McGill

Department of Earth and Planetary Sciences

Drift prospecting applied to iron oxide alkali-altered systems and iron oxide copper-gold deposits in the Great Bear magmatic zone, Northwest Territories, Canada

by

Philippe X. Normandeau

Department of Earth and Planetary Sciences
McGill University, Montreal

April 2018

A thesis submitted to McGill University in partial fulfillment of the requirements of the degree of Doctor of Philosophy

Earth & Planetary Sciences
McGill University
3450 University Street
Montréal, QC H3A 2A7
CANADA

Sciences de la Terre et des planètes
Université McGill
3450 Rue University
Montréal, (Québec) H3A 2A7
CANADA

(514) 398-6767
Fax: (514) 398-4680
http://www.eps.mcgill.ca

TABLE OF CONTENTS

LIST OF TABLES

LIST OF FIGURES

ABSTRACT

This thesis provides foundations for the development of glacial drift prospecting techniques applied to iron oxide alkali-alteration systems (IOAA) that can host deposits from the broad iron oxide apatite (IOA) and iron oxide copper-gold (IOCG) families. The potential of using drift prospecting as an exploration tool in these complex metasomatic systems is explored with a till matrix geochemical study and an indicator mineral study within the Great Bear magmatic zone (GBMZ). Both of these drift prospecting methods offer promising leads towards exploration vectors for IOA and IOCG mineralization as well as their IOAA system footprint in glaciated terrain.

The discontinuity of the till cover, the high compositional variability of the till due to heterogeneity within the source bedrock, the extensive size of alteration halos and the abundance of minor satellite mineralization in areas of interest complicate the application of surface exploration methods. However, Fe, Co, Ni, Cu, As, Mo, Bi, La, Th, U and W were identified as the most common potential vectoring elements towards mineralization in the GBMZ till matrix fraction based on a comparisons between a lithogeochemical dataset of the GBMZ (n= 707 samples) and a till geochemical dataset (n=101 samples). Anomalous concentration thresholds were established using the median values of elemental concentrations found in GBMZ background samples ± two times their standard deviation. Potential vectoring elements are dependent on the chosen analytical protocol, i.e. till matrix size fraction analyzed and digestion method used. In order to target the metasomatic halos of the mineralized systems, an innovative quantitative approach was developed based on the ratio of a selected element concentration from two analytical techniques. As such, mapping the ratios of the concentrations of either La or Th

obtained from a near-total digestion method over those obtained from a partial digestion method in the silt+clay-sized fraction of till defines a more consistent target than any element concentrations from any single digestion method used alone. This ratio reflects a variation in the element host mineral caused by metasomatic alteration. This approach was tested for the Sue Dianne deposit due to the higher number of till samples collected in its vicinity.

The potential of apatite to serve as an indicator of the presence of alteration systems and associated deposits in the GBMZ was also investigated. Apatite was selected due to its preservation in GBMZ till and its key role in the apatite-amphibole-magnetite assemblages as a signature alteration product of IOAA systems. The distinct fluorapatite chemistry that evolves within these systems can record metasomatic processes within IOA and IOCG deposits. Apatite from least-altered bedrock and from some IOAA systems have green to yellow-green cathodoluminescence responses. In contrast, apatite rich in REEs and poor in Mn, have a blue or blue and green-zoned cathodoluminescence response. REE-rich apatite crystals form during high temperature sodic-calcic-ferric/ferrous and calcic-ferric/ferrous metasomatism. As temperatures decline and the fluid chemistry evolves, localized REE leaching takes place within apatite and leads to the growth of secondary REE-bearing minerals. Apatite characteristics inherited from metasomatic history, such as irregular zoning, dissolution pits and mineral inclusions are visible in grains picked from the heavy mineral concentrates of till samples. Their presence may serve as a regional vector towards IOAA systems. The presence of blue cathodoluminescence response in apatite grains from till samples may serve as a local exploration tool for REE-rich IOA to IOCG prospects.

RÉSUMÉ

La présente étude établit les bases scientifiques nécessaires au développement de méthodes d'exploration glaciosédimentaire appliquées aux systèmes d'altérations alcalines à oxydes de fer pouvant servir d'hôtes aux gîtes de la famille des oxydes de fer-apatite (IOA) et oxyde de fer cuivre et or (IOCG). Le potentiel de la prospection glaciosédimentaire appliquée à ces sytèmes au métasomatisme complexe a été exploré par une étude géochimique de la matrice du till et une étude des minéraux indicateurs dans la zone magmatique du Grand lac de l'Ours (ZMGO). L'évaluation de ces deux méthodes d'exploration glaciosédimentaire a engendré des outils d'exploration prometteurs pouvant servir de vecteurs vers des minéralisations IOCG et IOA ainsi que vers l'empreinte de leurs systèmes d'altérations.

La couverture de till discontinue de la ZMGO, l'étendue des halos d'altérations et la présence de minéralisations mineures satellites dans les zones d'intérêt compliquent l'application de la prospection glaciosédimentaire. Le Fe, Co, Ni, Cu, As, Mo, Bi, La, Th, U et W ont toutefois été identifiés comme étant les éléments dans la matrice du till ayant le meilleur potentiel de vectorisation d'après des analyses de variance effectuées sur 707 échantillons d'une base de données de la lithogéochimie des roches encaissantes, alterées et mineralisées de la ZMGO et 101 échantillons de la géochimie du till, ainsi que des tests statistiques effectués en tenant compte de taux de confidence significatif. Les seuils de teneurs anormales de ces éléments ont été établis en utilisant les valeurs médianes des teneurs de fond dans la ZMGO ± deux fois leur déviation standard. L'identification d'éléments indicateurs de minéralisation est sensible au protocole analytique, i.e. la fraction granulométrique du till analysée et la méthode de digestion. Une méthode statistique innovatrice basée sur la cartographie des variations entre les minéraux

hôtes d'éléments sélectionnés a été développée de manière à cibler les halos d'altérations alcalines. Cette méthode exploite les rapports entre les concentrations de La ou de Th obtenues après digestion quasi totale et celles obtenues après digestion partielle de la fraction des silts et argiles du till et définit une cible plus nette que la concentration de quelconques éléments utilisés seuls. Cette approche a été testée au gîte Sue Dianne étant donné le nombre plus élevé d'échantillons prélevés autour de ce système.

Une méthode d'exploration spécifique aux systèmes d'altérations de la ZMGO et gîtes associés a été développée en utilisant l'apatite du till comme minéral indicateur. L'apatite a été sélectionnée pour une étude détaillée puisque ce minéral est préservé dans le till de la ZMGO et joue un rôle clé dans l'assemblage apatite-amphibole-magnétite, une signature des systèmes IOAA. Leur composition est un marqueur potentiel de leur processus de formation due au registre du métasomatisme. Les grains d'apatite provenant des roches moins altérées de la ZMGO, de même que la plupart des grains d'apatite provenant des systèmes IOAA et gîtes IOA et IOCG émettent, sous activation par cathodoluminescence, une lumière visible de couleur variant du vert au jaune et vert. En contraste, les grains d'apatite enrichis en terres rares et pauvres en Mn émettent une réponse bleue et/ou contiennent des zones irrégulières bleues et vertes. Ces grains d'apatite riches en terres rares sont le résultat de métasomatisme à haute température sodique calcique-fer et calcique-fer. Lors de la baisse de température subséquente et en fonction de l'évolution des fluides métasomatiques, une lixiviation localisée des terres rares prend place dans l'apatite et produit des phases minérales secondaires riches en terres rares. Les caractéristiques de l'apatite résultant de leur origine métasomatique et des altérations subséquentes, tel que des zones irrégulières, des traces de lixiviations et des inclusions de minéraux secondaires, sont visibles sur des grains récupérés de concentrés de minéraux lourds

des échantillons de till. Leur présence peut potentiellement servir d'outil de vectorisation régionale vers les systèmes IOAA. La présence de grains d'apatite à cathodoluminescence bleue est potentiellement un outil de vectorisation pour l'exploration de gîtes IOA à IOCG riches en terres rares.

ACKNOWLEDGMENTS

This work stems from the Geo-mapping for Energy and Minerals (GEM) IOCG/Multiple Metals Great Bear Region project of the Geological Survey of Canada (Natural Resources Canada) led by Dr. Louise Corriveau and conducted in partnership with the Wopmay Bedrock Mapping project of the Northwest Territories Geological Survey (NTGS) led by Val Jackson. Doctoral research funding was provided by the Research Affiliate Program of Natural Resources Canada and by the department of Earth and Planetary Science of McGill University. Field support was in part provided by the NTGS and helicopter support was provided by the Polar Continental Shelf Program of Natural Resources Canada. The Community Government of Gamètì and Fortune Minerals Ltd. are recognized for their active participation and collaborations. Thanks are due to Catherine Fontaine, Louis-Philippe Gélinas, Vincent Martel and Samuel Simard for astounding assistance in the field. The till geochemical datasets were made possible by Shauna Madore and her team at the Sedimentology Laboratory (GSC) for the management and preparation of till samples. XRD analysis were made possible by Alain Grenier and Jeanne Percival (GSC). Katherine Venance and Pat Hunt of the Geological Survey of Canada Microbeam Laboratory, Helen Campbell (McGill University) and the staff of the Deutsche GeoForschungsZentrum laboratory are recognized for their contributions with EMP analysis. Overburden Drilling Management (Stu Averill and Rémy Huneault) are thanked for the customized heavy mineral processing and indicator mineral picking. Hugh de Souza and his team at SGS Mineral Services completed the QEMSCAN analysis. John Stix (McGill University) and Jason Coumans (McGill University) are thanked for making the cathodoluminescence analysis possible. Ariane Castagner and Melissa Weber (Ottawa University) helped to prepare the appendices of Open File 7307 and Peter Bobrowsky (GSC) is thanked for providing a careful

review of this document. LA-ICP-MS measurements were made possible by Simon Jackson (GSC).

Insights, guidance, and in some cases, reviews, were provided by Robert Garrett (GSC), Eric Grunsky (GSC), Robert Martin (McGill University), Vincent Van Hinsberg (McGill University), Valerie Jackson (NTGS) and Luke Ootes (NTGS-BCGS) as well as Alain Plouffe (GSC). Jean-François Montreuil (INRS), Pedro Acosta (University of Alberta) and Madeline Lee (McMaster University) are thanked as fellow doctoral students involved within the IOCG/Multiple Metals Great Bear Region project for their team work, insights and a great time in the field. The author is also grateful to Cameron Butler and Philip Lypaczewski for their participation to this project during their undergraduate studies at McGill University, providing preliminary petrographic and cathodoluminescence observations. Jeffrey McKenzie, Galen Halverson and Kristy Thornton from McGill's Department of Earth and Planetary Sciences all helped with the thesis process.

This thesis benefited from exceptional participation from co-authors; Isabelle McMartin (GSC), Jeanne Paquette (McGill University), Louise Corriveau (GSC) and Daniel Harlov (GFZ). In addition, Isabelle and Jeanne are thanked for their devotion as supervisors and friends. Mentor and old time friend Louise is also thanked for leading the project that made this thesis possible. Parents, family and friends are mentioned for their encouragements and unfailing support. Scott Cairns and John Ketchum (NTGS) are thanked for their understanding and support while this project was completed in parallel to my responsibilities at the NTGS. My better half Danielle is to be recognized for nothing short of making the doctorate happen and for her ubiquitous awesomeness while seeing me through it. She is now also hard at work developing our newest life project which is expected this summer.

PREFACE

The present doctoral research resulted in four manuscripts corresponding to the chapters 2 3, 4 and 5 of this thesis. Chapter 2 is the report of an Open File published at the Geological Survey of Canada (GSC) entitled "Composition of till and bedrock across the Great Bear magmatic zone: Quaternary field database and analytical results from the GEM IOCG-Great Bear Project" (OF 7307: Normandeau and McMartin, 2013). I collected all samples and field observations in the summer of 2009 and 2010 in the Northwest Territories while receiving training from Dr. Isabelle McMartin, and I carried out the Quaternary geology analysis and interpretations presented in the report. The geochemical, indicator mineral and till matrix mineralogy results in this Open File originated from multiple private and GSC-housed laboratories while I made the field descriptions, ice-movement indicators, sample descriptions, pebble counts, binocular observations and scanning electron microscopy analyses. The GSC made this database available for public download under Dr. Isabelle McMartin's supervision (Appendix 1).

Chapter 3 consists of a manuscript tailored for submission to the journal *Geochemistry: Exploration, Environment, Analysis* entitled "Till geochemistry as a vector to iron oxide alkali-altered systems and iron oxide copper-gold deposits in the Great Bear magmatic zone, Northwest Territories, Canada". This manuscript presents the results of a series of statistical tests performed using univariate and multivariate techniques (i.e. Normandeau et al., 2011a,b,c; Normandeau et al., 2012a,b; Normandeau et al., 2013). I performed the statistical analyses on geochemical data from till samples that were compiled as part of GSC Open File 7307 as well as bulk lithogeochemical analyses provided by GSC colleagues found in GSC Open File 7643 (Corriveau et al., 2015). This manuscript benefited from text editing and critical comments from

my co-authors Dr. Isabelle McMartin, Dr. Jeanne Paquette and Dr. Louise Corriveau. Manuscript reviews were also provided by Dr. Alain Plouffe, Dr. Robert Garrett and Dr. Vincent van Hinsberg.

Chapter 4 consists of a manuscript entitled "Characterization of Fluorapatite within Iron Oxide Alkali Alteration Systems of the Great Bear magmatic zone: A Potential Metasomatic Process Record.", currently accepted and in queue to be released in the next issue of *The Canadian Mineralogist*. I benefited from text editions by co-authors Dr. Daniel Harlov, Dr. Louise Corriveau, Dr. Isabelle McMartin and Dr. Jeanne Paquette. The manuscript was reviewed by Dr. John Hanchar and an anonymous reviewer during the publication process. I selected and characterized the apatite grains using three different data sources; 1) laser ablation analysis that I performed with expert assistance from Dr. Simon Jackson (see Appendix 2 for the full datasets), 2) microprobe analysis that were performed at the GSC Microbeam Laboratory under the supervision of co-author Dr. Isabelle McMartin, and 3) microprobe analysis performed at the GeoForschungsZentrum laboratory under the supervision of co-author Dr. Daniel Harlov. I also performed the cathodoluminescence analysis as well as the scanning electron microscopy analysis at McGill University. Helen Campbell offered guidance on the scanning electron microscope operation and provided advice on the optimum instrumental configuration. Petrographic descriptions of some thin sections used in Chapter 4 were performed by Philip Lypaczewski under co-supervision by myself and Dr. Jeanne Paquette. I compiled these observations and added a preliminary interpretation of the apatite petrogenesis, which was released as GSC Open File 7319 (Lypaczewski, Normandeau et al., 2013). This report is included in this thesis as Appendix 3.

Chapter 5 consists of the manuscript to be submitted as a joint Northwest Territories Geological Survey (NTGS)- GSC Open File report, prepared as a complement to the apatite study in GBMZ bedrock. It incorporates my interpretations on the analysis of apatite grains recovered from till samples which are not included in Chapter 4. A portion of this work was presented at the Yellowknife Geoscience Forum (Normandeau et al., 2014a). The manuscript edition was performed by Dr. Isabelle McMartin. An overview of the work contained in chapter 4 and 5 was presented at the Geological Association of Canada and Mineralogical Association of Canada annual meeting in 2016 (Normandeau et al., 2016).

REFERENCES

Normandeau, P.X., McMartin, I., Paquette J., Corriveau, L., 2011a, Drift prospecting applied to iron oxide copper-gold exploration in the Great Bear magmatic zone, Northwest Territories. Canadian Quaternary Association (CANQUA), 15th biennial meeting, Québec, QC. August 28-31.

Normandeau, P.X., McMartin, I., Paquette, J., Corriveau, L., 2011b, Till geochemical signatures of iron oxide copper-gold mineralization in the Great Bear magmatic zone, Northwest Territories, Canada. In: B.J. Fischer and D.M. Watson (compilers), 39th Annual Yellowknife Geoscience Forum Abstracts. Northwest Territories Geoscience Office, Yellowknife, NT, YKGSF Abstracts Volume 2011, p. 115–116.

Normandeau, P.X. McMartin, I. Paquette, J. Corriveau, L., 2011c, Drift prospecting applied to iron oxide copper gold exploration in the Great Bear magmatic zone, Northwest Territories, Canada. Geological & Mineralogical Association of Canada (GAC-MAC) annual meeting, Ottawa, ON, April 25-27.

Normandeau, P.X., McMartin, I., Paquette, J., Corriveau, L., 2012a, Till geochemical signatures of iron oxide copper-gold mineralization in the Great Bear magmatic zone, Northwest Territories, Canada. 2012 SEG Canada Minerals Colloquium at Prospectors and Developers Association of Canada (PDAC) annual meeting, Toronto, ON, March 5.

Normandeau, P.X., McMartin, I., Paquette, J., Corriveau, L., Montreuil, J.F., 2012b, Geochemical signatures of IOCG mineralization and alteration in till. Goldschmidt 2012, Program with Abstracts.

Normandeau, P.X. and McMartin, I., 2013, Composition of till and bedrock across the Great Bear magmatic zone: field database and analytical results from the GEM IOCG-Great Bear Project: Geological Survey of Canada, Open File 7307, 26 p.

Normandeau, P.X., McMartin, I., Paquette, J., Corriveau, L., 2013, Prospection glaciosédimentaire appliquée aux gisements IOCG: signatures multivariées des altérations. 81e congrès de l'ACFAS, session ressources minérales-DIVEX, May 2013.

Normandeau, P.X., Corriveau, L., Paquette, J., and McMartin, I., 2014, Apatite as an Indicator Mineral to IOCG Deposits in the Great Bear Magmatic Zone, Northwest Territories, Canada. In: D. Irwin and P.X. Normandeau (compilers), 42nd Annual Yellowknife Geoscience Forum Abstracts, Northwest Territories Geoscience Office, Yellowknife, NT. YKGSF Abstracts Volume 2014. p. 53.

Normandeau, P.X. McMartin, I., Corriveau, L., Harlov D. E. and Paquette, J., 2016, Fluorapatite in till as an indicator mineral for iron oxide alkali-alteration systems, Great Bear magmatic zone, Northwest Territories, Canada. Geological & Mineralogical Association of Canada (GAC-MAC) annual meeting, Whitehorse, YT, June 1-3.

Normandeau, P.X., Harlov, D.E., Corriveau, L., Paquette, J., McMartin, I., in press, Characterization of fluorapatite within iron oxide alkali-calcic alteration systems of the Great Bear magmatic zone: a potential metasomatic process record: The Canadian Mineralogist.

Lypaczewski, P., Normandeau, P. X., Paquette, J. and McMartin, I., 2013, Petrographic and cathodoluminescence characterization of apatite from the Sue Dianne and Brooke Zone IOCG mineralization systems, Great Bear magmatic zone, Northwest Territories: Geological Survey of Canada, Open File 7319, 18 p.

CHAPTER 1: General Introduction

Formerly known for its vein-type uranium and silver mines, the Great Bear magmatic zone (GBMZ) is currently the most prospective iron oxide copper-gold (IOCG) mineral belt in Canada (Corriveau et al., 2010). It was selected as a study area under Natural Resources Canada's Geomapping for Energy and Minerals (GEM) Program at the Geological Survey of Canada (GSC). Specifically, the IOCG-Great Bear Project was implemented to refine the genetic models and exploration criteria of IOCG deposits using their host iron oxide alkali-alteration systems (IOAA) and their association to iron-oxide apatite deposits (IOA). In this context, an applied Quaternary research activity was created in partnership between the GSC and McGill University to provide the foundations for the application of geochemical and indicator mineral exploration for IOAA systems and their potential IOCG and IOA deposits in glaciated terrain.

1.1. DRIFT PROSPECTING

Drift prospecting refers to exploration methods based on our understanding of glacial sediment transport and erosional processes to locate exposed and buried economical mineralization in formerly glaciated terrain (Klassen, 2001). It relies on the identification of anomalies within glacial sediments and the ability to trace these anomalies back to their source, i.e. glacially eroded bedrock of economic interest. Such anomalies can take a variety of forms including chalcopyrite-rich boulders, sand-sized gold grains or high copper concentrations in the matrix fraction of glacial sediments. Anomalies are defined differently according to the drift prospecting method used. For example, the presence of a specific texture on a single sand-size grain of garnet can be meaningful in diamond exploration, but a geochemical anomaly is an

elemental concentration that needs to exceed a predefined statistical threshold to set it apart from background.

The application of any drift prospecting method relies on the reconstruction of glacial flow directions. These can be evaluated through the mapping and relative chronology of glacial erosional and depositional landforms (i.e. McMartin and Paulen, 2009, for a review of methods). Ice-flow directions and entrainment models may then be used to predict dispersal fan geometry (i.e. Klassen, 2001; Stanley, 2009; Hooke et al., 2013). Assessment of dispersal profiles for a given area may also be done through the mapping of anomalies around a known source. Various drift prospecting methods differ primarily in sample media and size fraction of the glacial sediment used, but also in the sampling and analytical methods.

Drift prospecting methods have been used in Canada since the beginning of the last century (see Paulen and McMartin, 2009, and references herein). Analytical techniques developed in the last decades enable their application to an increasing variety of deposit types (McClenaghan, 1994; Kaszycki et al., 1996; McClenaghan et al., 2000; Klassen, 2003; Lehtonen et al., 2005; Campbell, 2009; Sarala et al., 2009; Barnet and Averill., 2010; McClenaghan et al., 2011; McClenaghan and Peter, 2016). The present study assess till matrix geochemistry and indicator minerals as prospecting methods applied to IOAA systems and IOA-IOCG deposits in the GBMZ. Both of these modern, conventional tools offer the potential to target bedrock metasomatic alterations and mineralization.

1.1.1. Till geochemistry

Surficial geochemistry is a widely used inexpensive exploration method. Historically, geochemical anomalies were identified through proportional symbol plots (Harris et al., 2001).

More advanced statistical treatments and spatial pattern representations through geographical information systems (GIS) rapidly became customary (Grunsky and Smee, 1999; Grunsky, 2010). As geochemical data consist of multi-element sets, multivariate analysis may be used, for instance, to weigh the relative importance of provenance and transport distance variations on separate subsets of elements. In glaciated terrain, basal till mainly reflects source bedrock composition modified by glacial dispersal; weathering processes are minimal and have been active only since deglaciation in the uppermost portion of the till (0 to 2 m) (McMartin and McClenaghan, 2001). As with indicator minerals, till geochemistry from samples collected below the post-glacial solum reflects a first order physical dispersal method. When surveying for specific elements, understanding the physical segregation of the mineral grains containing these elements during glacial transport may help design appropriate protocols using well-defined particle size fractions, therefore accentuating the contrast between anomalies and background data (McClenaghan et al., 2013). Past studies have also demonstrated the feasibility of till geochemical methods in forested areas and/or areas affected by glaciolacustrine submergence, notably in the Abitibi Greenstone Belt for gold grain based exploration (McClenaghan, 2001).

1.1.2. Indicator minerals

Indicator mineral methods use 'clastic' indicators, i.e., sand grains usually recovered from the 0.25 to 2 mm size fraction of glacially transported sediments giving a signal attributable to mechanical dispersal processes alone (Thorleifson, 2009). Indicator mineral species must: 1) resist glacial attrition and post-glacial weathering, 2) carry a distinctive signature from the bedrock source, 3) be easily identifiable, and 4) be recoverable from the bulk sample through conventional gravity and density separation (typically S.G. > 3.2). Often, abundance alone of the indicator minerals in till is sufficient to serve as an exploration tool (McClenaghan, 2005).

Changes in the size and texture and morphology of individual grains from their aspect in the host rock can provide useful information such as travel distance between the sample location and their bedrock source (McClenaghan et al., 2000; McClenaghan, 2005). Also, the major, minor and trace element content of indicator grains can impart a signature distinctive enough to allow a match with specific deposit types (McClenaghan, 2005). Such information may allow the identification of the grain provenance when the chosen indicator mineral species are also found in the regional bedrock.

Indicator mineral based exploration has led to important discoveries in Canada including the Lac de Gras kimberlite field in the late 1980s (Carlson et al., 1999). The unusual major and trace element composition of kimberlite ultrabasic rocks and mantle xenoliths results in a diverse and distinctive mineralogy and mineral chemistry in glacially derived sediment. Diamond exploration based on indicator minerals of kimberlite affinity is now a well-established technique in glaciated terrain (McClenaghan and Kjarsgaard, 2001).

1.2. STUDY AREA – DRIFT PROSPECTING IN THE GREAT BEAR MAGMATIC ZONE

The GBMZ is a volcanic and plutonic felsic to intermediate Andean type calc-alkaline belt (Hildebrand et al. 1987, 2010; Jackson et al. 2013). It is exposed between the western margin of the Slave Craton to the east and the Phanerozoic cover to the west. At the eastern border, the Wopmay fault separates the GBMZ from the metamorphic rocks of the Wopmay Orogen (Hildebrand et al., 1987; Jackson, 2006, 2008; Jackson and Ootes, 2010). The GBMZ is host to two IOCG deposits of economic interest, the NICO Co-Au-Bi deposit and the Sue Dianne Cu-Ag-(U-Au) deposit. These deposits, as well as many IOAA systems of the GBMZ, have been

the subject of recent petrological, mineral chemistry, geochemical, geochronological, isotopic and economic geology studies (Gandhi et al. 1996, 2013; Corriveau et al. 2010a,b; Mumin et al. 2007, 2010; Potter et al. 2013a,b; Acosta-Góngora et al. 2014, 2015; DeToni 2016; Montreuil et al. 2015, 2016a, 2016b). These studies framed the GBMZ IOAA alteration zones into a prograding metasomatic facies evolution model linked to the genesis of IOA to IOCG deposits. Overprinting prograde and retrograde alterations, as well as the juxtaposition of alteration types, increase with proximity to the ore zones (Corriveau et al., 2010b; Montreuil et al., 2015, 2016a, 2016b). In the GBMZ, unaltered protoliths in the IOAA systems are rare due to the intensity of metasomatism and its spatial extent which, as also observed in other IOCG districts worldwide, often exceed 300 km^2 (Barton and Johnson, 2004; Mumin, 2015; Mumin et al., 2007, 2010; Porter, 2010).

Glacial flow directions in the GBMZ have not been the subject of any systematic study. Streamlined landform compilations (Prest et al., 1968; Clark, 1993; Dyke and Prest, 1987; Dyke, 2004) provide a general assessment of a west-southwest dominant glacial flow direction in the southern part of the GBMZ, but little data were previously compiled for the central and northern parts of the GBMZ prior to the current research. The sediment cover of the GBMZ is largely composed of a thin (< 2 m) and discontinuous till with large areas of exposed bedrock (Fulton, 1995). It possesses weak soil development (10 to 40 cm depth for lower B-horizon) and discontinuous permafrost. Its vegetation cover is a transitional boreal forest with areas of tundra in the northern part. The Glacial Lake McConnell (11.8 – 8.3 ka BP, Smith, 1994) covered most of the GBMZ below 300 m *(a.s.l.*).

An orientation study conducted at the NICO Co-Au-Bi magnetite-group IOCG deposit (McMartin et al., 2009a,b, 2011a,b) initiated the development of a drift prospecting method to

IOCG deposits in the southern GBMZ. This study demonstrated the potential of As, Bi, Co, Au, Cu, Sb, W and Cd as pathfinder elements in till geochemistry at NICO. Iron oxide grain composition and gold grain abundance were identified as potential indicator mineral methods towards IOCG in glaciated terrain (McMartin et al., 2011a; Sappin et al., 2014). Chalcopyrite, arsenopyrite and pyrite were noted to be present in some cases down-ice of mineralization but were not always preserved in the shallow till of the southern GBMZ. The use of gold grains as an indicator of the presence of IOA-IOCG deposits throughout the GBMZ was addressed in Normandeau et al. (2014). Modified shaped gold grain contents correlate well with highly reshaped gold grain contents and are most often from known sources of gold within short transport distances. This suggests that the reshaping of gold grains took place either rapidly during glacial transport or in situ caused by wave action from Glacial Lake McConnell. Chalcopyrite grains may also be preserved, in some cases, in till directly down-ice of their bedrock source but are not always present in the IOA-IOCG deposits and alteration systems of interest (Normandeau et al., 2011).

1.3. OBJECTIVES OF THE THESIS

The objectives of the research presented in this thesis are (1) to provide a Quaternary geology framework for interpreting the history and nature of glacial sediments in the GBMZ, (2) to examine spatial patterns of elemental concentrations in till and bedrock across the GBMZ and to evaluate statistical methods to identify mineral deposit signatures and IOAA alteration systems in glacial sediments, and (3) to develop an indicator mineral approach, by characterizing the nature of apatite grains in bedrock and in till. Drift prospecting methods for IOAA systems and their associated deposits have never been developed before in glaciated terrain with the

exception of targeted studies under the same GEM IOCG-Great Bear Project. As such, the present work expands on the preliminary findings of McMartin et al. (2011a,b) for the NICO Co-Au-Bi magnetite-group IOCG deposit by comparing the signatures of a broad range of IOA to IOCG mineralization and IOAA systems located throughout the GBMZ.

The development of drift prospecting methods applied to the spectrum of IOA to IOCG deposits and related hydrothermal alterations of the GBMZ first requires an understanding of the surficial geology context to constrain dispersal fan geometry, transport distance and to assess the suitability of GBMZ till as a sampling medium. The second chapter of this thesis summarizes some aspects of the surficial geology of the GBMZ and contains glacial dispersal interpretations based on striation measurements and pebble counts in till.

The third chapter investigates till geochemical signatures of IOAA systems and IOA to IOCG deposits. It builds on the recent characterization of GBMZ lithogeochemistry signatures (Corriveau et al., 2015; Montreuil et al., 2013, 2015, 2016a, 2016b). These results are combined with till geochemistry results from the GBMZ background, from the Sue Dianne Cu-Ag-(U-Au) magnetite to hematite group IOCG deposit and from several polymetallic showings of the GBMZ.

Chalcopyrite and gold grains were identified in till sampled down-ice (~ 1 km and less) of known mineralized outcrop within the GBMZ (McMartin et al., 2009a,b, 2011a,b; Normandeau et al., 2011; Normandeau et al., 2014) yet their use as indicator minerals is limited by variable abundances in mineralization and/or variable preservation in glacial sediments. Apatite was investigated as a novel indicator mineral that has the potential to identify alteration systems. The goal of this approach was to identify alteration signatures that are applicable to the

variety of IOA-IOCG deposits in the GBMZ and to provide larger targets than the mineralization. Chapter 4 documents the potential of apatite crystals to record metasomatic processes related to the IOA-IOAA deposits and other alteration systems in the GBMZ using thin sections and disaggregated samples of altered and mineralized bedrock. Chapter 5 investigates these characteristics in apatite grains picked in heavy mineral concentrates from till samples. This chapter therefore addresses the characterization of apatite as a new potential indicator mineral for IOA-IOCG deposits in glaciated terrain.

REFERENCES

Acosta-Góngora, P., Gleeson, S., Samson, I., Ootes, L. and Corriveau, L., 2014, Trace element geochemistry of magnetite and its relationship to Cu-Bi-Co-Au-Ag-UW mineralization in the Great Bear magmatic zone, NWT, Canada: Economic Geology, v. 109, p. 1901–1928.

Acosta-Góngora, G.P., Gleeson, S.A., Samson, I., Ootes, L. and Corriveau, L., 2015, Gold refining by bismuth melts in the iron oxide-dominated NICO Au-Co-Bi (±Cu±W) deposit, NWT, Canada: Economic Geology, v. 110, p. 291–314.

Barnett, P. J. and Averill, S., 2010, Heavy mineral dispersal trains in till in the area of the Lac des Iles PGE deposit, Northwestern Ontario, Canada. Geochemistry: Exploration, Environment, Analysis, v. 10, p. 391–399.

Barton, M.D. and Johnson, D.A., 2004, Footprints of Fe-oxide (Cu-Au) systems. Center for Global Metallogeny, University of Western Australia, Special Publication, v. 33, p. 112–116.

Campbell, J. E., 2009, Drift prospecting for uranium in the Athabasca Basin, Saskatchewan. In: R. C. Paulen and I. McMartin (eds), Application of till and stream sediment Heavy mineral and Geochemical Methods to Mineral Exploration in Western and Northern Canada, Geological Association of Canada, GAC short course Notes 18, p. 207–214.

Carlson, J.A., Kirkley, M.B., Thomas, E.M. and Hillier, W.D., 1999, Recent Canadian Kimberlite Discoveries. In: J.J. Gurney, J.L. Gurney, M.D. Pasco and S.H. Richardson (eds), The J.B. Dawson Volume, Proceedings of the VII International Kimberlite, Cape Town, p. 81–89.

Clark, C.D., 1993, Mega-scale glacial lineations and cross-cutting ice-flow landforms. Earth Surface Processes and Landforms, v. 18, p. 1–29.

Corriveau L., Mumin A.H. and Setterfield T., 2010a, IOCG environments in Canada: Characteristics, geological vectors to ore and challenges. In: T.M. Porter (ed), Hydrothermal iron oxide copper–gold and related deposits: A global perspective, Volume 4–advances in the understanding of IOCG deposits, Porter Geoscience Consultancy Publishing, Adelaide, p. 311–343.

Corriveau, L., Williams, P.J. and Mumin, A.H., 2010b, Alteration vectors to IOCG mineralization from uncharted terranes to deposits. In: L. Corriveau and A.H. Mumin (eds.), Exploring for iron oxide copper-gold deposits, Geological Association of Canada, Short Course Notes 20, p. 89–110.

Corriveau, L., Lauzière, K., Montreuil, J.F., Potter, E., Hanes, R. and Prémont, S., 2015, Dataset of geochemical data from iron oxide alkali-altered mineralizing systems of the Great Bear magmatic zone, Northwest Territories: Geological Survey of Canada, Open File 7643.

DeToni, A.F., 2016, Systèmes à oxydes de fer et altérations en éléments alcalins, zone magmatique du Grand lac de l'Ours. Unpublished M.Sc. thesis, Québec Canada, Université du Québec, Institut national de la Recherche scientifique, Centre – Eau Terre Environnement, 738 p.

Dyke, A.S., 2004, An outline of North American deglaciation with emphasis on central and northern Canada: Developments in Quaternary Sciences, v. 2, p. 373–424.

Dyke, A.S. and Prest, V.K., 1987, Late Wisconsinan and Holocene history of the Laurentide ice sheet: Géographie physique et Quaternaire, v. 41, p. 237–263.

Fulton, R.J.C., 1995, Surficial materials of Canada: Geological Survey of Canada, Map 1880A.

Gandhi, S.S., Prasad, N. and Charbonneau, B., 1996, Geological and geophysical signatures of a large polymetallic exploration target at Lou Lake, southern Great Bear magmatic zone, Northwest Territories: Geological Survey of Canada, Current Research - 1996, p. 147–158.

Gandhi, S.S., Potter, E.G. and Fayek, M., 2013, Polymetallic U-Ag veins at Port Radium, Great Bear magmatic zone, Canada: Main botryoidal pitchblende stage cuts 1.74 Ga diabase dykes and has REE signatures diagnostic of unconformity-type deposits: Geological Survey of Canada, Open File 7493, 1 p.

Grunsky, E.C., 2010, The interpretation of geochemical survey data: Geochemistry: Exploration, Environment, Analysis, v. 10, p. 27–74.

Grunsky, E. C., Smee, B. W., 1999, The differentiation of soil types and mineralization from multi-element geochemistry using multivariate methods and digital topography: Journal of Geochemical Exploration, v. 67, p. 287–299.

Harris, J. R. Wilkinson, L. and Bernier, M., 2001, Analysis of geochemical data for mineral exploration using a GIS – A case study from Swayze greenstone belt, northern Ontario, Canada. In: McClenaghan, M. B., Bobrowsky, P. T., Hall, G. E. M., Cook, S.J. (eds), Drift exploration in glaciated terrain, Geological Society, London, Special Publications, v. 185, p. 152–165.

Hildebrand, R.S., Hoffman, P.F. and Bowring, S.A., 1987, Tectono-magmatic evolution of the 1.9-Ga Great Bear magmatic zone, Wopmay Orogen, northwestern Canada: Journal of Volcanology and Geothermal Research, v. 32, p. 99–118.

Hildebrand, R.S., Hoffman, P.F. and Bowring, S.A., 2010, The Calderian orogeny in Wopmay orogen (1.9 Ga), northwestern Canadian Shield. Geological Society of America Bulletin, v. 122, 794–814.

Hooke, R.L., Cummings, D.I., Lesemann, J.-E. and Sharpe, D.R., 2013, Genesis of dispersal plumes in till: Canadian Journal of Earth Sciences, v. 50. p. 847–855.

Jackson, V.A., 2006, Preliminary geologic map of part of the southern Wopmay Orogen (parts of NTS 86B and 86C); descriptive notes to accompany 1:100,000 scale map. Northwest Territories Geoscience Office, Yellowknife, NT, NWT Open Report 2006-004, 1 map, scale 1:100,000, and accompanying report, 41 p.

Jackson, S.E., 2008, Calibration strategies for elemental analysis by LA-ICP-MS. In: P. Sylvester (ed.), Laser ablation-ICP-MS in the Earth sciences, Mineral Association of Canada, Short Course Series, v. 40, p. 69–188.

Jackson, V.A., and Ootes, L., 2010, Preliminary geologic map of the south-central Wopmay orogen (parts of NTS 86B, 86C, and 86D); results from 2009: Northwest Territories Geological Survey, Open Report 2010-004, 1 p.

Jackson, V.A., van Breemen, O., Ootes, L., Bleeker, W., Bennett, V., Davis, W.J., Ketchum, J., Smar, L. and McFarlane, C., 2013, U–Pb zircon ages and field relationships of Archean basement and Proterozoic intrusions, south-central Wopmay Orogen, NWT: implications for tectonic assignments 1, 2: Canadian Journal of Earth Sciences, v. 50, 979–1006.

Kaszycki, C.A., Nielsen, E. and Gobert, G., 1996, Surficial geochemistry and response to volcanic-hosted massive sulphide mineralization in the Snow Lake region. In: G.F. Bonham-Carter, A.G. Galley and G.E.M. Hall, (eds), Extech I: A Multidisciplinary approach to massive sulphide research in the Rusty Lake-Snow Lake greenstone belts, Manitoba: Geological Survey of Canada, Bulletin, v. 426, p. 139–154.

Klassen, R. A., 2001, A quaternary geological perspective on geochemical exploration in glaciated terrain. In: M.B. McClenaghan, P.T. Bobrowsky, G.E.M. Hall and S.J. Cook (eds), Drift exploration in glaciated terrain, Geological Society, London, Special Publications, v. 185, p. 1–19.

Klassen, R., 2003, The geochemical and physical properties of till, Bathurst Mining Camp, New Brunswick, Canada. Massive Sulfide Deposits of the Bathurst Mining Camp, New Brunswick, and Northern Maine, Economic Geology Monograph, v. 11, p. 661–678.

Lehtonen, M., Marmo, J., Nissinen, A., Johanson, B. and Pakkanen, L., 2005, Glacial dispersal studies using indicator minerals and till geochemistry around two eastern Finland kimberlites: Journal of Geochemical Exploration, v. 87, p. 19–43.

McClenaghan, M.B., 1994, Till geochemistry in areas of thick drift and its application to gold exploration, Matheson area, northeastern Ontario: Exploration and Mining Geology, v. 3, p. 17–30.

McClenaghan, M. B., 2001, Regional and local-scale gold grain and till geochemical signatures of lode Au deposits in western Abitibi Greenstone Belt, central Canada. In: M.B. McClenaghan, P.T. Bobrowsky, G.E.M. Hall and S.J. Cook (eds), Drift exploration in glaciated terrain, Geological Society, London, Special Publications, v. 185, p. 201–224.

McClenaghan, M. B. and Kjarsgaard, B. A., 2001, Indicator mineral and geochemical method for diamond exploration in glaciated terrain in Canada. In: M.B. McClenaghan, P.T. Bobrowsky, G.E.M. Hall and S.J. Cook (eds) 2001, Drift exploration in glaciated terrain, Geological Society, London, Special Publications, v. 185. p. 83–124.

McClenaghan, M.B., Thorleifson, L.H. and DiLabio, R.N.W., 2000, Till geochemical and indicator mineral methods in mineral exploration. Ore Geology Reviews, v. 16, p. 145–166.

McClenaghan, M. B. 2005, Indicator mineral methods in mineral exploration: Geochemistry: Exploration, Environment, Analysis, v. 5, p. 233–245.

McClenaghan, M.B., Layton-Matthews, D. and Matile, G., 2011, Till geochemical signatures of magmatic Ni–Cu deposits, Thompson Nickel Belt, Manitoba, Canada: Geochemistry: Exploration, Environment, Analysis, v. 11, p. 145–159.

McClenaghan, M.B., Plouffe, A., McMartin, I., Campbell, J.E., Spirito, W.A., Paulen, R.C., Garrett, R.G. and Hall, G.E.M., 2013, Till sampling and geochemical analytical protocols used by the Geological Survey of Canada: Geochemistry: Exploration, Environment, Analysis, v. 13, p. 285–301.

McClenaghan, M.B. and Peter, J.M., 2016, Till geochemical signatures of volcanogenic massive sulphide deposits: an overview of Canadian examples: Geochemistry: Exploration, Environment, Analysis, v. 1, 24–47.

McMartin, I. and McClenaghan, M.B., 2001, Till geochemistry and sampling techniques in glaciated shield terrain: a review. In: M.B. McClenaghan, P.T. Bobrowsky, G.E.M. Hall and S.J. Cook (eds), Drift exploration in glaciated terrain, Geological Society, London, Special Publications, v. 185, p. 19–43.

McMartin, I. and Paulen, R.C., 2009, Ice-flow indicators and the importance of ice-flow mapping for drift prospecting. In: R.C. Paulen and I. McMartin (eds), Application of till and stream sediment Heavy mineral and Geochemical Methods to Mineral Exploration in Western and Northern Canada, Geological Association of Canada, GAC short course Notes 18, p. 15–34.

McMartin, I., Corriveau, L. and Beaudoin, G., 2009a, Heavy mineral and till geochemical signatures of the NICO Co-Au-Bi deposit, Great Bear magmatic zone, Northwest Territories, Canada. In: D.R. Lentz, K.G. Thorne and K.-L. Beal (eds), Proceedings, 24th International Applied Geochemistry Symposium (IAGS 2009), Fredericton, New Brunswick, June 2009, p. 553–556.

McMartin, I., Corriveau, L., Beaudoin, G., Averill, S. and Kjarsgaard, I., 2009b, Heavy mineral signature of the NICO Co-Au-Bi deposit, Great Bear magmatic zone, Northwest Territories, Canada. In: B. McClenaghan and H. Thorleifson (eds), Indicator mineral methods in mineral exploration, Workshop B, 24th International Applied Geochemistry Symposium (IAGS 2009), Fredericton, New Brunswick, June 2009, p. 71–81.

McMartin, I., Corriveau, L. and Beaudoin, G., 2011a, An orientation study of the heavy mineral signature of the NICO Co-Au-Bi deposit, Great Bear magmatic zone, Northwest Territories, Canada: Geochemistry: Exploration, Environment, Analysis, v. 11, p. 293–307.

McMartin, I., Corriveau, L., Beaudoin, G., Averill, S.A. and Kjarsgaard, I., 2011b, Results from an orientation study of the heavy mineral and till geochemical signatures of the NICO Co-Au-Bi deposit, Great Bear magmatic zone, Northwest Territories, Canada: Geological Survey of Canada, Open File 6723.

Montreuil, J.-F., Corriveau, L. and Grunsky, E., 2013, Compositional data analysis of hydrothermal alteration in IOCG systems, Great Bear magmatic zone, Canada: to each alteration type its own geochemical signature: Geochemistry: Exploration, Environment, Analysis, v. 13, p. 229–247.

Montreuil, J.-F., Corriveau, L. and Potter, E.G., 2015, Formation of albitite-hosted uranium within IOCG systems: the Southern Breccia, Great Bear magmatic zone, Northwest Territories, Canada: Mineralium Deposita, v. 50, p. 293–325.

Montreuil, J.-F., Potter, E.G., Corriveau, L., and Davis, W.J., 2016a, Element mobility patterns in magnetite-group IOCG systems: The Fab IOCG system, Northwest Territories, Canada. Ore Geology Reviews, v. 72, p. 562–584.

Montreuil, J.F., Corriveau, L. and Potter, E.G., 2016b, On the relation between alteration signature and metal endowment of iron oxide alkali altered systems, southern Great Bear magmatic zone (Canada). In A Special Issue Devoted to Proterozoic Iron Oxide-Apatite-(+REE) and Iron Oxide-Copper-Gold and Affiliated Deposits of Southeast Missouri, USA, and the Great Bear Magmatic Zone, Northwest Territories, Canada (Slack, J. F., Corriveau, L. & Hitzman, M. W.): Economic Geology, v. 111, p. 1803–1814.

Mumin, A.H., ed., 2015, Echo Bay IOCG thematic map series: geology, structure and hydrothermal alteration of a stratovolcano complex, Northwest Territories, Canada: Geological Survey of Canada, Open File 7807, 19 p.

Mumin, A.H., Corriveau, L., Somarin, A.K., and Ootes, L., 2007, Iron oxide copper-gold-type polymetallic mineralisation in the Contact Lake Belt, Great Bear Magmatic Zone, Northwest Territories, Canada. Exploration and Mining Geology, v. 16, p. 187–208.

Mumin, A.H., Somarin, A.K., Jones, B., Corriveau, L., Ootes, L. and Camier, W.J., 2010, The IOCG-porphyry-epithermal continuum in the Great Bear Magmatic Zone, Northwest Territories, Canada. In: L.Corriveau and A.H. Mumin (eds.), Exploring for Iron-Oxide Copper-Gold deposits: Canada and global analogues. Geological Association of Canada, Short Course Notes, v. 20, p. 59–78.

Normandeau, P.X., McMartin, I., Paquette, J., Corriveau, L., 2011, Drift prospecting applied to iron oxide copper-gold exploration in the Great Bear magmatic zone, Northwest Territories, Canada. Geological Association of Canada – Mineralogical Association of Canada annual meeting, Ottawa, ON, May 25-27, p. 154.

Normandeau, P.X., McMartin, I., Jackson, V.A., Corriveau, L. and Paquette, J., 2014, Kimberlite Indicator Minerals and Gold Grains in Till from the Great Bear Magmatic Zone and Wopmay Metamorphic Zone, Northwest Territories, Canada. In: D. Irwin and P.X. Normandeau (compilers), 42nd Annual Yellowknife Geoscience Forum Abstracts, Northwest Territories Geoscience Office, Yellowknife, NT, YKGSF Abstracts Volume 2014. p. 97.

Paulen, R. and McMartin, I., 2009, Introduction. In: R.C. Paulen and I. McMartin (eds), Application of till and stream sediment Heavy mineral and Geochemical Methods to Mineral Exploration in Western and Northern Canada; Geological Association of Canada, GAC short course Notes 18.

Porter, T., 2010, Current understanding of iron oxide associated-alkali altered mineralized systems: Part 1- An overview; Part 2 –A review. In: T.M. Porter (ed.), Hydrothermal iron oxide copper-gold and related deposits: A global perspective, v. 3, 5–106.

Potter, E.G., Corriveau, L. and Montreuil, J.-F., 2013a, Iron oxide-copper-gold ±uranium in the Great Bear Magmatic Zone: Nature of uranium in IOCG systems. Geological Survey of Canada, Open File 7254, 1 p.

Potter, E.G., Montreuil, J.-F. and DeToni, A., 2013b, Geology and hydrothermal alteration of the Fab Lake region, Northwest Territories: Geological Survey of Canada, Open File 7339, 27 p.

Prest, V.K., Grant, D.R. and Rampton, V.N., 1968, Glacial Map of Canada: Geological Survey of Canada Map 1253A.

Sappin, A.A., Dupuis, C., Beaudoin, G., McMartin, I. and McClenaghan, M.B., 2014, Optimal ferromagnetic fraction representative of iron oxide compositional variations in till samples along ice-flow paths: Case studies from the Sue-Dianne IOCG and Thompson magmatic Ni-Cu deposits, Canada: Geochemistry: Exploration, Environment, Analysis. v. 14, p. 315–329

Sarala, P., Pulkkinen, E., Ojala, V.J., Peltoniemi-Taivalkoski, A., 2009, Gold exploration using till at Petäjälehto, northern Finland, Geochemistry: Exploration, Environment, Analysis, v. 9, p. 247–255

Smith, D.G., 1994, Glacial Lake McConnell: paleogeography, age, duration, and associated river deltas, Mackenzie River basin, western Canada. Quaternary Science Reviews, v. 13, p. 829–843.

Stanley, C. R., 2009, Geochemical, mineralogical, and lithological dispersal models in glacial till: physical process constraints and application in mineral exploration. In: R.C. Paulen and I. McMartin (eds), Application of till and stream sediment Heavy mineral and Geochemical Methods to Mineral Exploration in Western and Northern Canada, Geological Association of Canada, GAC short course Notes 18, p. 35–47.

Thorleifson, L.H., 2009, Till geochemical and indicator mineral methods in mineral exploration: history and status, 24th International Applied Geochemistry Symposium (IAGS 2009), Fredericton, New Brunswick.

RATIONALE OF CHAPTER 2

Prior to this research, the Quaternary geology of the GBMZ had only been studied at a reconnaissance scale. The only information regarding the surficial geology of this region came from 1:1 million and national scale glacial feature compilations and generalized surficial materials maps established through air photo interpretations. The GSC Open File report constituting the following chapter contains glacial dispersal interpretations based on the collection of surficial geology observations at 270 sites across the GBMZ including striation measurements, and the lithological analysis of the pebble fraction of 101 till samples. These results establish the ground work necessary for the till sample classifications found throughout the thesis. In addition, this report serves as an outlet for the massive quantity of information gathered during the two summers of field work performed in 2009 and 2010 within this publicly funded project. As such, this report outlines the sampling strategies as well as the analytical protocols and methodology employed, and provides a quality control study. This thesis includes a table of contents of the various datasets released in the Open File publication in the first appendix; the actual datasets are available for download from the Natural Resources Canada (http://geoscan.nrcan.gc.ca) as Open File 7307.

CHAPTER 2: Composition of till and bedrock across the Great Bear magmatic zone: Quaternary field database and analytical results from the GEM IOCG-Great Bear Project

2.1. INTRODUCTION

An applied Quaternary activity under the Geological Survey of Canada five year Geo-mapping for Energy and Minerals Program (GEM) was started in the Great Bear magmatic zone (GBMZ) of the Northwest Territories to characterize the heavy mineral and geochemical signature of iron oxide copper gold (IOCG) deposits in derived glacial sediments. The GBMZ (Fig. 2.1) is now considered the most prospective setting for IOCG and affiliated deposits in Canada (Corriveau, 2007; Corriveau et al., 2010). It includes two economic IOCG deposits, the magnetite-group NICO Au-Co-Bi-Cu deposit and the nearby magnetite- to hematite-group Sue Dianne Cu-Ag-(Au) deposit, as well as several other polymetallic occurrences, prospects, and deposits, many of which fall within the larger family of iron oxide alkali-altered (IOAA) alteration and mineralizing systems (Mumin et al., 2007, 2010; Corriveau et al. 2010; Porter, 2010). An orientation study at the NICO deposit originally completed as part of the TGI-3 initiative showed that the composition of iron oxide grains in till compared to that of bedrock, gold grain abundance, size and shape, as well as pathfinder elements (i.e. As-Bi-Co-Au-Cu-Sb-W-Cd) in surface till, had potential to fingerprint the mineralization at NICO (McMartin et al., 2009a, 2009b, 2011a, 2011b). As a follow up to this initial study, a doctoral research project at McGill University was undertaken to develop a drift prospecting method to IOCG exploration across the GBMZ using pathfinder and alteration-related elements in glacial sediments, and the indicator mineral method. This work is part of the joint government-industry-academia IOCG-

Great Bear Multiple Metals GEM project designed to refine IOCG±U exploration criteria and genetic models as well as increase our ability in finding IOCG mineralization in the GBMZ and in other Canadian settings. The purpose of this Open File publication is to release the complete Quaternary datasets collected as part of the GEM IOCG-Great Bear Project in 2009 and 2010. Initial results are discussed in Normandeau et al. (2011a, 2011b, 2011c, 2012). Research is ongoing on the characterization of apatite as an indicator of IOCG mineralization and the use of multivariate elemental signatures in glacial sediments (Lypaczewski et al., 2013; Normandeau et al., in press, in prep a, in prep b.). Iron oxide composition in the ferromagnetic fraction of till from the GBMZ is also under study (McMartin et al., 2011c, in prep.; Dupuis et al., 2012a, 2012b; Sappin et al., 2014).

2.2. REGIONAL SETTING

2.2.1. Location and physiography

The project area lies between latitudes N 63.5° and 66.7° and longitudes W 116.2° and 118.4° and includes the community of Gameti (Fig. 2.2). Drainage is towards the Arctic Ocean via rivers that drain into the MacKenzie River drainage basin. For much of the study area, elevations range from 170 m to 450 m above sea level (a.s.l.) (Fig. 2.2). Supracrustal rocks and the variety of hydrothermal alteration zones they host generally form prominent ridges striking south-southeast/north-northwest. These ridges have relief exceeding 100 m and are dominated by exposed bedrock draped in places by thin, discontinuous till (<2 m thick). Great Bear intrusive rocks form more poorly drained lowlands often covered by thin till. The area lies within the Western Taiga Shield Terrestrial Ecozone of Canada at the northern edge of the boreal

coniferous forest (Wiken, 1986). It is part of the Coppermine river Upland Ecoregion of Canada having a mean annual temperature of approximately -7.5° C (summer mean of 9° C; winter mean of -24.5°C) and a mean annual precipitation of 200-300 mm (http://ecozones.ca/english/region/68.html). It is characterized by extensive discontinuous permafrost for much of the area. The northernmost part of the area (north of Port Radium – Echo Bay) is underlain by continuous permafrost. In the southern part of the GBMZ, brunisolic static cryosols have developed on the glacial sediments. Vegetation in the latter area is dominated by a mixed deciduous and conifer open forest cover. Turbic and Static Cryosols developed on sandy diamicton and glaciofluvial deposits are the dominant soils in the north where lichen-shrub tundra vegetation is more prevalent.

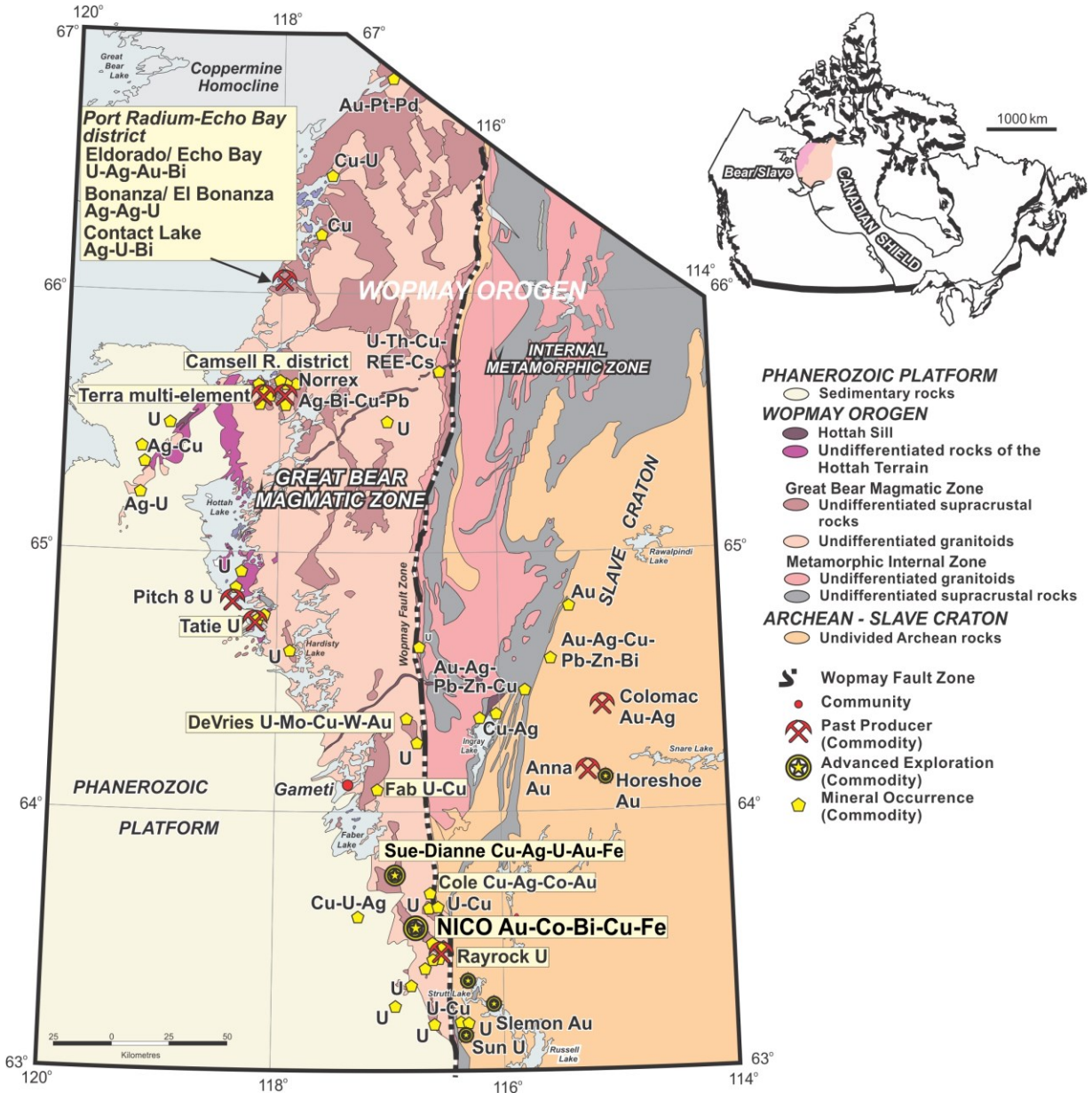

Figure 2.1: The Great Bear magmatic zone bedrock geology, mineral occurrences and past-producing mines (modified from Corriveau et al., 2010). Inset map locates the Wopmay orogen (Bear Province) and adjacent Slave craton at the western edge of the Canadian Shield.

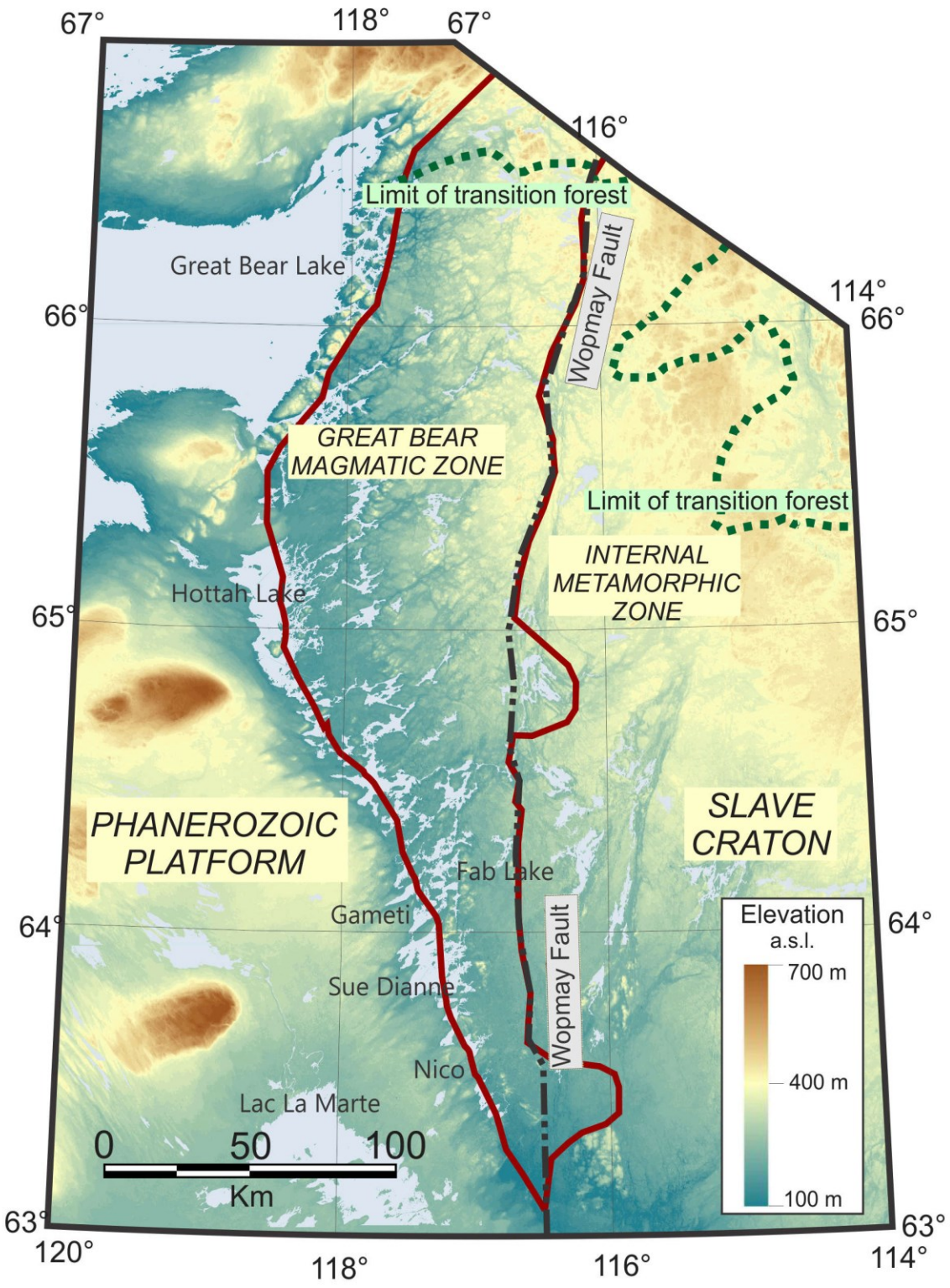

Figure 2.2: DEM generated from ASTGTM (30 m Aster digital elevation model). Study area is outlined in red. Thick green line represents the limit of transition forest, Atlas of Canada, 2003.

2.2.2. Bedrock geology and mineralization

The Great Bear magmatic zone is a Palaeoproterozoic 1.87-1.85 Ga calcalkaline volcano-plutonic arc accreted to the western margin of the Archean Slave craton during the short-lived Calderian Orogeny responsible for the Wopmay Orogen at 1.88 Ga (Bowring and Grotzinger, 1992; Hildebrand et al., 2010). It is exposed between the Archean Slave Craton in the east and the Phanerozoic Cover to the west (Fig. 2.1). Formerly known for its vein-type uranium and silver mines, the Great Bear magmatic zone is currently the most prospective IOCG mineral belt in Canada (Corriveau et al., 2010). IOCG hydrothermal systems of the GBMZ encompass a broad range of hydrothermal alteration types formed at the expense of a variety of volcanic, sedimentary, plutonic and metamorphic rock types. Their evolution history is well constrained within an IOCG alteration sequencing model (i.e. Corriveau et al., 2010).

The magnetite group IOCG NICO deposit is located in the southern part of the GBMZ, about 160 km northwest of Yellowknife. It is an economically significant source of Au-Co-Bi-Cu-Fe with pre-production reserves of 33 Mt at 1.02 g/t Au, 0.11% Co, 0.14% Bi and 0.04 % Cu (Fortune Minerals Limited news release, February 02, 2012). Mineralization at NICO consists of three surface and sub-surface tabular zones, up to 1.5 km in length, that are hosted in hydrothermally-altered and locally brecciated marine siltstone and wacke of the ca. 1.88 Ga Treasure Lake Group below their unconformity with overlying 1.87 Ga felsic volcanic rocks of the Faber Group (Goad et al., 2000a, 2000b; Gandhi et al., 2001; Gandhi and van Breemen, 2005). The magnetite to hematite-group IOCG Sue Dianne deposit is located 25 km north of the NICO deposit. It is an iron-hosted, polymetallic deposit with indicated resources of 8.4 Mt @ 0.8 % Cu and 3.2 g/t Ag (Hennessey and Puritch, 2008). It is hosted in the Faber Lake volcanic sequence and was formed in well-preserved rhyodacite ignimbrite sheets during the development

of a structural-hydrothermal diatreme breccia complex. These volcanic rocks are intruded by various felsic porphyry dykes and sills and quartz veins in the vicinity of the deposit. The Port Radium-Echo Bay district hosts polymetallic mineral showings with typical features of iron oxide-apatite deposits (e.g., K-2 and Mag Hill prospects at depth and the past-producing Echo Bay mine area) and magnetite- to hematite-group IOCG deposits (e.g. K-2, Mile Lake, Breccia Island, Hoy Bay and Birchtree) in the classification scheme of Williams (2010). The Camsell River district is centered on the past-producing Terra (Ag-Ni±Co-Bi) and Norex vein-type deposits (Badham, 1972, 1975; Hildebrand, 1986) hosted among Kiruna-type and IOCG-type alteration and mineralization (Walker and Rajnovich, 2007; Acosta et al., 2014). Other extensive IOAA-type and IOCG hydrothermal systems of the GBMZ include Fab, Damp, Hump, Cole, Ham, JLD, Sunil, Peanut, Esther, DeVries, Dennis and Hailstone. Detailed descriptions of these systems are provided in Montreuil et al. (2016).

2.2.3. Quaternary geology

During the last Wisconsinan glaciation, the GBMZ was affected by Keewatin Sector Ice of the Laurentide Ice Sheet (e.g. Dyke and Prest, 1987) and lay west of a major ice divide in Keewatin (Dyke, 2004). Only reconnaissance-scale Quaternary mapping with limited field work is available for the study area. The Glacial Map of Canada depicts streamlined forms oriented west-southwest to west, striations predominantly indicating a westerly flow and a handful of esker segments (Prest et al., 1968). Areas of maximum glacial lake coverage located within the depression between Great Slave and Great Bear lakes are also shown on this map. The Surficial Materials Map of Canada (Fulton, 1995) and the 1:1 million scale glacial features compilation of Aylsworth and Shilts (1989) show the study area as a drift-poor area (>80% bedrock outcrop)

with small areas of undifferentiated materials, mainly thin till. A series of north-south moraine ridges in the eastern portion of the GBMZ, part of the Forcier Moraine identified by St-Onge et al. (1981) and the Rebesca Moraine, indicate major ice recessional positions within the GBMZ (Fig. 2.3).

Field observations collected as part of the project indicate that the sediment cover over the GBMZ is dominated by discontinuous, thin (<2 m) silty sand till. Above 270 m a.s.l., till is rare but can be found as lee-side deposits of prominent outcrops. Late during deglaciation, Glacial Lake McConnell occupied most of the area below 300 m a.s.l. from ca. 8.5 to 10.5 ka BP (Dyke, 2004) as a result of glacioisostatic depression reversing the regional drainage in the Great Bear, Great Slave and Athabasca lake basins (e.g., Lemmen et al., 1994; Smith, 1994). Evidence for reworking of glacial sediments by glaciolacustrine processes is present in areas covered by the glacial lake as veneers of silt and clay in topographic depressions, specifically around lake basins up to 10 m above actual water levels, or as veneers of winnowed till and littoral sands overlying the glacial deposits. Multiple shoreline levels indicated by paleobeaches of sorted and well-rounded cobbles (8 to 20 cm in size) were found in certain areas. These are characterized by little to no vegetation cover.

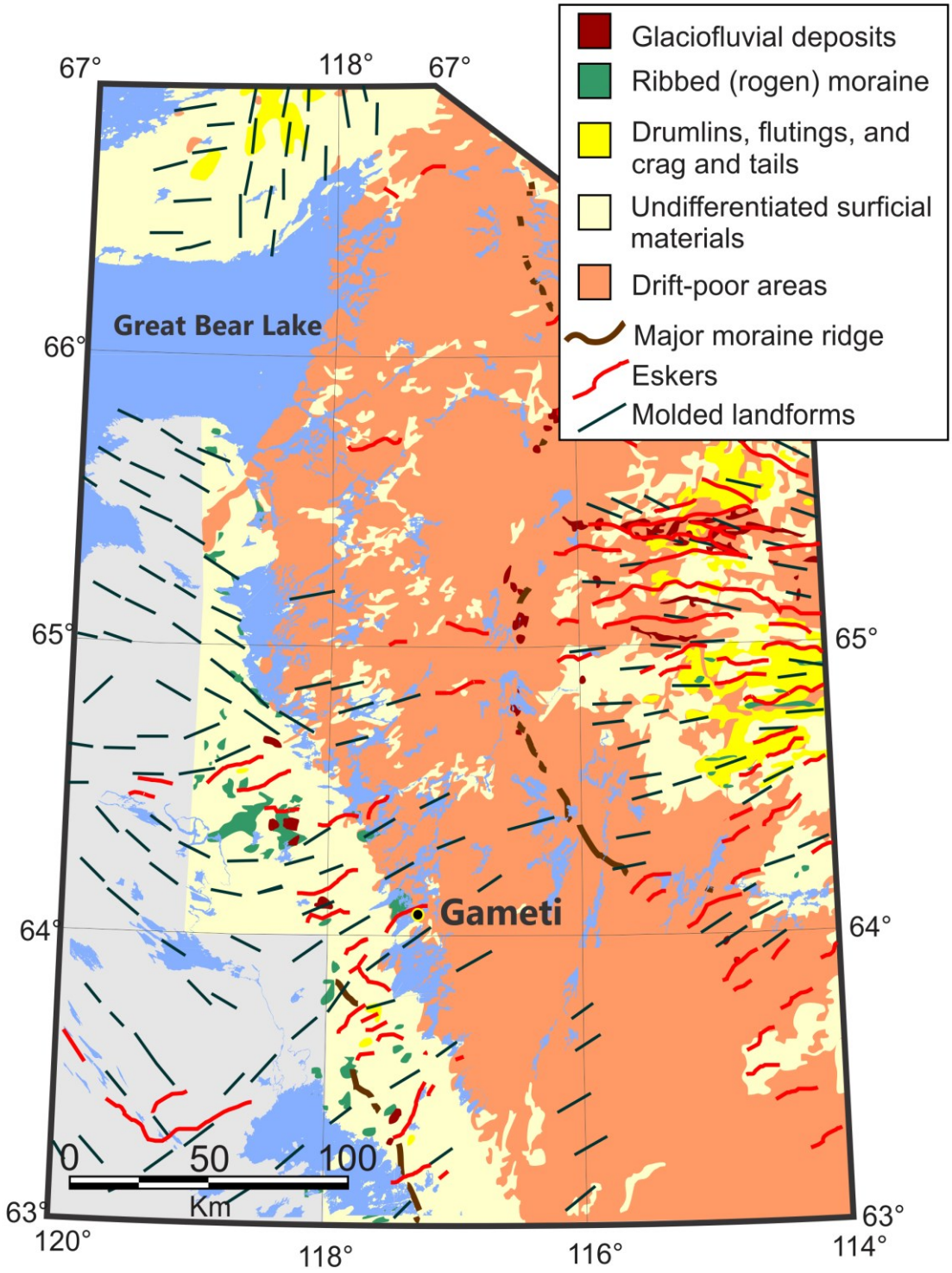

Figure 2.3: Regional Quaternary map for the study area. Location of major eskers and streamlined forms are derived from Fulton (1995); areas of streamlined drift, ribbed moraine, glaciofluvial deposits, drift-poor terrain and undifferentiated materials are from Aylsworth and Shilts (1989). The location of major moraine ridges are also shown. Areas in grey were unmapped by Aylsworth and Shilts (1989).

Ice-flow indicators measured on bedrock near sampling sites or along lake shorelines indicate that the area was influenced primarily by ice flowing to the west-southwest south of Hottah Lake and to the west-northwest north of the lake (see Appendix 1-II for full datasets). Three distinct ice-flow phases were recorded in the study area (Fig. 2.4). Ice-flow indicators associated with Phases 1 and 2 consist of relict features preserved on protected (west) sides of outcrops. Phase 1 is better preserved and more commonly observed in the central part of the GBMZ, and is concordant with megascale ice-flow indicators present west of the GBMZ over the Phanerozoic cover (Prest et al., 1968). It is north bound in the southern GBMZ and shifts towards the northwest in the central GBMZ. Observations of Phase 2 ice-flow indicators, trending towards the south-southwest (210°), are confined south of the 64$_{th}$ parallel. The orientation of Phase 3 indicators range from 225° to 305° across the GBMZ, gradually shifting from west-southwestward in the southern part of the GBMZ to west-northwestward in the north. Phase 3 is the dominant ice-flow direction and is consistent with megascale streamlined forms present within and east of the study area.

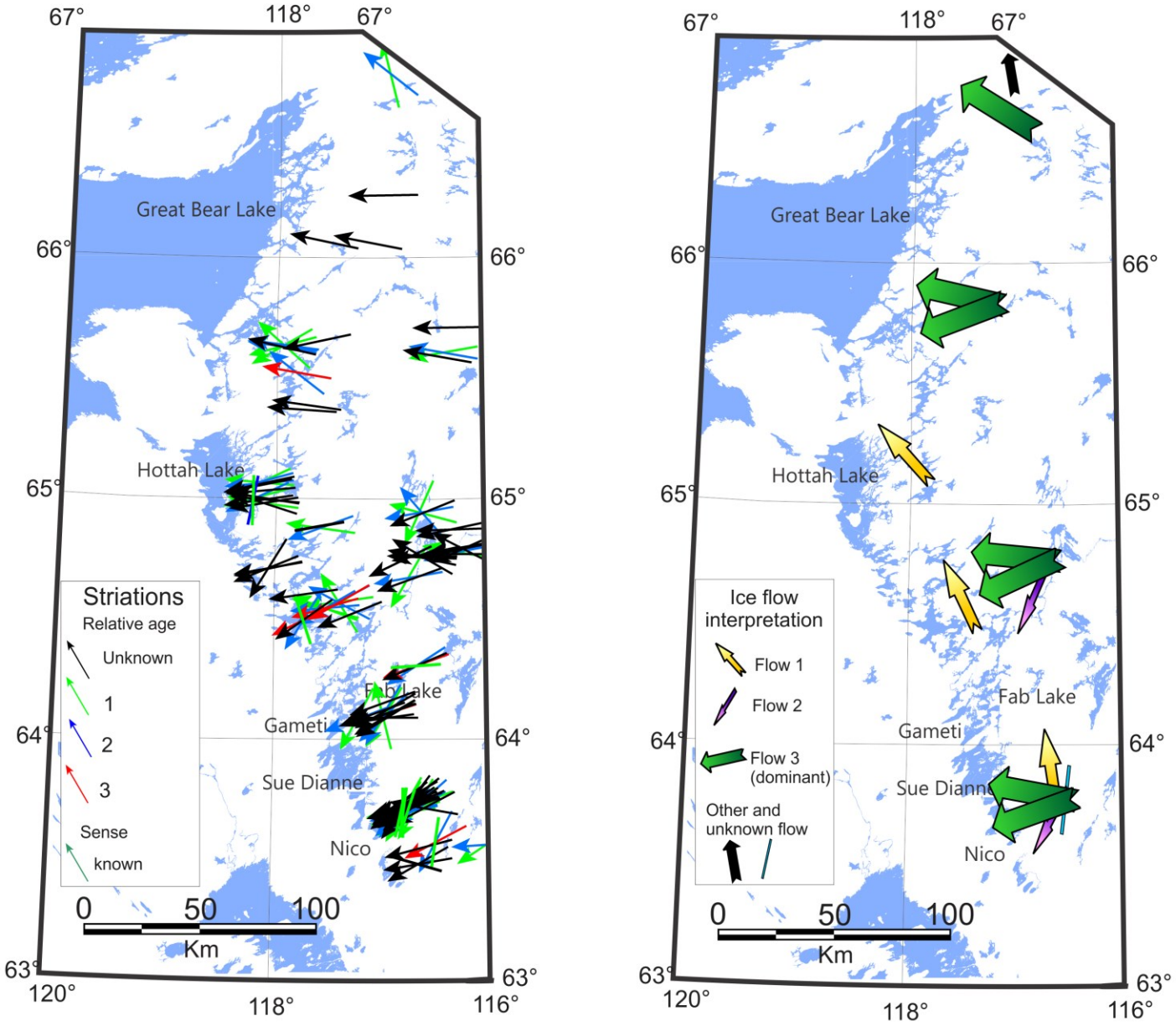

Figure 2.4: Erosional ice-flow indicator map showing trends and relative ages at each site (left map). Interpreted phases of ice-flow are shown on the map to the right.

Pebble lithology data show that till has a local provenance with a short distance of glacial transport (see Appendix 1-XI for full datasets). For example, dispersal of heavily metasomatized clasts is observed less than 800 m down-ice of the Sue Dianne deposit (Normandeau et al., 2011a). Dispersal train orientations are coherent with the dominant flow directions.

2.3. METHODS

2.3.1 Field procedures

Field data collection

Field work was completed from June 10 to July 24 in 2009 and June 29 to July 30 in 2010 by Philippe Normandeau with assistance from Isabelle McMartin and Louise Corriveau, as well as from a number of project participants from the GSC and the NTGS, students and local hires. Field activities in 2009 were concentrated around the Sue Dianne and NICO deposits, and showings at Hardisty, Fab, Isabelle, Grant and Little Crapeau lakes, and in 2010 around showings and hydrothermal systems at Fab, DeVries, Hottah and Grouard lakes, and in the Terra-Mine area (Fig. 2.1). Access was by helicopter, float plane, boat or foot from Fortune Minerals Ltd. NICO camp, Gameti community, Grouard Lake GSC camp and NTGS field camps. Field work involved sampling site description, ice-flow indicator mapping, and till and bedrock sampling. A total of 270 sites were visited and are described in Appendix 1-I.

Ice-flow indicator mapping

The orientation and sense of 165 small-scale erosional ice-flow indicators were measured from 106 sites in 2009 and 2010 (Fig. 2.4). Indicators included striations, grooves, moulded outcrop, crescentic fractures, and roches moutonnées (Fig. 2.5a). The sense of ice flow movement was derived from crescentic fractures and roches moutonnées, where present, or from stoss and lee topography (general shape of outcrop). Relative ages of striated facets were established at 30 sites. Detailed ice-flow indicator measurements and descriptions are provided in Appendix 1-II.

Till sampling

A total of 101 till samples were collected across the entire GBMZ in 2009 and 2010 in the vicinity of known deposits and showings hosted within large IOCG-type alteration systems (Fig. 2.6). Samples were collected proximal to, up-ice, and down-ice from mineralization, hydrothermally-altered host rocks and least-altered bedrock. Detailed sampling was completed around the Sue Dianne deposit and the Fab Lake showing. Samples were collected in the upper C-horizon soils developed on till from hand dug pits, at an average depth of 50 cm, to obtain relatively unaltered material (Fig. 2.5b). At each site, one small sample (~ 3 kg) and one large sample (8-26 kg; mean=16 kg) were collected. Permafrost or sometimes bedrock was encountered at the bottom of holes. Special care was taken to exclude layers of organic material or heavily oxidized clasts. Winnowed and modified tills were avoided as much as possible during sampling. One sample per block of about 25 samples was collected as a field duplicate to test site variability; it was taken randomly within each block (total of two samples per year). Of

the 101 samples, 6 samples were collected <25 km up-ice (east) from the GBMZ, in the Wopmay internal metamorphic zone and in the Slave Province and represent non-altered background sites. Detailed till sample locations and descriptions are provided in Appendix 1-III.

Figure 2.5: Photographs of 1) southwestward (208°) deep striae preserved on the lee side of surface striated by younger west-southwestward flow (249°) near Gameti. Arrows indicate sense of flow (left photo); 2) hand-dug hole in C-horizon soil developed on till with small and large sample bags collected at sample site (right photo).

Bedrock sampling

A total of 71 representative 1 to 3 kg surface bedrock samples were collected in 2009 and 2010 for indicator mineral recovery at most till sample sites, in the vicinity of and at nearby surface deposits and showings (Fig. 2.6). In addition, 24 smaller (118 to 1313 g) leftover crushed bedrock samples collected in 2009 and 2010 by project participants for lithogeochemistry were selected in 2011 for indicator mineral processing and recovery. Detailed bedrock sample locations and descriptions are given in Appendix 1-III.

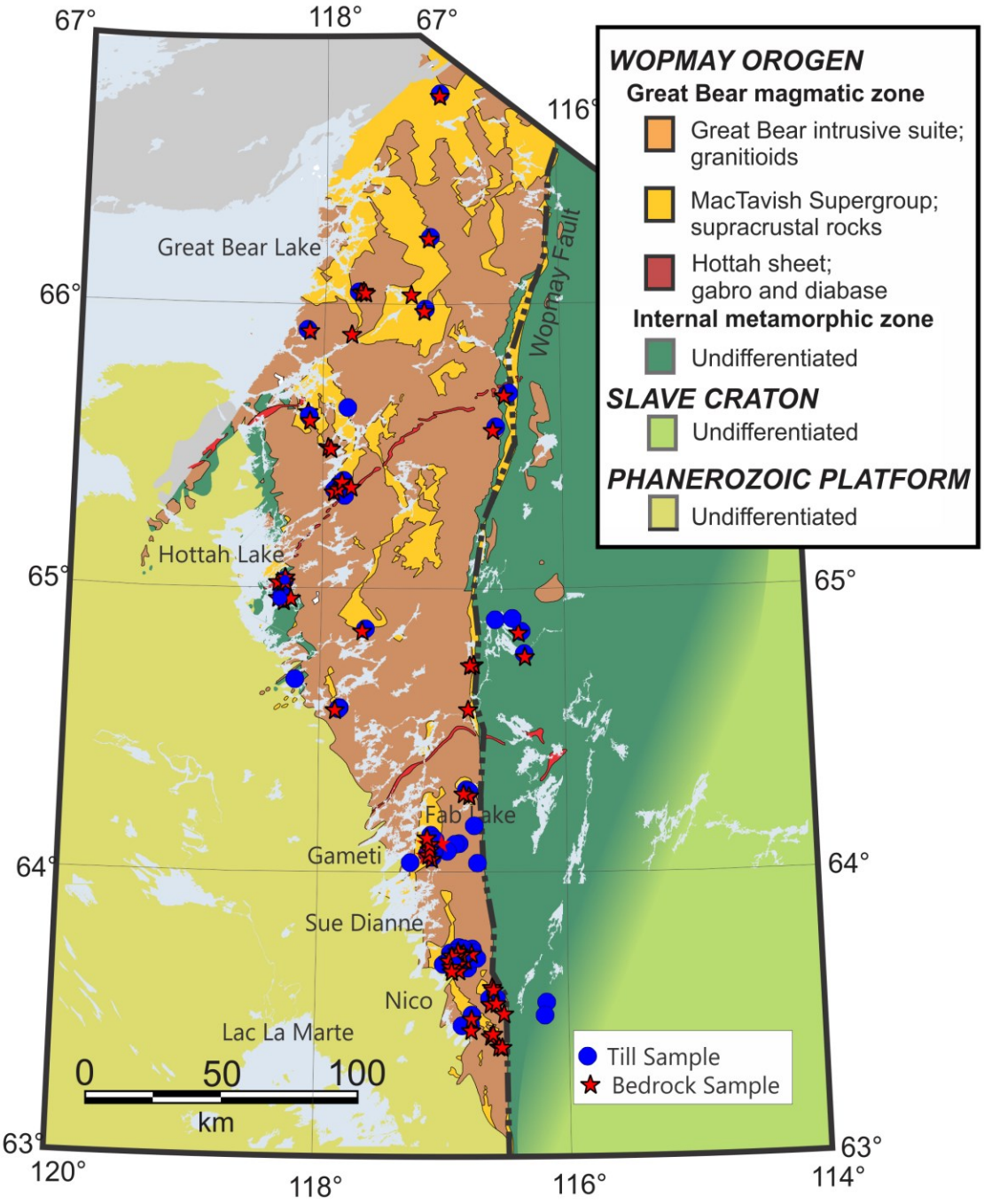

Figure 2.6: Sample location map. Detailed description and location of the samples are given in Appendix 1-III.

2.3.2. Analytical procedures

Sample preparation

Preparation of each of the two till sample sizes was different (Fig. 2.7). The clay-sized fraction (<0.002 mm) of about 300-500 g from the small 3-kg samples was separated by centrifugation and decantation in GSC's Sedimentology Laboratory using the methods described in Girard et al. (2004). A 2- kg split of all 3-kg samples was air-dried and dry-sieved in the Sedimentology Laboratory using a stainless steel 230 mesh screen to obtain the <0.063 mm fraction for geochemical analysis. An order of processing from the potentially least metal-rich to the most metal-rich samples was given and followed in each sample batch (2009 and 2010) to limit cross-contamination. The remainder (<800 g) of the original 3-kg till samples was archived at the GSC, Ottawa. The large till samples were shipped to Overburden Drilling Management Ltd. (ODM) for processing and the production of heavy mineral concentrates. Samples were disaggregated in water and screened at 2 mm to produce a non-ferromagnetic heavy mineral concentrate (NF-HMC) for picking indicator minerals and a ferromagnetic fraction (FM-HMC) for further studies on iron oxides. The oversize material was wet-sieved to collect the 4-9 mm fraction for lithological analysis. Samples collected near mineralized zones with potentially high concentrations of sought indicator minerals were processed at the end of the batch in each year to limit cross-contamination, and results are given in the order they are listed in the ODM raw data file in Appendix 1-XII. Sample preparation and analytical procedures for all till samples are summarized in Figure 2.7.

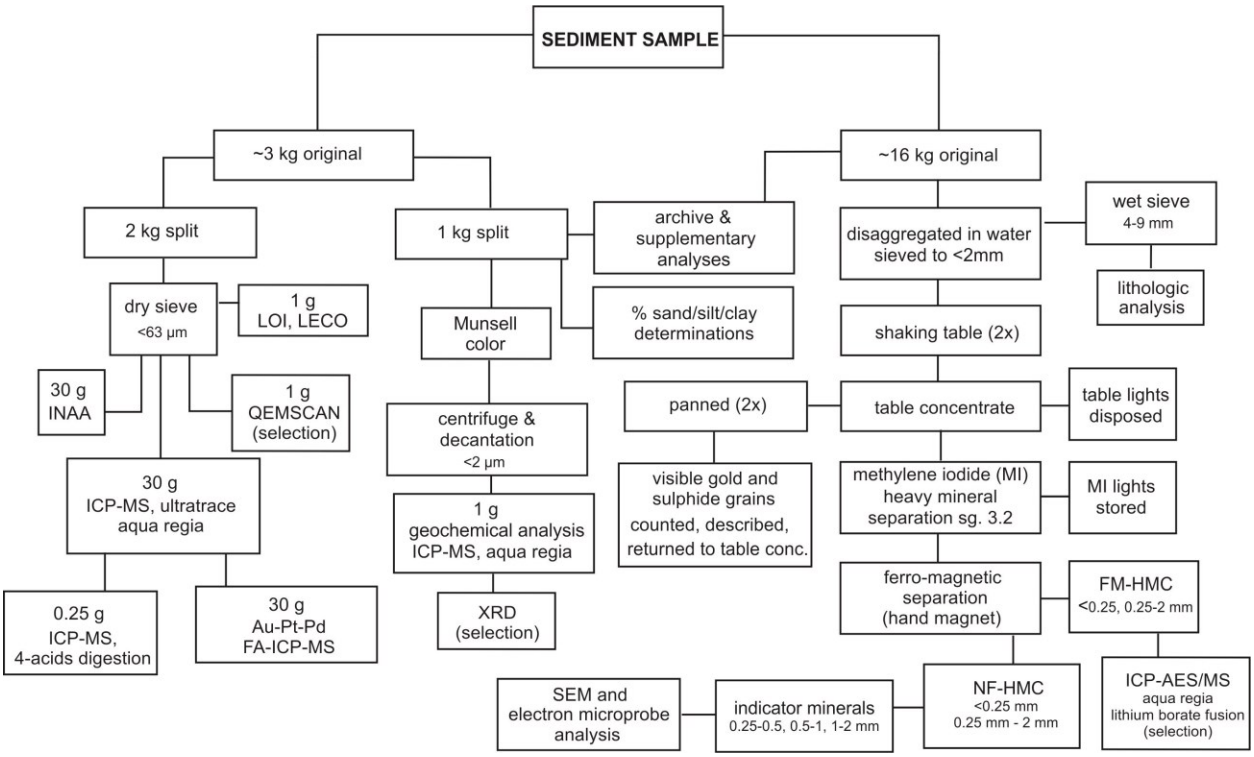

Figure 2.7: Generalized flow sheet showing steps in till sample processing.

Bedrock samples were examined at ODM and described, to determine processing characteristics, optimum sample size and processing sequence (See Appendix 1-III for ODM bedrock logs). All bedrock samples were disaggregated to reduce rock fragment/mineral grain size to <2 mm using an electric pulse disaggregator (EPD Spark-2) (e.g. Cabri et al., 2008). Highly mineralized samples were processed at the end of the batch in each year to limit cross-contamination, and results are given in the order they are listed in the ODM raw data file in Appendix 1-XII. All disaggregated bedrock samples were processed at ODM for heavy mineral separation, panning and indicator mineral picking (Fig. 2.8).

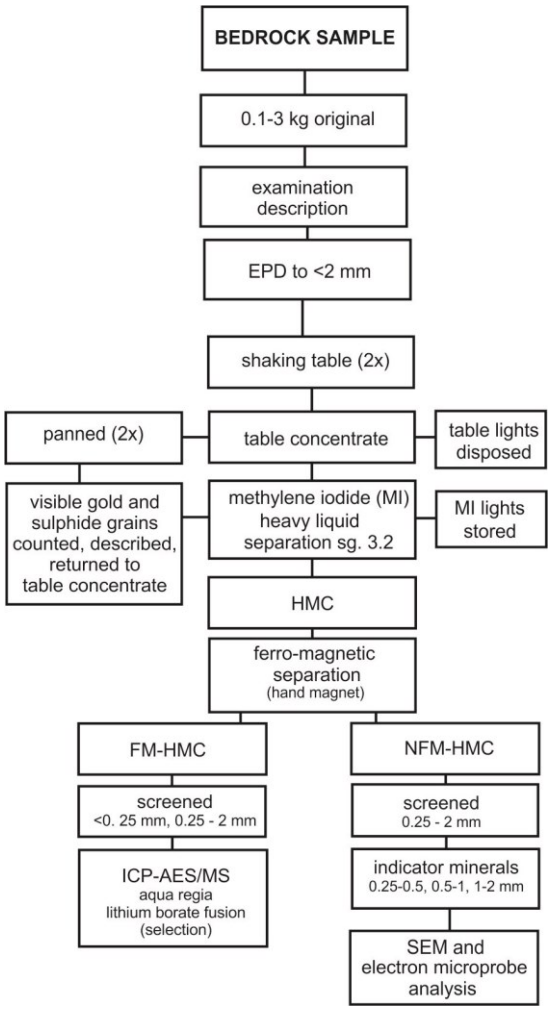

Figure 2.8: Generalized flow sheet showing steps in rock sample processing for indicator mineral analysis.

Till matrix geochemistry

Approximately 1 g of the clay-sized fraction (<0.002 mm) of till was analyzed at Acme Analytical Laboratories Ltd., Vancouver, for a suite of trace and major elements using ICP-MS, following a hot (95°C) modified aqua regia digestion (HCl-HNO_3, 1:1) (Group 1DX: 37 elements). In addition, approximately 30 g of the silt+clay-sized fraction (<0.063 mm) were

analyzed at Acme for a suite of trace, major and rare earth elements using ultratrace ICP-MS, following a hot (95°C) modified aqua regia digestion (HCl-HNO_3, 1:1) (Group 1F06-1F09: 65 elements); a separate 0.25 g split of the same fraction was analyzed at Acme using ultratrace ICP-MS, 4-acid digestion (HNO_3-$HClO_4$-HF dissolved in HCl: Group 1T-MS: 43 + REE elements). Gold, Pt and Pd concentrations were also determined on 30 g of the silt+clay-sized fraction at Acme by Pb-fire assay/ICP-MS (Group 3B-MS). About 30 g of the same fraction was analysed at Activation Laboratories Ltd. for Au and a suite of trace, major and rare earth elements using INAA (Group 1D Enhanced: Au + 34 elements). Detection limits and analytical results are presented by the respective analytical methods in Appendices IV, V, VI and VII.

QA/QC analysis of till geochemical determinations

Reliability (accuracy and precision) of analytical data returned from commercial laboratories was determined by including analytical ('blind') duplicates, analytical standards and silica blanks within the till sample suite submitted to the labs. To monitor potential cross-contamination and to purge the sieves, silicic acid blanks were inserted and sieved during the sieving process and sent for analysis (with <0.063 mm pulps only). Field duplicates were submitted to evaluate sediment heterogeneity within a site. QA/QC procedures generally followed the protocols developed for till samples collected as part of GEM projects and implemented in 2010 (Spirito et al., 2011). Results of the QA/QC statistics and plots discussed below are included in the respective appendices for the geochemical results.

Precision

Analysis of analytical duplicate samples was used to monitor analytical precision of the till matrix geochemical results. In every analytical batch (2009 and 2010), 2 to 4 laboratory duplicates prepared by the GSC Sedimentology Laboratory were inserted randomly. The results for the two laboratory duplicate samples inserted with the 2010 clay fraction pulps indicate that the analytical precision is very good to excellent for all elements analyzed by ICP-MS after a modified aqua regia digestion (RSD≤10%), except for Na (RSD=15%) and Au (RSD=21%). In contrast, the precision in 2009 was only high for Ba, La and Zn (RSD<10%) using the same method; the four laboratory duplicates inserted with the 2009 samples indicate that this method was less precise for all the other elements (RSD=10-20%), and not precise for Al, Au, Ti and W (RSD=21-29%). There may have been a problem with the laboratory instruments in that batch although Acme's internal laboratory duplicate results were reproducible; alternatively, a mistake in the laboratory duplicate preparation and labelling at the GSC may have happened in 2009. Ag, B, Cd, Hg, S, Se, and Te levels are near or below the lower detection limit in the laboratory duplicates for both years, therefore the precision cannot be properly evaluated for these elements. The results for the laboratory duplicate samples inserted with the silt+clay fraction pulps indicate that the analytical precision is good to very good for many elements analyzed by ultratrace ICP-MS after a modified aqua regia digestion (RSD≤10%). This method is somewhat less precise (RSD=10-20%) for Be, Bi (2010), Dy, Er, Gd (2009), Hf (2009), Ho (2010), Lu (2009), Na (2010), Nb (2010), Ni (2010), Sb (2010), Tb (2010), Tm (2009), U (2009) and Yb (2009), and even less so (RSD>20%) for Ag, Au, Mo and Sn (2009). Au (2009: 210%) and Mo (2010: 45%) are specially not reproducible. B, Cd, Ge, Hg, In, Pd, Pt, Re, S, Se, Ta, Te levels are near or

below the lower detection limit in laboratory duplicates, therefore the precision for these elements cannot be properly evaluated with this method. For the 4-acid digestion, laboratory duplicates indicate that the analytical precision is very good to excellent for most elements, but somewhat less precise (RSD=10-20%) for Ag, As (2010), Cd (2010), Nd (2010) and Tb (2009). This method is not very precise for Cd (2009), Mo (2010), Sn (2009) and W (RSD=26-40%). Au, Be, Bi, In, Lu, Re, S, Sb, Se, Tm and W levels in laboratory duplicates are near or below the detection limit with the 4-acid digestion, therefore the precision cannot be properly evaluated for these elements. With the neutron activation method, reproducibility appears to be good for most elements (RSD<10%). This method is somewhat less precise for As (2010), Cr (2009), Eu (2010), Nd (2009), U and Yb (2009) (RSD=15-24%), and even less so for Ba (2009: 32%), Cs (2010: 47%) and Rb (2009: 69%). It is not very reliable (RSD>97%) for Au, Mo (2010) and Ta although levels detected for these elements were close to their lower detection limits in the duplicates. Precision for Ag, Br, Ca, Cs, Hg, Ir, Ni, Sb, Se, Sn, Sr, Tb, W and Zn cannot be properly evaluated since the results of the lab duplicate analysis are below or near the lower detection limit. For the FA-ICP-MS method, Au and Pd levels in laboratory duplicates are too close to the detection limit for the precision to be properly evaluated. Precision of Pt determinations are good in 2009 (RSD=14%) and poor in 2010 (RSD=53%) although Pt levels are rather low in the laboratory duplicates.

Accuracy

Analysis of standards was used to monitor analytical accuracy of the geochemical results. In every analytical batch (2009 and 2010), 2 to 3 control reference samples (CANMET

Standards TDB-1, UM-2, UM-4, Till 4) were inserted. Some of the standards had insufficient material for analysis (noted "not/ss" in results files), and others had no certified, provisional or informational values for comparison. The evaluation of the accuracy is therefore largely qualitative for some methods. The accuracy in the ICP-MS analysis by modified aqua regia digestion is good for most elements as results are generally within 10% of the mean of values from the informational analysis available for TDB-1 and Till 4 (GSC internal database). Values above 10% of the mean are shown in red in the QA/QC report standard sheets. Al, Na and Pb are less accurate using this method. The accuracy in the ultratrace ICP-MS analysis by modified aqua regia digestion is very good (based on TDB-1, Till 4 and UM-4 standard results), except for a few elements such as Ag, Au, Fe, Hg, Pd and Sb which are somewhat (but inconsistently) less accurate between batches. The 4-acid digestion is generally very accurate except for Cd, Mo, Nb, P and W which are less accurate, mainly when comparing results of the TDB-1 standard with the certified values. The accuracy in the INAA analysis is generally good for most elements except for Au, Ba (with TDB-1), Br, Rb and U, elements that are consistently less accurate (above 10% of certified, provisional or mean of informational values). For the FA-ICP-MS method, the accuracy is very good using the results of the UM-4 standard which contains more PGMs. Results of silica blanks are very low for all elements using all methods indicating that contamination was minimal during the various batch analyses. Only Zr was higher reaching as much as 52 ppm in some samples (ICP-MS, modified aqua regia), likely the result of zircon grains in the silica blanks.

Field variability

Results of the two field duplicate samples collected each year within 5-10 m of the original sampling sites indicate that the sediment is fairly homogeneous in composition within a site. Variability between each of the 4 field duplicate sample sites exceeds the variability within sets of duplicate data. Complete geochemical datasets along with sample preparation methods and additional results of the QA/QC analysis are reported in Appendix 1.

Till matrix color and texture

Munsell Color codes were determined on dry samples at the GSC Sedimentology Laboratory using a Munsell Soil Color Chart for the 2009 samples and a spectrophotometer for the 2010 samples. In addition, approximately 200-300 g from the 3-kg till samples was used for textural analysis of the till matrix: the <2 mm (-10 mesh) fraction of the samples was separated by dry-sieving; the classes of sizes greater than 0.063 mm are determined using wet sieving followed by dynamic digital image processing using a CAMSIZER Particle Size Analysis System. The classes of sizes smaller than 0.063 mm are determined using a Lecotrac LT-100 Particle Size Analyser. The results of the matrix colour and textural determinations (>2 mm, 2-0.063 mm, 0.063-0.002 mm, <0.002 mm) are presented in Appendix 1-VIII.

Till matrix organic and inorganic carbon content

Total, inorganic and organic carbon were determined with a LECO CR-412 Carbon Analyzer instrument on the <0.063 mm fraction of all till samples (1350°C). A small portion of the same fraction of all samples that had total C > 0.1% was analyzed for loss-on-ignition (LOI). LOI helps to give a measure of the degree to which the sample geochemistry has been modified by post-depositional weathering and/or organic matter incorporation. Results for LOI are expressed as % weight loss of the dry weight after heating a small portion at 500°C for one hour (Girard et al., 2004). The results of the LOI and LECO analysis are given in Appendix 1-IX. Laboratory duplicates and in-house standards were also inserted for the till matrix carbon analysis at GSC's Sedimentology Laboratory. Results for these and for laboratory repeats are part of Appendix 1-IX.

Till matrix mineralogy

To evaluate the potential for finer-grained and/or lighter-weight indicator minerals in till, and to gain a better understanding of the fine till fraction geochemistry, an experiment using Quantitative Evaluation of Materials by Scanning Electron Microscopy (QEMSCAN™) of ten selected till samples was completed in collaboration with SGS Mineral Services in Lakefield, Ontario (de Souza et al., 2011). Samples were collected from the Sue Dianne deposit area except for one which was collected near Hottah Lake. Approximately 1 g of the silt-and-clay sized fraction (<0.063 mm) of till was mounted on 30 mm polished section and coated with a thin layer of carbon to ensure conductivity while in the SEM chamber. QEMSCAN utilizes both the back-

scattered electron (BSE) signal intensity as well as an Energy Dispersive X-ray Signal (EDS) at each measurement point. EDS signals are used to assign mineral identities to each measurement point by comparing the EDS spectrum against a mineral species identification program (SIP) or database. A bulk modal analysis (BMA) giving mineral identities and proportions (% mineral mass) and mean grain size by frequency (μm) for each mineral identified, and the grain size distribution (% mass of grain size) in each sample are given in Appendix 1-Xa. The mineralogy of the clay-sized fraction (<0.002 mm) of 14 selected till samples was determined by X-ray powder diffraction analyses at the Geological Survey of Canada, using a Bruker D8 Advance Powder Diffractometer equipped with a Lynx-Eye detector, with Co Kα radiation set at 40 kV and 40 mA. The samples were also x-rayed following saturation with ethylene glycol (24 hours in desiccator) and heat treatment (2 hours at 550 °C). The selection included samples collected down-ice from the Sue Dianne deposit, and various showings across the GBMZ. Initial identification of minerals was made using EVA software with comparison to reference mineral patterns using Powder Diffraction Files (PDF) of the International Centre for Diffraction Data (ICDD) and other available databases. Quantitative analysis was carried out using TOPAS, a PC-based program that performs Rietveld refinement (RR) of XRD spectra. Detailed methods and results of the XRD analysis are presented in Appendix 1-Xb.

Till clast lithology

The >2.0 mm material from the large bulk till samples was wet-sieved to separate the 4-9 mm fraction for lithological analysis. Pebbles from all till samples were visually examined using a binocular microscope (minimum of 170 clasts counted per sample) at McGill University.

Pebbles were grouped into the following lithological categories: intrusive, metamorphic (2009 samples only), non-metamorphosed sedimentary, supracrustal, magnetic, altered (visible metasomatic alteration), quartz, gabbro, schist, concretion, heavily weathered, hematite breccia, or others undifferentiated (2010 samples only). Results were calculated by % clasts counted of the total sample and are presented in Appendix 1-XI.

Till and bedrock heavy mineral processing

The large bulk till and the bedrock samples were processed at Overburden Drilling Management Ltd. (ODM), Ottawa, for recovery of the heavy mineral fraction and indicator mineral picking, including gold grains. The <2 mm (matrix) fraction of the till samples were processed using a double-run across the shaking table. The table preconcentrate was then panned to recover any gold, sulphide and platinum group minerals. After tabling and panning, the preconcentrate was further refined using heavy liquid (S.G. 3.0 and 3.2) and ferromagnetic (FM) separations. The non-ferromagnetic heavy mineral concentrates (NF-HMC) were screened at 0.25 mm. The 0.25-2 mm fraction NF-HMC (S.G. >3.2) was used for indicator mineral picking. The ferromagnetic fraction (FM-HMC) was also screened at 0.25 mm and the 0.25-2 mm fraction FM-HMC was used for the study of iron oxides (i.e. Dupuis et al., 2012a, 2012b). Bedrock samples were processed to recover heavy minerals, using a method similar to that used for the till samples. The disaggregated bedrock samples were pre-concentrated with respect to density using a shaking table. Samples were tabled twice to increase gold recovery. Visible gold, sulphide and platinum group grains recovered from this table concentrate and/or by subsequent panning were counted and described, then returned to the table concentrate after examination.

Heavy liquid separation using methylene iodide (S.G. 3.0 and 3.2) was used to produce a final heavy mineral concentrate (HMC) from the table concentrate. After a ferromagnetic separation, the NFM-HMC was sieved to obtain the sand fraction (0.25-2 mm) for picking. The 0.18 mm-0.25 mm fraction was also prepared for future reference. The ferromagnetic fraction (FM-HMC) was sieved (0.25-2 mm) for further examination. The total number of gold grains recovered, the weights of table feed, table preconcentrates, NFM- and FM- HMCs for both bedrock and till samples are presented in Appendix 1-XII. The FM-HMC fractions of selected bedrock and till samples collected in 2007 (McMartin et al., 2011b) and in 2009 and 2010 (this report) were analyzed for geochemistry to evaluate the metal contents and potential pathfinder elements in this fraction. The <0.25 mm and pulverized 0.25-2 mm FM-HMC fractions were analyzed at Acme Analytical Laboratories Ltd. for a selected suite of base metals using ICP-MS after a hot modified aqua regia digestion (Group 1DX: 14 elements), and for whole rock analysis by ICP-ES and total trace elements by ICP-MS following a lithium metaborate/tetraborate fusion and dilute nitric digestion (Group 4A-4B: 46 elements). Results for the geochemical analysis of the <0.25 mm and pulverized 0.25-2 mm FM-HMC of all samples, together with laboratory duplicate results, are presented in Appendix 1-XIIIa and 1-XIIIb. Interpretation of these results is currently under study (McMartin et al., in prep.)

Indicator mineral picking

Prior to indicator mineral examination and selection, the 0.25-2 mm NFM-HMCs (S.G.>3.2) recovered from till and bedrock samples were sieved to 0.25-0.5 mm, 0.5-1 mm and 1-2 mm. The 0.25-0.5 mm fraction of bedrock and till samples was further refined using a

Carpco® electromagnetic separator to produce fractions with different paramagnetic characteristics to help reduce the volume of concentrate to be visually examined (Averill and Huneault, 2006). All fractions were examined under a stereoscopic microscope at ODM to determine the abundance of potential IOCG and metamorphosed or magmatic massive sulphide (MMSIM®) indicator minerals. Bedrock samples were examined first. Checks were performed on selected grains using SEM-energy dispersive x-ray spectrometer (EDS) to confirm mineral identity. Selected grains considered having possible IOCG affinities (mainly sulphides, silicates, some oxides) were picked and mounted for further study. Because of their abundance in some bedrock samples, no more than 20 to 50 representative grains of the same mineral species were selected per sample for further study (mainly allanite, andradite, apatite, actinolite, hematite, chalcopyrite, polymineralic grains). Selected iron oxide grains from the ferro-magnetic fraction of selected bedrock and till samples were picked, mounted and microprobed at Laval University. These results are reported elsewhere (Dupuis et al., 2012a, 2012b; Sappin et al., 2014). Appendix 1-XII includes all raw grain counts from visual identification of possible IOCG indicator minerals for the 0.25-2 mm NFM-HMCs (S.G.>3.2).

QA/QC analysis of heavy mineral processing and indicator mineral picking

Following the new QA/QC protocols developed for till samples as part of GEM Projects (Spirito et al., 2011), 'blank' samples consisting of weathered Silurian-Devonian granite (grus) (Plouffe et al., 2013) were inserted at the beginning and through the till sample batch in 2010 to monitor potential cross-contamination introduced during heavy mineral separation. 'Blind' duplicates (sub-split of field duplicates) were also used to evaluate the precision of the mineral

separation and identification method. One to two gold grains were found in 5 of the 6 blanks during panning and gold grain counts in 2010, in agreement with known values of gold grains in this blank material (Plouffe et al., 2013). Expected hornblende/titanite-zircon assemblages with no PGMs nor specific potential indicator minerals were found in the blanks. Results for the blind and the field duplicates indicate that gold grain counts are reproducible, and that the sediment collected 5-10 m apart is fairly homogeneous. The results of potential indicator mineral picking in the blind and field duplicate samples indicate minor sediment heterogeneity at the sample site, and a good reproducibility of the results. Although the mineral assemblages are similar, single grains of andradite, Mn-epidote, sapphirine, red rutile, loellingite, chalcopyrite and gahnite were sometimes found in the field duplicate, in the blind duplicate or in the original. All panning results and weights for the blanks, blind and field duplicate samples are reported in Appendix 1-XII. With the 2009 bedrock samples, crushed vein quartz (i.e., mineral blank) was processed at the beginning, and through the sample batches to monitor contamination from laboratory equipment and carryover. Unfortunately, four heavily mineralized samples from Voisey's Bay (Ni-Cu) and Nevada (Au) were introduced in one of the 2009 bedrock sample batches on the EPD at ODM (batch # 4761). This resulted in significant carryover contamination in the quartz blanks (QC-1 to QC-4) and in some of the samples. This contamination included >0.25 mm chromite grains from Voisey's Bay and ruby corundum from Nevada. In addition, minor carryover contamination occurred in the same batch in heavy silicate minerals (almandine, hornblende and pyroxene) from the large number of till samples processed in this laboratory. In the end however, none of these grains were picked as potential indicator minerals. The suspected chromite grains resulting from contamination were removed in a separate bedrock sample results sheet for that batch in Appendix 1-XII ("MMSIM Chromite Removed") and highlighted in the

final results sheet ("Bedrock – MMSIM"). The micropanning results were even more susceptible to inter-sample EPD contamination than the >0.25 mm sand-sized fraction picked for indicator minerals. The QC quartz blanks contained fine grained chalcopyrite and pyrite as a result of carryover contamination from other bedrock samples and one sample contained a single grain of cinnabar probably as a result of carryover from the Nevada sample. The second batch of bedrock samples submitted to ODM in 2009 (#4937) showed no contamination related to EDP processing in the fine fraction. One to three silt-sized pyrite grains were found in each blank of the second batch but these could have been introduced during panning and are considered insignificant. To better monitor the carryover contamination experienced in 2009 with the EPD, quartz blanks were inserted between each single bedrock sample collected in 2010, and between the leftover crushed bedrock samples collected in 2009 and 2010. No mineralized samples from outside sources were introduced between these sample batches. Carryover from inter-sample contamination during sample processing still occurred in the very fine fraction of bedrock samples as shown in the micropanning results of the quartz blanks (mainly pyrite and arsenopyrite). More importantly, a significant fine grained galena contamination occurred from the EPD carryover of a previously processed galena ore sample in the batch of coarsely crushed bedrock samples (leftover lithogeochemistry samples). All galena counts within this batch (quartz blanks and regular samples) should therefore be disregarded (batch #5730). It is important to note that the coarser >0.25 mm fraction was not affected by this carryover. A single grain of chalcopyrite was found in a quartz blank processed in 2010. All picking results for the blank samples processed with the bedrock samples are reported in Appendix 1-XII.

Binocular and SEM photographs of selected grains

Picked grain texture from selected indicator mineral species from till and disaggregated bedrock samples were studied under binocular and scanning electron microscope (SEM). Backscattered electron images (BSE) and energy dispersive X-ray spectroscopy analysis (EDX) were taken using the Hitachi S-3200N variable pressure SEM at the GSC Microbeam Laboratory for the 2009 samples and using the Hitachi S-3000N variable pressure SEM at the Facility for Electron Microscopy Research (FER) at McGill University for the 2010 samples. The beam was set at 25 kV in variable pressure mode (set at 20 Pa). Single-point, non-quantitative compositional data were obtained using EDX with the INCA analysis software. Readings were averaged over a live time period of 50 seconds and taken at multiple locations as to provide complete identification of polymineralic grains. Representative binocular and BSE data as well as an observation summary document are provided in Appendix 1-XIV.

Electron microprobe analysis

Selected visually identified indicator minerals and some background grains (total of 433 grains from 2009 and 496 grains from 2010) were mounted on 25-mm epoxy-impregnated stubs at SGS Lakefield Research Laboratory. In the 2010 batches, only the Cr-pyrope, Cr-diopside, olivine, chromite, hematite, apatite and malachite grains were selected for microprobe analysis. The rest of the grains were mounted but are archived for further studies. The grains were analyzed to confirm their identity and quantify their chemical composition. Analyses were conducted at the GSC Microbeam Laboratory using a CAMECA SX50 electron microprobe

(EMP) equipped with four wavelength-dispersive spectrometers. Operating conditions were 20 kV accelerating voltage, and 10 nA beam current using a focused spot. Count times on peak were 10 seconds, with 5 seconds off-peak. The raw data were processed with the ZAF matrix correction. Standards comprise a range of natural and synthetic pure metals, simple oxides and simple compounds. The analysed grains were classified (or re-classified when necessary) by K. Venance (GSC) and I. Kjarsgaard (2009 results only) on the basis of their chemical composition. Theoretical chemical compositions of mineral end-members (LeMaitre, 1982) were used to calculate cut-off values (at approximately 50:50 mol %) for members of binary solid solution series. Some of grain mounts were not suitable for work on a per-grain basis. EMP work on grain mounts at the GSC is done in automated mode: the coordinates of clean spots away from cracks and impurities are loaded off-line. Some of the grains were heterogeneous (comprised of multiple phases) or the phase of interest comprised only a minor component of the grain. Therefore the totals are sometimes too low or too high and re-classification was not possible or approximate. The final mineral classification (2009 sample only) and chemistry results for the 0.25-2 mm NFM-HMC are provided in Appendix 1-XV.

2.4. SUMMARY

This Open File report releases the Quaternary field database and analytical results from the 2009 and 2010 field seasons of the GEM IOCG-Great Bear Project. The datasets are presented in a format easily importable in a geographic information system (GIS). Quaternary field observations were recorded at 270 field stations; 154 of these included either surface expression and/or material modifier description and/or ice-flow indicator measurements (n=165). They depict a discontinuous till cover, sparingly affected by glaciolacustrine reworking below 300 m a.s.l., and a dominant ice-flow direction gradually shifting from west-southwestward in the southern part of the GBMZ to west-northwestward in the north.

Samples collected include 101 till samples from C-horizon soils, primarily for geochemical and indicator mineral analysis, taken in relation to known mineralization, alteration zones and least altered bedrock, as well as 95 surface bedrock samples for indicator mineral recovery purposes. Analytical results include till matrix texture and color, matrix carbon, pebble analysis, as well as extensive till matrix geochemistry performed on the <0.002 mm and/or <0.063 mm fraction using ICP-MS modified aqua regia digestion, ICP-MS 4-acid digestion, INAA, and fire assay/ICP-MS. Till matrix geochemistry QA/QC analysis was determined using field and analytical duplicates as well as control reference samples (silica blanks and analytical standards). Analytical precision analysis indicates results to be reproducible with precision generally classified as good to very good for most elements in results from both years. Limitations include many elements with values too close or below detection limits in the analytical duplicates. Problematic elements recurring over multiple analytical techniques include: Ag, Au, B, Cd, Hg, In, S, Sb, Se, Re and W. Measurement accuracy analysis shows that results are generally within 10% of the mean standard value available for most elements. Limitations

include insufficient material for analysis of some standards. Blank sample analyses show minimal contamination between samples. Field duplicate geochemical analyses suggest the sediment is fairly homogeneous within a site although insufficient data is available to do a full analysis of variance.

Mineralogy of the till <0.063 mm fraction of 10 selected samples was determined using QEMSCAN™, giving mineral species identity and proportion under bulk modal analysis, mean grain size frequency per species and grain size distribution per sample. Mineralogy of the till <0.002 mm fraction of 14 selected samples was determined using XRD, giving mineral species identity and proportions.

Heavy mineral processing, gold grain counts and indicator mineral picking of potential IOCG affinities were completed on all till and disaggregated bedrock samples. Contamination, grain carryover, reproducibility and site heterogeneity were evaluated using blanks, as well as laboratory and field duplicates. Results indicate minor sediment heterogeneity at the till sample site and a good reproducibility. However, low abundance of some mineral species in till samples may allow for single grain occurrence in only one of both duplicate samples. In 2009, carryover contamination during EPD processing in a specific quartz blank, and to a lesser extent in the following sample, was caused by four heavily mineralized samples from Voisey's Bay (Ni-Cu) and Nevada (Au) introduced in one of the bedrock sample batches. Results suspected to have been affected were removed in a separate sheet.

Textural analysis of representative grains from selected species was performed using binocular, SEM-EDX and SEM-backscatter. Picked grain composition of 433 grains from 2009 and selected species from 496 grains from 2010 was determined using electron microprobe through single point per grain analysis.

2.5. ACKNOWLEDGMENTS

This work was conducted as part of IOCG-Great Bear Project within the Geo-mapping for Energy and Minerals (GEM) Program under the leadership of Louise Corriveau at the Geological Survey of Canada. We are grateful to the following: the IOCG-Great Bear Project participants for assistance in the field; Shauna Madore and her team (GSC) for the management and analysis of till samples at the Sedimentology Laboratory; Alain Grenier and Jeanne Percival (GSC) for the XRD analysis; Katherine Venance and Pat Hunt (GSC) for electron microprobe and SEM analysis; Overburden Drilling Management (Stu Averill and Rémy Huneault) for the customized heavy mineral processing and indicator mineral picking; Fortune Minerals Ltd. for logistical support at NICO in 2009; NTGS for field support at Hardisty and Grant Lake camps; the Community Government of Gamètì for their active participation and collaboration; PCSP (project 00410) for helicopter support; and Hugh de Souza and his team at SGS Mineral Services for the QEMSCAN analysis. Ariane Castagner and Melissa Weber (Ottawa U.) helped to prepare the appendices. Peter Bobrowsky (GSC) is thanked for providing a careful review.

2.6. REFERENCES

Acosta-Góngora, P., Gleeson, S., Samson, I., Ootes, L. and Corriveau, L., 2014, Trace element geochemistry of magnetite and its relationship to Cu-Bi-Co-Au-Ag-UW mineralization in the Great Bear magmatic zone, NWT, Canada: Economic Geology, v. 109, p. 1901–1928.

Averill, S.A. and Huneault, R., 2006, Overburden Drilling Management Ltd: Exploring heavy minerals: EXPLORE, Newsletter of the Association of Applied Geochemists, v. 133, p. 1–5.

Aylsworth, J. M. and Shilts, W. W., 1989, Glacial features around the Keewatin Ice divide: Districts of MacKenzie and Keewatin: Geological Survey of Canada, Paper 88–24, 21 p.

Badham, J.P.N., 1972, The Camsell River – Conjuror Bay Area, Great Bear Lake, N.W.T: Canadian Journal of Earth Science, v. 9, p. 1460–1468.

Badham, J.P.N., 1975, Mineralogy, paragenesis and origin of the Ag-Ni, Co arsenide mineralization, Camsell River, N.W.T.; Canada: Miner Deposita, v. 10, p. 153–175.

Bowring, S.A. and Grotzinger, J.P., 1992, Implications of new chronostratigraphy for tectonic evolution of Wopmay orogen, northwest Canadian Shield; American Journal of Science, v. 292, p. 1–20.

Cabri, L.J., Rudashevsky, N.S., Rudashevsky, V.N. and Oerthür, T., 2008, Electric-Pulse Disaggregation (EPD), Hydroseparation (HS) and their use in combination for mineral processing and advanced characterization of ores; Canadian Mineral Processors 40th Annual Meeting, Proceedings, Paper 14, p. 211–235.

Corriveau, L., 2007, Iron oxide-copper-gold deposits: a Canadian perspective; *in* Goodfellow W.D. (ed) Mineral deposits of Canada: a synthesis of major deposit-types, district metallogeny, the evolution of geological provinces and exploration methods: Geological Association of Canada, Mineral Deposit Division, Special Publication 5, p. 307–328.

Corriveau, L., Williams, P.J. and Mumin, H., 2010, Alteration vectors to IOCG mineralization – from unchartered terranes to deposits; *in* Corriveau, L. and Mumin, H. (eds) Exploring for Iron Oxide Copper-Gold Deposits: Canada and Global Analogues: Geological Association of Canada, Short Course Volume 20, p. 89–110.

de Souza, H., Gibbs, K., Gunning, C. and Prout, S., 2011, Use of automated mineralogy for identification of multicommodity indicator minerals; 25th International Applied Geochemistry Symposium 2011, Program and Abstracts, p. 57–58, Rovaniemi, Finland.

Dupuis, C., Sappin, A.-A., Pozza, M., Beaudoin, G., McMartin, I. and McClenaghan, M.B., 2012a, Iron oxide compositions in till samples from the Sue-Dianne IOCG deposit, NWT and the Pipe Ni-Cu deposit, Manitoba: Geological Survey of Canada, Open File 7310, 8 p.

Dupuis, C., Sappin, A.A., Pozza, M., Beaudoin, G., McMartin, I. and McClenaghan, M.B., 2012b, Iron oxide compositional variations in tills along ice-flow paths: Case studies from Sue-Dianne IOCG, and Thompson Ni-Cu deposits, Canada; 22nd V.M. Goldschmidt Conference, Abstract_CD, p. 483, Montréal, Canada.

Dyke, A.S., 2004, An outline of North American deglaciation with emphasis on central and northern Canada; *in* Ehlers, J. and Gibbard, P.L. (eds) Quaternary glaciations - extent and chronology, part II, North America: Developments in Quaternary Science, v. 2, p. 373–424.

Dyke, A. S. and Prest, V. K., 1987, Late Wisconsinan and Holocene history of the Laurentide Ice Sheet: Géographie physique et Quaternaire, v. 41, p. 237–263.

Fulton, R.J. (compiler), 1995, Surficial materials of Canada: Geological Survey of Canada, Map 1880A, Scale 1: 5 000 000.

Gandhi, S.S. and van Breemen, O., 2005, SHRIMP U-Pb geochronology of detrital zircons from the Treasure Lake Group – new evidence for Paleoproterozoic collisional tectonics in the southern Hottah terrane, northwestern Canadian Shield: Canadian Journal of Earth Sciences, v. 42, p. 833–845.

Gandhi, S.S., Mortensen, J.K., Prasad, N. and van Breemen, O., 2001, Magmatic evolution of the southern Great Bear continental arc, northwestern Canadian Shield: Geochronological constraints: Canadian Journal of Earth Sciences, v. 38, p. 767–785.

Garrett, R.G., 1969, The determination of sampling and analytical errors in exploration geochemistry: Economic Geology, v. 64, p. 568–569.

Garrett, R.G., 1983, Sampling Methodology; in Howarth R.J. (ed) Statistics and Data Analysis in Geochemical Prospecting; Handbook of Exploration Geochemistry, Vol. 2 (G.J.S. Govett, series ed); Elsevier, Amsterdam, Chapter 4, p. 83–110.

Girard, I, Klassen, R.A. and Laframboise, R.R., 2004, Sedimentology laboratory manual, Terrain Sciences Division: Geological Survey of Canada, Open File 4823, 134 p,

Goad, R.E., Mumin, A.H., Duke, N.A., Neale, K.L., Mulligan, D.L. and Camier, W.J., 2000a, The NICO and Sue- Dianne Proterozoic, iron oxide-hosted, polymetallic deposits, Northwest Territories: Application of the Olympic Dam model in exploration: Exploration and Mining Geology, v. 9, p. 123–140.

Goad, R.E., Mumin, A.H., Duke, N.A., Neale, K.L. and Mulligan, D.L., 2000b, Geology of the Proterozoic iron oxide-hosted NICO cobalt-gold-bismuth and Sue-Dianne copper-silver deposits, Southern Great Bear Magmatic Zone, Northwest Territories, Canada; *in* Porter, T.M. (ed) Hydrothermal Iron Oxide Copper-Gold and Related deposits: A Global Perspective; Volume 1, PGC Publishing, Adelaide, p. 249–267.

Hennessey B.T. and Puritch, E., 2008, A technical report on a mineral resource estimate for the Sue-Dianne deposit, Mazenod Lake area, Northwest Territories, Canada; Fortune Minerals Limited, Tech Rep, 125 p.

Hildebrand, R.S., 1986, Kiruna-type deposits: their origin and relationship to intermediate subvolcanic plutons in the Great Bear Magmatic Zone, northwest Canada: Economic Geology, v. 81, p. 640–659.

Hildebrand, R.S., Hoffman, P.F. and Bowring, S.A., 2010, The Calderian Orogeny in Wopmay Orogen (1.9 Ga), northwestern Canadian Shield: Geological Society of America Bulletin, v. 122, p. 794–814.

LeMaitre, R.W., 1982, Numerical Petrology - Statistical Interpretation of Geo-chemical data; Developments in Petrology, vol. 8, Elsevier Science Publishing, Amsterdam, New York, 281 p.

Lemmen, D.S., Duk-Rodkin, A. and Bednarski, J.M., 1994, Late glacial drainage systems along the northwestern margin of the Laurentide Ice Sheet: Quaternary Science Reviews, v. 13, p. 805–828.

Lypaczewski, P., Normandeau, P. X., Paquette, J. and McMartin, I., 2013, Petrographic and cathodoluminescence characterization of apatite from the Sue Dianne and Brooke Zone IOCG mineralization systems, Great Bear magmatic zone, Northwest Territories: Geological Survey of Canada, Open File 7319, 18 p.

McMartin, I., Corriveau, L. and Beaudoin, G., 2009a, Heavy mineral and till geochemical signatures of the NICO Co-Au-Bi deposit, Great Bear magmatic zone, Northwest Territories, Canada; *in* Lentz, D.R., Thorne, K.G. and Beal, K.-L. (eds), Proceedings, 24th International Applied Geochemistry Symposium (IAGS 2009), Fredericton, New Brunswick, June 2009, p. 553–556.

McMartin, I., Corriveau, L., Beaudoin, G., Averill, S. and Kjarsgaard, I., 2009b, Heavy mineral signature of the NICO Co-Au-Bi deposit, Great Bear magmatic zone, Northwest Territories, Canada; *in* McClenaghan, B. and Thorleifson, H. (eds) Indicator mineral methods in mineral exploration, Workshop B, 24th International Applied Geochemistry Symposium (IAGS 2009), Fredericton, New Brunswick, June 2009, p. 71–81.

McMartin, I., Corriveau, L. and Beaudoin, G., 2011a, An orientation study of the heavy mineral signature of the NICO Co-Au-Bi deposit, Great Bear magmatic zone, Northwest Territories, Canada: Geochemistry: Exploration, Environment, Analysis, v. 11, p. 293–307.

McMartin, I., Corriveau, L., Beaudoin, G., Averill, S.A. and Kjarsgaard, I., 2011b, Results from an orientation study of the heavy mineral and till geochemical signatures of the NICO Co-Au-Bi deposit, Great Bear magmatic zone, Northwest Territories, Canada: Geological Survey of Canada, Open File 6723, 23 p.

McMartin, I., Corriveau, L., Beaudoin, G., Jackson, S. and Normandeau, P.X., 2011c, Magnetite composition applied to drift prospecting methods for IOCG exploration in the Great Bear magmatic zone, Canada: Results from the NICO Au-Co-Bi deposit; 25th International Applied Geochemistry Symposium 2011, Program and Abstracts, p. 90–91, Rovaniemi, Finland.

McMartin, I., Beaudoin, G., Jackson, S. and Normandeau, P.X., *in prep,* Magnetite composition in glacial sediments derived from IOCG deposits, Great Bear Magmatic Zone.

Montreuil, J.-F., Corriveau, L. and Potter, E.G., 2016, On the relation between alteration signature and metal endowment of iron oxide alkali altered systems, southern Great Bear magmatic zone (Canada). In A Special Issue Devoted to Proterozoic Iron Oxide-Apatite-(+REE) and Iron Oxide-Copper-Gold and Affiliated Deposits of Southeast Missouri, USA, and the Great Bear Magmatic Zone, Northwest Territories, Canada (Slack, J. F., Corriveau, L. & Hitzman, M. W.): Economic Geology, v. 111, p. 1803–1814.

Mumin, A.H., Corriveau, L., Somarin, A.K. and Ootes, L., 2007, Iron oxide copper-gold-type polymetallic mineralization in the Contact Lake Belt, Great Bear Magmatic Zone, Northwest Territories, Canada: Exploration and Mining Geology, v. 16, p. 187–208.

Mumin, H., Somarin, A.K., Jones, B., Corriveau, L., Ootes, L. and Camier, J., 2010, The IOCG-porphyry-epithermal continuum of deposits types in the Great Bear Magmatic Zone, Northwest Territories, Canada; *in* Corriveau, L. and Mumin, H. (eds) Exploring for Iron Oxide Copper-Gold Deposits: Canada and Global Analogues; Geological Association of Canada, Short Course Volume 20, p. 59–79.

Normandeau, P.X., McMartin, I., Paquette, J. and Corriveau, L., 2011a, Drift prospecting applied to iron oxide copper gold exploration in the Great Bear Magmatic Zone, Northwest Territories, Canada; Geological Association of Canada-Mineralogical Association of Canada, Joint Annual Meeting, Abstracts Volume vol. 34, Ottawa, Ontario, May 2011, p.154.

Normandeau, P.X., McMartin, I., Paquette, J. and Corriveau, L., 2011b, Drift prospecting applied to Iron Oxide Copper Gold exploration in the Great Bear Magmatic Zone, Northwest Territories, Canada; Geohydro 2011, Proceedings of the joint meeting of the Canadian Quaternary Association and the Canadian Chapter of the International Association of Hydrogeologists, Quebec City, Quebec, August 2011, Doc. 2128.

Normandeau, P.X., McMartin, I., Paquette, J. and Corriveau, L., 2011c, Till geochemical signatures of iron oxide copper-gold mineralization in the Great Bear magmatic zone, Northwest Territories, Canada. In: B.J. Fischer, and D.M. Watson (eds), 39th annual Yellowknife Geoscience Forum Abstracts, Northwest Territories Geoscience Office, Volume 2011, p. 115–116.

Normandeau, P.X., McMartin, I., Paquette, J., Corriveau, L., and Montreuil, J.F., 2012, Multivariate till geochemical signatures of iron oxide copper-gold mineralization in the Great Bear magmatic zone, Northwest Territories, Canada; Goldschmidt 2012, Program with Abstracts.

Normandeau, P.X., McMartin, I., Paquette, J. and Corriveau, L., 2013, Prospection glaciosédimentaire appliquée aux gisements IOCG: signatures multivariées des altérations hydrothermales, ACFAS 2013.

Normandeau, P.X., McMartin, I., Paquette, J. and Corriveau, L., in prep, Till geochemistry as a vector to iron oxide alkali-altered systems and iron oxide copper-gold deposits in the Great Bear magmatic zone, Northwest Territories, Canada.

Normandeau, P.X., Harlov, D.E., Corriveau, L., Paquette, J., McMartin, I., in press, Characterization of fluorapatite within iron oxide alkali-calcic alteration systems of the

Great Bear magmatic zone: a potential metasomatic process record: The Canadian Mineralogist.

Plouffe, A., McClenaghan, M. B., Paulen, R. C., McMartin, I., Campbell, J. E. and Spirito, W., 2013, Processing of glacial sediments for the recovery of indicator minerals: protocols used at the Geological Survey of Canada: Geochemistry: Exploration, Environment, Analysis, v. 13, p. 303–316.

Porter, T.M., 2010, Current understanding of iron oxide associated-alkali altered mineralised systems: Part 1 – An overview; *in* Porter TM (ed) Hydrothermal iron oxide copper-gold and related deposits: A global perspective, volume 3, Advances in the understanding of IOCG deposits, PGC Publishing, Adelaide, p. 5–32.

Prest, V.K., Grant, D.R. and Rampton, V.N., 1968, Glacial Map of Canada: Geological Survey of Canada, Map 1253A, Scale 1:5 000 000.

Sappin, A.-A., Dupuis, C., Beaudoin, G., McMartin, I. and McClenaghan, B.B., 2013, Optimal ferromagnetic fraction representative of iron oxide compositional variations in till samples along ice-flow paths: Case studies from the Sue-Dianne IOCG and Thompson magmatic Ni-Cu deposits, Canada: Geochemistry: Exploration, Environment, Analysis, v. 14, p. 315–329.

Spirito, W.A., McClenaghan, M.B., Plouffe, A., McMartin, I., Campbell, J.E., Paulen, R.C., Garrett, R.G. and Hall, G.E.M., 2011, Till sampling and analytical protocols for GEM projects: From field to archive: Geological Survey of Canada, Open File 6850, 83 p.

Smith, D.G., 1994, Glacial Lake McConnell: Paleogeography, age, duration, and associated river deltas, Mackenzie River Basin, Western Canada: Quaternary Science Reviews, v. 13, p. 829–843.

St-Onge, D.A., Geurts, M.A., Guay, F., Dewez, V., Landriault, F. and Léveillé, P., 1981, Aspects of the deglaciation of the Coppermine River region, District of McKenzie: *in* Current Research, Part A, Geological survey of Canada, Paper 81-1A, p. 327–331.

Walker, E.C. and Rajnovich, L., 2007, Cooper Minerals exploration for IOCG-type deposits within the Terra Property, Great Bear Magmatic Zone, NWT; NTGO, YKGSF Abstracts Volume 2007, p. 65.

Wiken, E.B., 1986, Terrestrial Ecozones of Canada. Ecological Land Classification; Series No. 19, Environment Canada. Hull, Quebec, 26 p.

Williams, P.J., 2010, Classifying IOCG deposits; *in* Corriveau L. and Mumin A.H. (eds) Exploring for iron oxide copper-gold deposits: Canada and global analogues: Geological Association of Canada, Short Course Notes 20, p. 13–22.

RATIONALE OF CHAPTER 3

The surficial geology of the GBMZ was summarized in the previous chapter based on field observations including striation measurements, and the nature of glacial transport was characterized using interpreted glacial directions and the lithological analysis of the pebble fraction of till samples. Till samples can now be classified with respect to their spatial relationship to glacial dispersal trains. Chapter 3 explores the relation between the till geochemical results provided in the previous chapter and the lithogeochemistry of GBMZ bedrock samples. This chapter makes use of analysis of variance to test potential vectors towards IOA to IOCG mineralization and IOAA systems within the till matrix geochemistry datasets. Experimental statistical tests are performed where a large number of till samples in the vicinity of a single deposit allowed for significant results. This is monitored through a constant control of the confidence level. Elements whose results did not prove to be reliable through the data quality study described in Chapter 2 were abandoned. These include one or more set of analysis for Ag, Au, B, Cd, Hg, In, P, S, Sb, Se, Re and, in some cases, W.

CHAPTER 3: Till geochemistry as a vector to iron oxide alkali-altered systems and iron oxide copper-gold deposits in the Great Bear magmatic zone, Northwest Territories, Canada

3.1. ABSTRACT

Recent advances in the characterization of iron-oxide alkali-altered systems and associated iron-oxide apatite and iron-oxide copper-gold deposits of the Great Bear magmatic zone (GBMZ) are used to test pathfinder elements as exploration vectors towards mineralization and alterations in this prospective glaciated region. Analysis of variance within lithogeochemical (n= 707 samples) and till geochemical datasets (n=101 samples) are compared. Results show that the vectoring potential of till geochemistry in the GBMZ is limited by the absence of a continuous till cover, the variability of elemental enrichments within IOA to IOCG mineralization as well as the complexity and size of the alteration systems. Within these limitations, Fe, Co, Ni, Cu, As, Mo, Bi, La, Th, U and W were identified as potential vectoring elements in till due to their anomalous concentrations down-ice of various outcropping mineralization within the study area. For instance, Fe, Co, Cu and Mo are established as the most useful vectoring elements in till toward the Sue Dianne deposit and Fe, Co, Ni, Cu, Mo, W, Bi and U towards the Fab system. GBMZ till composition reflects local provenance with till geochemical anomalies found up to 2 km down-ice of the Sue Dianne deposit and Fab system. At the Sue Dianne deposit, the La and Th ratios obtained after a near-total digestion over those obtained after a partial digestion within the silt and clay-sized fraction of till define a more consistent anomaly near mineralization compared to single element concentrations. Additional

testing using a larger number of till samples in an area of continuous till cover, down-ice, up-ice and over unaltered background of an isolated point source is recommended to further develop the elemental ratio method for exploration of iron oxide alkali-altered systems.

3.2. INTRODUCTION

Till geochemistry is widely used in mineral exploration in glaciated terrain as till is widespread, has a relatively simple transport history and has a composition that reflects its source material. Hence, anomalous concentrations of metals or other pathfinder elements in till can be traced back to potential bedrock sources (e.g., McClenaghan et al., 2000, 2013; McClenaghan and Kjarsgaard 2001; Klassen 2001b; Paulen and McMartin, 2009; McMartin et al., 2016). Here, we test wether till geochemistry can be used to identify iron oxide copper-gold (IOCG) deposits in the Great Bear magmatic zone (GBMZ, Northwest Territories, Canada). Suites of pathfinder elements in till have been defined through case studies for a broad range of mineral deposits, including magmatic Ni-Cu-PGEs, Cu porphyry, volcanogenic massive sulphides, uranium, gold and diamonds (e.g., McClenaghan, 1994; Kaszycki et al., 1996; Levson, 2002; Klassen, 2003; Lehtonen et al., 2005; Campbell, 2009; McClenaghan et al., 2011; McClenaghan and Peter, 2016; Hashmi et al., 2015). The potential for geochemical exploration applied to IOCG has been demonstrated in non-glaciated hyperarid settings using lag talus samples (Benavides et al., 2008a,b; Fabris et al., 2013, 2015). However, very few studies using till composition have been conducted near IOCG deposits, and these were focusing on indicator minerals (McMartin et al., 2011a,b; Sappin et al., 2014). Recently, an orientation study at the NICO Co-Au-Bi magnetite-group IOCG deposit in the GBMZ, showed the potential of As, Bi,

Co, Au, Cu, Sb, W and Cd as pathfinder elements in till (McMartin et al., 2009, 2011b). The present work builds on this study and aims to evaluate a full suite of elements that can be used as exploration vectors in the GBMZ. To this end, till sampling surveys were completed at the Sue Dianne Cu-Ag-Au magnetite to hematite-group IOCG deposit and the Fab system U-Th-Cu magnetite-group IOCG showings, as well as in the vicinity of several polymetallic showings within the larger family of IOAA systems (Mumin et al., 2007, 2010; Corriveau et al. 2010b; Porter 2010). The mineralization and extensive alteration halos of these systems (Williams et al., 2005; Corriveau et al., 2010b) are characterized by specific lithogeochemical signatures (Montreuil et al. 2013, 2015, 2016b). This study compares these signatures with till geochemistry. Potential pathfinder elements, in addition to the known ore elements, are determined from a comprehensive lithogeochemistry database (Corriveau et al., 2015). The spatial distribution as well as statistical significance of these element concentrations in till are evaluated to assess their mineral exploration applicability for IOCG deposits and IOAA systems.

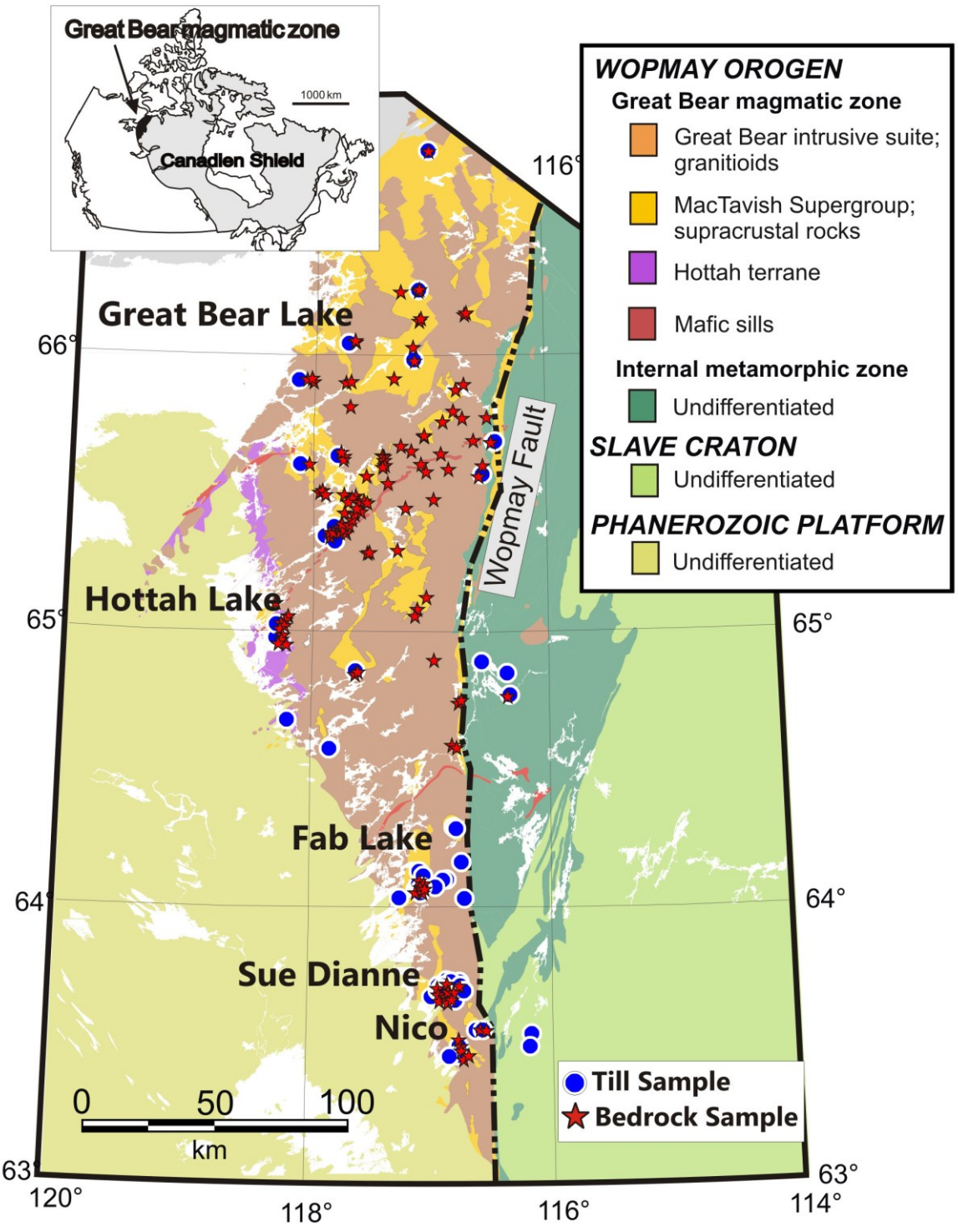

Figure 3.1: (**a**) The Great Bear magmatic zone (GBMZ) in Canada; (**b**) General geology of the GBMZ (modified from Corriveau et al., 2010b) with till and bedrock sample locations.

3.2 STUDY AREA

3.2.1. Geochemistry of iron oxide alkali alteration systems and iron oxide copper-gold deposits

A wide range of elements of economic potential can be enriched in IOAA systems and IOCG deposits. They can contain enrichment of Cu, Au, Ag, Co, Bi, Fe, Mo, Ni, PGE, Pb, REE, Th, U, V and/or Zn (Corriveau et al., 2010a). The metasomatic alterations associated with these systems are characterized by the addition of alkali metals and iron (Porter, 2010), and may extend hundreds of square kilometers (Barton and Johnson, 2004). The extent and intensity of these halos explain the rarity of unaltered protoliths for many of the IOAA metasomites in the GBMZ and worldwide (Mumin et al., 2007, 2010; Mumin, 2015). Corriveau et al. (2010b) provide a conceptual framework for the alteration zoning (Hitzman et al., 1992; Barton and Johnson, 1996; Williams et al., 2005; Corriveau, 2007). Five sequential stages of alteration are described: (1) early high-temperature sodic-calcic alteration, (2) calcic-ferric alteration, (3) high-temperature potassic ferric alteration, (4) skarn type alteration, only if a carbonate rich protolith is involved, and (5) low-temperature (LT) potassic-ferric alteration. The high intensity of these alterations results in complete replacement of the protolith mineralogy with or without textural preservation. Overprinting prograde and retrograde alterations, as well as the juxtaposition of alteration types, increase with proximity to the ore zones (Corriveau et al., 2010a; Montreuil et al., 2015, 2016b).

3.2.2. Bedrock geology of the Great Bear magmatic zone

The GBMZ (Fig. 3.1) is a volcanic and plutonic felsic to intermediate Andean type calc-alkaline belt (Hildebrand et al., 1987, 2010) resulting from the Calderian Orogeny responsible for the Wopmay Orogen (1.88 Ga, Hildebrand et al., 2010; Jackson et al., 2013). It is exposed between the western margin of the Slave Craton to the east and the Phanerozoic cover to the west. Remnants of an older arc in suture with the Slave Craton also outcrop at the western margin of the GBMZ (i.e. Hottah Terrane; Hildebrand et al., 1987). To the east, the Wopmay fault separates the GBMZ from metamorphic rocks of the Wopmay Orogen (Hildebrand et al., 1987; Jackson, 2006, 2008; Jackson and Ootes, 2010). Many IOAA systems of the GBMZ have been the subject of recent petrological, mineral chemistry, geochemical, geochronological, isotopic and economic geology studies which outline the potential for undiscovered deposits in the GBMZ (Gandhi et al., 1996; Mumin et al., 2007; Corriveau et al., 2010a, b; Mumin et al., 2010; Gandhi et al., 2013; Potter et al., 2013a, b; Acosta-Góngora et al., 2014, 2015; DeToni, 2016; Montreuil et al., 2015, 2016b).

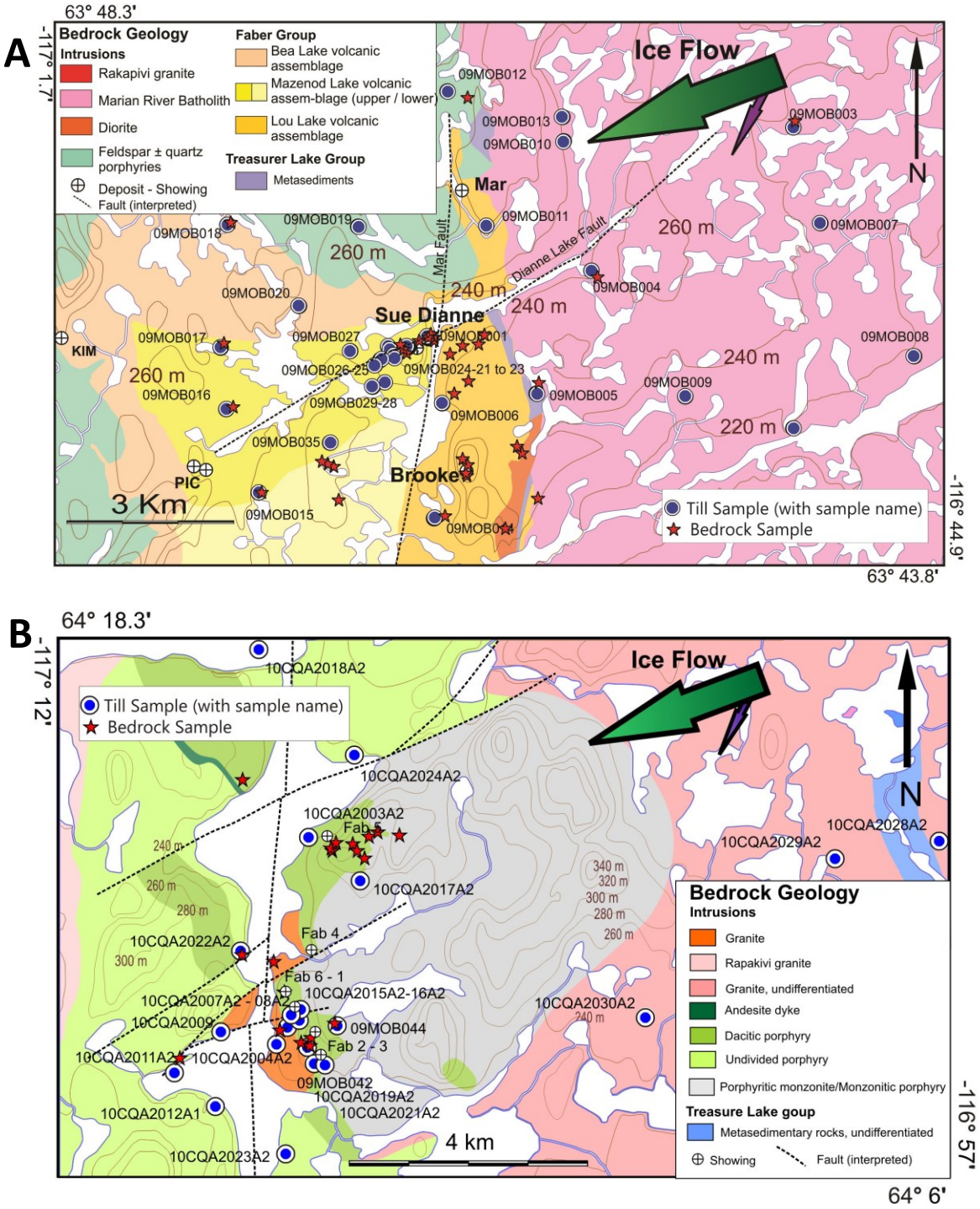

Figure 3.2: (**a**) Bedrock geology of the Sue Dianne deposit area and sample location, after Camier (2002); (**b**) Geology of the Fab system area and sample location, modified from Potter et al. (2013b), Gandhi (1988) and Jackson (2008).

Montreuil et al. (2013) identified systematic behaviors of elements related to alteration types in the GBMZ. Strong positive correlations between K and Al, Rb and Ba are visible in most types of alterations as well as strong positive correlations between Fe and Co, Ni and Cu. Multivariate analysis shows the following elemental enrichment in each alteration type: 1) Sr in sodic alteration ; 2) Co, Mg, Mn, Ni, P, Zn ± Fe in calcic-ferric/ferrous alteration; 3) all REEs but Eu in calcic-ferric/ferrous and potassic-ferric/ferrous alterations; 4) Al, Ba, Nb, Rb, Si, Ta, U, Th and Zr in potassic alterations, ; and 5) Ag, Au, Cu, Mo, Pb, PGEs, REEs and Zn in low temperature potassic-ferric/ferrous alterations. While being enriched within the sodic alteration, Sr is strongly decoupled from Ca due to incompatibility with amphiboles. Enrichment in Ag, Au, Bi, Co, Cu, Ni, Th, U and Y+REEs is observed in the high temperature potassic-ferric/ferrous alteration of prospects and deposits of the southern GBMZ. As well, an increase of the less mobile high field strength elements (HFSE) Nb, Ta and Th, and a decrease in REEs, are associated with the earlier sodic alteration (e.g., Ester zone and MHF prospect (Montreuil et al., 2016b)).

3.2.3. The Sue Dianne IOCG system

The Sue Dianne Cu-Ag-(U-Au) deposit (Fig. 3.2a) is hosted in a hydrothermal breccia complex occurring in the Faber Group volcanic rocks at the intersection of the Mar and Dianne Lake faults (Goad et al., 2000a,b; Camier 2002). Major ore minerals are chalcopyrite, bornite, chalcocite and covellite. The alteration zonation is well exposed within 1 km of the Sue Dianne deposit and extends up to 7 km along the main Dianne Lake Fault trend (Camier, 2002; Mumin et al., 2010). The predominant IOCG alteration types outcropping at the Sue Dianne Ag-Cu deposit are high temperature potassic and potassic-ferric/ferrous alterations. These are locally superimposed by a low temperature calcic alteration with epidote and allanite. High-temperature

sodic and calcic alterations are the predominant peripheral alterations and are also present, in small proportion, in the immediate vicinity of the outcropping mineralization (Montreuil et al., 2016b). An envelope of quartz and quartz-epidote veins, breccia and stockworks overprint the potassic alteration (Mumin et al., 2010). Alteration minerals including quartz, sericite, K-felspar, hematite, chlorite, fluorite, epidote, andradite, magnetite and albite decrease in abundance with increasing distance from mineralization. The same alterations and associated mineralogy are present at the nearby Brooke Zone (Bi-Cu-Mo-LREE) showing, characterized with high Mo, W and LREE concentrations with lesser Bi and Th (Montreuil et al., 2016b). Both systems are enriched in LREE when compared to host rocks. REEs are hosted primarily in apatite and allanite with minor monazite and retrograde britholite (Lypaczewski et al., 2013; Normandeau et al., in press). Further mention of the Sue Dianne system includes both the Sue Dianne deposit and Brooke Zone showing.

3.2.4. The Fab IOCG system

The Fab system (Fig. 3.2b) includes eight historical showings of U-Cu-Fe, and/or F (Gandhi, 1988) along with many newly identified U and Th showings and anomalies (Potter et al., 2013a,b). This magnetite-group IOCG system has a large alteration footprint, outcropping over an area of 5 by 10 km (Potter et al., 2013b). Least altered and weakly to moderately albitized precursor hypabyssal intrusions are cross-cut by high-temperature calcic alteration that grades into a transitional calcic-potassic-ferric/ferrous alteration which, with increasing intensity of K-feldspar, develops large breccia zones, intense high-temperature potassic-ferric/ferrous alteration zones and zones of base and specialized metal mineralization (Acosta-Góngora et al., 2014; Montreuil et al., 2016a). Both historical and newly identified showings are found within or near hydrothermal magnetite-rich veins and breccias as well as magnetite-apatite-actinolite

veins. Some of these veins contain up to 10 % apatite with or without biotite, muscovite, chlorite and scheelite (DeToni, 2016; Lypaczewski et al., 2013; Normandeau et al., in press). U± Cu showings contain combinations of pitchblende, chalcopyrite, pyrite, apatite and fluorite (Gandhi 1988) with traces of hematite (Potter et al., 2013a) and are located in the central area of the Fab system (Fig. 3.2b). The U and Th showings are limited to the northern part of the Fab system and are within amphibole-magnetite veins and breccias without sulphides.

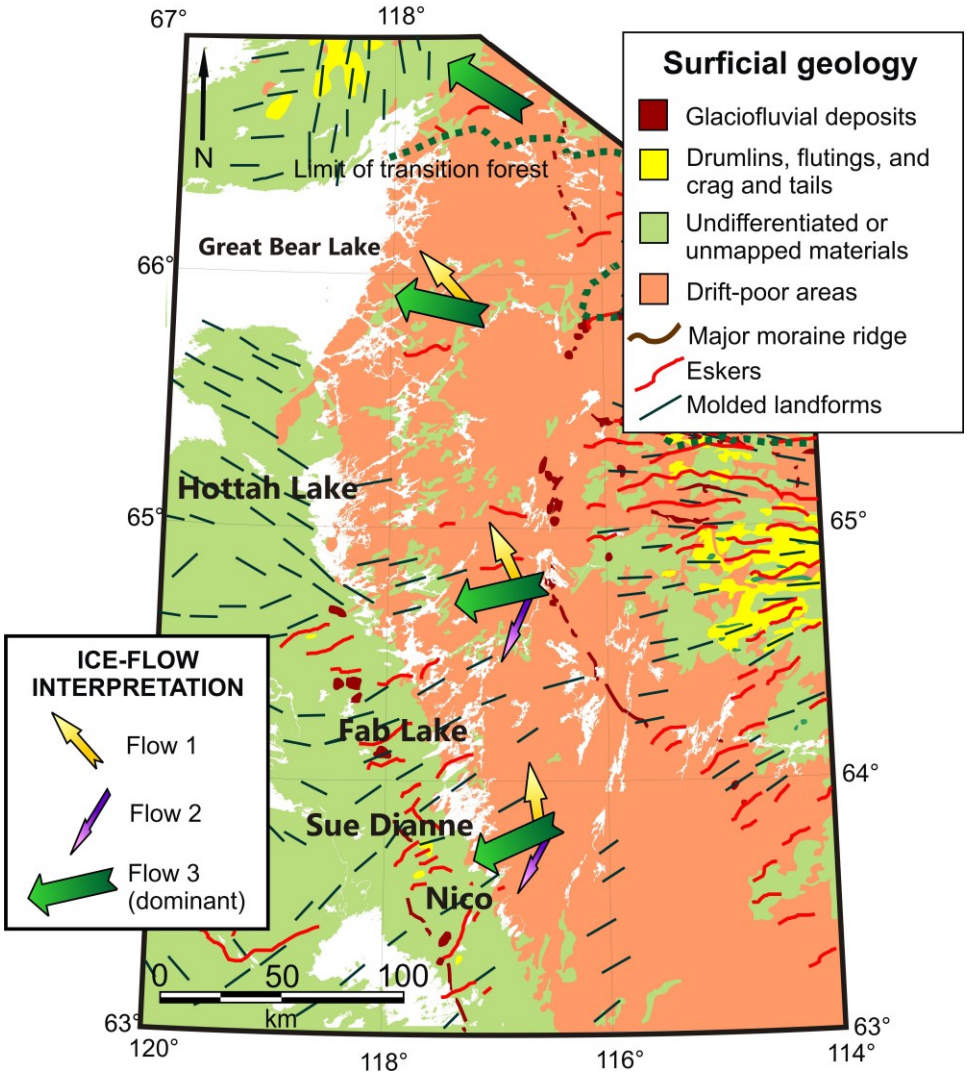

Figure 3.3: Simplified interpretation of ice-flow directions within the GBMZ modified from Normandeau and McMartin (2013). Regional surficial geology modified after Aylsworth and Shilts (1989) and Fulton (1995). Undifferentiated and unmapped areas are mostly till.

3.2.5. Quaternary geology

Physiography and surficial sediments

In the GBMZ, supracrustal rocks and the variety of hydrothermal alteration zones they host, tend to form prominent ridges striking SSE to NNW. These ridges have relief exceeding 100 m and are dominated by exposed bedrock draped by a thin and discontinuous till cover generally less than 2 m thick. The intrusive rocks of the GBMZ commonly form poorly drained lowlands (170 to 250 m above sea level - a.s.l) with a generally continuous thin till cover (Fig. 3.3; Aylsworth and Shilts, 1989; Fulton, 1995; Normandeau and McMartin 2013). Glaciofluvial deposits are scarce, with only a few isolated esker segments present (Fig. 3.3). Raised glaciolacustrine beaches and till partly winnowed by waves, ice and currents are found below the maximum elevation of Glacial Lake McConnell at 300 m a.s.l. (Lemmen et al., 1994; Smith, 1994). Glaciolacustrine sediment veneers occur in lowlands and in protected embayments above modern lake levels.

Glacial geology and glacial transport

The GBMZ was covered by the western part of the Keewatin Sector of the Laurentide Ice Sheet during the last glaciation (Dyke and Prest, 1987; Dyke and Dredge, 1989; Dyke, 2004). Glacial Lake McConnell (11.8 – 8.3 ka BP, Lemmen et al., 1994; Smith, 1994) invaded the lowlands between Great Bear and Great Slave lakes as the ice retreated to the east during deglaciation (12 - 10 ka, Dyke et al., 2003; Dyke, 2004). Ice-flow indicators show that the study area was influenced primarily by ice flowing to the WSW south of Hottah Lake and to the WNW north of the lake (Normandeau and McMartin, 2013). Three distinct phases of ice flow are

present in the area (Fig. 3.3). Phase 1 (360° to 308°) and phase 2 (210°) consist of relict features preserved on the western sides of outcrops, protected from ice flow during phase 3. Phase 3 ice-flow indicators range in orientation from 225° to 305° across the GBMZ, gradually shifting from west-southwestward in the south to west-northwestward in the north. Phase 3 is the dominant ice-flow direction and is consistent with compilations of streamlined landforms from air photo interpretation and remote sensing observations (Prest et al., 1968; Dyke and Prest, 1987; Clark, 1993).

Till pebble lithologies suggest a short distance of glacial transport over the GBMZ. For example, heavily metasomatized clasts (4 to 9.8 mm) are dispersed less than 800 m to the west (down-ice) of the Sue Dianne deposit (Normandeau et al., 2011; Normandeau and McMartin, 2013). For most showings and deposits of the GBMZ, the presence of multiple outcropping mineralization, at a scale similar to the glacial transport distances, adds complexity to the dispersal trains interpretation as they can rarely be confidently interpreted as single point source for anomalies in till.

3.3. METHODS

3.3.1. Sampling procedures and analytical approach

Whole rock geochemistry analyses of 707 samples from Corriveau et al. (2015) lithogeochemical database were selected to best represent the source bedrock of 101 till samples collected in the field. Selected lithogeochemical results are from the Sue Dianne deposit and Fab systems, from other IOAA systems where till samples were collected, and from background sites with barren lithologies in the GBMZ (Table 3.1). The location of these samples is shown in Figure 3.1. A distribution analysis using Tukey box plots (Tukey, 1977; Reimann *et al.,* 2008; Grunsky, 2010) of economic and accessory enriched elements within the GBMZ (Na, Ca, K, V, Cr, Mn, Fe, Co, Ni, Cu, As, Mo, La, Yb, W, Bi, Th and U) was performed using the log-transformed lithogeochemistry in order to identify potential geochemical indicators common to all the sampled mineralized occurrences. Selection of these elements was based on reported enrichments by Mumin et al. (2010) in addition to established pathfinder elements noted in till at the NICO deposit by McMartin *et al.* (2009, 2011a). Bedrock samples collected from IOCG ore zones, breccia and showings, or from IOAA systems containing large amounts of sulfides and/or hydrothermal magnetite and/or hematite, were classified as "mineralized" (n=107). Selections were made independent of elemental concentrations or alteration type. Within these mineralized samples, 25 are from the Sue Dianne and 10 from the Fab systems (Table 3.1). GBMZ background samples (n=215) were selected to represent the least altered GBMZ host rocks.

A total of 101 till samples were collected in C-horizon soils across the entire GBMZ (Fig. 3.1, Table 3.1) focussing on the Sue Dianne (n=30) and Fab systems (n=23) (Fig. 3.2). Till samples were also collected near other known showings within large IOCG-type alteration systems (n=25). To assess the range of geochemical background values, till samples were collected away from any known IOAA system in the GBMZ (n=9) as well as in the Wopmay internal metamorphic zone (n=4) and in the Slave Province (n=2) (rf. Normandeau and McMartin (2013) for detailed sampling methods). The low thickness, discontinuity and the variable preservation state of the GBMZ till placed constraints on the choice of sample locations during field work. For these reasons, a grid-like pattern of sample locations, typical of exploration programs, was not possible. Nonetheless, till could be sampled at various distances down-ice and up-ice of outcropping mineralization (Table 3.1 and 3.3).

Table 3.1: Number of samples

System	Till				Bedrock		
	Down-ice*	up-ice**	Background	Total	Mineralized	Non mineralized	Total
Sue Dianne	10	1	19	30	25	63	88
Fab	13	2	8	23	10	20	30
Other IOAA	25	-	-	25	72	302	374
GBMZ host rock	-	-	9	9	-	215	215
Slave Craton and Wopmay metamorphic zone	-	-	5	5	-	-	-

* Down-ice distances varies from 200 to 2 000 m

** Up-ice distances are less than 200 m at Sue Dianne system and less than 500 m at Fab system

3.3.2. Analytical methods

Till samples were dry-sieved to obtain the <0.063 mm (silt and clay fraction). The <0.002 mm (clay fraction) was obtained through centrifugation and decantation. Approximately 1 g of the <0.002 mm of till was analyzed at ACME Labs, Vancouver using inductively coupled plasma – mass spectrometry (ICP-MS) following a hot (95°C) modified aqua regia digestion (HCl-HNO3, 1:1). In addition, approximately 30 g of the <0.063 mm were analyzed using ICP-MS following the modified aqua regia digestion; a separated 0.25 g split of the same fraction was analyzed using ICP-MS, 4-acid digestion (HNO3-HClO4-HF dissolved in HCl). About 30 g of the <0.063 mm fraction was analysed at Activation Laboratories Ltd. using instrumental neutron activation (INA). Quality assurance (QA) and quality control (QC) procedures followed the protocols developed as part of GEM projects (Spirito et al. 2011). Results are reproducible and accurate with the differences between measured and certified values for the standards falling at or below 10%. Elements with high relative standard deviation (≥ 30%) or accuracies worse than 10% for specific methods and/or batches were excluded from the present study. These include one or more data sets of analyses for Ag, Au, B, Cd, Hg, In, P, S, Sb, Se, Re and, in some cases, W. Variability between each of the 4 field duplicate sample sites exceeds the variability within sets of duplicate data. More information is available in Normandeau and McMartin (2013). Bedrock sampling methods and lithogeochemical analytical procedures are presented in Montreuil et al. (2013) and Corriveau et al. (2015).

The choice of the size fraction and analytical methods used in this study varies depending on the element. Chalcophile elements and/or most base metals concentrations (i.e., Ni, Cu, As, Mo, Bi) are from the modified aqua regia digestion on the clay-size fraction (<0.002 mm) to enhance contrasts between anomalous and background values. W data were also obtained after

modified aqua regia digestion yet the silt and clay-size fraction (<0.063 mm) was used as they were, in this case, more reliable then the clay-size fraction (Normandeau and McMartin, 2013). These elements are typically hosted either within sulphides and clays minerals or scavenged onto clays minerals and secondary oxides dominantly present in the clay-sized fraction of till (Cole and Rose, 1984; Tarvainen, 1995; Peuraniemi et al., 1997; McClenaghan et al., 2000; Klassen, 2001a,b). All of these phases are dissolved with partial digestion including a modified aqua (Shilts, 1975, Koljonen and Malisa, 1991; Niskavaara, 1995; Shilts, 1996).

Data from the stronger 4-acid digestion on the silt and clay-size fraction (<0.063 mm) is used for the lithophile and most siderophile elements (i.e. Na, K, Ca, Fe, Co, La, Yb, Th, U). These elements are used to investigate the potential effect of IOAA alteration of the host rocks in till. Major rock forming minerals such as feldspar are much less affected by modified aqua regia digestion than sulphides and phyllosilicates (Foster, 1973; Snäll and Liljefors, 2000) and tend to reach a terminal size in the sand- and silt-size fractions of glacial sediments (Dreimanis and Vagners, 1971; Klassen, 2001a,b). Due to the nature of IOAA fluids, the alkali content of these resistant rock forming phases needs to be considered here. In contrast to the 4-acid digestion, alkali results obtained from a partial digestion such as modified aqua regia primarily targets the phyllosilicate minerals present in this size fraction. Comparisons between geochemical results obtained with these different digestion methods and size fractions are used to obtain insight into till mineralogy (Lahtinen et al., 1993; Tarvainen, 1995; McClenaghan et al., 2000, 2011) and host mineral phases modal size fractions (Mäkinen, 1995; Tarvainen, 1995). In particular, strong correlations between geochemical results obtained with a partial digestion method and those obtained with a total or near total digestion method for the same element indicate that the element in question dominantly resides in a mineral phase dissolved in the partial leach (Dolezal

et al., 1968). Na, Mo, W and Bi were not used in this analysis as results from both partial and total digestion were not available (Normandeau and McMartin, 2013).

3.3.3. Till geochemistry data preparation

Preparation of the till geochemistry data included the conversion of the geochemical results to a common unit of measurement (i.e. ppm) and the substitution of results falling below their respective analytical detection limits to half of that value (e.g. reported values of <1 ppm was set to 0.5 ppm). This substitution was applied when the amount of values falling below detection was no greater than 10% of the dataset as suggested by Reimann et al. (2008) to minimize the censoring effect on further statistical procedures (Sanford et al., 1993; Grunsky, 2010). Elements were excluded when more than 10% of their values in the data set fell below their analytical detection limit. Results from each pair of duplicates were averaged to single values. Numerical data analyses were carried out in most part in the R programming environment (R Project, 2016) with extensive use of the 'rgr' Applied Geochemistry EDA package (Garrett, 2012, 2013).

3.4. DATA ANALYSIS AND RESULTS

3.4.1. Lithogeochemistry

Tukey box plots (Fig. 3.4) and Kruskal-Wallis analysis of variance (Kruskal and Wallis, 1952; Hollander et al., 1973; Reimann et al., 2008) (Table 3.2) are used to compare data from two categories of samples, 'mineralized' and 'GBMZ background' bedrock samples. Elements are listed in order of decreasing contrast between mineralized and background samples. The Kruskal-Wallis Z-test (Dunn, 1964; Gibbons, 1976) is a non-parametric median based test and

was chosen for its robustness, since we cannot assume equality of variance within mineralized samples or background samples, in addition to the absence of normality in the data distribution. A positive result indicates that, within a 95% confidence interval, the median of the mineralized sample is significantly different from the median of the GBMZ background sample. When significant, the difference is expressed as either higher (H) or lower (L) in Table 3.2. Based on these methods, as a whole, 'mineralized' bedrock samples (line 1 in Table 3.2) have higher values for Fe, Cu, Co, As, Ni, Mo, W, U and Bi and lower values for Na and Th than GBMZ background samples. The range of the element distributions observed in Figure 3.4 also varies between the mineralized and background samples. For all studied elements but Fe, Mn and Cr, mineralized samples have greater spread than background samples.

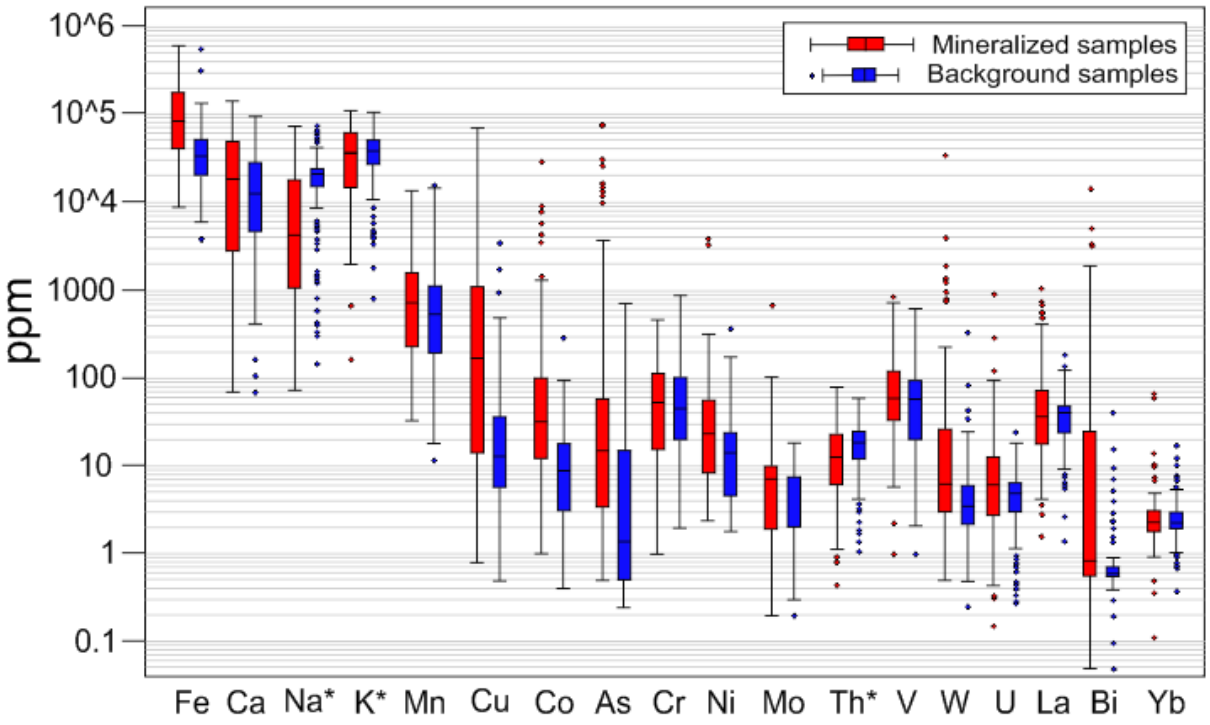

Figure 3.4: Tukey boxplot of the mineralized (n = 107) and GBMZ background (n = 215) lithogeochemical samples, in order of highest to lowest contrast between medians (*with Na, K, La and Th having higher medians in the background). Highest contrasts represent elements most likely to be anomalous in till collected down-ice from IOCG systems within the GBMZ.

Additional Kruskal-Wallis Z-tests were performed to investigate the differences of elemental abundances between and within the Sue Dianne and Fab system samples (Table 3.2). Samples from the Sue Dianne system have a higher median value of Na, K, As, W, La, Th, U, and Bi abundances as well as a lower median value of Ca and Ni abundances than samples representing the GBMZ background. Within the Sue Dianne sample subsets, mineralized samples show higher median abundance values of Fe, Cu, Co, Mo, W, U, and Bi than non-mineralized samples, while their Na, Th, and Yb median abundances are lower. Samples belonging to the Fab system have higher median values for Ca, As, Th, U, La and Yb as well as a lower median of Na than those representing the GBMZ background. Within the Fab system subset, mineralized samples show higher median abundance values of Cu than non-mineralized host rock samples. While Mn, Cr and V may be remobilized in IOAA and IOCG systems (Mumin et al., 2010; Montreuil et al., 2013), their abundances, in the present dataset, do not differentiate any sampling category. These elements were therefore excluded from any further numerical analysis.

3.4.2. Till geochemistry

Elemental distribution

The concentrations of the investigated elements established in the previous section (Na, K, Ca, Fe, Co, Ni, Cu, As, Mo, La, Yb, W, Bi, Th and U) are presented by till location in Table 3.3. Threshold is here defined as the median till value of the GBMZ background samples ± 2 times the standard deviation. The grouping of local background samples for the Sue Dianne and Fab systems was based on till sample location and the results of the pebble lithological analysis (Normandeau and McMartin, 2013).

Table 3.2: Kruskal-Wallis test results discriminating populations within the lithogeochemistry datasets at the 95% confidence level. Populations can be distinguished based on a relatively higher (H) or lower (L) median with respect to the median of the second population; (-) indicates where populations cannot be distinguished. Population tested refers to the various sample subsets presented in Table 3.1.

Population tested	Fe	Ca	Na	K	Mn	Cu	Co	As	Cr	Ni	Mo	Th	V	W	U	La	Bi	Yb
Mineralized samples vs. GBMZ background	H	-	L	-	-	H	H	H	-	H	H	L	-	H	H	-	H	-
All of Sue Dianne system vs. GBMZ background	-	L	H	H	-	-	-	H	-	L	-	H	-	H	H	H	H	-
Mineralized vs. non mineralized samples in the Sue Dianne system	H	-	L	-	-	H	H	-	-	-	H	L	-	H	H	-	H	L
All of Fab system samples vs. GBMZ background	-	H	L	-	-	-	-	H	-	-	-	H	-	-	H	H	-	H
Mineralized vs. non mineralized samples in the Fab system	-	-	-	-	-	H	-	-	-	-	-	-	-	-	-	-	-	-

Table 3.3: Concentrations of selected elements in the <0.063 mm and the < 0.002 mm fractions of till samples analyzed by ICP-MS after a 4-acid digestion and by ICP-MS after a modified aqua regia digestion respectively. Values higher than the median background plus 2 standard deviations are in bold and values lower than the median background minus 2 standard deviations are in italic. For W, results are from ICP-MS after a modified aqua regia digestion on the < 0.063 mm fraction (see text). Distances down-ice are measured with respect to Sue Dianne deposit and Fab showings, parallel to predominant ice-flow direction (WSW).

Setting	Sample(s)	Na	K	Ca	Fe	Co	La	Yb	Th	U	W*	Ni	Cu	As	Mo	Bi
		ppm	ppm	ppm	ppm	ppm	ppm	ppm	ppm	ppm	ppm	ppm	ppm	ppm	ppm	ppm
		ICP-MS after a 4-acid digestion <0.063 mm fractions									ICP-MS after an aqua regia digestion < 0.002 mm fraction					
IOAA showings within the GBMZ																
	Median (n=25)	20100	25600	10400	21800	8.5	37.4	1.7	15.6	3.8	0.70	43.4	81.3	8.6	1.2	1.9
Hottah Lake	median (n=8)	22085	26250	14400	21250	8.2	40.6	1.8	15.3	3.0	0.70	33.4	62.9	6.1	0.7	1.4
Stew Zone (NICO area)	09MOB037	19180	20100	10400	25700	9.3	36.0	*1.2*	14.6	3.8	0.50	**61.0**	42.2	8.3	0.4	1.2
LCL	09MOB043	23390	22400	12200	19200	12.2	30.3	1.4	13.7	2.8	0.50	**85.3**	85.2	**25.7**	1.0	1.5
UR	09MOB041	20420	22200	10000	18500	5.6	31.3	2.0	**22.9**	7.1	0.90	27.2	55.3	12.6	3.4	**2.4**
Dry	10CQA2061A2	*14520*	25600	8400	20900	9.3	41.6	2.0	15.6	5.6	0.20	41.9	75.0	6.8	1.5	**2.7**
DV-3	10CQA2034A2	15830	29200	9600	**49400**	**16.1**	**69.9**	**2.7**	**30.6**	6.4	0.50	49.0	82.1	19.7	1.9	1.0
DV-8	10CQA2031A2	18480	29800	10500	**36600**	12.6	**77.2**	2.4	**29.6**	6.9	0.90	53.7	124.6	**29.5**	4.0	2.0
Grouard Lake South	10CQA2041A2	16650	29700	10200	33400	10.6	**83.4**	**4.3**	**34.1**	**16.0**	**2.70**	34.9	**274.5**	6.3	**4.6**	**3.4**
Jackpot-McPhoo	10CQA2052A2	16360	23200	8700	**36500**	**14.0**	33.7	1.4	12.2	3.8	0.20	**54.2**	44.8	**16.4**	1.7	2.1
Jackpot-McPhoo	10CQA2055A2	18230	22700	9800	29200	12.6	41.1	1.5	13.5	4.1	0.20	62.7	85.9	**14.4**	2.1	1.6
MRB	09MOB032	20340	23500	11100	*16700*	5.8	*26.6*	1.3	*10.6*	2.3	0.40	61.0	81.3	11.7	0.6	*0.9*
HS-1 (NICO area)	09MOB030	19690	24500	9800	29900	**13.0**	36.1	*1.2*	18.9	2.5	0.90	**83.1**	**161.2**	**42.1**	0.7	**2.6**
OUR (NICO area)	09MOB036	22860	20200	12100	17600	7.0	36.3	*1.2*	13.2	2.1	0.40	50.1	**128.3**	**37.2**	1.6	**2.8**
Lou Lake (NICO area)	09MOB038	20100	21500	8600	20200	6.0	*29.1*	*1.1*	11.8	2.3	0.20	30.9	36.7	12.0	0.9	1.7
Rainy Lake 1 (Terra mine area)	10CQA2046A2	19590	27200	9700	25800	9.0	32.0	1.7	13.0	3.0	0.80	49.3	**175.2**	**25.9**	2.4	**3.5**
UR	09MOB040	18870	22000	8000	22900	7.8	45.8	2.5	**32.7**	**17.7**	1.10	28.9	59.4	8.6	0.6	1.6
Torrie Lake - Unnamed	10CQA2059A2	15080	26900	8100	29200	10.6	**56.5**	2.5	20.4	8.9	0.50	47.2	**170.3**	6.9	1.2	**2.8**
Tatie	09MOB045	17230	25600	8400	19400	5.3	31.6	2.0	16.9	6.8	0.90	20.1	29.4	5.5	1.2	1.3
GBMZ background and other samples																
GBMZ background	Median (n=9)	18840	24900	11400	25700	8.7	41.0	2.0	16.0	3.3	0.60	38.2	76.0	8.8	1.1	1.6
	Standard dev.	2332	2819	1848	4268	2.1	5.6	0.3	2.5	2.4	0.30	9.2	24.8	3.8	1.7	0.3
Slave Craton and east of the Wopmay fault zone	Median (n=5)	**23760**	23200	13400	25100	9.0	34.0	*1.0*	16.0	3.0	0.2	51.0	66.0	10.0	1.0	0.9

Table 3.3. (Continued)

Setting	Sample	Na ppm	K ppm	Ca ppm	Fe ppm	Co ppm	La ppm	Yb ppm	Th ppm	U ppm	W* ppm	Ni ppm	Cu ppm	As ppm	Mo ppm	Bi ppm
		ICP-MS after a 4-acid digestion <0.063 mm fractions									ICP-MS after an aqua regia digestion < 0.002 mm fraction					
Sue Dianne deposits and local background	Median (n=30)	21520	22750	11100	24000	11.2	38.2	1.3	16.2	3.0	0.20	67.1	88.1	10.8	0.8	0.9
Down-ice (< 200m)	09MOB002	*7060*	*13600*	*4100*	28100	5.4	34.3	*1.3*	*10.5*	6.9	0.30	20.0	**1189.0**	9.1	**12.1**	4.5
Down-ice (< 500m)	09MOB021	21580	25500	12400	31800	**15.0**	43.0	*1.3*	16.7	3.8	0.20	**77.4**	114.9	8.6	0.7	*0.7*
Down-ice (< 500m)	09MOB022	*12490*	23800	*9100*	**52200**	**43.2**	**60.4**	1.7	16.5	**9.4**	0.60	**93.8**	**347.9**	14.9	2.3	**2.8**
Down-ice (< 500m)	09MOB023	**23660**	23500	14000	23800	9.6	37.9	1.6	14.9	3.1	0.20	**68.0**	103.1	9.5	0.3	*0.9*
Down-ice (< 500m)	09MOB024	21790	24000	12600	30600	**14.9**	41.7	*1.3*	18.5	4.2	0.20	**73.5**	**173.1**	9.5	0.6	1.0
Down-ice (< 1000m)	09MOB025	22590	23500	14100	24000	11.0	32.1	1.4	13.0	2.3	0.20	48.8	51.4	7.9	0.6	1.0
Down-ice (< 1000m)	09MOB026	18400	*21800*	*9600*	**35600**	12.7	30.9	*1.1*	*10.5*	2.3	0.30	50.3	80.8	**26.8**	2.4	2.2
Down-ice (< 1000m)	09MOB027	18940	23300	10500	31500	**13.2**	40.0	*1.3*	17.9	3.1	0.30	**74.2**	92.9	12.9	0.7	1.8
Down-ice (< 1000m)	09MOB028	20190	24300	10800	22700	8.9	43.6	*1.3*	15.9	3.0	0.20	54.9	49.3	8.0	0.5	*0.7*
Down-ice (< 1000m)	09MOB029	16400	27800	*9000*	33500	**15.0**	34.4	1.4	15.5	3.0	0.40	**74.6**	95.5	13.5	2.0	1.1
Up - ice (< 200m)	09MOB001	21810	*20400*	11300	21100	12.1	32.1	*1.2*	17.6	2.4	0.30	**138.9**	111.2	**28.5**	1.7	1.4
Sue Dianne deposit local background																
Marian River Batholith	Median (n=7)	21700	*22000*	12000	22500	8.4	31.9	*1.2*	15.7	3.0	0.20	**62.7**	69.3	9.6	0.8	0.8
Undifferentiated porphyry	Median (n=9)	21640	22600	10900	23300	9.8	34.9	*1.2*	16.5	2.5	0.20	**57.1**	85.3	10.9	0.8	1.0
Undifferentiated volcanic	Median (n=3)	21460	*21500*	12100	23300	11.3	44.0	1.6	18.7	3.3	0.30	**70.9**	90.6	14.8	1.0	0.9
Fab system and local background	Median (n=23)	21520	22750	11100	24000	**11.2**	38.2	1.3	16.2	3.0	0.50	**62.4**	78.2	9.6	2.0	1.0
Down-ice (< 200m)	09MOB042	11780	13400	10200	**51600**	**13.9**	40.2	1.8	17.8	**8.1**	**1.30**	27.6	57.1	**17.0**	**17.4**	**3.0**
Down-ice (< 250m)	10CQA2016A2	18430	26000	11900	**34500**	**13.3**	**56.8**	1.9	**21.5**	5.1	0.50	**65.4**	**435.4**	12.4	2.7	1.1
Down-ice (< 250m)	10CQA2019A2	*8250*	*13300*	*5000*	22800	7.5	44.9	1.5	19.4	**9.8**	0.90	24.2	94.1	4.8	**4.9**	*0.9*
Down-ice (< 250m)	10CQA2021A2	*5320*	*11800*	*3700*	*11700*	*2.9*	*26.2*	*1.1*	*9.5*	4.2	**1.40**	*6.7*	**318.1**	3.4	**7.7**	*0.7*
Down-ice (< 300m)	10CQA2007A2	17300	27000	10800	28300	8.6	49.6	1.9	18.8	4.6	0.30	48.4	61.5	7.0	**7.9**	*0.8*
Down-ice (< 500m)	10CQA2003A2	17110	24300	10900	28800	9.7	40.1	1.4	15.7	5.7	0.40	43.3	43.9	4.6	**5.6**	1.1
Down-ice (< 500m)	10CQA2004A2	17580	23100	10800	32900	**13.9**	33.8	*1.2*	13.9	2.9	0.50	**67.8**	78.2	**19.4**	3.4	1.3
Down-ice (< 500m)	10CQA2008A2	20810	28100	13900	29600	11.7	51.3	2.0	19.0	3.6	0.70	**69.0**	**130.3**	**16.8**	3.9	**2.2**
Down-ice (< 500m)	10CQA2015A2	*9410*	*14600*	7200	**62500**	**35.7**	31.5	1.1	15.1	3.8	**1.30**	36.8	68.6	9.2	**14.7**	**2.8**
Down-ice (< 2000m)	10CQA2009	16060	25600	12950	**43800**	**19.9**	**53.0**	1.6	**22.5**	**8.9**	0.50	**62.4**	46.9	6.2	0.9	*0.6*
Down-ice (< 2000m)	10CQA2011A2	18500	24100	11100	28700	9.8	31.6	*1.3*	12.5	2.4	0.40	**65.6**	46.8	14.8	2.3	1.1
Down-ice (< 2000m)	10CQA2012A1	20540	27000	14300	25900	11.4	36.9	1.6	15.5	2.9	0.50	51.8	27.2	5.2	2.0	*0.7*
Down-ice (< 2000m)	10CQA2022A2	16370	29400	13100	**37100**	**18.0**	**65.0**	2.2	**22.8**	**9.2**	0.30	**64.8**	57.8	5.3	0.5	*0.6*
Up - ice (< 500m)	Average (n=2)	20595	24850	12700	29000	12.3	**59.1**	2.2	19.4	4.5	0.45	56.2	66.0	8.2	0.9	*0.8*
Fab system local background																
Undifferentiated porphyry	Median (n=3)	19390	25600	13900	26900	11.1	**71.2**	2.1	**27.3**	5.6	0.60	61.1	111.7	**17.0**	2.0	1.2
Undifferentiated granit	Median (n=5)	17760	28000	10500	**39600**	**17.3**	51.7	1.6	**22.1**	5.3	0.30	**77.1**	96.3	10.2	1.5	1.0

At the Sue Dianne system, maximum contents of Na, Fe, Co, La, Yb, U, W, Cu, Mo and Bi occur in till samples collected less than 500 m down-ice of the deposit (Table 3.3). The highest Cu concentration of the entire dataset is found in a sample collected less than 200 m down-ice of the Sue Dianne deposit (Table 3.3; Fig. 3.5a). Ni is clearly anomalous in all Sue Dianne samples compared to the GBMZ background. Co, Cu and Bi, and to some extent Fe, Mo and U (Fig. 3.5d) are sporadically high down-ice of the deposit in comparison to the local background.

Within the Fab system, highest contents of Na, Fe, Co, U , W, Cu, As and Mo occur in samples collected less than 500 m down-ice of the showings (Table 3.3). In contrast, highest contents of La, Th and Ni are found in the local background or up-ice from the showings. The second highest Cu concentration of the entire till dataset occurs in a sample located less than 250 m down-ice of one of the Fab showings (Table 3.3; Fig. 3.5a). In summary within the Fab area till samples, mainly Fe, Co, La, Th and Ni are often anomalous in the entire system and local background with respect to the GBMZ background, and U, W, Cu, Mo and Bi are sporadically high down-ice of the deposit in comparison to the local background.

The highest contents of K, Ca, La, Yb, Th, U, W and Bi are found in till samples collected directly down-ice or in the vicinity of various IOAA showings within the GBMZ (Table 3.3). No K or Ca values are higher than the anomalous threshold and few Na and Yb values are. Anomalously low values for K, Ca, Na and Yb, however, are more common. Fe, La, Yb, Th, U, W, Cu, As, Mo and Bi display highest contrast, with anomalous values reaching at least twice the median value.

Results presented above indicate that Ni concentrations with respect to GBMZ background, as well as mainly Cu and Bi contents with respect to local backgrounds, are regularly anomalous in the till samples of both Sue Dianne and Fab systems. However, results show highly variable elemental concentrations within each of these detailed sampling areas. This spatial variability is illustrated in Figure 3.5 where high and low values often occur in close proximity such as 50 meters. In both the Sue Dianne and Fab systems areas, many samples collected down-ice from the deposits or showings do not display consistent elemental enrichments. In addition, specific samples that are anomalous in certain elements may differ greatly from one to another in the concentrations of other elements. For example, while 09MOB002 and 09MOB022 contain the highest Cu and U value down-ice of the Sue Dianne deposit, they differ significantly in most other elemental contents (Table 3.3). For many elements, both highest and lowest contents are measured in samples located down-ice of mineralization (e.g. Na, Co and Mo).

Figure. 3.5.

A)

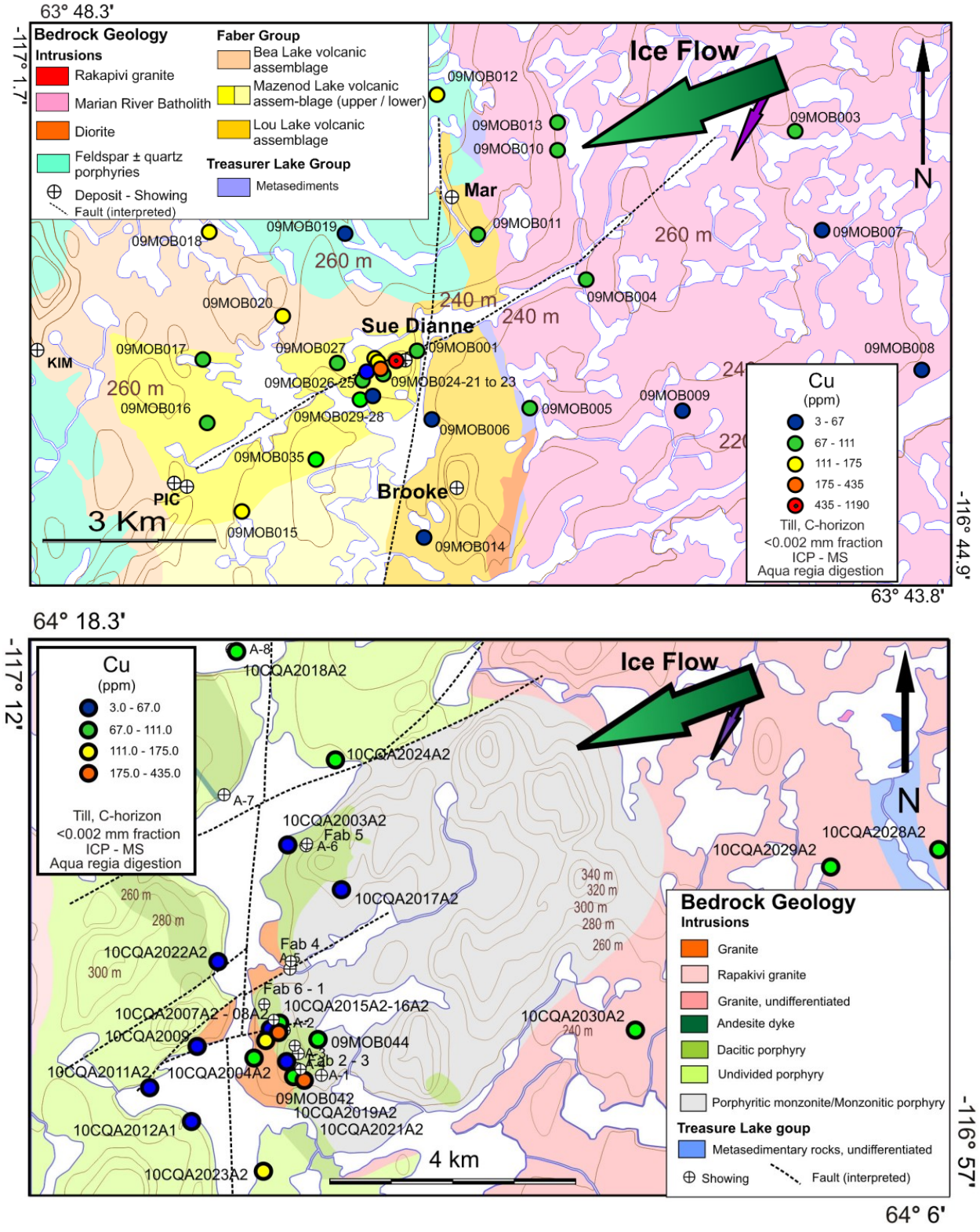
63° 48.3'
-117° 1.7'
Bedrock Geology
Intrusions
Rakapivi granite
Marian River Batholith
Diorite
Feldspar ± quartz porphyries
Deposit - Showing
Fault (interpreted)
Faber Group
Bea Lake volcanic assemblage
Mazenod Lake volcanic assem-blage (upper / lower)
Lou Lake volcanic assemblage
Treasurer Lake Group
Metasediments
Ice Flow
N
09MOB012
09MOB013
09MOB010
09MOB003
Mar
09MOB019
09MOB018
09MOB011
09MOB007
260 m
240 m
09MOB020
09MOB004
Sue Dianne
09MOB017
09MOB027
09MOB001
09MOB008
KIM
09MOB026-25
09MOB024-21 to 23
09MOB009
09MOB016
09MOB005
09MOB029-28
09MOB006
09MOB035
Brooke
PIC
3 Km
09MOB015
09MOB014
Cu
(ppm)
3 - 67
67 - 111
111 - 175
175 - 435
435 - 1190
Till, C-horizon
<0.002 mm fraction
ICP - MS
Aqua regia digestion
-116° 44.9'
63° 43.8'
64° 18.3'
-117° 12'
Cu
(ppm)
3.0 - 67.0
67.0 - 111.0
111.0 - 175.0
175.0 - 435.0
Till, C-horizon
<0.002 mm fraction
ICP - MS
Aqua regia digestion
A-8
10CQA2018A2
Ice Flow
N
10CQA2024A2
A-7
10CQA2003A2
Fab 5
A-6
10CQA2028A2
10CQA2029A2
10CQA2017A2
260 m
280 m
340 m
320 m
300 m
280 m
260 m
Fab 4
A-5
10CQA2022A2
300 m
Fab 6 - 1
10CQA2007A2 - 08A2
10CQA2015A2-16A2
10CQA2030A2
240 m
10CQA2009
A-2
09MOB044
A-3
Fab 2 - 3
10CQA2011A2
10CQA2004A2
A-4
A-1
09MOB042
10CQA2019A2
10CQA2012A1
10CQA2021A2
4 km
10CQA2023A2
Bedrock Geology
Intrusions
Granite
Rapakivi granite
Granite, undifferentiated
Andesite dyke
Dacitic porphyry
Undivided porphyry
Porphyritic monzonite/Monzonitic porphyry
Treasure Lake goup
Metasedimentary rocks, undifferentiated
Showing
Fault (interpreted)
-116° 57'
64° 6'

Figure. 3.5. (Continued)
B)

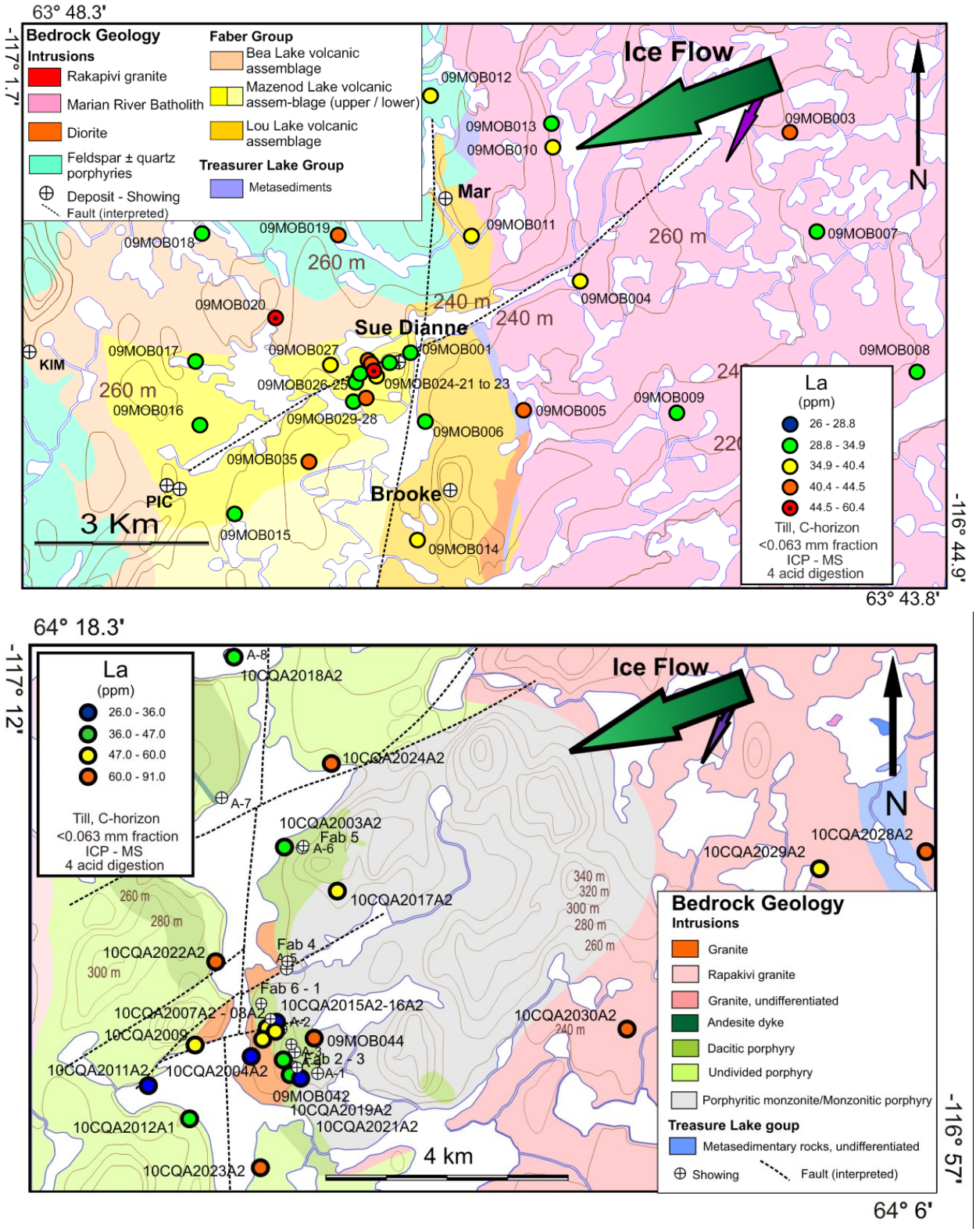

Figure. 3.5. (Continued)
C)

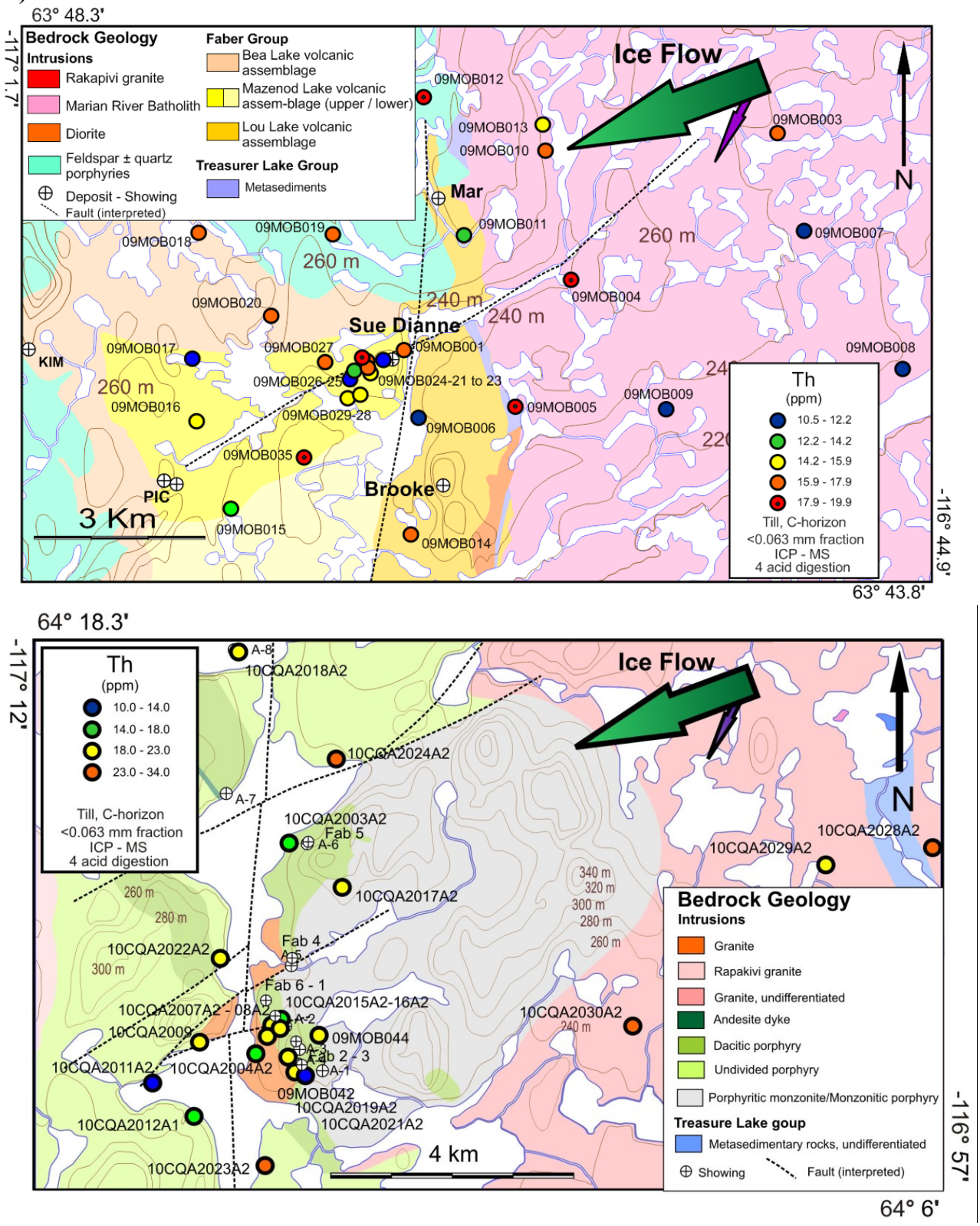

Figure. 3.5. (Continued)
D)

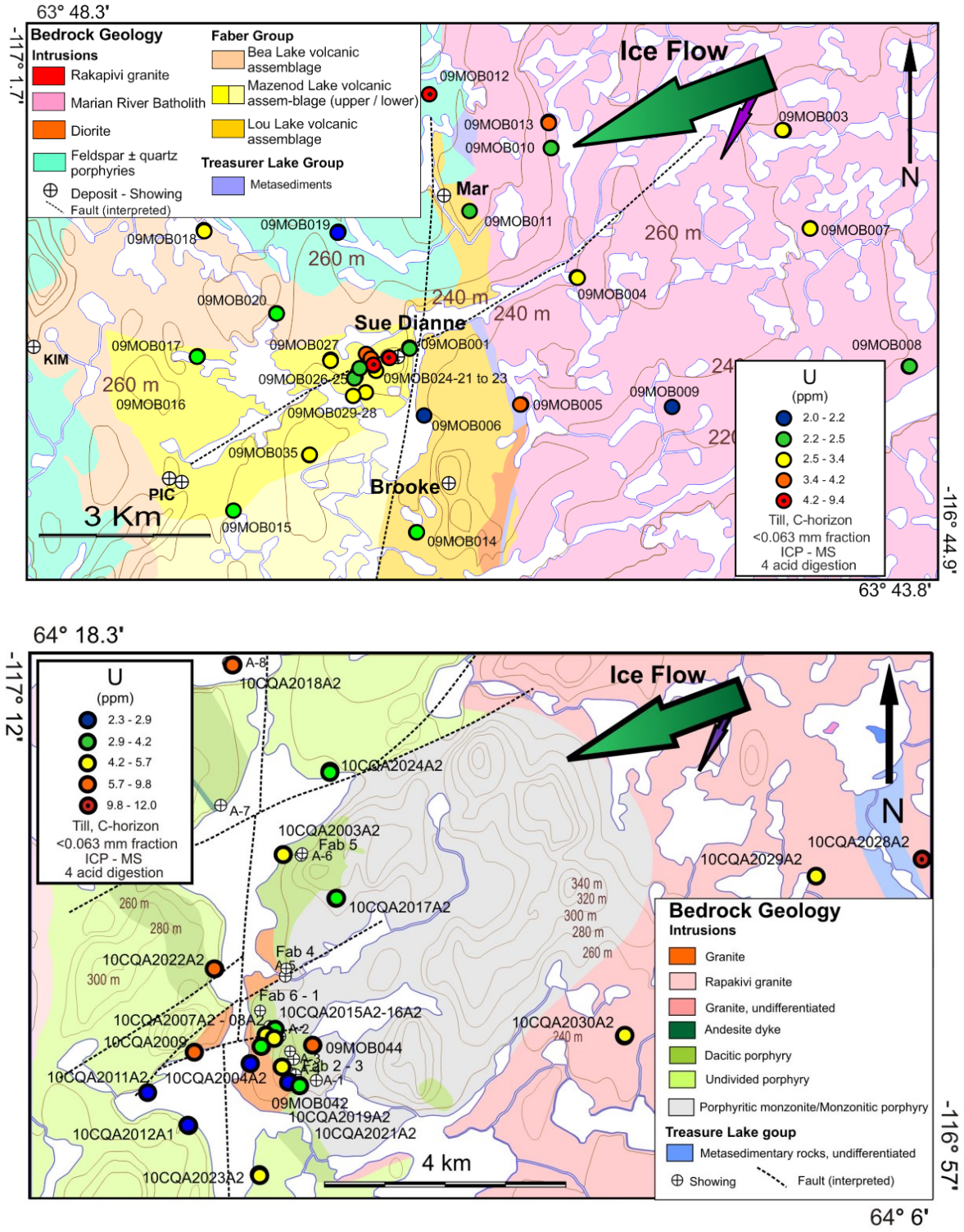

Figure 3.5: **(a)** Cu content within the clay-sized fraction (< 0.002 mm) of till C-horizon as determined by modified aqua regia / ICP-MS in the Sue Dianne and Fab areas as an example of the base metal distribution. **(b)** La, **(c)** Th and **(d)** U contents within the silt and clay-sized fraction (< 0.063 mm) of till C-horizon as determined by 4-acid / ICP-MS as examples of lithophile element distribution.

Statistical significance of elemental enrichments and depletions.

The till geochemical dataset was submitted to a Kruskal-Wallis analysis of variance (Kruskal and Wallis, 1952; Hollander et al., 1973) to identify elements that show significant differences in median concentrations between samples down-ice of deposits/showings and the up-ice and background populations (Table 3.4). A confidence interval of 90% was chosen here to account for the smaller number of till samples than bedrock samples. Consecutive tests were performed for each investigated element as the response variable, and the selected population ('collected down-ice' or 'background') as the factor variable. These tests were performed using all till samples and the Sue Dianne and Fab subsets. Tests were repeated for both sets of digestion methods and both analyzed size fractions.

Results show that enrichments in Ca, W, Bi and U as well as depletions in Na, Co, Ni and Th are significant in samples collected directly down-ice of IOCG mineralization and/or IOAA systems in comparison to all background samples (Table 3.4). The results are dependent on the digestion method used and size fraction analyzed. Samples from the Sue Dianne deposit area show the most significant results; enrichments of K, Ca, Fe, Cu, As and Bi as well as depletions of Na and Th can all be observed in at least one analytical technique. Within the silt and clay-size fractions (< 0.063 mm), similar discriminations are obtained between partial and near total digestion results, with the exception of As. Despite the presence of many elemental enrichments in samples down-ice of the Fab system compared to local background samples (Cu, Mo, W, and U; Table 3.3, Fig. 3.5), no enrichment is systematic enough to allow a significant discrimination with the Kruskal-Wallis analysis of variance (Table 3.4). However, lower medians of La and Th are present down-ice of the Fab showings for all analytical techniques. Most elements have lower median values down-ice of the showings in the clay-size fraction (< 0.002 mm). These

contrasts highlight the complexity of the IOAA alteration system, where element remobilizations may be enriched in mineralization and depleted in the surrounding metasomatised bedrock or vice versa and the difficulty of predicting the presence of an IOAA system using elemental concentrations alone.

Comparison between geochemical dissolution methods and size fractions

To gain a better understanding of the till mineralogy and associated till geochemical composition in the GBMZ samples, a rank based regression analysis (Kloke and McKean, 2012) was performed between the partial (modified aqua regia) and near total (4-acid) geochemical results on elements where both sets of results were available (Table 3.5). Very strong rank based correlations (Spearman $r > 0.95$, $p > 0.99$) between elemental contents obtained by modified aqua regia and 4-acid digestions exist for most investigated base metals (Fe, Co, Ni, Cu) as well as for U in the silt and clay-size fraction of till (Table 3.5). These relationships indicate that the minerals hosting these elements within the silt and clay-size fraction are similar in species and mostly susceptible to partial dissolution across all the sampling areas. Rank based correlations between digestion methods for As, La and Th are strong ($r>0.75$; $p > 0.99$) for all sampling areas. In contrast, rank based correlations for K and Ca within specific sampling groups vary from strong ($r > 0.75$) to weak ($r < 0.6$). This suggests a host mineral variation between the various sampling groups for K and Ca. While these tests are performed on a small number of samples ($n = 8$ to 25), confidence remains very high ($p > 0.99$), indicating a statistical significance.

Table 3.4: Krustal-Wallis test results discriminating populations within the till geochemistry at the 90% confidence interval. Samples collected down-ice of an IOCG deposit or showing can be distinguished based on a higher (H) or lower (L) median value than the median background value; (-) indicates where populations cannot be distinguished and (na) indicates where results are not available for the specific element and analytical technique.

Population tested	Digestion method and size fraction	Na	K	Ca	Fe	Co	Ni	Cu	As	Mo	La	Yb	W	Bi	Th	U
Sample collected down-ice of all showings or deposits (from < 200m to < 2000m), tested against all background samples	aqua regia, < 0.063 mm	na		H	-	-	-	-	-	na	-	-	H	H	-	-
	4 acid, < 0.063 mm	L	-	-	-	-	-	-	-	na	-	-	na	-	-	H
	aqua regia, <0.002 mm	-	-	H	-	L	L	-	-	-	-	na	na	H	L	-
Samples collected down-ice of the Sue Dianne deposit (from < 200m to < 1000m), tested against the local background	aqua regia, < 0.063 mm	na	H	-	H	-	-	H	H	na	-	-	-	H	-	-
	4 acid, < 0.063 mm	L	H	-	H	-	-	H	-	na	-	-	na	na	-	-
	aqua regia, <0.002 mm	L	H	H	H	-	-	-	-	-	-	na	na	H	L	-
Samples collected down-ice of the Fab system (from < 500m to < 2000m, tested against the local background	aqua regia, < 0.063 mm	na	-	-	-	-	-	-	-	na	L	L	-	-	L	-
	4 acid, < 0.063 mm	-	-	-	-	-	-	-	-	na	L	-	na	na	L	-
	aqua regia, <0.002 mm	L	L	-	-	L	L	L	L	-	L	na	na	-	L	L

Table 3.5: Spearman r and probability of acceptance (p) of rank based correlation between partial (modified aqua regia) digestion and near total digestion (4-acid) results in the < 0.063 mm fraction of till.

Rank based regression analysis	K		Ca		Fe		Co		Ni		Cu		As		La		Th		U	
	r	p	r	p	r	p	r	p	r	p	r	p	r	p	r	p	r	p	r	p
All samples (n=92)	<0.60	>0.99	0.66	>0.99	0.99	>0.99	0.99	>0.99	0.98	>0.99	0.99	>0.99	0.88	>0.99	0.91	>0.99	0.88	>0.99	0.97	>0.99
GBMZ background (n=9)	<0.60	<0.95	<0.6	<0.95	1.00	>0.99	1.00	>0.99	0.95	>0.99	0.95	>0.99	0.83	>0.99	0.78	>0.99	0.92	>0.99	0.98	>0.99
Within other IOAA system (n=25)	<0.60	0.99	0.61	>0.99	0.98	>0.99	0.97	>0.99	0.94	>0.99	0.98	>0.99	0.77	>0.99	0.96	>0.99	0.97	>0.99	0.98	>0.99
Sue Dianne deposit local background (n=19)	<0.60	0.99	0.84	>0.99	0.97	>0.99	0.98	>0.99	0.98	>0.99	0.99	>0.99	0.95	>0.99	0.94	>0.99	0.91	>0.99	0.96	>0.99
Down-ice of Sue Dianne deposit (n=10)	0.62	0.97	<0.6	<0.95	0.98	>0.99	0.96	>0.99	1.00	>0.99	1.00	>0.99	1.00	>0.99	0.92	>0.99	0.87	>0.99	0.99	>0.99
Fab system local background (n=8)	0.62	<0.95	0.99	>0.99	1.00	>0.99	0.96	>0.99	1.00	>0.99	0.99	>0.99	0.95	>0.99	0.95	>0.99	0.88	>0.99	0.99	>0.99
Down-ice of Fab system (n=13)	0.83	>0.99	0.85	>0.99	0.98	>0.99	0.96	>0.99	0.98	>0.99	0.93	>0.99	0.86	>0.99	0.97	>0.99	0.86	>0.99	1.00	>0.99

Rank based regression analyses were constructed to further investigate those bivariate relationships as strong correlations in two sample subsets do not necessarily reflect the same association. These regression analysis were performed using the rfit R package (Kloke and McKean, 2012) and are presented on biplots for As, La, U and Th, using samples collected in the Sue Dianne system area only (Fig. 3.6a). The Sue Dianne area subset was chosen for this analysis because of the larger number of samples (down-ice and background). For La and Th, samples collected down-ice from the Sue Dianne deposit have slightly higher values with near-total digestion compared to partial digestion results whereas the results for local background samples tend to fall slightly below the 1:1 ratio (Fig. 3.6a). This indicates that till samples collected down-ice of Sue Dianne contain resistant La and Th minerals, not affected by modified aqua regia. Alternatively, resistant mineral phases common to all samples may be more enriched in La and Th only in samples down-ice of Sue Dianne. The following analysis will test whether this difference in mineral association can be used to discriminate samples of interest better than single element concentrations.

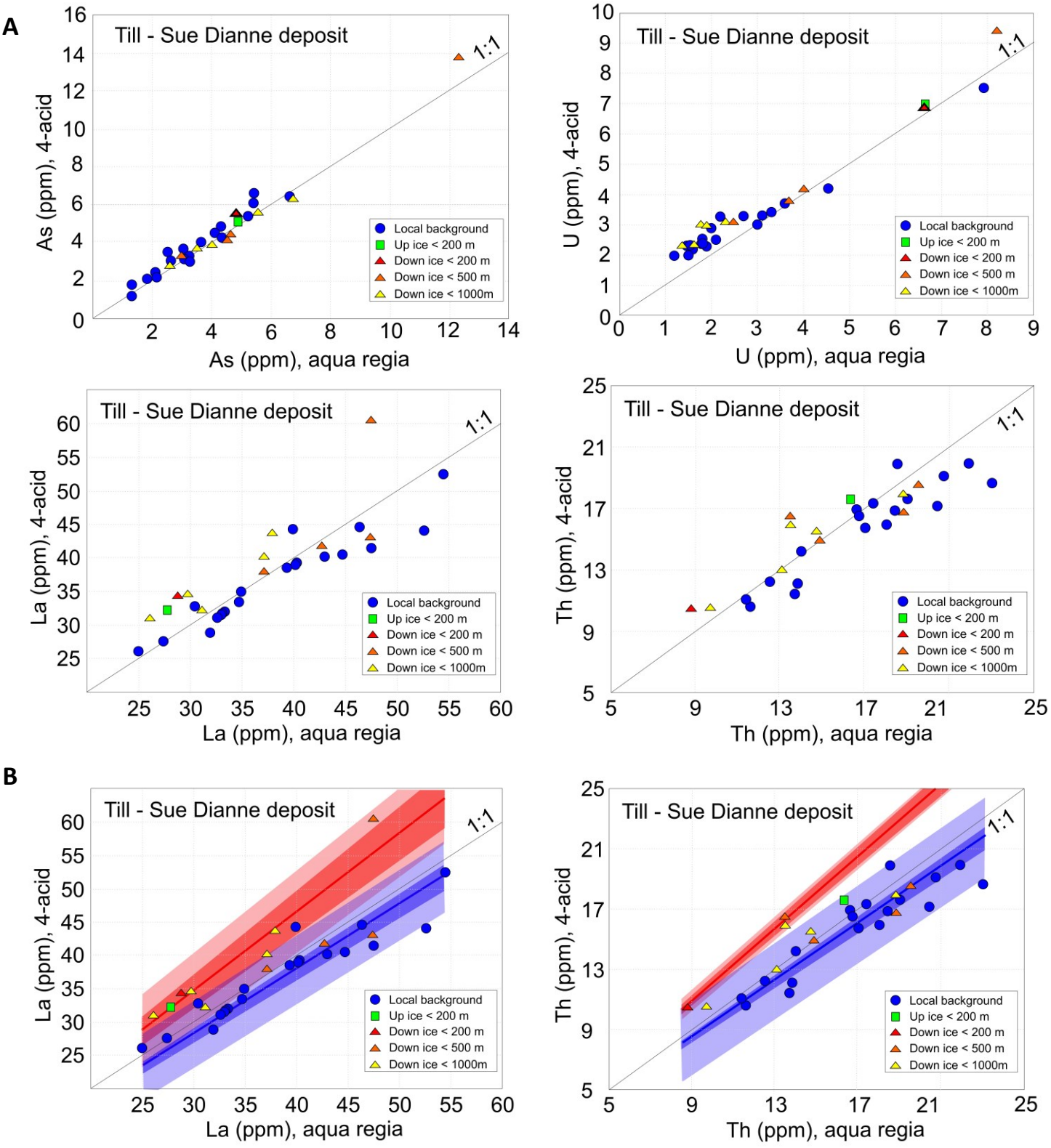

Figure 3.6: (**a**) Bi-plots of partial (modified aqua regia) digestion and near total digestion (4-acid) in the < 0.063 mm fraction of till samples collected in the Sue Dianne area for As, La, Th and U. (**b**) Mixture of regression models discriminating two sample populations based on linear regressions for La and Th (line: regression, dark envelope: 95% confidence interval, pale envelope: prediction band).

La and Th analytical results from the Sue Dianne system were submitted to a cluster-wise mixture of regression analysis (R package 'mixreg'; Turner, 2000) as a test for detecting mineralization. This technique presumes that a number of data distributions (e.g., La determined after a modified aqua regia digestion and La after a 4-acid digestion) are each composed of multiple unknown components 'mixed together' (e.g. La in till derived from altered and unaltered bedrock). This technique attempts to distinguish sub-populations by clustering samples based on their affinity to a bivariate relation (cluster-wise regression) using an iterative procedure with an arbitrary starting configuration of clusters (bootstrapping) (see Everitt and Hand (1981) and Titterington et al. (1985) for examples). This approach was chosen for; 1) its compliance with the present constraint of having both regressions based on a single predictor (partial digestion value), and 2) its low computational demands, originating from the sole use of linear regression models, allowing for step-wise covariance calculations necessary for the estimation of the confidence interval. The model was constrained to converge towards two regressions not allowed to intercept. Equality of variance between each sub-population was not presumed. Results are represented in Figure 3.6b. For both La and Th, one of the resulting output sub-populations has the following characteristics: 1) it contains a much smaller number of samples than the other, 2) its regression diverges from the 1 to 1 ratio, 3) it contains a smaller number of samples exclusively within its prediction bands (7 out of 23 for La and 3 out of 28 for Th), and 4) it contains few of the local background samples within the 95% confidence interval. This sub-population, identified by the model, might therefore be interpreted as successfully representing the samples affected by the Sue Dianne deposit geochemical signal, based on the bivariate relationship between the two digestion methods.

La and Th ratio maps better highlight the dispersal train down-ice of the Sue Dianne deposit (Fig. 3.7) in comparison with the scattered enrichments and/or depletions observed with the single elemental abundances, or with the Cu map (Fig. 3.5a). The ratio method for both La and Th, defines an anomalous zone extending 2.7 km southwest from the mineralized zone, i.e. down-ice along the last phase of ice movement. Background values have less variations; for example, samples outside the dispersal train with high La or Th abundance (Fig. 3.5b and c) are no longer anomalous (Fig. 3.7). Also of interest are samples 09MOB013 and 09MOB010 taken over the Marian River batholith less than 500 m apart, in which La and Th contents are variable but digestion ratios are similar, and both non anomalous. Sample 09MOB001 collected close but up-ice of the deposit shows a high La digestion ratio while the abundance was not anomalous.

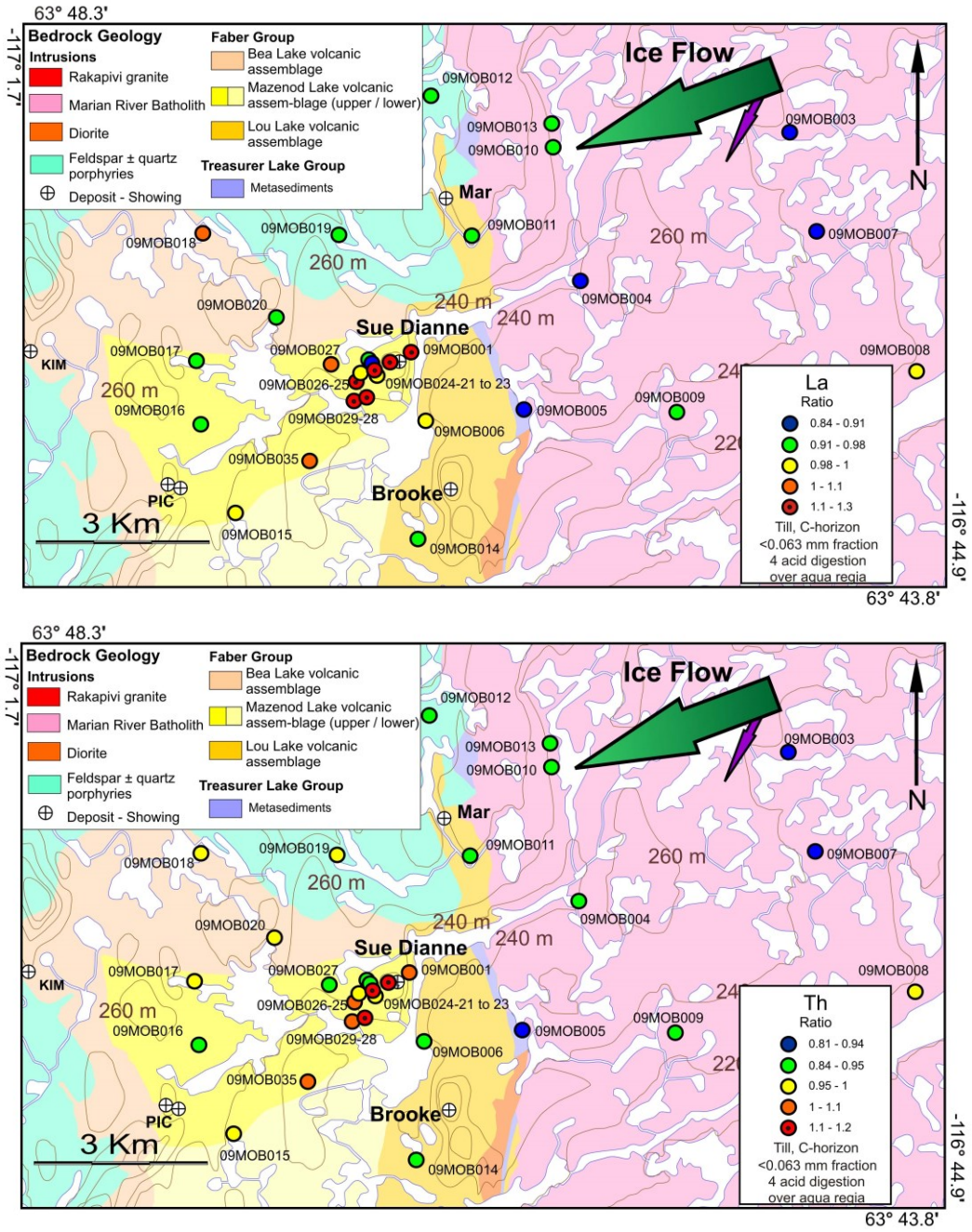

Figure 3.7: La and Th ratios of near total (4 acid) digestion concentrations over partial (modified aqua regia) digestion concentrations within the silt and clay-sized fraction (< 0.063 mm) of till C-horizon.

3.5. DISCUSSION

3.5.1. Elemental abundance in till associated with IOCG mineralization and IOAA systems

A number of elements (Na, K, Ca, Fe, Co, Ni, Cu, As, Mo, La, Yb, W, Bi, Th and U) have shown the potential to be influenced by the presence of IOCG mineralization and IOAA systems in the lithogeochemistry and to be reflected in the till geochemistry. This relation is not systematically visible through analysis of variance, but is reflected through the presence of anomalous elemental concentrations up to 2 km down-ice of the various deposits and showings examined in the GBMZ. Fe and Co through the near total digestion of the silt and clay-size fraction and Ni, Cu, As and Mo through the partial digestion of the clay-size fraction of till are the most consistently promising elements throughout the multiple IOCG mineralization and IOAA systems studied. Other elements of interest are sporadically found to be in anomalous concentrations in till related to some IOAA systems and IOCG deposits. These elements include La, Th and U through the near total digestion of the silt and clay-size fraction, W through the partial digestion of the silt and clay-size fraction and Bi through the partial digestion of the clay-size fraction. Of these, La and Th where not found to be systematically enriched in the mineralized bedrock samples but may be linked to the systems alteration halos as they may be remobilized by the IOAA metasomatism (Montreuil et al., 2013; Potter et al., 2013b*;* Acosta-Góngora et al., 2014).

Elements with vectoring potential to IOCG deposits and IOAA systems in till are highly variable throughout the GBMZ. High variability is also present between sampling sites in the individual dispersal trains mapped out from the Sue Dianne and Fab system areas. The vectoring capabilities of elemental abundance maps are therefore limited by the high geochemical

variability of the till. The large range of values observed in the lithogeochemical database suggests that the till geochemistry variability can be due to variability within the source bedrock.

The till matrix mineralogy also reflects variability between sampling sites as observed in previous results (Normandeau and McMartin, 2013). For example, the silt and clay fraction of selected till samples comprises 8 to 20 wt% k-feldspars, 15 to 36 wt% plagioclase, 1 to 7 wt% chlorite and 1 to 42 wt% clay minerals. The clay size fraction varies from containing trace amounts to 28 wt% k-feldspar, 1 to 37 wt% plagioclase and trace amounts to 25 wt% chlorite. While one of the major clay minerals in all samples is illite, illite content varies from trace amounts to 32 wt%.

3.5.2. Digestion method ratios in till with respect to the Sue Dianne IOCG deposit alterations

The relationship between partial and near total digestion results found in till samples collected down-ice of the Sue Dianne deposit can be used successfully as a discriminant factor through a cluster-wise regression analysis for La and Th, the main elements that show slightly distinct concentrations between the two digestion methods. The use of digestion method ratios (near total over partial digestion results) for La and Th provides means of better delineating the dispersal train from the Sue Dianne deposit with less variability than the use of single elemental abundance. Samples collected down-ice of the deposit systematically have higher ratios for these elements than in the local background samples in which the ratios approach one.

The main La and REE-bearing minerals at the Sue Dianne deposit are metasomatic apatite and allanite as well as minor monazite and britholite, while magmatic apatite is the main REE mineral in the barren and less altered host rocks (Lypaczewski et al., 2013; see Chapter 4 of this thesis: Normandeau et al., in press). Sue Dianne LREE enrichment in bedrock is associated

with the high and low temperature potassic-ferric/ferrous alteration and, and to a lesser extent, to the following low temperature calcic-ferric alteration (Camier, 2002; Montreuil et al., 2016b). REE remobilization from apatite to secondary phases such as monazite and/or allanite due to alkali rich fluid evolution has been described from laboratory experiment (Harlov and Förster, 2004; Harlov et al., 2005; Budzyń et al., 2011), documented in the IOAA Kiruna district (Harlov et al. 2002, 2007) and Bafq district (Bonyadi et al., 2011), and is currently under study at the Sue Dianne deposit (Montreuil et al., 2016b; Normandeau et al., in press). The efficiency of the La ratios at detecting mineralization likely results from REEs being hosted in mineral species more resistant to partial digestion (e.g. monazite and allanite) down-ice of the deposit. In till derived from barren and less altered rocks the REEs are more likely hosted in mineral susceptible to partial digestion (e.g., apatite). Therefore, a tentative association can be made between La digestion method ratio variations results and the potassic-ferric/ferrous as well as calcic-ferric/ferrous alteration phases at the Sue Dianne System where a high ratio in till samples would indicate altered source rocks. Th host minerals were not identified within the least altered host rocks at Sue Dianne, yet Th enrichment occurs during the low temperature calcic-ferric alteration and is associated with minor thorite and britholite (Camier, 2002; Lypaczewski et al., 2013; Ootes et al., 2010; Potter et al., 2013a,b; Acosta-Góngora et al., 2014; Montreuil et al., 2016b, Normandeau et al., in press). Th ratio variations might result from the calcic-ferric/ferrous stage only.

3.5.3. Limitations of the till geochemical method in the GBMZ

Several limitations to the application of the till geochemical method exist in the GBMZ. The presence of multiple outcropping mineralization throughout and/or close to the sampled areas at the Sue Dianne deposits and Fab system prevented the deposits/showings to act as single point sources for geochemical anomalies in till, and added complexity to the dispersal trains

interpretation. In addition, the non-uniform till distribution in the GBMZ also caused restrictions to sampling locations. The use of a digestion ratio mapping method suggested for the Sue Dianne deposit area remains to be tested around other deposits and showings. The low amount of samples in the Fab system area (n= 23) was insufficient to further test this potential vectoring tool. Bedrock alteration mapping related to IOCG and IOAA systems remains a challenge due of overprinting and retrograde alterations as well as the juxtaposition of alteration types (Corriveau et al., 2010b; Montreuil et al., 2015; Montreuil et al., 2016b). This complicates the elaboration of a relationship between a geochemical anomaly in till and a single type of alteration. Because of these limitations, it is difficult to identify single elements that can be used to evaluate proximity to IOCG alteration without resorting to bivariate relationships as demonstrated with La and Th digestion method ratios at the Sue Dianne deposit area.

3.7. CONCLUSIONS

Till near known mineralized zone throughout the GBMZ are commonly enriched in Fe, Co, Ni, Cu, As, Mo, Bi, La, Th, U and W. All investigated IOAA systems contain one or a combination of these elements in anomalous concentrations down-ice of outcropping mineralization, even in a context of low sampling density. The vectoring potential of till geochemistry in the GBMZ however, remains limited by the discontinuous till cover, the variability of elemental enrichments within IOA to IOCG mineralization as well as the complexity and size of the alteration systems.

The Sue Dianne deposit mineralization is enriched in Fe, Co, Cu, Mo, W, Bi and U as shown through the lithogeochemical analysis of mineralized samples versus barren samples. Of these elements, Fe and Co, through the near total digestion of the silt and clay-size fraction, and

Cu, Mo and Bi, through the partial digestion of the clay-size fraction of till, have the best potential to be used as vectors to mineralization.

The Fab system is enriched in Ca, As, La, Yb, Th, Cu and U as shown through the lithogeochemical analysis with respect to the GBMZ. Of the various anomalous values in the till geochemistry in the Fab system, only U, determined by the near total digestion of the silt and clay-size fraction, and Cu determined by the partial digestion of the clay-size fraction, concord with the lithogeochemical enrichments. However, Fe, Co, Mo, W, Ni and Bi in Fab system till may also sporadically be anomalous relative to the GBMZ background.

Na, Ca and K concentrations in till determined by the near total digestion of the silt and clay-size fraction are influenced by IOAA and IOCG alteration yet a systematic relation is elusive. La and Th ratios of near total digestion concentrations over partial digestion concentrations within the silt and clay-sized fraction of till provides the largest anomalous signal in the Sue Dianne deposit area, extending over 2.7 km southwest from the main mineralization, parallel to the last ice-flow movement. This ratio based method also provides insight into the potential direct transfer of a bedrock alteration signature into the till mineralogy. As such, the fine fraction of till in which La preferentially resides in minerals most resistant to acid digestion reflects potassic-ferric/ferrous as well as calcic-ferric/ferrous alteration. Further testing of the ratio method in more alteration systems is needed to assess its applicability to other deposits.

3.8. ACKNOWLEDGMENTS

This work stems from the Geomapping for Energy and Minerals (GEM) IOCG/Multiple Metals Great Bear Region project at the Geological Survey of Canada (GSC; Natural Resources Canada) conducted in partnership with the Wopmay Bedrock Mapping project of the Northwest Territories Geological Survey. The first author was funded by the Research Affiliate Program of Natural Resources Canada. Processing of till samples for grain size separation and geochemical analyses were supervised by Shauna Madore at the Sedimentology Laboratory of the GSC. Alain Plouffe provided comments and suggestions as part of the GSC internal review process. Thanks are due to Catherine Fontaine, Louis-Philippe Gélinas, Vincent Martel and Samuel Simard for astounding assistance in the field.

3.9. REFERENCES

Acosta-Góngora, G.P., Gleeson, S.A., Samson, I.M., Ootes, L. and Corriveau, L., 2014, Trace element geochemistry of magnetite and its relationship to Cu-Bi-Co-Au-Ag-UW mineralization in the Great Bear magmatic zone, NWT, Canada: Economic Geology, v. 109, p. 1901–1928.

Acosta-Góngora, G.P., Gleeson, S.A., Samson, I.M., Ootes, L. and Corriveau, L., 2015, Gold refining by bismuth melts in the iron oxide-dominated NICO Au-Co-Bi (±Cu±W) deposit, NWT, Canada: Economic Geology, v. 110, p. 291–314.

Aylsworth, J.M. and Shilts, W.W., 1989, Glacial features around the Keewatin ice divide: districts of Mackenzie and Keewatin: Geological Survey of Canada, Paper 88–24, 21 p.

Barton, M.D. and Johnson, D.A., 1996, Evaporitic-source model for igneous-related Fe oxide–(REE-Cu-Au-U) mineralization: Geology, v. 24, p. 259–262.

Barton, M.D. and Johnson, D.A., 2004, Footprints of Fe-oxide (Cu-Au) systems. Center for Global Metallogeny, University of Western Australia, Special Publication, v. 33, p. 112–116.

Benavides, J., Kyser, T.K., Clark, A.H., Stanley, C. and Oates, C., 2008a, Application of molar element ratio analysis of lag talus composite samples to the exploration for iron oxide–copper–gold mineralization: Mantoverde area, northern Chile: Geochemistry: Exploration, Environment, Analysis, v. 8, p. 369–380.

Benavides, J., Kyser, T.K., Clark, A.H., Stanley, C. and Oates, C., 2008b, Exploration guidelines for copper-rich iron oxide–copper–gold deposits in the Mantoverde area, northern Chile: the integration of host-rock molar element ratios and oxygen isotope compositions: Geochemistry: Exploration, Environment, Analysis, v. 8, p. 343–367.

Bonyadi, Z., Davidson, G.J., Mehrabi, B., Meffre, S. and Ghazban, F., 2011, Significance of apatite REE depletion and monazite inclusions in the brecciated Se–Chahun iron oxide–apatite deposit, Bafq district, Iran: Insights from paragenesis and geochemistry: Chemical Geology, v. 281, p. 253–269.

Budzyń, B., Harlov, D.E., Williams, M.L. and Jercinovic, M.J., 2011, Experimental determination of stability relations between monazite, fluorapatite, allanite, and REE-epidote as a function of pressure, temperature, and fluid composition: American Mineralogist, v. 96, p. 1547–1567.

Camier, W.J., 2002, The Sue-Dianne Fe-oxide Cu-Ag-Au breccia complex, southern Great Bear Magmatic Zone, Northwest Territories, Canada. University of Western Ontario, London, Ontario, 220 p.

Campbell, J. E., 2009, Drift prospecting for uranium in the Athabasca Basin, Saskatchewan, in R. C. Paulen and I. McMartin (eds), Application of till and stream sediment Heavy mineral and Geochemical Methods to Mineral Exploration in Western and Northern Canada; Geological Association of Canada, GAC short course Notes 18, p. 207–214.

Clark, C.D., 1993, Mega-scale glacial lineations and cross-cutting ice-flow landforms: Earth Surface Processes and Landforms, v. 18, p. 1–29.

Cole, D.R. and Rose, A.W., 1984, Distribution and mode of occurrence of zinc and lead in glacial soils: Journal of Geochemical Exploration, v. 20, p. 137–160.

Corriveau, L., 2007, Iron oxide-copper-gold deposits: a Canadian perspective, in Goodfellow, W.D., ed., Mineral deposits of Canada: a synthesis of major deposit-types, district metallogeny, the evolution of geological provinces and exploration methods: Geological Association of Canada, Mineral Deposit Division, Special Publication, v. 5, p. 307–328.

Corriveau, L., Lauzière, K., Montreuil, J.F., Potter, E., Hanes, R. and Prémont, S., 2015, Dataset of geochemical data from iron oxide alkali-altered mineralising systems of the Great Bear magmatic zone, Northwest Territories: Geological Survey of Canada, Open File 7643, 24 p.

Corriveau, L., Mumin, A.H. and Setterfield, T., 2010a, IOCG environments in Canada: Characteristics, geological vectors to ore and challenges, in Porter T.M., ed, Hydrothermal iron oxide copper-gold and related deposits: A global perspective volume 4-advances in understanding of IOCG deposits: Porter Geoscience Consultancy Publishing, Adelaide, p. 311–343.

Corriveau, L., Williams, P.J. and Mumin, A.H., 2010b, Alteration vectors to IOCG mineralization from uncharted terranes to deposits, in Corriveau, L., and Mumin, A.H., eds., Exploring for iron oxide copper-gold deposits. Geological Association of Canada, Short Course Notes Volume 20, p. 89–110.

DeToni, A.F., 2016, Systèmes à oxydes de fer et alterations en élémeents alcalins, zone magmatic du Grand Lac de l'Ours. Unpublished Master's thesis, Université du Québec, Institut national de la Recherche scientifique, Centre – Eau Terre Environnement, 738 p.

Dolezal, J., Povondra, P. and Sulcek, Z., 1968, Decomposition Techniques in Inorganic Analysis. American Elsevier Publishing Company Inc, New York, 224 p.

Dreimanis, A. and Vagners, U., 1971, The dependence of the composition of till upon the rule of bimodal composition. VII International Conference, Études sur le Quaternaire dans le Monde 2. INQUA, Paris, p. 787–789.

Dunn, O.J., 1964, Multiple comparisons using rank sums: Technometrics, v. 6, p. 241–252.

Dyke, A.S., 2004, An outline of North American deglaciation with emphasis on central and northern Canada: Developments in Quaternary Sciences, v. 2, p. 373–424.

Dyke, A.S. and Dredge, L., 1989, Quaternary geology of the northwestern Canadian Shield. In Chapter 3 of Quaternary Geology of Canada and Greenland. (eds) R.J. Fulton: Geological Survey of Canada, Geology of Canada, v. 1, p.189–214.

Dyke, A.S., Moore, A. and Robertson, L., 2003, Deglaciation of North America: Geological Survey of Canada, 2 Sheets, 1:30,000,000 scale.

Dyke, A.S. and Prest, V.K., 1987, Late Wisconsinan and Holocene history of the Laurentide ice sheet: Géographie physique et Quaternaire, v. 41, p. 237–263.

Everitt, B.S. and Hand, D.J., 1981, Finite mixture distributions. Monographs on applied probability and statistics. Chapman and Hall, London, New York. 85 p.

Fabris, A.J., Halley, S., Van Der Wilen, S., Keeping, T. and Gordon, G., 2013, IOCG-style mineralisation in the central eastern Gawler Craton, SA; characterisation of alteration, geochemical associations and exploration vectors. Department of Innovation, Manufacturing, Trade, Resources and Energy, South Australia, Adelaide, Report Book 2013/00014.

Fabris, A.J., Van Der Wilen, S., Keeping, T. and Gordon, G., 2015, Geochemical Footprint of IOCG Deposits Beneath Thick Cover: Insights From The Olympic Cu-Au Province, South Australia. 27th International Applied Geochemistry Symposium, April 20–24, 2015.

Foster, J.R., 1973, The efficiency of various digestion procedures on the extraction of metals from rocks and rock forming minerals. Canadian Institute of Mining Bulletin, 66, p. 85–92.

Fulton, R.J.C., 1995, Surficial materials of Canada: Geological Survey of Canada, Map 1880A, 1:5 000 000 scale.

Gandhi, S.S., 1988, Volcano-plutonic setting of U-Cu bearing magnetite veins of FAB claims, southern Great Bear magmatic zone, Northwest Territories: in Current Research, Part C, Geological Survey of Canada, Paper 88-1C, p. 177–188.

Gandhi, S.S., Potter, E.G. and Fayek, M., 2013, Polymetallic U-Ag veins at Port Radium, Great Bear magmatic zone, Canada: Main botryoidal pitchblende stage cuts 1.74 Ga diabase dykes and has REE signatures diagnostic of unconformity-type deposits: Geological Survey of Canada, Open File 7493, 1 p.

Gandhi, S.S., Prasad, N. and Charbonneau, B., 1996, Geological and geophysical signatures of a large polymetallic exploration target at Lou Lake, southern Great Bear magmatic zone, Northwest Territories: Geological survey of Canada, Current Research Paper, p. 147–158.

Garrett, R.G., 2012, The GSC Applied Geochemistry EDA Package. Version 1.12. https://cran.r-project.org/package=rgr

Garrett, R.G., 2013, The 'rgr'package for the R Open Source statistical computing and graphics environment-a tool to support geochemical data interpretation: Geochemistry: Exploration, Environment, Analysis, v. 13, p. 355–378.

Gibbons, J., 1976, Nonparametric Methods for Quantitative Analysis. Holt, Rinehart and Winston, New York, 463 p.

Goad, R.E., Mumin, A.H., Duke, N., Neale, K. and Mulligan, D., 2000a, Geology of the Proterozoic iron oxide-hosted, NICO cobalt-gold-bismuth, and Sue Dianne copper-silver deposits, southern Great Bear magmatic zone, Northwest Territories, Canada. In Porter T.M. ed, Hydrothermal iron oxide copper-gold and related deposits a global perspective volume 1: Porter Geoscience Consultancy Publishing, Adelaide, p. 249–268.

Goad, R.E., Mumin, A.H., Duke, N., Neale, K.L., Mulligan, D.L. and Camier, W.J., 2000b, The NICO and Sue-Dianne Proterozoic, iron oxide-hosted, polymetallic deposits, Northwest Territories: Application of the Olympic Dam model in exploration: Exploration and Mining Geology, v. 9, p. 123–140.

Grunsky, E.C., 2010, The interpretation of geochemical survey data: Geochemistry: Exploration, Environment, Analysis, v. 10, p. 27–74.

Harlov, D.E., Andersson, U.B., Förster, H.-J., Nyström, J.O., Dulski, P. and Broman, C., 2002, Apatite–monazite relations in the Kiirunavaara magnetite–apatite ore, northern Sweden: Chemical Geology, v. 191, p. 47–72.

Harlov, D.E. and Förster, H.-J., 2004, Fluid-induced nucleation of (Y+ REE)-phosphate minerals within apatite: Nature and experiment. Part II. Fluorapatite: American Mineralogist, v. 88, p. 1209–1229.

Harlov, D.E., Wirth, R. and Förster, H.-J., 2005, An experimental study of dissolution–reprecipitation in fluorapatite: fluid infiltration and the formation of monazite: Contributions to Mineralogy and Petrology, v. 150, p. 268–286.

Harlov, D.E., Wirth, R. and Hetherington, C.J., 2007, The relative stability of monazite and huttonite at 300–900 C and 200–1000 MPa: metasomatism and the propagation of metastable mineral phases: American Mineralogist, v. 92, p. 1652–1664.

Hashmi, S., Ward, B.C., Plouffe, A., Leybourne, M.I., and Ferbey, T., 2015, Geochemical and mineralogical dispersal in till from the Mount Polley Cu-Au porphyry deposit, central British Columbia, Canada. Geochemistry: Exploration, Environment, Analysis, v. 15, p. 234–249.

Hildebrand, R.S., Hoffman, P.F. and Bowring, S.A., 1987, Tectono-magmatic evolution of the 1.9-Ga Great Bear magmatic zone, Wopmay Orogen, northwestern Canada: Journal of Volcanology and Geothermal Research, v. 32, p. 99–118.

Hildebrand, R.S., Hoffman, P.F. and Bowring, S.A., 2010, The Calderian orogeny in Wopmay orogen (1.9 Ga), northwestern Canadian Shield: Geological Society of America Bulletin, v. 122, p. 794–814.

Hitzman, M.W., Oreskes, N. and Einaudi, M.T., 1992, Geological characteristics and tectonic setting of proterozoic iron oxide (Cu + U + Au + REE) deposits: Precambrian Research, v. 58, p. 241–287.

Hollander, M., Wolfe, D.A. and Chicken, E., 2013, Nonparametric statistical methods. John Wiley & Sons, 828 p.

Jackson, V.A., 2006, Preliminary geologic map of part of the southern Wopmay Orogen (parts of NTS 86B and 86C); descriptive notes to accompany 1:100,000 scale map; Northwest Territories Geoscience Office, Yellowknife, NT: NWT Open Report 2006-004, 1 map, scale 1:100,000, and accompanying report, 41 p.

Jackson, V.A., 2008, Preliminary geologic map of part of the southern Wopmay Orogen (parts of NTS 86B and 86C; 2007 updates); descriptive notes to accompany 1:100 000 scale map: Northwest Territories Geoscience Office, NWT Open Report 2008–007.

Jackson, V.A. and Ootes, L., 2010, Preliminary geologic map of the south-central Wopmay orogen (parts of NTS 86B, 86C, and 86D); results from 2009: Northwest Territories Geoscience Office, NWT Open Report 2010–004.

Jackson, V.A., van Breemen, O., Ootes, L., Bleeker, W., Bennett, V., Davis, W.J., Ketchum, J., Smar, L. & McFarlane, C., 2013, U–Pb zircon ages and field relationships of Archean basement and Proterozoic intrusions, south-central Wopmay Orogen, NWT: implications for tectonic assignments 1, 2: Canadian Journal of Earth Sciences, v. 50, p. 979–1006.

Kaszycki, C.A., Nielsen, E. and Gobert, G., 1996, Surficial geochemistry and response to volcanic-hosted massive sulphide mineralization in the Snow Lake region. In: Bonham-Carter, G.F., Galley, A.G. & Hall, G.E.M. (eds) Extech I: A Multidisciplinary approach to massive sulphide research in the Rusty Lake-Snow Lake greenstone belts: Manitoba. Geological Survey of Canada, Bulletin, v. 426, p. 139–154.

Klassen, R., 2003, The geochemical and physical properties of till, Bathurst Mining Camp, New Brunswick, Canada. Massive Sulfide Deposits of the Bathurst Mining Camp, New Brunswick, and Northern Maine: Economic Geology Monograph, v. 11, p. 661–678.

Klassen, R.A., 2001a, The interpretation of background variation in regional geochemical surveys–an example from Nunavut, Canada: Geochemistry: Exploration, Environment, Analysis, v. 1, p. 163–173.

Klassen, R.A., 2001b, A Quaternary geological perpective on geochemical exploration in glaciated terrain: Geological Society, London, Special Publications, v. 185, p. 1–17.

Kloke, J.D. and McKean, J.W., 2012, Rfit: Rank-based estimation for linear models: The R Journal, v. 4, p. 57–64.

Koljonen, T. and Malisa, E., 1991, Solubility in aqua regia of selected chemical elements occurring in the fine fraction of till, in Pulkkinen, E., ed., Environmental geochemistry in northern Europe: Geological Survey of Finland, Special Paper 9, p. 49–52.

Kruskal, W.H. and Wallis, W.A., 1952, Use of ranks on one-criterion variance analysis: Journal of the American Statistical Association, v. 47, p. 583–621.

Lahtinen, R., Lestinen, P. and Savolainen, H., 1993, The use of total and partial dissolution till geochemical data in delineating favourable areas for Ni prospects: an example from the Tampere– Hämeenlinna area, southern Finland: Geological Survey of Finland, Special Paper 18, p. 101–111.

Lehtonen, M., Marmo, J., Nissinen, A., Johanson, B. and Pakkanen, L., 2005, Glacial dispersal studies using indicator minerals and till geochemistry around two eastern Finland kimberlites: Journal of Geochemical Exploration, v. 87, p. 19–43.

Lemmen, D.S., Duk-Rodkin, A. and Bednarski, J.M., 1994, Late glacial drainage systems along the northwestern margin of the Laurentide Ice Sheet: Quaternary Science Reviews, v. 13, p. 805–828.

Levson, V.M., 2002, Quaternary geology and till geochemistry of the Babine Porphyry Copper Belt, British Columbia (NTS 93 L/9,16, M/1, 2, 7, 8); British Columbia Ministry of Energy and Mines, and Petroleum Resources, Victoria, B.C., Bulletin 110, 278 p.

Lypaczewski, P., Normandeau, P.X., Paquette, J. and McMartin, I., 2013, Petrographic and cathodoluminescence characterization of apatite from the Sue-Dianne and Brooke Zone IOCG mineralization systems, Great Bear magmatic zone, Northwest Territories, Canada: Geological Survey of Canada, Open File 7319, 18 p.

Mäkinen, J., 1995, Effects of grinding and chemical factors on the generation and composition of the till fine fraction: an experimental study: Journal of Geochemical Exploration, v. 54, p. 49–62.

McClenaghan, M.B., 1994, Till geochemistry in areas of thick drift and its application to gold exploration, Matheson area, northeastern Ontario: Exploration and Mining Geology, v. 3, p. 17–30.

McClenaghan, M.B., Thorleifson, L.H. and DiLabio, R.N.W., 2000, Till geochemical and indicator mineral methods in mineral exploration: Ore Geology Reviews, v. 16, p. 145–166.

McClenaghan, M.B. and Kjarsgaard, B.A., 2001, Indicator mineral and geochemical methods for diamond exploration in glaciated terrain in Canada: Geological Society, London, Special Publications, v. 185, p. 83–123.

McClenaghan, M.B., Layton-Matthews, D. and Matile, G., 2011, Till geochemical signatures of magmatic Ni–Cu deposits, Thompson Nickel Belt, Manitoba, Canada: Geochemistry: Exploration, Environment, Analysis, v. 11, p. 145–159.

McClenaghan, M.B., Plouffe, A., McMartin, I., Campbell, J.E., Spirito, W.A., Paulen, R.C., Garrett, R.G. & Hall, G.E.M., 2013, Till sampling and geochemical analytical protocols used by the Geological Survey of Canada: Geochemistry: Exploration, Environment, Analysis, v. 13, p. 285–301.

McClenaghan, M. and Peter, J., 2016, Till geochemical signatures of volcanogenic massive sulphide deposits: an overview of Canadian examples: Geochemistry: Exploration, Environment, Analysis, v. 1, p. 27–47.

McMartin, I., Corriveau, L. and Beaudoin, G., 2009, Heavy mineral and till geochemical signatures of the NICO Co-Au-Bi deposit, Great Bear magmatic zone, Northwest Territories, Canada; in Lentz, D.R., Thorne, K.G. and Beal, K.-L. (eds). Proceedings, 24th International Applied Geochemistry Symposium (IAGS 2009), Fredericton, New Brunswick, 555–556.

McMartin, I., Corriveau, L. and Beaudoin, G., 2011a, An orientation study of the heavy mineral signature of the NICO Co-Au-Bi deposit, Great Bear magmatic zone, NW Territories, Canada: Geochemistry: Exploration, Environment, Analysis, v. 11, p. 293–307.

McMartin, I., Corriveau, L., Beaudoin, G., Averill, S. and Kjarsgaard, I., 2011b, Results from an orientation study of the heavy mineral and till geochemical signatures of the NICO Co-Au-Bi deposit, Great Bear magmatic zone, Northwest Territories, Canada: Geological Survey of Canada, Open File 6723, 23 p.

McMartin, I., Dredge, L.A., Grunsky, E.C. and Pehrsson, S., 2016, Till geochemistry in west-central Manitoba: interpretation of provenance and mineralization based on glacial history and multivariate data analysis: Economic Geology. v. 111, p. 1001–1020.

Montreuil, J.-F., Corriveau, L. and Potter, E.G., 2015, Formation of albitite-hosted uranium within IOCG systems: the Southern Breccia, Great Bear magmatic zone, Northwest Territories, Canada: Mineralium Deposita, v. 50, p. 293–325.

Montreuil, J.F., Corriveau, L. and Grunsky, E., 2013, Compositional data analysis of hydrothermal alteration in IOCG systems, Great Bear magmatic zone, Canada: to each alteration type its own geochemical signature: Geochemistry: Exploration, Environment, Analysis, v. 13, p. 229–247.

Montreuil, J.F., Potter, E.G., Corriveau, L. and Davis, W.J., 2016a, Element mobility patterns in magnetite-group IOCG systems: The FAb IOCG system, Northwest Territories, Canada: Ore Geology Reviews, v. 72, p. 562–584.

Montreuil, J.F., Corriveau, L. and Potter, E.G., 2016b, On the relation between alteration signature and metal endowment of iron oxide alkali altered systems, southern Great Bear magmatic zone (Canada). In A Special Issue Devoted to Proterozoic Iron Oxide-Apatite-(+REE) and Iron Oxide-Copper-Gold and Affiliated Deposits of Southeast Missouri, USA, and the Great Bear Magmatic Zone, Northwest Territories, Canada (Slack, J. F., Corriveau, L. & Hitzman, M. W.): Economic Geology, v. 111, p. 1803–1814.

Mumin, A.H., 2015, Echo Bay IOCG thematic map series: geology, structure and hydrothermal alteration of a stratovolcano complex, Northwest Territories, Canada: Geological Survey of Canada, Open File 7807, 19 p.

Mumin, A.H., Corriveau, L., Somarin, A. and Ootes, L., 2007, Iron oxide copper-gold-type polymetallic mineralization in the Contact Lake belt, Great Bear magmatic zone, Northwest Territories, Canada: Exploration and Mining Geology, v. 16, p. 187–208.

Mumin, A.H., Somarin, A.K., Jones, B., Corriveau, L., Ootes, L. and Camier, W.J., 2010, The IOCG-porphyry-epithermal continuum in the Great Bear Magmatic Zone, Northwest Territories, Canada. in Corriveau, L., Mumin, H. (eds). Exploring for Iron-Oxide Copper-Gold deposits: Canada and global analogues. Geological Association of Canada, Short Course Notes Volume 20, p. 59–78.

Niskavaara, H., 1995, A comprehensive scheme of analysis for soils, sediments, humus and plant samples using inductively coupled plasma atomic emission spectrometry (ICP-AES): Current Research. Geological Survey of Finland, Special Paper 20, p. 167–175.

Normandeau, P.X. and McMartin, I., 2013, Composition of till and bedrock across the Great Bearmagmatic zone: Quaternary field database and analytical results from the GEM IOCG-Great Bear Project: Geological Survey of Canada, Open File 7307, 26 p.

Normandeau, P.X., McMartin, I., Paquette, J. and Corriveau, L., 2011, Drift prospecting applied to iron oxide copper gold exploration in the Great Bear Magmatic Zone, Northwest Territories, Canada. Geological Association of Canada-Mineralogical Association of Canada, Joint Annual Meeting, Ottawa, Ontario, p. 154.

Normandeau, P.X., Harlov, D.E., Corriveau, L., Paquette, J., McMartin, I., in press, Characterization of fluorapatite within iron oxide alkali-calcic alteration systems of the Great Bear magmatic zone: a potential metasomatic process record: The Canadian Mineralogist.

Ootes, L., Goff, S., Jackson, V.A., Gleeson, S.A., Creaser, R.A., Samson, I.M., Evensen, N., Corriveau, L. & Mumin, A.H., 2010, Timing and thermochemical constraints on multi-element mineralisation at the Nori/RA Cu–Mo–U prospect, Great Bear magmatic zone, Northwest Territories, Canada: Mineralium Deposita, v. 45, p. 549–566.

Paulen, R.C. and McMartin, I., 2009, Application of till and stream sediment Heavy mineral and Geochemical Methods to Mineral Exploration in Western and Northern Canada. Geological Association of Canada, Short Course Notes 18, 222 p.

Peuraniemi, V., Aario, R. and Pulkkinen, P., 1997, Mineralogy and geochemistry of the clay fraction of till in northern Finland: Sedimentary Geology, v. 111, p. 313–327.

Porter, T., 2010, Current understanding of iron oxide associated-alkali altered mineralized systems: Part 1- An overview; Part 2 –A review, in Porter, T.M., ed., Hydrothermal iron oxide copper-gold and related deposits: A global perspective, v. 3, p. 5–106.

Potter, E.G., Corriveau, L., and Montreuil, J.-F., 2013a, Iron oxide-copper-gold ±uranium in the Great Bear Magmatic Zone: Nature of uranium in IOCG systems: Geological Survey of Canada, Open File 7254, 1 p.

Potter, E.G., Montreuil, J.-F., and DeToni, A., 2013b, Geology and hydrothermal alteration of the Fab Lake region, Northwest Territories: Geological Survey of Canada, Open File 7339, 27 p.

Prest, V.K., Grant, D.R. and Rampton, V.N., 1968, Glacial Map of Canada: Geological Survey of Canada, Map 1253A. 1: 5 000 000 scale.

R_Project, 2016, The R Project for Statistical Computing, https://www.r-project.org/.

Reimann, C., Filzmoser, P., Garrett, R. and Dutter, R.. 2008, Statistical Data Analysis Explained: Applied Environmental Statistics with R. John Wiley and Sons, Ltd., 362 p.

Reimann, C., Filzmoser, P, and Garrett, R.G., 2005, Background and threshold: critical comparison of methods of determination: Science of the Total Environment, v. 346, p. 1–16.

Reimann, C. and Garrett, R.G., 2005, Geochemical background - Concept and reality: Science of the Total Environment, v. 350, p. 12–27.

Sanford, R.F., Pierson, C.T. and Crovelli, R.A., 1993, An objective replacement method for censored geochemical data: Mathematical geology, v. 25, p. 59–80.

Sappin, A.A., Dupuis, C., Beaudoin, G., McMartin, I. and McClenaghan, M.B., 2014, Optimal ferromagnetic fraction representative of iron oxide compositional variations in till samples along ice-flow paths: Case studies from the Sue-Dianne IOCG and Thompson magmatic Ni-Cu deposits, Canada: Geochemistry: Exploration, Environment, Analysis.v. 14, p. 315–329

Shilts, W.W., 1975, Principles of geochemical exploration for sulphide deposits using shallow samples of glacial drift. Canadian Institute of Mining and Metallurgy Bulletin, v. 68, p. 73–80.

Shilts, W.W., 1996, Drift exploration, in Menzies, J., ed., Glacial environments, sediment forms and techniques: Butterworth Heinemann Ltd., p. 411–439.

Smith, D.G., 1994, Glacial Lake McConnell: paleogeography, age, duration, and associated river deltas, Mackenzie River basin, western Canada: Quaternary Science Reviews, v. 13, p. 829–843.

Snäll, S. and Liljefors, T., 2000, Leachability of major elements from minerals in strong acids: Journal of Geochemical Exploration, v. 71, p. 1–12.

Spirito, W., McClenaghan, M.B., Plouffe, A., McMartin, I., Campbell, A.R., Paulen, R.C., Garrett, R.G. & Hall, G.E.M., 2011, Till sampling and analytical protocols for GEM projects: from field to archive: Geological Survey of Canada, Open File 6850, 85 p.

Tarvainen, T., 1995, The geochemical correlation between coarse and fine fractions of till in southern Finland: Journal of Geochemical Exploration, v. 54, p. 187–198.

Titterington, D.M., Smith, A.F. and Makov, U.E., 1985, Statistical analysis of finite mixture distributions. Wiley New York, 243 p.

Tukey, J.W., 1977, Exploratory Data Analysis. Addison-Wesley Publishing Compagny, 688 p.

Turner, T.R., 2000, Estimating the propagation rate of a viral infection of potato plants via mixtures of regressions. Journal of the Royal Statistical Society: Series C (Applied Statistics), v. 49, p. 371–384.

Wiken, E.B., 1986, Terrestrial Ecozones of Canada. Ecological Land Classification; Series No. 19, Environment Canada. Hull, Quebec, 26 p.

Williams, P.J., Barton, M.D., Johnson, D.A., Fontboté, L., De Haller, A., Mark, G., Oliver, N.H.S. & Marschik, R., 2005, Iron oxide copper-gold deposits: geology, space-time distribution, and possible modes of origin: Economic Geology, p. 371–405.

RATIONALE OF CHAPTER 4

Vectors towards IOA to IOCG mineralization and IOAA systems within the till matrix geochemistry were sought in Chapter 3. Despite limitations, mainly due to the complexity and variability of the studied systems, Fe, Co, Ni, Cu, As, Mo, Bi, La, Th, U and W were established as common potential vector elements to mineralization within the GBMZ. Specifically La and Th ratios of near total digestion concentrations to partial digestion concentrations were used to target the alteration halo of the Sue Dianne deposit. As such, these ratios may offer more consistent anomalies and larger targets provided that they can be further tested in other systems with higher sample density. The following two chapters consist of an apatite study to establish the potential of this mineral as a vector towards the IOA to IOCG mineralization and alteration systems of the GBMZ. Chapter 4 describes the results and interpretations of investigation of apatite in bedrock samples. The investigation makes use of microprobe geochemical characterizations of apatite grains from disaggregated bedrock samples included in the Open File report of Chapter 2 as well as laser ablation supplementary data included in Appendix 2. Additional microprobe results from GBMZ samples were provided by co-author Dr. Daniel Harlov (University of Johannesburg). This chapter was recently accepted for publication in The Canadian Mineralogist and is currently in press.

CHAPTER 4: Characterization of fluorapatite within iron oxide alkali alteration systems of the Great Bear magmatic zone: A potential metasomatic process record

4.1. ABSTRACT

Fluorapatite-amphibole-magnetite assemblages are a signature alteration product in iron oxide alkali-alteration (IOAA) systems that can host iron oxide-apatite (IOA) and iron oxide Cu-Au (IOCG) deposits. The distinct fluorapatite chemistry that evolves within these systems can record metasomatic processes within IOA and IOCG deposits. Rare-earth element (REE)-rich fluorapatite forms during high temperature sodic-calcic-ferric/ferrous and calcic-ferric/ferrous metasomatism. As temperature declines and the fluid chemistry evolves, localized REE leaching takes place within fluorapatite and leads to secondary allanite and monazite crystallization. Such processes have been observed experimentally and inferred in IOA deposits (*e.g.*, Kiruna district in Sweden, Bafq district in Iran). In the present study, fluorapatite grains in thin section and hand-picked from disaggregated bedrock samples from a series of areas including the Fab system, Brooke Zone, Mag Hill, the JLD showing, the Terra mine and the Dennis showing from the Great Bear magmatic zone (GBMZ, Northwest Territories, Canada) are examined. Dark irregular zones observed under scanning-electron microscope backscattered images have lower REE contents when measured using electron probe microanalyzer and/or laser ablation inductively coupled plasma mass spectrometry. REE remobilization and precipitation of secondary allanite and monazite during metasomatic alteration of the fluorapatite is inferred based on petrographic evidence and dissolution pits in the REE-depleted zones of fluorapatite. Allanite is the most common secondary REE-rich phase and can be explained by the

predominance of calcic alteration during the low temperature stage alteration. Fluorapatite grains with Mn content above 500 ppm and where LREE leaching occurred have green or green to yellow cathodoluminescence responses. Single grains of fluorapatite also record an atypical decoupling of U and Th interpreted to be caused by potassic-ferric/ferrous alteration. This metasomatism leads to fluorapatite grains with localized increases in Th content near fractures and edges (*e.g.* from ~50 to ~1000 ppm). The identification of these textural characteristics, geochemical signatures, and cathodoluminescence responses in fluorapatite from the systems covered by this study is a significant first step in the development of an indicator mineral exploration method in prospecting IOA and IOCG deposits in the GBMZ.

4.2. INTRODUCTION

Fluorapatite is an ubiquitous accessory mineral (Hughes and Rakovan, 2002; Pan and Fleet, 2002; Piccoli and Candela, 2002; Hughes and Rakovan 2015) and is present as a major mineral in iron oxide-apatite (IOA) and as a minor accessory mineral in iron oxide-copper-gold (IOCG) deposits worldwide (*e.g.*, Benavides et al., 2007; Mumin et al., 2010; Rusk et al., 2010; Lypaczewski et al., 2013; Krneta et al., 2015; DeToni, 2016). IOA deposits, otherwise known as Kiruna-type magnetite-apatite deposits, include Kirunavaara and other deposits of the Norrbotten region, northern Sweden (Frietsch and Perdahl, 1995; Nyström and Henriquez, 1989, 1994; Harlov et al., 2002; Edfelt et al., 2005; Westhues et al., 2016), Grängesberg ore body, central Sweden (Jonsson et al., 2016), the Great Bear magmatic zone (GBMZ) of northern Canada (Hildebrand, 1986; Montreuil et al., 2013, 2015, 2016a, 2016b; Corriveau et al., 2016), Pea Ridge, Missouri, USA (Aleinikoff et al., 2016; Harlov et al., 2016; Hofstra et al., 2016; Johnson et al., 2016), Yangtze river valley, southeastern China (Mao et al., 2011; Hu et al., 2014), and the Bafq district of Iran (Torab and Lehmann, 2007; Daliran et al., 2010; Bonyadi et al., 2011).

The structure of fluorapatite can accommodate a large number of trace to major elements via a variety of substitutions (Pan and Fleet, 2002; Hughes and Rakovan, 2015). Commonly, the rare-earth elements (REE^{3+}) may substitute for Ca^{2+} in two distinct sites (M1 and M2) via a series of coupled substitution reactions, most importantly $Na^{+} + REE^{3+} \Leftrightarrow 2Ca^{2+}$, and $Si^{4+} + REE^{3+} \Leftrightarrow P^{5+} + Ca^{2+}$ (Hughes et al., 1991; Fleet and Pan, 1997, 1995; Pan and Fleet, 2002), though other less common charge-balance mechanisms are also possible such as $2(Mg, Mn, Fe)^{2+} + REE^{3+} \Leftrightarrow P^{5+} + Ca^{2+}$ (Bonyadi et al., 2011; see also Pan and Fleet, 2002).

Characterization of natural apatite and experimental studies have demonstrated the ability of this mineral to record geochemical conditions during crystallization and subsequent metasomatic alteration (Harlov et al., 2002, 2003, 2005, 2007; Bouzari et al., 2011; Budzyń et al., 2011; Harlov, 2015). These studies have identified that fluid chemistry, rather than pressure, temperature, or the original apatite composition, is the major controlling factor for the REE remobilization associated with apatite metasomatism. This metasomatism is responsible for irregular compositional zonation visible in backscattered electron (BSE) or cathodoluminescence (CL) images, dissolution pits preferentially aligned with the c axis of fluorapatite grains and the presence of REE-bearing mineral inclusions such as monazite, xenotime, allanite, REE-fluorides, and REE-carbonatites within the apatite or associated with the fluorapatite.

The present study describes and interprets the textural and compositional variations of fluorapatite within six selected iron oxide alkali-alteration (IOAA) systems from the GBMZ. By doing so, this study provides insight into the relationship between the fluid-rock interaction responsible for the relative stability of monazite versus allanite within these systems as well as the remobilization of U and Th resulting from metasomatism. This study also emphasizes

utilizing CL to characterize natural fluorapatite as record of metasomatic process (*e.g.*, Harlov et al., 2002; Dempster, et al., 2003; Harlov and Förster, 2004; Bonyadi et al., 2011; Mao et al., 2015; Zirner et al., 2015; Harlov, 2015).

4.3. GEOLOGICAL SETTING

4.3.1. Great Bear magmatic zone

The Great Bear magmatic zone (GBMZ) (Fig. 4.1) is a volcanic and plutonic felsic to intermediate Andean type calc-alkaline belt (Hildebrand et al., 1987, 2010) that formed subsequently to the Calderian Orogeny responsible for the Wopmay Orogen (1.88 Ga; Hildebrand et al., 2010; Jackson et al., 2013). It is exposed between the western margin of the Slave Craton to the east and a Phanerozoic cover to the west. The GBMZ is host to many past producing U and Ag deposits resulting from broad IOAA metasomatic systems (Mumin et al., 2010; Gandhi et al., 2013). IOAA systems from the GBMZ have been the subject of recent petrological, mineral chemistry, geochemical, geochronological, isotopic, and economic geology studies that offer a context for this study (*e.g.*, Mumin et al., 2007, 2010; Corriveau et al., 2010a, 2010b, 2016; Acosta-Góngora et al., 2014, 2015; Montreuil et al., 2013, 2015, 2016a, 2016b; Potter et al., 2013a, 2013b;DeToni, 2016).

The GBMZ IOAA zones are framed into a model of prograde, metasomatic facies that provides a link with the genesis of GBMZ ores (Corriveau et al., 2010a, 2010b, 2016). Overprinted prograde and retrograde alterations, as well as the juxtaposition of alteration types, increase with proximity to the ore zones (Corriveau et al., 2010b; Montreuil et al., 2015, 2016b). Unaltered rocks in the GBMZ are rare due to the extent and the intensity of the alteration systems, which

often exceed 300 km^2 in surface area (Barton and Johnson, 2004; Mumin et al., 2007, 2010, Porter, 2010; Mumin, 2015). The most common protoliths are supracrustal rocks and porphyritic sub-volcanic intrusions. The least altered protoliths are hypabyssal intrusions, which are the only rocks for which chemical changes, induced by fluid-rock interaction, can be quantified by mass-balance calculations (Montreuil et al., 2016b). Late, polyphase granitic intrusions were emplaced throughout the GBMZ after major regional scale metasomatism (Hildebrand et al., 2010). Local metasomatism took place proximal to and within those granitic intrusions during emplacement. The present study is based on samples from deposits and prospective localities from six IOAA systems in the GBMZ and on samples from the least altered granitic rocks. A brief description of each IOAA system follows. In these descriptions 'showing' refers to anomalous concentrations of mineral commodities as found in the NWT mineral database (Normin, 2016). Table 4.1 indicates the samples and the alteration types present in the samples for each locality.

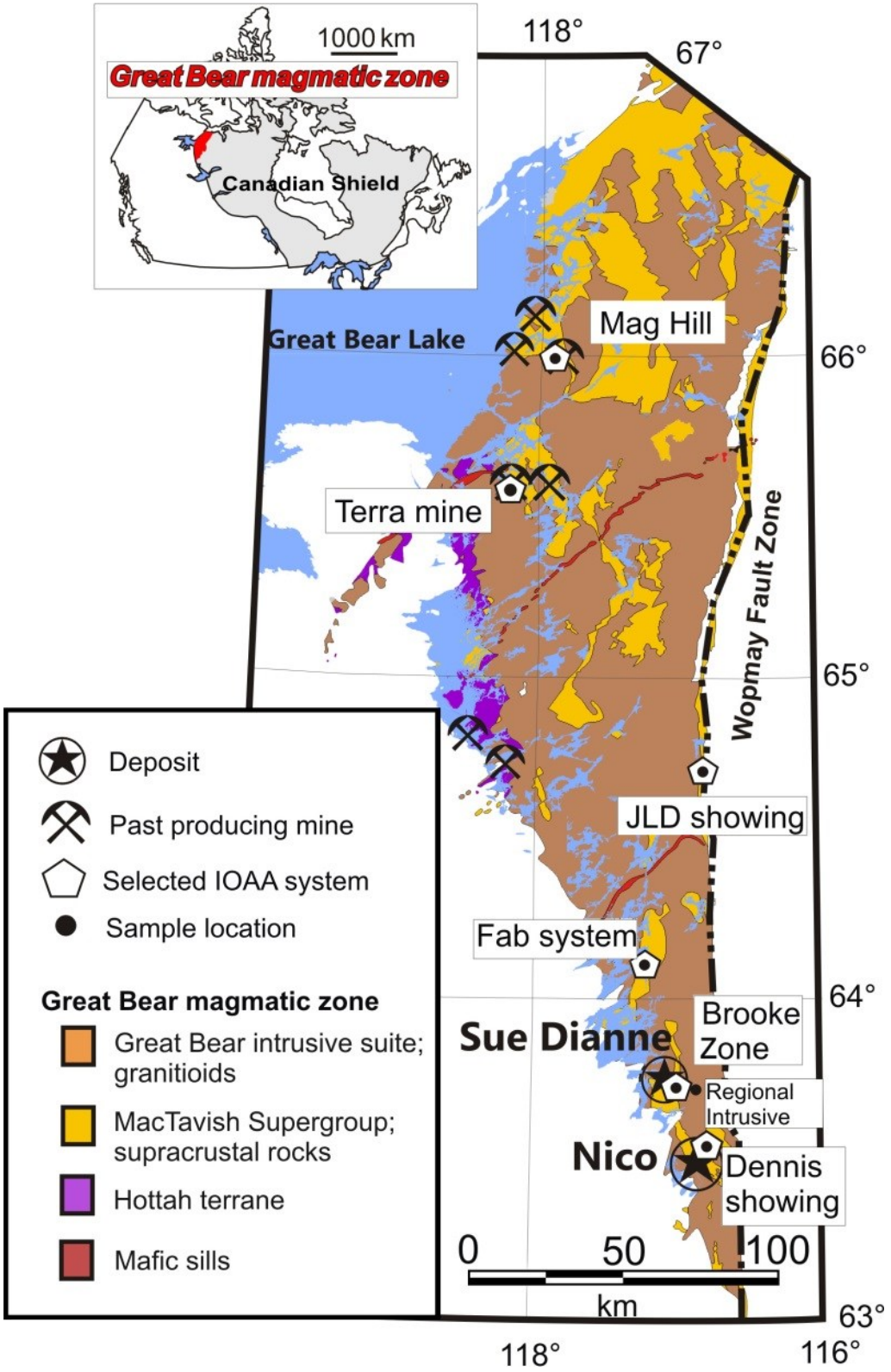

Figure 4.1: Study areas in the Great Bear magmatic zone with sample locations. Geology modified from Hoffman and Hall (1993).

Table 4.1: List of locality, samples, alteration types and analytical technique used

Source	Sample	Alteration type	CL	BSE	EPMA	LA-ICP-MS	Sample type
Fab system	11UPA86B4	(HT) Ca-Fe, weak (LT) Fe	x	-	-	4	Thin section
Brooke Zone	09CQA026E01	(HT to LT) K-Fe, (LT), Ca-Fe, Si	x	x	31	-	Thin section
	09CQA109F02	(HT to LT) K-Fe, (LT), Ca-Fe, Si	x	x	-	-	Thin section
Mag Hill	CQA-05-110A	(HT) Na-Ca-Fe	-	x	41	-	Thin section
JLD showing	09CQA1170D3	(HT) Ca-Fe, Si	x	x	27	3	Disaggregated
Terra mine	09CQA0128B2	(HT) Ca-Fe, (HT) K-Fe, (LT) K-Fe, Si	x	-	-	5	Disaggregated
	3507A	(HT) Ca-Fe, (HT) K-Fe, (LT) K-Fe, Si	x	x	49	4	Thin section
Dennis showing	09CQA1045C8	(HT) Na, (HT) Na-Ca-Fe to (HT) Ca-Fe to (LT) Ca-Fe	x	x	44	4	Disaggregated
	09CQA1045E4	(HT) Na, (HT) Na-Ca-Fe to (HT) Ca-Fe	x	x	45	4	Disaggregated
Regional intrusive	09CQA1010A4	weak- post IOAA; (LT) K, (LT) Ca	x	x	3	-	Disaggregated
	09CQA0011B01	weak; (HT) Na, (LT) K +- Fe	x	x	35	-	Thin section

x analyses available, - analyses not available, or number of analyses

4.3.2. Fab system

The Fab system includes U-, Cu-, Fe-, and/or F-bearing showings (Gandhi, 1988) as well as U and Th showings (Potter et al., 2013a, 2013b). This magnetite-group IOCG system displays an alteration footprint of approximately five by ten kilometers. The least altered and weakly to moderately albitized precursor hypabyssal intrusive body is cross-cut by high-temperature calcic-ferric/ferrous alteration that grades into a transitional calcic-potassic-ferric/ferrous alteration. The prograde alteration phase consists of high-temperature potassic-ferric/ferrous alteration, leading to U, Cu, Fe, and F mineralization (Acosta-Góngora et al., 2014; Montreuil et al., 2016a). Showings are found within or near hydrothermal magnetite-rich veins and breccias as well as magnetite-apatite-actinolite veins and breccias, many hosting potassic minerals such as biotite or having intense K-feldspar haloes (Corriveau et al., 2016). Some of these veins contain up to 10% fluorapatite with or without biotite, muscovite, chlorite, and scheelite (Lypaczewski et al., 2013; Corriveau et al., 2016; DeToni, 2016). The sample from one of the Fab system showings (11PUA086B04, Table 4.1) is from a large, Th-rich composite vein-like replacement zone consisting in part of coarse grained (> 3 mm) amphibole, biotite, and fluorapatite (Corriveau et al., 2016).

4.3.3. Brooke Zone

The Brooke Zone (Bi-Cu-Mo-LREE) prospect (Montreuil et al., 2016b), much like the neighboring Sue Dianne Cu-Ag-(U-Au) deposit (Goad et al., 2000a, 2000b; Camier, 2002), is hosted in a hydrothermal breccia complex occurring in the Faber Group volcanic rocks at the intersection of the Mar and Dianne Lake faults. The two samples from the Brooke Zone (09CQA-0026E1 and 09CQA-109F02; Table 4.1) are representative of the observed outcropping alteration. The protolith was affected by high temperature potassic-ferric/ferrous alteration (magnetite, K-feldspar), which evolved to low temperature potassic-ferric (hematite-K-feldspar-chlorite) alteration. Quartz and quartz-epidote veins, breccia, and stockworks overprint the potassic and potassic-ferric/ferrous alteration halo (Mumin et al., 2010). The Brooke Zone prospect differs from the Sue Dianne deposit by having a higher concentration of Mo, W, and LREE with minor Bi and Th in the whole rock geochemistry (Montreuil et al., 2016b).

4.3.4. Mag Hill

The Mag Hill sector of the Port Radium-Echo Bay district is one of the best studied depth to surface profiles across Fe oxide alkali alteration systems in the GBMZ (Mumin et al., 2007, 2010; Somarin and Mumin 2014; Mumin, 2015; Corriveau et al., 2016). Sample CQA-05-110A is part of the sodic-calcic-ferric/ferrous alteration zone within the Mag Hill V-rich IOA prospect. Sericitized and hematized albite, chloritized amphibole, magnetite with hematite replacement along grain margins, fluorapatite with inclusions of monazite, pyrite, K-feldspar, quartz, chalcopyrite, and tourmaline are found within these rocks (DeToni, 2016).

4.3.5. JLD showing

The historic JLD U and Cu showings are hosted in magnetite and chlorite rich bodies (Gill, 1969). The showings are characterized by intense magnetite ± amphibole, high temperature, calcic-ferric/ferrous alteration parageneses within veins and replacement zones. In contrast to the other systems covered in this study, those that formed proximal to the Wopmay fault zone (Fig. 4.1), such as the JLD showing, have been commonly affected by high temperature recrystallization postdating the GBMZ IOAA systems (Jackson et al., 2013). Sample 09CQA1170D3 (Table 4.1) consists of mostly fine-grained (0.05 – 0.1 mm) to locally, coarsely, recrystallized (0.5–2 mm) magnetite (80%), cryptocrystalline quartz (10%), plagioclase (5%), pyrite (2% as wispy layers and stringers), and accessory fluorapatite, fluorite, and allanite.

4.3.6. Terra mine

The past producing Ag, Ni, Bi, and U Terra mine consists of a vein-type mineralization that cross-cuts alkali metasomatism and IOA mineralization in the IOAA system of the Camsell River district (Shegelski, 1973; Badham, 1975; Badham and Morton, 1976; Hildebrand, 1986; Acosta-Góngora et al., 2014). This system is hosted in a volcano-sedimentary caldera sequence (Hildebrand 1986). It is extensively albitized at its base and evolves upwards, temporally and spatially, to zones of moderate to intense albitization, stratabound to anastomosing, and finally massive replacement with high temperature calcic-ferric/ferrous alteration parageneses. Precursor rocks are thinly bedded clastic, volcaniclastic, and carbonate rocks that are locally extensively brecciated. In this alteration zone, massive magnetite-apatite mineralization bodies occur. Both brecciated and non-brecciated examples of magnetite-apatite mineralization from these zones were studied (Table 4.1). In each case, fluorapatite crystals are highly fractured and contain monazite inclusions. Sample 3507A is brecciated and possesses > 85% coarse magnetite,

fluorapatite, and traces of calcite in an interstitial matrix of magnetite and clay (Lypaczewski et al., 2013). Sample 09CQA0128B2 is a non-brecciated sample that is 80% magnetite, 15% fluorapatite, and 5% cryptocrystalline quartz patches.

4.3.7. Dennis showing

The Dennis Th showing occurs within skarns and calcic-ferric/ferrous alteration among pervasively and intensely albitized sedimentary rocks. The alteration sequence is as follow: 1) high temperature sodic (albite) alteration; 2) skarns (clinopyroxene and garnet) and sodic-calcic-ferric/ferrous (albite, clinopyroxene and/or amphibole) alteration in the form of replacement and breccia fills; 3) Th-bearing, high temperature, calcic-ferric/ferrous alteration as replacement veins (magnetite, amphibole, with and without fluorapatite) amongst; 4) assemblages of low temperature potassic-ferric/ferrous alteration (K-feldspar, hematite, sericite, carbonates); and 5) late-stage low temperature calcic-ferric (epidote) alteration. The Dennis showing is located 9 km north-east of the NICO magnetite-group IOCG deposit in the southern part of the GBMZ. It differs from the NICO deposit by lacking high temperature potassic-ferric/ferrous alteration and Co-Au-Bi mineralization (Montreuil et al., 2016b). Sample 09CQA1045E4 from the Dennis showing is weakly magnetic and consists of irregular 0.5 – 2 mm patches of fine-grained (0.3 – 0.5 mm) skarn with hedenbergite (80%), titanite (20%) and magnetite (1%) after albite. Sample 09CQA1045C8 is non-magnetic and contains patches (0.5 – 5 mm) of epidote and cross-cutting patches (0.5 – 2 mm) of actinolite amongst partially hematized magnetite as well as late calcite filled hairline fractures. This sample illustrates a low temperature calcic-ferric/ferrous overprint on high temperature calcic-ferric/ferrous alteration that forms in sodic-calcic-ferric/ferrous alteration zones resulting in the pseudo-pegmatitic textures described in Corriveau et al. (2010a, b).

4.3.8. Regional intrusive rocks

Two of the least altered granitic samples (Corriveau et al., 2016) were used to characterize the GMBZ regional fluorapatite. They serve as a contrast to fluorapatite found in the IOAA systems described in this study. Both samples are from the vicinity of the Sue Dianne deposit and the Brooke Zone prospect. The first sample (09CQA0011B01) is from a syn-IOAA medium to coarse grained granitic dike that crosscuts amphibole-magnetite altered volcaniclastic rocks of the Faber Group. It shows moderate albitization along margins and fractures of K-feldspar grains and overprint by patchy K-feldspar alteration. In contrast, the second sample (09-CQA-1010A4) is from a late-stage granite with minor potassic alteration and local epidote veins, which postdates the IOAA systems.

4.4. ANALYTICAL METHODS

The data used in this study represent a compilation from the multidisciplinary IOCG-Great Bear Project of the Geological Survey of Canada. Hence, fluorapatite both from disaggregated samples designed for an indicator mineral study in unconsolidated sediments and from thin sections were used (Table 4.1).

4.4.1. Sample disaggregation

Sample dissagregation was performed at Overburden Drilling Management Ltd using an electric pulse disaggregator (EPD Spark-2) (*e.g.* Cabri et al., 2008). To follow standard exploration studies using detrital indicator minerals, fluorapatite from disaggregated bedrock samples were picked within the 0.25 mm to 1 mm size fraction. Therefore, the presence of fluorapatite grains smaller than 0.25 mm or bigger than 1 mm in disaggregated samples cannot be evaluated.

4.4.2. Cathodoluminescence microscopy

Qualitative cathodoluminescence (CL), optical microscopy, and photomicrography were conducted at the department of Earth and Planetary Sciences of McGill University using a Reliotron III cold-cathode low-vacuum unit mounted on a Leitz petrographic microscope stage. The beam was set to a 4.0 kV voltage at a 0.5 mA current. A QImaging Retiga EXi camera with an exposure time of 3 to 4 seconds was used for image acquisition. This short exposure time was used to reduce the loss of signal through time (luminescence aging; Murray and Oreskes, 1997).

4.4.3. Scanning electron microscopy (SEM)

Backscattered electron (BSE) images and energy dispersive X-ray spectra (EDX) of fluorapatite from disaggregated samples were acquired using a Hitachi S-3200N variable pressure SEM at the Geological Survey of Canada Microbeam Laboratory. The Hitachi S-3000N variable pressure SEM at the Facility for Electron Microscopy Research (FEMR) at McGill University was used for samples in thin section. In each case, a 25 kV electron beam was used in variable pressure mode (set at 20 Pa). Single-point, semi-quantitative compositional data were obtained using EDX with INCA analysis software. Readings were integrated over a period of 50 seconds.

4.4.4. Electron probe microanalyzer (EPMA)

Fluorapatite grains, hand-picked from the non-ferromagnetic heavy mineral concentrate fraction of disaggregated bedrock samples, were mounted in 25-mm epoxy-impregnated stubs and polished at SGS Lakefield Research Laboratory. Electron probe microanalyzer (EPMA) analyses of these grains were conducted at the Geological Survey of Canada Microbeam Laboratory (GSCML) using a CAMECA SX50 EPMA equipped with four wavelength-dispersive spectrometers. Operating conditions were 20 kV accelerating voltage, 10 nA beam current, and a 10 μm beam spot. Count times on peak were 10 seconds, with 5 seconds off-peak. Analytical standards included the natural Durango fluorapatite (Young et al., 1969) for Ca, P, and F, and synthetic oxides for all other elements found in Table 4.2. The raw data were processed using the ZAF matrix correction.

EPMA analyses of fluorapatite and monazite grains in thin section were made on a JEOL JXA-8500F HYPERPROBE equipped with a thermal field emission gun at the Deutsche GeoForschungsZentrum Potsdam. EPMA operating conditions for the fluorapatite were 20 kV, 20 nA and a 15 μm electron beam spot, and for the monazite were 20 kV, 50 nA, and a 1 μm diameter electron beam spot. Count times on peak as well as off-peak were 30 seconds for P, Ca, F, and Cl, and 50 seconds for all other elements found in Table 4.2 and 4. Analytical standards included pure metals for Th and U, vanadinite for Pb, synthetic REE phosphates prepared by Jarosewich and Boatner (1991), and natural minerals, such as the Durango fluorapatite (Young et al., 1969), and synthetic oxides for all other elements found in Table 4.2. The analytical errors for the REEs depend on the absolute abundances of each element. Relative errors are estimated to be < 1% at the > 10 wt% level, 5 – 10% at the 1 wt% level, 10 – 20% at the 0.2 to 1 wt%

level, and 20 – 40% at the < 0.1 wt% level (Jackson 2008). For concentrations below 0.1 wt%, the analytical precision for the actinides is approximately 10%. Detection limits were approximately 200 to 300 ppm for all elements analyzed. EPMA measurement of Cl and F in the fluorapatite was made according to guidelines outlined in Stormer et al. (1993) and Goldoff et al. (2012). The raw data were processed using the JEOL software.

4.4.5. Laser ablation inductively coupled plasma mass spectrometry (LA-ICP-MS)

Laser ablation inductively coupled plasma mass spectrometry (LA-ICP-MS) was performed on polished thin sections as well as on grains from disaggregated bedrock samples at the Geological Survey of Canada facility in Ottawa (Jackson, 2008). The system consists of a Photon-Machines Analyte 193 excimer laser ablation (λ = 193 nm) with Helex ablation cell and an Agilent 7700x quadrupole ICP-MS. A laser spot size of 10 μm was used for all samples. Spots analysis and line scan analysis were used. Line scan analysis had a scanning speed of 10 μm/sec and pre-analysis ablation lines were performed. The Durango fluorapatite and the NIST610 glass reference were used as standards. Recalibration was performed after every 15 consecutive set of analyses and for each sample change. Quantitative calibration was made using the Ca content of the fluorapatite from the EPMA analyses when available. A stoichiometric Ca concentration was used in the other cases. Data integration was performed after selective rejection of contaminated data by mineral and fluid inclusions using GLITTER software (Van Achter-bergh et al., 2001).

4.5. MINERALOGY AND PETROLOGY

4.5.1. Fluorapatite textural description and mineralogical association

Based on their textural characteristics and mineralogical associations, two distinct types of fluorapatite crystals were identified.

1) Type 1: Large (100–300 μm) subhedral to euhedral fluorapatite often within or next to epidote rich veins with or without scheelite (Figs. 4.2). This type of fluorapatite does not occur as aggregates and does not have pitted edges. No monazite or allanite inclusions were observed in this fluorapatite.

2) Type 2: Fine to coarse grained fluorapatite (20 μm - 3 mm), often found as aggregates in a dull hematite stained groundmass with or without cryptocrystalline quartz (Fig. 4.3). Grains are anhedral to subhedral and show pitted edges as well as numerous dissolution pits. These fluorapatite crystals are often fractured and/or scattered throughout the matrix of the breccia. They commonly contain inclusions of allanite and/or monazite and/or hematite and/or a fluid phase. Allanite is also observed as a fracture filling mineral crosscutting Type 2 fluorapatite (Figs. 4.3, 4.4). Larger (0.2–3 mm) fluorapatite crystals of this type occur with either massive magnetite or with hematite, clays, and chlorite ± biotite aggregates (*e.g.*, 3507A, Fig. 4.5; 11UPA86B4, Fig. 4.6).

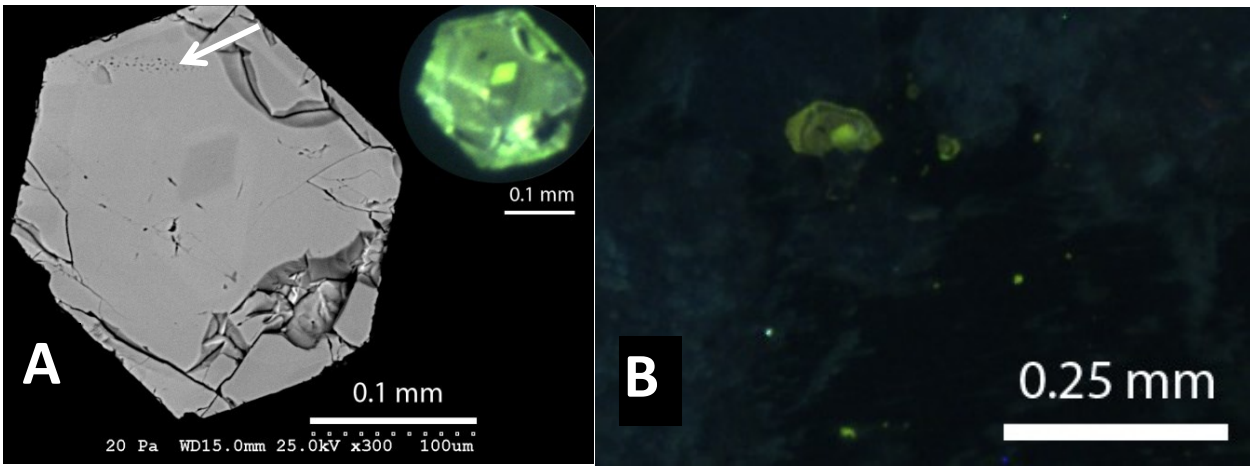

Figure 4.2: Type 1 fluorapatite. **(A)** Concentric zoning in euhedral fluorapatite disaggregated from sample 09CQA1010A4 post-iron oxide alkali-alteration (IOAA) regional granitic intrusive. The arrow indicates a group of closely packed secondary fluid inclusions, not to be confused with dissolution pits. **(B)** Concentric zonations in subhedral fluorapatite from sample 09CQA0011B01 from a syn-IOAA regional granitic intrusive.

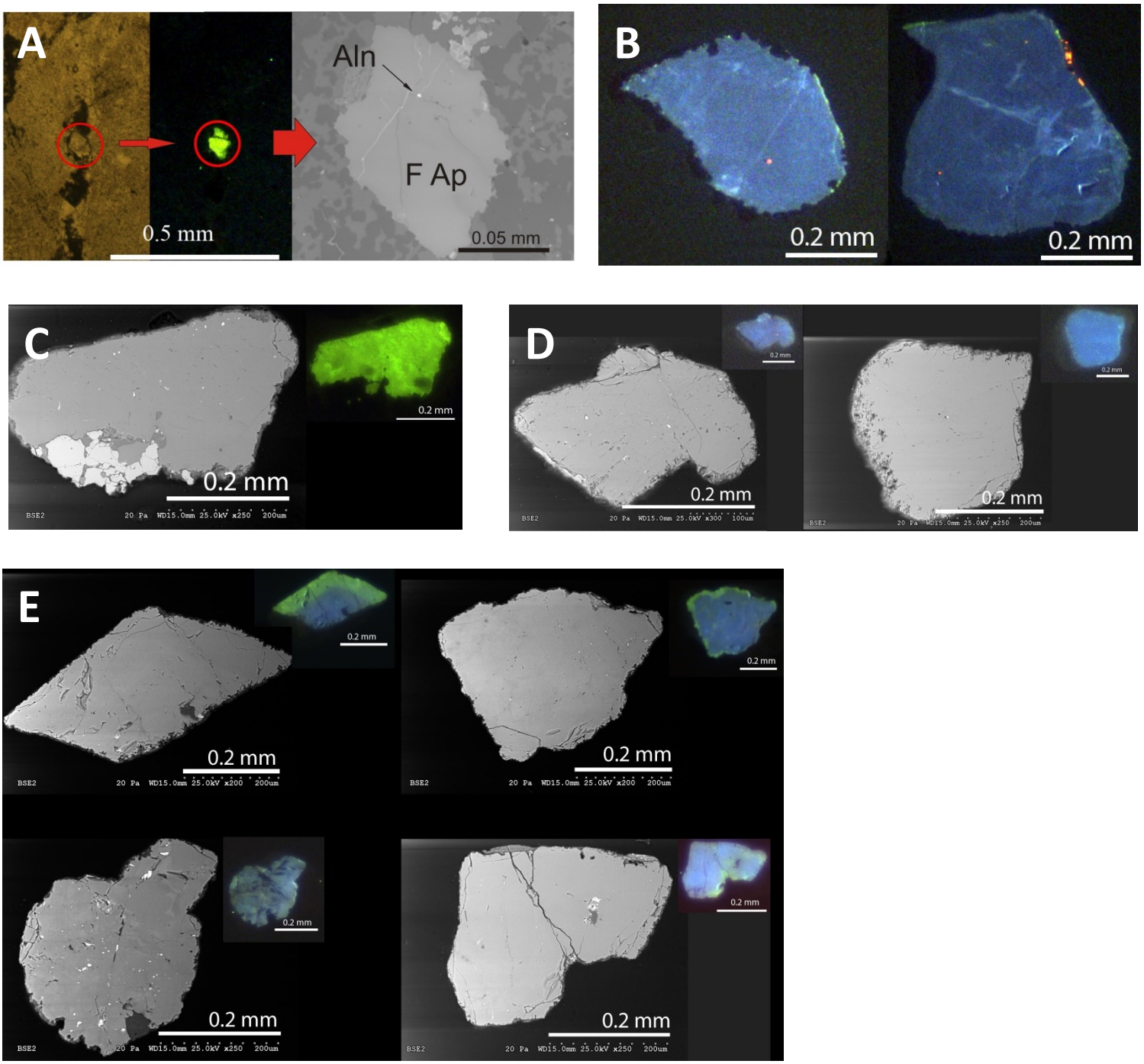

Figure 4.3: Type 2 fluorapatite. (**A)** Transmitted light, cathodoluminescence, and backscattered electron images of a pitted fluorapatite grain within thin section 09CQA026E1 from the Brooke Zone system. (**B**). Blue cathodoluminescence response of fluorapatite in sample 09CQA128B2 from the Terra mine with thin green zones along a crystal edge free of notches. A calcite inclusion is visible as orange cathodoluminescence response. (**C-E**). Backscattered electron and cathodoluminescence images of fluorapatite within sample 109CQA170D3 from the JLD showing (**C**) and within samples 09CQA1045E4 (**D**) and 09CQA1045C8 (**E**) from the Dennis showing.

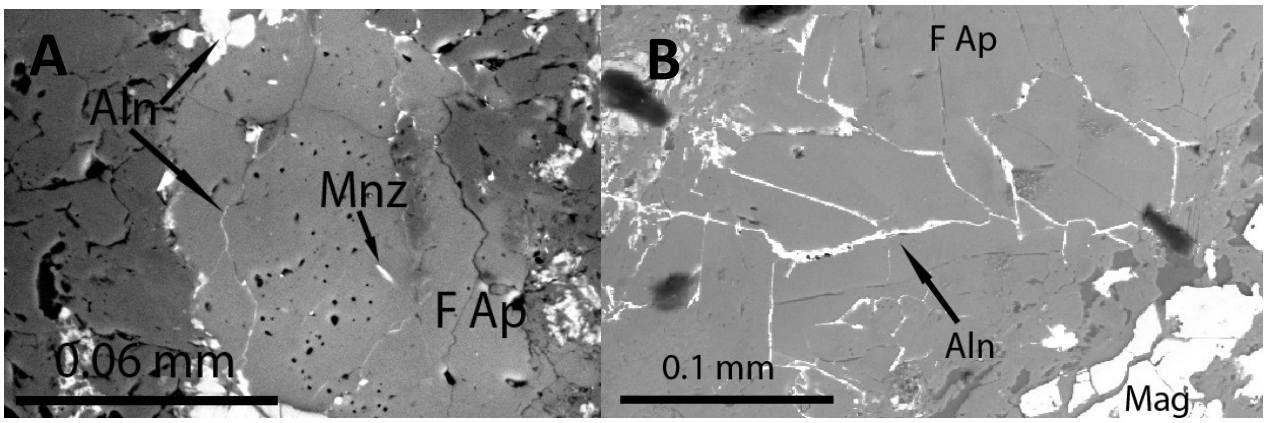

Figure 4.4: Type 2 Fluorapatite. (**A**) Backscattered electron images of fluorapatite in sample 09CQA109F2 from the Brooke Zone. Fluorapatite (FAp) containing numerous dissolution pits and monazite inclusions. (**B**) Fracture fills in fluorapatite filled with allanite (Aln).

Type 1 fluorapatite occurs in the regional intrusive rock samples as well as in both Brooke Zone altered samples. The most pristine-looking fluorapatite grain of Type 1 is in sample 09CQA1010A4 from a regional post IOA alteration granite (Fig. 4.2). Type 2 fluorapatite is present in all the altered samples studied but not in the two specimens of least altered regional granitic intrusive rocks. The most numerous mineral inclusions and irregular pitted edges as well as dissolution pits are found in fluorapatite grains from sample 3507A in the Terra mine (Figs. 4.5, 4.9).

The occurrence of fluorapatite crystals smaller than 0.25 mm at the Dennis and JLD showings cannot be addressed as these localities are only represented by disaggregated samples. Their mineralogical association is also unknown. It should be noted, however, that allanite and epidote were also hand-picked from samples from the JLD showing (09CQA1170D03) and the Dennis showing (09CQA1045C8) (Normandeau and McMartin 2013). Fluorapatite from these samples at the JLD and Dennis showings all contain numerous dissolution pits, jagged edges, and fractures, typical of Type 2.

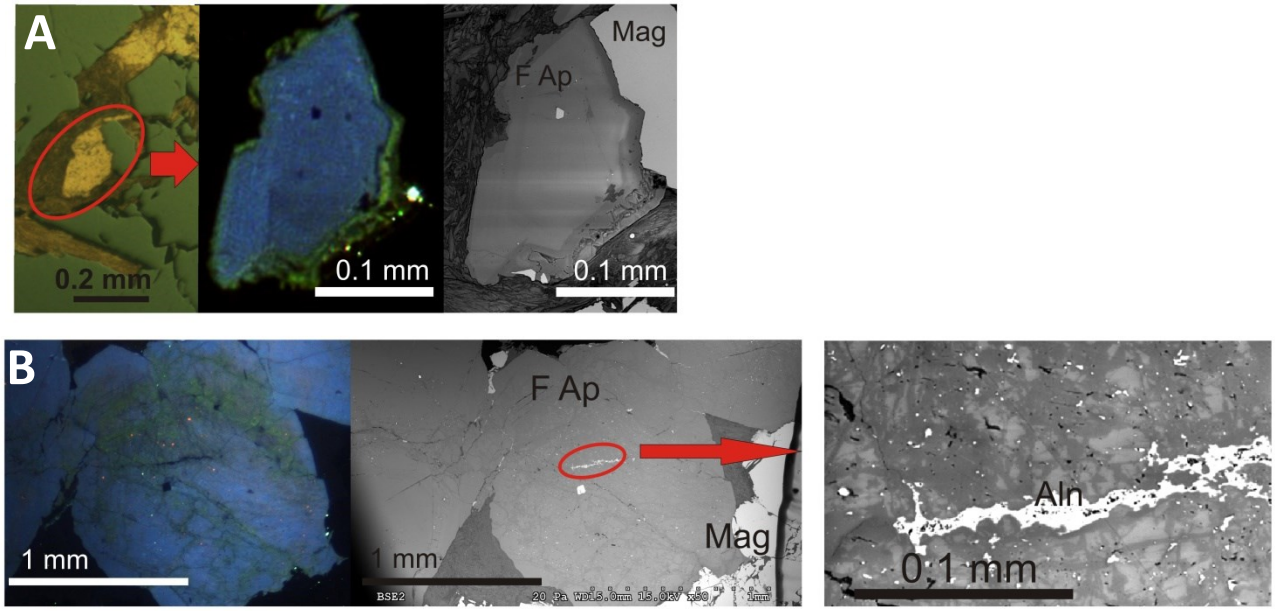

Figure 4.5: Type 2 fluorapatite: **(A)** Reflected light, cathodoluminescence, and backscattered electron images of a fluorapatite-magnetite breccia from the Terra mine. **(B)** Green and blue cathodoluminescence zones in fluorapatite are cross correlated with the dark and bright backscattered electron zones, respectively, from sample 3507A. Dissolution pits and allanite filled fractures are present.

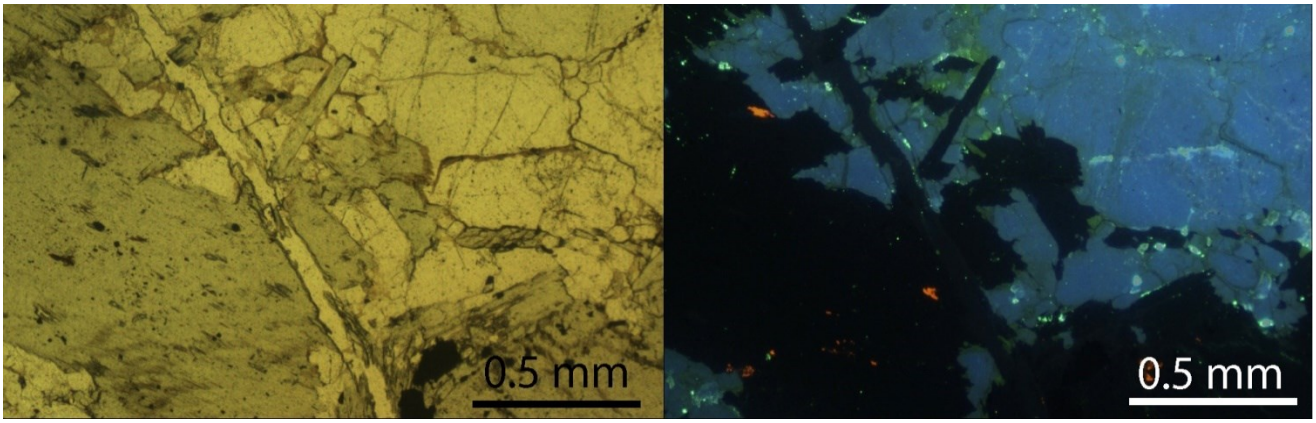

Figure 4.6: Transmitted light and cathodoluminescence microscopy of Type 2 fluorapatite (blue in cathodoluminescence) from chlorite aggregates (dark in cathodoluminescence) in sample 11UPA86B4 from the Fab system.

4.5.2. Fluorapatite cathodoluminescence and backscattered electron textures

All fluorapatite grains from thin sections and disaggregated bedrock had a strong response to CL activation. Two distinct colors were observed in CL: either yellow-green to green, or blue. In the thin sections, other minerals showing response to CL activation include bright light blue scheelite, faint blue feldspars, and red-orange calcite. Fluorapatite crystals show CL zoning as: 1) patchy irregular zones distinct in their intensity and hue of the green color response (*e.g.*, Fig. 4.3a, c); 2) green zones, within a generally blue fluorapatite, either irregularly following the edges of crystals or filling crystal fractures or discontinuous stringers (*e.g.*, Fig. 4.5); 3) rare concentric zoning within green zones (*e.g.*, Fig. 4.2); and, in a single case, 4) a possible growth zonation from a blue core to a green zone at the rim (*e.g.*, Fig. 4.3e).

Fluorapatite grains with a blue CL response are present in samples from the Terra mine, Dennis showing, and the Fab system. They are the larger millimeter sized fluorapatite grains of Type 2 associated with a coarser grained, pseudo-pegmatitic, sodic-calcic-ferric/ferrous, and calcic-ferric/ferrous alteration. Samples from the Dennis showing and the Terra mine also show accessory calcite visible as CL red-orange micron-size grains in fractures and along the rims of the fluorapatite grains (*e.g.*, Fig. 4.3b). In fluorapatite from the Dennis showing, green zones are more frequent in grains from low temperature alteration sample 09CQA1045C8 than in skarn sample 09CQA1045E4 (Figs. 4.3d, 4.3e). Low temperature alteration sample 09CQA1045C8 also contained a single grain of fluorapatite, which showed a blue zone at the grain core and an overgrowth green zone at the rim (Fig. 4.3e). Fluorapatite grains, hand-picked from a disaggregate sampled from the high temperature calcic-ferric/ferrous alteration of the JLD

showing, have an irregular green patchy CL zoning, frequent dissolution pits, and occasional mineral inclusions of allanite.

Fluorapatite grains from the regional intrusive rock sample, which postdates the IOAA system, have concentric zoning as well as a euhedral shape with no traces of dissolution along the crystal edges. This concentric zoning is visible in the BSE images as contrasting shades of grey in which the darker BSE zones correlate with a brighter green CL response (Fig. 4.2). Dissolution pits are absent in the fluorapatite grains from the regional intrusive rock sample postdating the IOAA system (sample 09CQA1010A4). Secondary fluid inclusions, observed in this sample (Fig. 4.2), are distinct from dissolution pits by being closely packed and forming a line crossing concentric crystal zones rather than being either randomly distributed within the crystal or only present in a specific crystal zone.

4.5.3. Chemical variation of fluorapatite

The fluorapatite mineral chemistry from each of the systems described above is presented in Table 4.2 (EPMA) and Table 4.3 (LA-ICP-MS). When available, chemical data from individual zones within the grains are presented (*i.e.*, sample 3507A from the Terra mine, and sample 09CQA0011B01 from the syn-IOAA regional intrusive rock, Table 4.2).

Fluorapatite from regional intrusive rocks are relatively rich in REEs (average REE oxide = 1.63 and 1.65 wt%, Table 4.2) and are exceeded only in sample 3507A from the Terra mine (average REE oxide = 2.12 wt%) while other samples range from 0.35 to 0.84 wt%. Fluorapatite grains from the Terra mine also stand out in Table 4.2 by having the highest Na values (average Na_2O = 0.19 wt%) compared to a range of 0.01 to 0.07 wt% for the other samples. Fluorapatite

from the JLD showing is high in Mn (average MnO = 0.23 wt% compared to a range of 0.02 to 0.11 wt% for other samples). Comparison between the different zones within fluorapatite grains from the same localities indicates higher REEs, higher Na, and lower Ca average values in bright BSE zones compared to dark BSE zones, both for sample 09CQA0011B01 as well as for regional intrusive sample 3507A (Terra mine).

Table 4.2: Mean fluorapatite electron probe microanalyzer analytical results (wt %)

Source	Sample	P_2O_5	SiO_2	ThO_2	UO_2	Y_2O_3	La_2O_3	Ce_2O_3	Pr_2O_3	Nd_2O_3	Sm_2O_3	Gd_2O_3	Dy_2O_3	Er_2O_3	Yb_2O_3	CaO	SrO	MnO	FeO*	Na_2O	F	Cl	H_2O**	Sum	O=(F+Cl)	Total	REE
Brooke zone	09CQA0026E01																									
	all (n=31)	42.24	*0.00*	*0.00*	*0.00*	0.09	0.04	0.07	0.04	0.07	0.03	0.02	0.03	0.04	0.02	54.91	0.00	0.11	0.10	0.05	3.72	0.02	0.17	101.71	1.57	100.14	0.45
	1 - σ std. dev	0.32	0.00	0.02	0.01	0.07	0.05	0.07	0.04	0.06	0.04	0.03	0.04	0.05	0.02	0.53	0.01	0.03	0.04	0.03	0.42	0.01	0.11	0.70	0.18	0.66	0.22
Mag Hill	CQA-05-110A																									
	all (n=41)	42.52	*0.00*	*0.00*	*0.00*	0.05	0.02	0.06	0.02	0.05	0.04	0.04	0.02	0.04	0.01	55.72	0.02	0.04	0.15	0.03	3.58	0.09	0.22	102.66	1.53	101.13	0.35
	1 - σ std. dev	0.22	0.00	0.01	0.00	0.03	0.04	0.05	0.04	0.05	0.05	0.05	0.03	0.05	0.02	0.21	0.02	0.02	0.13	0.02	0.29	0.02	0.13	0.38	0.12	0.38	0.16
JLD showing	09CQA1170D3																									
	all (n=27)	40.51	0.31	-	-	0.25	0.03	0.05	-	0.07	0.04	-	-	-	-	55.12	0.06	0.23	0.13	0.03	-	-	-	101.03	-	-	0.44
	1 - σ std. dev	0.72	0.30	-	-	0.11	0.04	0.07	-	0.08	0.05	-	-	-	-	0.63	0.02	0.07	0.20	0.02	-	-	-	0.93	-	-	0.18
Terra mine	3507A																									
	all (n=49)	41.48	*0.00*	*0.00*	*0.00*	0.10	0.50	0.95	0.10	0.30	0.05	0.05	0.02	0.03	0.02	54.03	*0.00*	0.02	0.13	0.19	3.46	0.23	0.14	101.82	1.51	100.31	2.12
	1 - σ std. dev	0.89	0.00	0.02	0.01	0.06	0.41	0.78	0.08	0.22	0.05	0.04	0.03	0.05	0.03	1.63	0.01	0.02	0.09	0.15	0.31	0.17	0.08	0.88	0.11	0.82	1.54
	dark (n=19)	42.52	*0.00*	*0.00*	*0.00*	0.05	0.03	0.03	0.04	0.04	0.02	0.03	0.02	0.03	0.02	55.95	*0.00*	0.01	0.11	0.02	3.76	0.03	0.18	102.80	1.59	101.22	0.31
	1 - σ std. dev	0.18	0.00	0.01	0.00	0.04	0.04	0.03		0.04	0.03	0.04	0.03	0.05	0.03	0.14	0.01	0.01	0.10	0.02	0.31	0.03	0.12	0.26	0.13	0.22	0.12
	bright (n=22)	40.80	*0.00*	0.04	*0.00*	0.13	0.80	1.54	0.14	0.46	0.06	0.05	0.02	0.05	0.02	52.81	*0.00*	0.02	0.16	0.31	3.26	0.36	0.15	101.18	1.46	99.72	3.27
	1 - σ std. dev	0.41	0.00	0.02	0.01	0.04	0.23	0.38	0.08	0.06	0.06	0.04	0.02	0.04	0.02	0.79	0.01	0.02	0.08	0.07	0.12	0.06	0.06	0.51	0.04	0.51	0.75
Dennis showing	09CQA1045C8																									
	all (n=44)	40.06	0.35	-	-	0.09	0.17	0.34	-	0.14	0.03	-	-	-	-	55.32	0.05	0.02	0.09	0.01	-	-	-	100.63	-	-	0.78
	1 - σ std. dev	0.85	0.18	-	-	0.09	0.09	0.18	-	0.12	0.04	-	-	-	-	0.46	0.02	0.02	0.35	0.02	-	-	-	1.22	-	-	0.37
	09CQA1045E4																									
	all (n=45)	39.92	0.45	-	-	0.05	0.20	0.42	-	0.13	0.03	-	-	-	-	55.21	0.06	0.01	0.13	0.02	-	-	-	100.47	-	-	0.84
	1 - σ std. dev	0.76	0.28	-	-	0.07	0.10	0.16	-	0.12	0.05	-	-	-	-	0.56	0.03	0.03	0.29	0.02	-	-	-	0.94	-	-	0.31
Regional intrusive	09CQA1010A4																									
	all (n=3)	40.17	0.69	-	-	0.28	0.27	0.68	-	0.34	0.06	-	-	-	-	54.87	0.06	0.05	0.08	0.03	-	-	-	102.26	-	-	1.63
	1 - σ std. dev	0.60	0.32	-	-	0.25	0.11	0.23	-	0.11	0.01	-	-	-	-	0.89	0.02	0.02	0.02	0.01	-	-	-	0.84	-	-	0.65
	09CQA0011B01																									
	all (n=35)	41.26	*0.01*	*0.00*	*0.00*	0.47	0.11	0.33	0.06	0.30	0.08	0.13	0.08	0.06	0.03	54.34	*0.00*	0.11	0.23	0.07	3.60	0.02	0.14	101.40	1.52	99.88	1.65
	1 - σ std. dev	0.62	0.04	0.01	0.00	0.23	0.09	0.20	0.05	0.15	0.06	0.08	0.06	0.05	0.03	0.59	0.01	0.03	0.11	0.03	0.24	0.02	0.08	0.60	0.10	0.55	0.72
	dark (n=7)	41.22	*0.00*	*0.00*	*0.00*	0.45	0.11	0.31	0.07	0.27	0.07	0.11	0.06	0.06	0.02	54.42	*0.00*	0.12	0.31	0.05	3.60	0.03	0.15	101.41	1.52	99.89	1.55
	1 - σ std. dev	0.55	0.00	0.01	0.00	0.17	0.11	0.26	0.05	0.14	0.06	0.09	0.06	0.05	0.02	0.66	0.00	0.02	0.09	0.03	0.29	0.02	0.07	0.50	0.12	0.39	0.87
	bright (n=3)	40.45	0.07	*0.00*	*0.00*	0.82	0.07	0.51	0.07	0.45	0.15	0.23	0.14	0.12	0.05	53.50	*0.00*	0.13	0.35	0.08	3.55	0.06	0.19	100.93	1.51	99.42	2.60
	1 - σ std. dev	0.69	0.10	0.01	0.00	0.23	0.04	0.26	0.05	0.20	0.06	0.04	0.07	0.01	0.05	0.64	0.00	0.03	0.02	0.01	0.33	0.02	0.08	0.60	0.13	0.46	0.87

Concentration in Italics are statistically not significant due to detection limits

*Total Fe as FeO

** calculated assuming the (F,Cl,OH) site is filled

Table 4.3: Mean fluorapatite laser ablation inductively coupled plasma mass spectrometry analytical results (wt%)

Source	Sample	P_2O_5	SiO_2	ThO_2	UO_2	Y_2O_3	La_2O_3	Ce_2O_3	Pr_2O_3	Nd_2O_3	Sm_2O_3	Eu_2O_3	Gd_2O_3	Tb_2O_3	Dy_2O_3	Ho_2O_3	Er_2O_3	Tm_2O_3	Yb_2O_3	Lu_2O_3	CaO	SrO	MnO	FeO*	Na_2O	Total	REE
Terra mine	09CQA0128B2 - 3507A																										
	all (n=9)	42.1	0.59	0.02	0.00	0.26	1.22	2.37	0.23	0.79	0.11	0.01	0.08	0.01	0.05	0.01	0.02	0.00	0.01	0.00	55.0	0.05	0.02	0.24	0.20	103.41	5.16
	1 - σ std. dev	1.2	0.18	0.00	0.00	0.02	0.18	0.29	0.03	0.10	0.01	0.00	0.01	0.00	0.00	0.00	0.00	0.00	0.00	0.00	0.0	0.00	0.00	0.32	0.03	1.51	0.64
Fab system	11UPA86B4																										
	all (n=4)	41.7	0.23	0.01	0.00	0.09	0.35	0.66	0.06	0.19	0.02	0.00	0.02	0.00	0.01	0.00	0.01	0.00	0.01	0.00	55.0	0.01	0.01	0.06	0.05	98.49	1.43
	1 - σ std. dev	1.5	0.03	0.00	0.00	0.01	0.06	0.12	0.01	0.04	0.00	0.00	0.00	0.00	0.00	0.00	0.00	0.00	0.00	0.00	0.0	0.00	0.00	0.00	0.01	1.74	0.25
JLD showing	09CQA1170D3																										
	all (n=3)	41.2	0.19	0.00	0.00	0.47	0.02	0.09	0.02	0.11	0.06	0.01	0.08	0.01	0.08	0.01	0.04	0.00	0.03	0.00	55.3	0.01	0.30	0.08	0.03	98.14	1.04
	1 - σ std. dev	1.0	0.11	0.00	0.00	0.12	0.01	0.02	0.00	0.03	0.02	0.00	0.03	0.00	0.02	0.00	0.01	0.00	0.01	0.00	0.3	0.00	0.04	0.02	0.00	1.39	0.26
Dennis showing	09CQA1045C8																										
	all (n=4)	39.7	0.32	0.01	0.00	0.16	0.30	0.68	0.07	0.23	0.03	0.00	0.03	0.00	0.02	0.00	0.01	0.00	0.01	0.00	55.4	0.01	0.01	0.18	0.02	97.23	1.56
	1 - σ std. dev	1.1	0.14	0.01	0.00	0.05	0.19	0.38	0.03	0.10	0.01	0.00	0.01	0.00	0.01	0.00	0.00	0.00	0.00	0.00	0.5	0.00	0.00	0.26	0.00	0.40	0.75
	09CQA1045E4																										
	all (n=4)	39.3	0.42	0.03	0.02	0.08	0.53	1.03	0.09	0.26	0.03	0.00	0.02	0.00	0.01	0.00	0.01	0.00	0.00	0.00	55.0	0.01	0.01	0.04	0.02	96.92	2.06
	1 - σ std. dev	1.2	0.05	0.00	0.00	0.02	0.08	0.12	0.01	0.01	0.00	0.00	0.00	0.00	0.00	0.00	0.00	0.00	0.00	0.00	0.5	0.00	0.00	0.00	0.00	1.47	0.24

*Total Fe as FeO

Table 4.4: Individual monazite inclusion electron probe microanalyzer analytical results (wt %)

Source	Sample	P_2O_5	SiO_2	ThO_2	UO_2	Y_2O_3	La_2O_3	Ce_2O_3	Pr_2O_3	Nd_2O_3	Sm_2O_3	Gd_2O_3	Tb_2O_3	Dy_2O_3	Ho_2O_3	Er_2O_3	Yb_2O_3	Lu_2O_3	CaO	PbO	Total
Mag Hill	CQA-05-110A																				
	grain 1	29.26	0.35	1.12	0.03	0.51	16.96	34.01	3.31	10.17	0.92	0.52	0.03	0.22	0.00	0.03	0.00	0.00	1.68	0.12	99.23
	grain 2	30.78	0.10	0.47	0.02	0.40	19.37	32.68	2.84	8.49	0.67	0.39	0.00	0.12	0.05	0.00	0.06	0.04	3.76	0.04	100.31
Terra mine	3507A																				
	grain 1	28.83	0.78	0.72	0.03	0.66	20.97	33.35	2.56	7.93	0.63	0.43	0.00	0.18	0.06	0.10	0.02	0.00	1.29	0.02	98.59

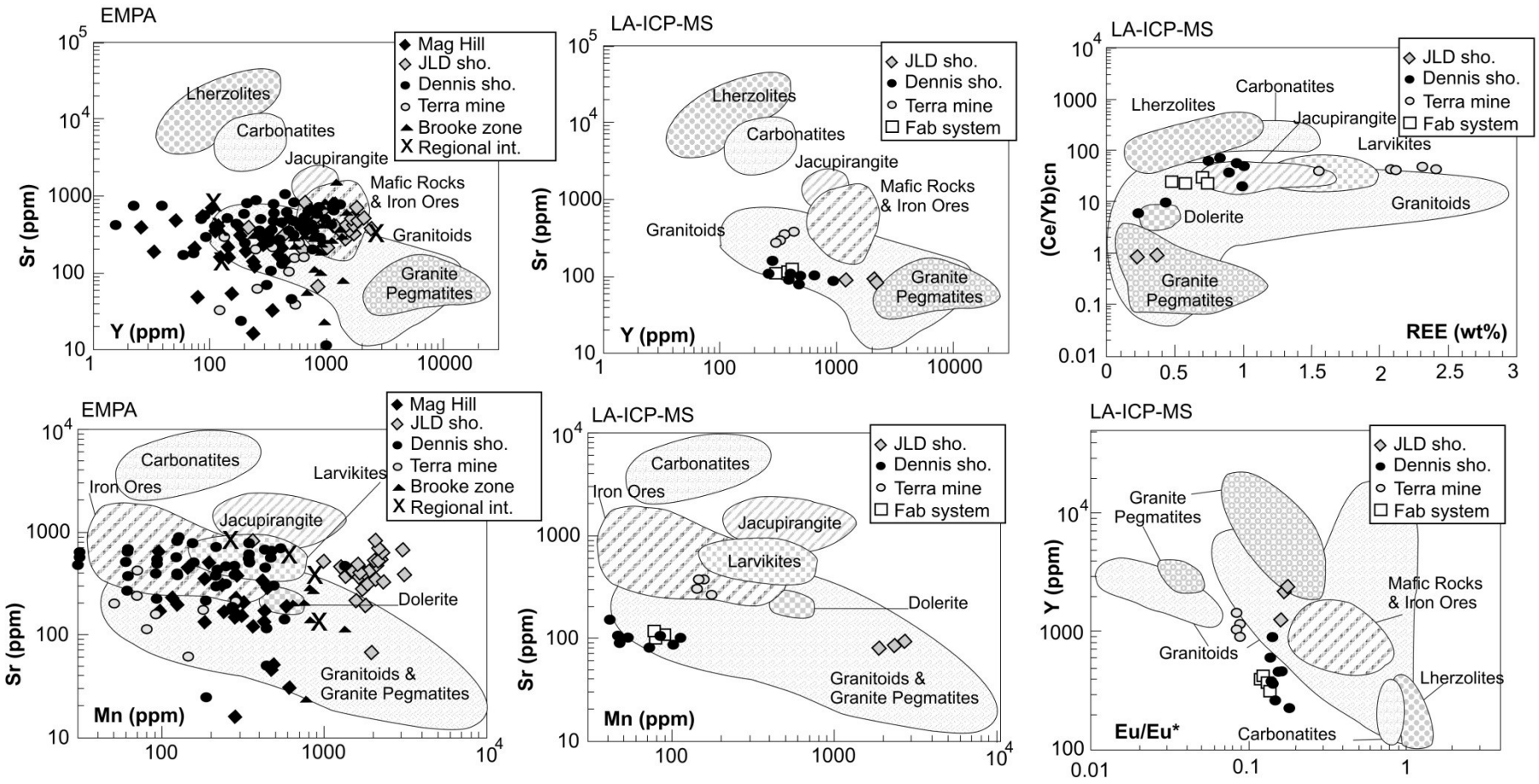

Figure 4.7: Fluorapatite analytical results from electron probe microanalyzer and from Laser ablation inductively coupled plasma mass spectrometry analyses plotted against discriminant diagrams from Belousova et al. (2002).

The REE content of fluorapatite grains, as determined by EPMA (Table 4.2), is consistent with the LA-ICP-MS data (Table 4.3) with the highest average Y+REE oxide value measured at 5.16 wt%. The lowest Y+REE oxide content (1.04 wt%), the lowest SiO_2 content (0.191 wt%), as well as the highest MnO content (0.3 wt%) are found for fluorapatite grains from the JLD showing (Table 4.3). Some representative analyses of EPMA monazite inclusions obtained from the GeoForschungsZentrum laboratory are presented in Table 4.4.

Fluorapatite compositions, obtained by EPMA and LA-ICP-MS, were plotted on the discriminant diagrams of Belousova et al. (2002) (Fig. 4.7). While these values are generally within the granite and Fe ore reference fields, a large degree of scatter is observed. Fluorapatite from the JLD showing are the most distinctive within the selected GBMZ localities, with the highest Mn and Y content and a lower Ce/Yb ratio. Fluorapatite from the Fab system and Dennis showings are similar to each other. Fluorapatite from the Terra mine have higher REE contents, and a slightly greater negative Eu anomaly. Fluorapatite grains from Mag Hill are relatively low in Y and Mn. In regional intrusive specimens, either syn- or postdating IOAA metasomatism, fluorapatite grains plot within or on the edge of the field for typical granitoids based on their Sr, Y, and Mn content (Fig. 4.7).

The chondrite-normalized patterns obtained from the LA-ICP-MS data (Fig. 4.8) show a consistent sharp drop from LREEs to HREEs for the Terra mine and Fab systems. Results from the Dennis showing vary between a sharp to a gradual decrease from LREEs to HREEs. Within this system, the steeper slope corresponds to sample 09CQA1045E4 only partially overprinted by low temperature alteration. Fluorapatite from the JLD showing have flatter profiles, which show a slight increase in HREE. All analyses show a moderate to high negative Eu anomaly.

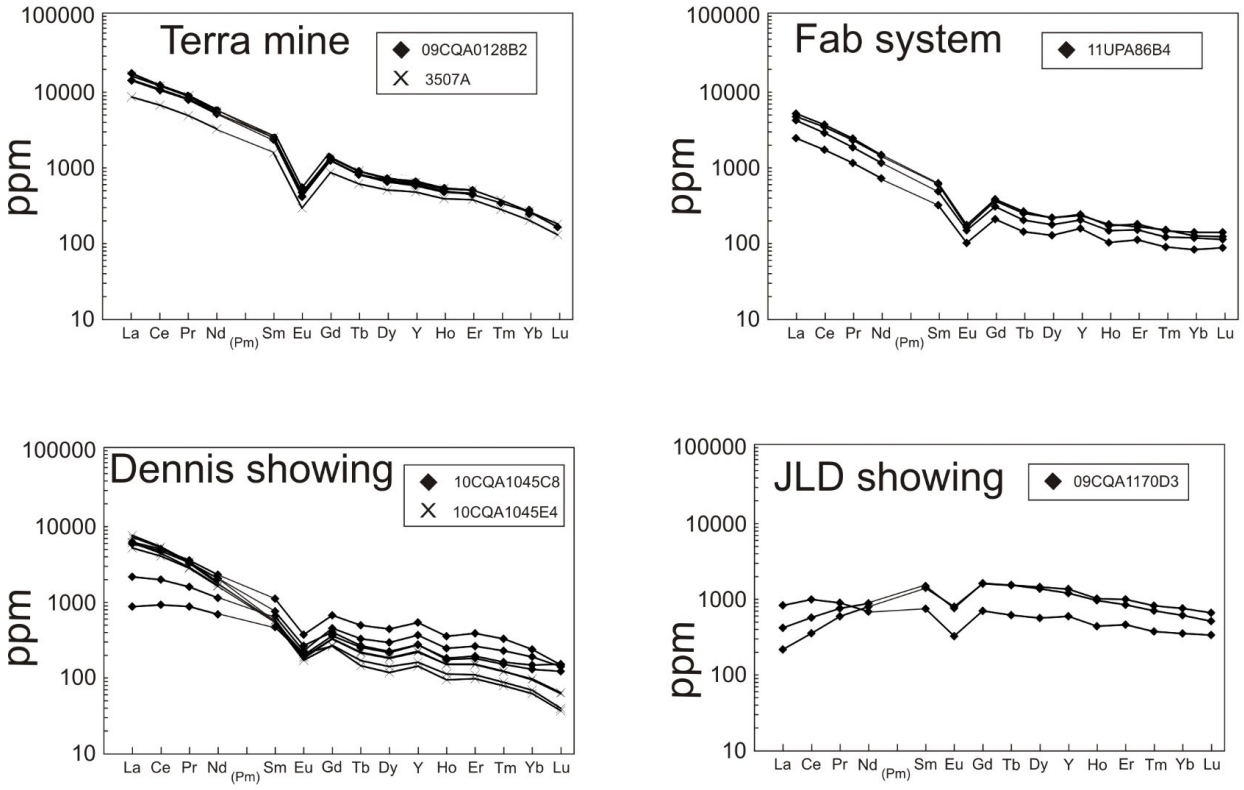

Figure 4.8: Chondrite normalized rare-earth element profiles from laser ablation inductively coupled plasma mass spectrometry analyses of fluorapatite from various alteration systems within the Great Bear magmatic zone.

4.6. DISCUSSION

4.6.1. Fluorapatite texture and iron oxide alkali-alteration

Type 1 fluorapatite from sample 09CQA1010A4 (regional post IOA alteration granitic intrusive) shows some traces of metasomatism, such as secondary fluid inclusions and patchy zonation overprinting the concentric zoning. Unlike fluorapatite from the IOAA systems, fluorapatite from this sample did not recrystallize during metasomatism and a magmatic concentric growth zoning is still preserved. While acknowledging the low number of analyses and the large standard deviation for the regional intrusive rock, fluorapatite postdating the alteration systems of the GBMZ (sample 09CQA1010A4) have the highest Si and REE contents suggesting the following coupled substitution reaction $Si^{4+} + (REE)^{3+} = Ca^{2+} + P^{5+}$ as the predominant substitution mechanism (cf. Pan and Fleet 2002)

The Type 2 fluorapatite grains are similar to fluorapatite grains from North Qôroq (Greenland) as described by Rae et al. (1996), which are found to co-exist with mafic Ca-rich mineral phases, including aegirine-augite and amphibole, and interpreted to be of metasomatic origin.

Recent work by Mao et al. (2016) discriminates apatite from various settings based on trace element composition. Their results highlight the high Na and low REE content of apatite from Kiruna type deposits when compared to other deposit types and apatite from unmineralized

rocks, as well as higher Mn content in apatite from the IOCG-type Wernecke breccia than their Kiruna-type examples. According to these results, fluorapatite from Terra mine are the most Kiruna-type like of the present study, but only if the composition is taken from the less metasomatised bright BSE zones within fluorapatite grains.

4.6.2. Fluorapatite cathodoluminescence activators and iron oxide alkali-alteration

Fluorapatite from typical unaltered granites worldwide exhibit a yellow CL response, which is attributed to Mn^{2+} activation (Roeder et al., 1987; Göetze, 2012). These contrast the blue-violet, lilac, and green-blue of REE^{3+} activated fluorapatite from carbonatites and other REE rich rocks (Kempe and Götze, 2002). A yellow to yellow-green CL response, attributed to Mn^{2+} activation, has also been observed in fluorapatite from porphyry systems (Bouzari et al., 2011). Other CL colors reported for fluorapatite include a pink-violet response attributed to Sm^{3+}, Dy^{3+}, and Nd^{3+} activation from alkaline and peralkaline rocks (*e.g.*, Mitchell and Platt, 1978; Mitchell et al., 1997).

The Mn and REE relative content can explain the change from the yellow-green and green to blue CL response. This is in line with Mn^{2+} activation generally dominating over the potential REE^{3+} activation responsible for the blue color (Mitchell and Platt, 1978; Kempe and Götze, 2002; Mitchell, 2014). Variations in CL intensity, leading to patchy yellow-green and green CL response zonation, are interpreted to be caused by a combination of Mn^{2+} self-quenching when it exceeds 2 wt% (Kempe and Götze, 2002) and/or Fe quenching of the Mn^{2+}

activator. Manganese enrichment in fluorapatite may have resulted from calcic-ferric/ferrous alterations within the IOAA systems during alkali metasomatism (Montreuil et al., 2013).

LREE enrichment is a characteristic feature of IOAA systems (Groves et al., 2010) and may be associated with calcic-ferric/ferrous or potassic-ferric/ferrous alteration, and their respective IOA and IOCG mineralization (Montreuil et al., 2013). In contrast, HREE enrichment is most pronounced in IOA mineralization with combined calcic-potassic-ferric/ferrous alteration or where intense potassic-ferric/ferrous alteration occurs within the immediate area of the IOA mineralization (Corriveau et al., 2016). LREE remobilization and precipitation of REE-rich minerals, such as monazite and allanite, take place during subsequent lower temperature alteration of fluorapatite (Montreuil et al., 2016b). The fluorapatite REE profiles for the Fab system, Terra mine, and Dennis showing (Fig. 4.8) are similar to those measured in the Se-Chahun IOA ore deposit (Bonyadi et al., 2011). On the other hand, the REE profiles for fluorapatite from the regional intrusive rocks and the JLD showing are similar to those of a pegmatitic granitic fluorapatite (Belousova et al., 2002) with the highest REE concentrations being at the transition from the LREEs to HREEs.

The present work suggests that fluorapatite with a green to yellow-green response within the GBMZ may represent either 1) primary magmatic fluorapatite with or without metasomatic dissolution (*e.g.*, Type 1 fluorapatite from the regional intrusive rocks); or 2) Mn-enriched metasomatized fluorapatite or fully recrystallized magmatic fluorapatite (*e.g.*, Type 2 fluorapatite from the JLD showing). A blue CL response is interpreted to be associated with a Mn-poor fluorapatite of metasomatic origin with no or little subsequent element remobilization. Green CL

zoning, within a generally blue CL fluorapatite, may be due to intensive leaching of LREE (*e.g.* Type 2 fluorapatite from Dennis showing) and/or enrichment of Mn due to calcic-ferric/ferrous alteration (*e.g.*, Type 2 fluorapatite from the Terra mine). In a single case (sample 09CQA1045C8 from the Dennis showing), a green CL growth zone at the rim of a blue CL fluorapatite suggests continuous crystal growth throughout this change in the geochemical environment. In all other cases, petrographic evidence suggests an episodic influx of fluids metasomatically altering fluorapatite grains already in place.

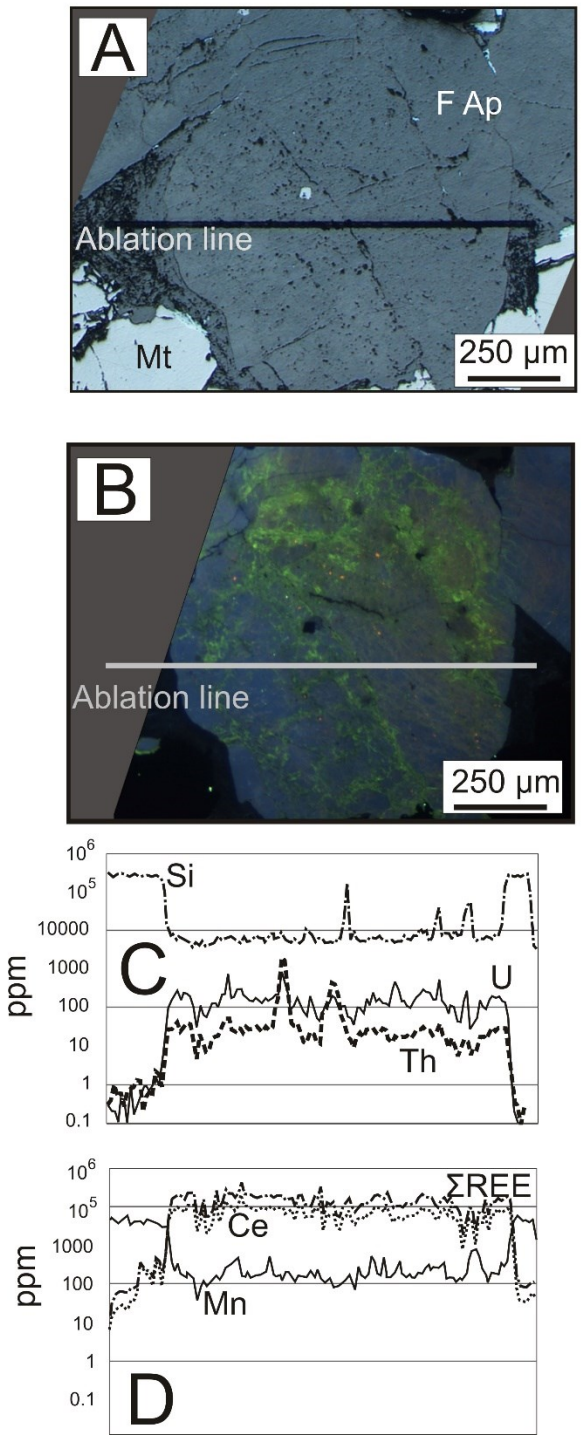

Figure 4.9: (**A**) Backscattered electron images, and (**B**) cathodoluminescence response of a Type 2 fluorapatite grain from sample 3507A from the Terra mine showing the location of selected Laser ablation inductively coupled plasma mass spectrometry (LA-ICP-MS) ablation lines (**C**). Silicon, U, and Th content from LA-ICP-MS ablation line across the fluorapatite. (**D**) Cerium, Mn, and REE content from LA-ICP-MS ablation line across the fluorapatite.

4.6.3. Secondary rare-earth element rich mineral in Great Bear magmatic zone fluorapatite

Fluorapatite from the GBMZ differs from those so far described in IOA deposits worldwide (*e.g.*, Bonyadi et al., 2011; Harlov et al., 2002; Krneta et al., 2015; Zirner et al. 2015) by having a greater abundance of dissolution pits and fractures as well as the predominance of allanite over monazite inclusions. Fluorapatite grains from the sodic-calcic-ferric/ferrous alteration at Mag Hill are the only ones in the present study where the inclusions are exclusively monazite. The predominance of calcic ± ferric/ferrous over sodic ± ferric/ferrous alteration during the latest stage of metasomatic alteration in the GBMZ may be why allanite preferentially forms as opposed to monazite, in accordance with previous experimental work (*e.g.*, Budzyń et al., 2011).

4.6.4. Uranium and thorium decoupling in Great Bear magmatic zone fluorapatite

An atypical decoupling of U and Th is observed as alteration evolves from the high temperature calcic-ferric/ferrous to potassic-ferric/ferrous leading to enrichment of the less mobile element (Th) over the more mobile element (U) (Acosta-Góngora *et al.* 2014, Gandhi, 1988, Montreuil *et al.* 2013, 2015, 2016a, Ootes *et al.* 2010, Potter *et al.* 2013a, 2013b). For example, the Th-rich amphibole-magnetite-apatite replacement veins of the Fab system are interpreted to be a reaction product between U-rich intrusive rocks and fluids forming high temperature calcic-ferric/ferrous alteration facies (Montreuil *et al.* 2016a). The higher Th content recorded in fluorapatite (compared to U) from these replacement veins (Table 3) is consistent with this explanation. While the full nature and chemistry of the fluids responsible for this decoupling is still under investigation, this mechanism would explain the measurable Th from U

compositional changes within the whole rock chemistry as well as gamma ray spectra of the host rock (Corriveau *et al.* 2010a, 2010b, Montreuil *et al.* 2013, 2016a). Figure 4.9 shows that the U and Th content within a single fluorapatite crystal may record this decoupling as the Th content is higher relative to U within areas along fractures and close to the grain boundary as opposed to the interior.

4.7. CONCLUSION

Fluorapatite from the GBMZ, for a set of selected systems, consistently displays textural features resulting from IOAA metasomatism. Dissolution pits and grain fractures are ubiquitous within the fluorapatite from these altered systems and within regional intrusive rock synchronous to these systems. Inclusions of monazite and allanite are present in fluorapatite from most of the samples. Allanite is the dominant, secondary, REE-bearing phase where late, low temperature calcic alteration is present. The CL response of fluorapatite from the GBMZ is green to yellow-green where the Mn^{2+} activator dominates and blue, originating from REE^{3+} activation otherwise. The latter is present in fluorapatite from the Terra mine and the Dennis showing. Patchy zonation within the CL response for a single fluorapatite grain, in most cases, indicates an originally LREE rich fluorapatite with localized LREE leaching. In the GBMZ fluorapatite, the patchy zonation seen in the BSE images and CL response, the Th and U content, and the presence of monazite and/or allanite inclusions all result from the metasomatic alteration of the IOAA systems, indicating the important role that fluorapatite can play as a tracer of the process and chemistry of alterations during mineralization. As these characteristics are present in single grains, planned future work includes a feasibility study of fluorapatite as an indicator mineral in glacial-sedimentary exploration within the GBMZ.

4.8. ACKNOWLEDGMENTS

This work stems from the Geomapping for Energy and Minerals (GEM) IOCG/Multiple Metals Great Bear Region project at the Geological Survey of Canada (Natural Resources Canada) conducted in partnership with the Wopmay Bedrock Mapping project of the Northwest Territories Geological Survey. The first author was funded by the Research Affiliate Program of Natural Resources Canada. LA-ICP-MS measurements were made under the supervision of Simon Jackson of Geological Survey (Ottawa). Katherine Venance and Pat Hunt of the Geological Survey of Canada Microbeam Laboratory and Dieter Rhede at the Deutsche GeoForschungsZentrum are recognized for their help in obtaining EPMA analyses for fluorapatite and monazite. The authors are also grateful to Cameron Butler and Philip Lypaczewski for their participation to this project during their undergraduate studies at McGill University. This paper constitutes the fourth chapter of the first author's PhD thesis at McGill University. Northwest Territories Geological Survey contribution number 2015 – 0093 and Natural Resources Canada ESS Contribution number 20150365. Dr. John Hanchar and an anonymous reviewer are thanked for their constructive comments.

4.9. REFERENCES

Acosta-Góngora, P., Gleeson, S., Samson, I., Ootes, L., and Corriveau, L., 2014, Trace element geochemistry of magnetite and its relationship to Cu-Bi-Co-Au-Ag-UW mineralization in the Great Bear magmatic zone, NWT, Canada: Economic Geology, v. 109, p. 1901–1928.

Acosta-Góngora, G.P., Gleeson, S.A., Samson, I., Ootes, L., and Corriveau, L., 2015, Gold refining by bismuth melts in the iron oxide-dominated NICO Au-Co-Bi (±Cu±W) deposit, NWT, Canada: Economic Geology, v. 110, p. 291–314.

Aleinikoff, J.N., Selby, D., Slack, J.F., Day, W.C., Pillers, R.M., Cosca, M.A., Seeger, C.M., Fanning, C.M. and Samson, I.M., 2016, U-Pb, Re-Os, and Ar/Ar geochronology of REE-rich breccia pipes and associated host rocks from the Mesoproterozoic Pea Ridge Fe-REE-Au deposit, St. Francois Mountains, Missouri, USA. In A Special Issue Devoted to Proterozoic Iron Oxide-Apatite-(+REE) and Iron Oxide-Copper-Gold and Affiliated Deposits of Southeast Missouri, USA, and the Great Bear Magmatic Zone, Northwest Territories, Canada (Slack, J. F., Corriveau, L. & Hitzman, M. W.): Economic Geology, v. 111, p. p. 1883-1914.

Badham, J., 1975, Mineralogy, paragenesis and origin of the Ag-Ni, Co arsenide mineralisation, Camsell River, NWT Canada: Mineralium Deposita, v. 10, p. 153–175.

Badham, J., and Morton, R., 1976, Magnetite-apatite intrusions and calc-alkaline magmatism, Camsell River, NWT: Canadian Journal of Earth Sciences, v. 13, p. 348–354.

Barton, M.D., and Johnson, D.A., 2004, Footprints of Fe-oxide (Cu-Au) systems: Center for Global Metallogeny, University of Western Australia, Special Publication, v. 33, p. 112–116.

Belousova, E., Griffin, W., O'Reilly, S.Y., and Fisher, N., 2002, Apatite as an indicator mineral for mineral exploration: Trace-element compositions and their relationship to host rock type: Journal of Geochemical Exploration, v. 76, p. 45–69.

Benavides, J., Kyser, T., Clark, A.H., Oates, C.J., Zamora, R., Tarnovschi, R., and Castillo, B., 2007, The Mantoverde iron oxide-copper-gold district, III region, Chile: The role of regionally derived, nonmagmatic fluids in chalcopyrite mineralization: Economic Geology, v. 102, p. 415–440.

Bonyadi, Z., Davidson, G.J., Mehrabi, B., Meffre, S., and Ghazban, F., 2011, Significance of apatite REE depletion and monazite inclusions in the brecciated Se–Chahun iron oxide–apatite deposit, Bafq district, Iran: Insights from paragenesis and geochemistry: Chemical Geology, v. 281, p. 253–269.

Bouzari, F., Hart, C., Barker, S., and Bissig, T., 2011, Porphyry Indicator Minerals (PIMS): A new exploration tool for concealed deposits in south-central British Columbia: Geoscience BC Report, 2011-17, 31 p.

Budzyń, B., Harlov, D.E., Williams, M.L., and Jercinovic, M.J., 2011, Experimental determination of stability relations between monazite, fluorapatite, allanite, and REE-epidote as a function of pressure, temperature, and fluid composition: American Mineralogist, v. 96, p. 1547–1567.

Cabri, L.J., Rudashevsky, N.S., Rudashevsky, V.N. and Oerthür, T. 2008. Electric-Pulse Disaggregation (EPD), Hydroseparation (HS) and their use in combination for mineral processing and advanced characterization of ores; Canadian Mineral Processors 40th Annual Meeting, Proceedings, Paper 14, p. 211-235.

Camier, W.J., 2002, The Sue-Dianne Fe-oxide Cu-Ag-Au breccia complex, southern Great Bear Magmatic Zone, Northwest Territories, Canada: University of Western Ontario, London, Ontario, 220 p.

Corriveau L., Mumin A.H., and Setterfield T., 2010a, IOCG environments in Canada: Characteristics, geological vectors to ore and challenges, in Porter T.M., ed, Hydrothermal iron oxide copper–gold and related deposits: A global perspective volume 4–advances in the understanding of IOCG deposits: Porter Geoscience Consultancy Publishing, Adelaide, p. 311–343.

Corriveau, L., Williams, P.J., and Mumin, A.H., 2010b, Alteration vectors to IOCG mineralization from uncharted terranes to deposits, in Corriveau, L., and Mumin, A.H., eds., Exploring for iron oxide copper-gold deposits: Geological Association of Canada, Short Course Notes 20, p. 89–110.

Corriveau, L., Montreuil, J.-F. and Potter, E., 2016, Alteration facies linkages amongst IOCG, IOA and affiliated deposits in the Great Bear magmatic zone, Northwest Territories, Canada. In A Special Issue Devoted to Proterozoic Iron Oxide-Apatite-(+REE) and Iron Oxide-Copper-Gold and Affiliated Deposits of Southeast Missouri, USA, and the Great Bear Magmatic Zone, Northwest Territories, Canada (Slack, J. F., Corriveau, L. & Hitzman, M. W.): Economic Geology, v. 111, p. 2045–2072.

Daliran, F., Stosch, H.-G., Williams, P.J., Jamali, H., and Dorri, M.-B., 2010, Early Cambrian iron oxide-apatite-REE (U) deposits of the Bafq district, East-Central Iran, in Corriveau, L., and Mumin, A.H., eds., Exploring for iron oxide copper-gold deposits: Canada and global analogues: Geological Association of Canada, Short Course Notes 20, p. 147–159.

Dempster, T.J., Jolivt, M., Tubrett, M.N., Braithwaite, C.J.R., 2003, Magmatic zoning in apatite: a monitor of porosity and permeability change in granites. Contributions to Mineralogy and Petrology, v. 145, p. 568–577.

DeToni, A.F., 2016, Systèmes à oxydes de fer et altérations en éléments alcalins, zone magmatique du Grand lac de l'Ours: Unpublished M.Sc. thesis, Québec Canada, Université du Québec, Institut national de la Recherche scientifique, Centre – Eau Terre Environnement, 738 p.

Edfelt, Å., Armstrong, R.N., Smith, M., and Martinsson, O., 2005, Alteration paragenesis and mineral chemistry of the Tjårrojåkka apatite–iron and Cu (-Au) occurrences, Kiruna area, northern Sweden: Mineralium Deposita, v. 40, p. 409–434.

Fleet, M.E., and Pan, Y., 1995, Site preference of rare earth elements in fluorapatite: American Mineralogist, v. 80, p. 329–335.

Fleet, M.E., and Pan, Y., 1997, Site preference of rare earth elements in fluorapatite: Binary (LREE+ HREE)-substituted crystals: American Mineralogist, v. 82, p. 870–877.

Frietsch, R., and Perdahl, J.A., 1995, Rare earth elements in apatite and magnetite in Kiruna-type iron ores and some other iron ore types: Ore Geology Reviews, v. 9, p. 489–510.

Gandhi, S.S., 1988, Volcano-plutonic setting of U-Cu bearing magnetite veins of FAB claims, southern Great Bear magmatic zone, Northwest Territories: Geological Survey of Canada, Paper 88-1C, p. 177–188.

Gandhi, S.S., Potter, E.G., and Fayek, M., 2013, Polymetallic U-Ag veins at Port Radium, Great Bear magmatic zone, Canada: Main botryoidal pitchblende stage cuts 1.74 Ga diabase dykes and has REE signatures diagnostic of unconformity-type deposits: Geological Survey of Canada, Open File 7493, 1 p.

Gill, F.D., 1969, J Jacobson, Wopmay River Area, Mackenzie: Northwest Territories Geological Survey, Mineral Exploration Report, Assesment Report 060420. 9 p.

Goad, R.E., Mumin, A.H., Duke, N., Neale, K., and Mulligan, D., 2000a, Geology of the Proterozoic iron oxide-hosted, NICO cobalt-gold-bismuth, and Sue Dianne copper-silver deposits, southern Great Bear magmatic zone, Northwest Territories, Canada, in Porter T.M., ed, Hydrothermal iron oxide copper–gold and related deposits: A global perspective volume 1: Porter Geoscience Consultancy Publishing, Adelaide, p. 249–268.

Goad, R.E., Mumin, A.H., Duke, N., Neale, K.L., Mulligan, D.L., and Camier, W.J., 2000b, The NICO and Sue-Dianne Proterozoic, iron oxide-hosted, polymetallic deposits, Northwest Territories: Application of the Olympic Dam model in exploration: Exploration and Mining Geology, v. 9, p. 123–140.

Göetze, J., 2012, Applications of cathodoluminescence microscopy and sprectroscopy in geosciences: Microscopic and Microanalysis, v. 18, p. 1270–1284.

Goldof, B., Webster, J.D., and Harlov, D.E., 2012, Characterization of fluor-chlorapatites by electron probe microanalysis with a focus on time-dependant intensity variation of halogens: American Mineralogist, v. 97, p. 1103–1115.

Groves, D.I., Bierlein, F.P., Meinert, L.D., and Hitzman, M.W., 2010, Iron oxide copper-gold (IOCG) deposits through earth history: Implications for origin, lithospheric setting, and distinction from other epigenetic iron oxide deposits: Economic Geology, v. 105, p. 641–654.

Harlov, D.E., 2015, Apatite: A fingerprint for metasomatic processes: Elements, v. 11, p. 171–176.

Harlov, D.E. , Meighan, C.,Kerr, I. and Samson, I. M., 2016 Mineralogy, chemistry, and fluid-aided evolution of the Pea Ridge Fe oxide-(Y + REE) deposit, southeast Missouri, USA. In A Special Issue Devoted to Proterozoic Iron Oxide-Apatite-(+REE) and Iron Oxide-Copper-Gold and Affiliated Deposits of Southeast Missouri, USA, and the Great Bear Magmatic Zone, Northwest Territories, Canada (Slack, J. F., Corriveau, L., & Hitzman, M. W.): Economic Geology, v. 111, p. 1963–1984.

Harlov, D.E., and Förster, H.J., 2004, Fluid-induced nucleation of (Y+ REE)-phosphate minerals within apatite: Nature and experiment. Part II. Fluorapatite: American Mineralogist, v. 88, p. 1209–1229.

Harlov, D.E., Andersson, U.B., Förster, H.-J., Nyström, J.O., Dulski, P., and Broman, C., 2002, Apatite–monazite relations in the Kiirunavaara magnetite–apatite ore, northern Sweden: Chemical Geology, v. 191, p. 47–72.

Harlov, D.E., Förster, H.J., and Schmidt, C., 2003, High PT experimental metasomatism of a fluorapatite with significant britholite and fluorellestadite components: Implications for LREE mobility during granulite-facies metamorphism: Mineralogical Magazine, v. 67, p. 61–72.

Harlov, D.E., Wirth, R., and Förster, H.J., 2005, An experimental study of dissolution–reprecipitation in fluorapatite: Fluid infiltration and the formation of monazite: Contributions to Mineralogy and Petrology, v. 150, p. 268–286.

Harlov, D.E., Wirth, R., and Hetherington, C.J., 2007, The relative stability of monazite and huttonite at 300–900 C and 200–1000 MPa: Metasomatism and the propagation of metastable mineral phases: American Mineralogist, v. 92, p. 1652–1664.

Hildebrand, R.S., 1986, Kiruna-type deposits; their origin and relationship to intermediate subvolcanic plutons in the Great Bear magmatic zone, Northwest Canada: Economic Geology, v. 81, p. 640–659.

Hildebrand, R.S., Hoffman, P.F., and Bowring, S.A., 1987, Tectono-magmatic evolution of the 1.9-Ga Great Bear magmatic zone, Wopmay Orogen, northwestern Canada: Journal of Volcanology and Geothermal Research, v. 32, p. 99–118.

Hildebrand, R.S., Hoffman, P.F., and Bowring, S.A., 2010, The Calderian orogeny in Wopmay orogen (1.9 Ga), northwestern Canadian Shield: Geological Society of America Bulletin, v. 122, p. 794–814.

Hoffman P.F., and Hall, L., 1993, Geology, Slave craton and environs, district of Mackenzie, Northwest Territories: Geological Survey of Canada, Open File 2559, scale 1:1 000 000.

Hofstra, A.H., Meighan, C.J., Song, X., Samson, I., Marsh, E.E., Lowers, H.A., Emsbo, P. and Hunt, A.G., 2016, Mineral thermometry and fluid inclusion studies of the Pea Ridge iron oxide-apatite-rare earth element deposit, Mesoproterozoic St. Francois Mountains terrane, southeast Missouri, USA. In A Special Issue Devoted to Proterozoic Iron Oxide-Apatite-(+REE) and Iron Oxide-Copper-Gold and Affiliated Deposits of Southeast Missouri, USA, and the Great Bear Magmatic Zone, Northwest Territories, Canada (Slack, J. F., Corriveau, L. & Hitzman, M. W.): Economic Geology, v. 111, p.1985-2016.

Hu, H., Li, J.-W., Lentz, D., Ren, Z., Zhao, X.-F., Deng, X.-D. and Hall, D., 2014, Dissolution–reprecipitation process of magnetite from the Chengchao iron deposit: Insights into ore genesis and implication for in-situ chemical analysis of magnetite: Ore Geology Reviews, v. 57, p. 393–405.

Hughes, J.M., and Rakovan, J., 2002, The crystal structure of apatite, Ca5 (PO4) 3 (F, OH, Cl): Reviews in Mineralogy and Geochemistry, v. 48, p. 1–12.

Hughes, J.M., and Rakovan, J.F., 2015, Structurally robust, chemically diverse: Apatite and apatite supergroup minerals: Elements, v. 11, p. 165–170.

Hughes, J.M., Cameron, M., and Mariano, A.N., 1991, Rare-earth-element ordering and structural variations in natural rare-earth-bearing apatites: American Mineralogist, v. 76, p. 1165–1173.

Jackson, S.E., 2008, Calibration strategies for elemental analysis by LA-ICP-MS, in Sylvester, P., ed., Laser ablation-ICP-MS in the Earth sciences: Mineral Association of Canada, Short Course Series, v. 40, p. 69–188.

Jackson, V.A., van Breemen, O., Ootes, L., Bleeker, W., Bennett, V., Davis, W.D., Ketchum, J., and Smar, L., 2013, Ages of basement and intrusive phases east of the Wopmay fault zone, south-central Wopmay Orogen, NWT: A field-based U–Pb zircon study: Canadian Journal of Earth Sciences, v. 50, p. 979–1006.

Jarosewich, E. and Boatner, L.A., 1991, Rare-Earth element refeerence sample for electron microprobe analysis. Geostandards and Geoanalytical Reasearch, v. 15, p. 397-399.

Johnson, C.A., Day, W.C. and Rye, R.O., 2016, Oxygen, hydrogen, sulfur, and carbon isotopes in the Pea Ridge magnetite-apatite deposit, southeast Missouri, and sulfur isotope comparisons to other iron deposits in the region. In A Special Issue Devoted to Proterozoic Iron Oxide-Apatite-(+REE) and Iron Oxide-Copper-Gold and Affiliated Deposits of Southeast Missouri, USA, and the Great Bear Magmatic Zone, Northwest Territories, Canada (Slack, J. F., Corriveau, L. & Hitzman, M. W.): Economic Geology, v. 111, p. 2017-2032.

Jonsson, E., Harlov, D.E., Majka, J., Högdahl, K. and Persson-Nilsson, K., 2016, Fluorapatite-monazite-allanite relations in the Grängesberg apatite-iron oxide ore district, Bergslagen, Sweden: American Mineralogist, v. 101, p. 1769–1782.

Kempe, U., and Götze, J., 2002, Cathodoluminescence (CL) behaviour and crystal chemistry of apatite from rare-metal deposits: Mineralogical Magazine, v. 66, p. 151–172.

Krneta, S., Ciobanu, C.L., Cook, N.J., Ehrig, K., and Kamenetsky, V.S., 2015, Apatite in the Olympic Dam Fe-oxide Cu-U-Au-Ag deposit: Proceeding of the 13th Biennial SGA Meeting, 24-27 August 2015, Nancy, France.

Lypaczewski, P., Normandeau, P.X., Paquette, J., and McMartin, I., 2013, Petrographic and cathodoluminescence characterization of apatite from the Sue-Dianne and Brooke Zone IOCG mineralization systems, Great Bear magmatic zone, Northwest Territories, Canada: Geological Survey of Canada. Open File 7319, 18 p.

Mao, J., Xie, G., Duan, C., Pirajno, F., Ishiyama, D. and Chen, Y., 2011, A tectono-genetic model for porphyry-skarn-stratabound Cu-Au-Mo-Fe and magnetite-apatite deposits along the Middle-Lower Yangtze River Valley, Eastern China: Ore Geology Reviews, v. 43, p. 294–314.

Mao, M., Rukhlov, A.S., Rowins, S.M., Spence, J., and Coogan, L.A., 2015, Detrital apatite trace-element compositions: A robust new tool for mineral exploration: British Columbia Ministry of Energy and Mines, British Columbia Geological Survey, GeoFile 2015-09, 1 p.

Mao, M., Rukhlov, A.S., Rowins, S.M., Spence, J. and Coogan, L.A., 2016, Apatite trace element composition: A robust new tool for mineral exploration: Economic Geology, v. 111, p. 1187–1222.

Mitchell, R.H., 2014, Cathodoluminescence of apatite, in Coulson, I.M., ed., Cathodoluminescence and its application to geoscience: Mineral Association of Canada, Short Course Series, v. 45, p. 143–167.

Mitchell, R.H., and Platt, R.G., 1978, Mafic mineralogy of ferroaugite syenite from the Coldwell alkaline complex, Ontario: Canada: Journal of Petrology, v. 19, p. 627–651.

Mitchell, R.M., Xiong, J., Mariano, A.N., and Fleet, M.E., 1997, Rare-earth element-activated cathodoluminescence in apatite: The Canadian Mineralogist, v. 35, p. 979–998.

Montreuil, J.-F., Corriveau, L., and Grunsky, E., 2013, Compositional data analysis of hydrothermal alteration in IOCG systems, Great Bear magmatic zone, Canada: to each alteration type its own geochemical signature: Geochemistry: Exploration, Environment, Analysis, v. 13, p. 229–247.

Montreuil, J.-F., Corriveau, L., and Potter, E.G., 2015, Formation of albitite-hosted uranium within IOCG systems: the Southern Breccia, Great Bear magmatic zone, Northwest Territories, Canada: Mineralium Deposita, v. 50, p. 293–325.

Montreuil, J.-F., Potter, E.G., Corriveau, L., and Davis, W.J., 2016a, Element mobility patterns in magnetite-group IOCG systems: The Fab IOCG system, Northwest Territories, Canada: Ore Geology Reviews, v. 72, p. 562–584.

Montreuil, J.-F., Corriveau, L. and Potter, E.G., 2016b, On the relation between alteration signature and metal endowment of iron oxide alkali altered systems, southern Great Bear magmatic zone (Canada). In A Special Issue Devoted to Proterozoic Iron Oxide-Apatite-(+REE) and Iron Oxide-Copper-Gold and Affiliated Deposits of Southeast Missouri, USA, and the Great Bear Magmatic Zone, Northwest Territories, Canada (Slack, J. F., Corriveau, L. & Hitzman, M. W.): Economic Geology, v. 111, p. 1803–1814.

Mumin, A.H., ed., 2015, Echo Bay IOCG thematic map series: geology, structure and hydrothermal alteration of a stratovolcano complex, Northwest Territories, Canada: Geological Survey of Canada, Open File 7807, 19 p.

Mumin, A.H., Corriveau, L., Somarin, A.K., and Ootes, L., 2007, Iron oxide copper-gold-type polymetallic mineralisation in the Contact Lake Belt, Great Bear Magmatic Zone, Northwest Territories, Canada: Exploration and Mining Geology, v. 16, p. 187–208.

Mumin, A.H., Somarin, A.K., Jones, B., Corriveau, L., Ootes, L., and Camier, W.J., 2010, The IOCG-porphyry-epithermal continuum in the Great Bear Magmatic Zone, Northwest Territories, Canada, in Corriveau, L., and Mumin, A.H., eds., Exploring for Iron-Oxide Copper-Gold deposits: Canada and global analogues: Geological Association of Canada, Short Course Notes, v. 20, p. 59–78.

Murray, J.R., and Oreskes, N., 1997, Uses and limitations of cathodoluminescence in the study of apatite paragenesis: Economic Geology, v. 92, p. 368–376.

Normandeau, P.X., and McMartin, I., 2013, Composition of till and bedrock across the Great Bear magmatic zone: Quaternary field database and analytical results from the GEM IOCG-Great Bear project: Geological Survey of Canada, Open File 7307, 22 p.

Normin, 2016 Northwest Territories Geological Survey: Geoscience Web site, URL http://www.nwtgeoscience.ca/normin.

Nyström, J.O. and Henriquez, F., 1989, Dendritic magnetite and miniature diaper-like concentrations of apatite: Two magmatic features of the Kiirunavaara iron ore: Geologiska Föreningens i Stockholm Förhandlingar, v. 111, p. 53–64.

Nyström, J.O. and Henriquez, F., 1994, Magmatic features of iron ores of the Kiruna type in Chile and Sweden: Ore textures and magnetite geochemistry: Economic Geology, v. 89, p. 820–839.

Ootes, L., Goff, S., Jackson, V.A., Gleeson, S.A., Creaser, R.A., Samson, I.M., Evensen, N., Corriveau, L., and Mumin, A.H., 2010, Timing and thermochemical constraints on multi-element mineralisation at the Nori/RA Cu–Mo–U prospect, Great Bear magmatic zone, Northwest Territories, Canada: Mineralium Deposita, v. 45, p. 549–566.

Pan, Y., and Fleet, M.E., 2002, Compositions of the apatite-group minerals: Substitution mechanisms and controlling factors: Reviews in Mineralogy and Geochemistry, v. 48, p. 13–49.

Piccoli, P.M., and Candela, P.A., 2002, Apatite in igneous systems: Reviews in Mineralogy and Geochemistry, v. 48, p. 255–292.

Potter, E.G., Corriveau, L., and Montreuil, J.-F., 2013a, Iron oxide-copper-gold ±uranium in the Great Bear Magmatic Zone: Nature of uranium in IOCG systems: Geological Survey of Canada, Open File 7254, 1 p.

Potter, E.G., Montreuil, J.-F., and DeToni, A., 2013b, Geology and hydrothermal alteration of the Fab Lake region, Northwest Territories: Geological Survey of Canada, Open File 7339, 27 p.

Porter, T.M., 2010, Current understanding of iron oxide associated-alkali altered mineralised systems: Part 1- An overview; Part 2 –A review, in Porter, T.M., ed., Hydrothermal iron oxide copper-gold and related deposits: A global perspective, volume 3-Advances in the understanding of IOCG deposits: Porter Geoscience Consultancy Publishing, Adelaide, p. 5–106.

Rae, D.A, Coulson,I.M., and Chambers, A.D., 1996, Metasomatism in the North Qôroq Centre, South Greenland: apatite chemistry and rare-earth element transport: Mineralogical Magazine, v. 60, p. 207–220.

Reisfeld, R., Gaft, M., Boulon, G., Panczer, C., and Jørgensen, C., 1996, Laser-induced luminescence of rare-earth elements in natural fluor-apatites: Journal of Luminescence, v. 69, p. 343–353.

Roeder, P.L., MacArthur, D., Ma, X.P., and Palmer, G.R., 1987, Cathodoluminescence and microprobe study of rare-earth elements in apatite: American mineralogist, v. 72, p. 801–811.

Rusk, B., Oliver, N., Cleverley, J., Blenkinsop, T., Zhang, D., Williams, P., and Habermann, P., 2010, Physical and chemical characteristics of the Ernest Henry iron oxide copper gold deposit, Australia; implications for IOGC genesis, in Porter, T.M. ed., hydrothermal iron oxide copper-gold & related deposits: A global perspective, v. 3–Advances in the understanding of IOCG deposits: Porter Geoscience Consultancy Publishing, Adelaide, p 1–18.

Shegelski, I.R.J., 1973, Geology and mineralogy of the Terra Silver mine, Camsell River, N.W.T.: Unpublished M.Sc. thesis, Toronto Canada, University of Toronto, 169 p.

Somarin, A., and Mumin, A.H., 2014, P-T composition and evolution of paleofluids in the Paleoproterozoic Mag Hill IOCG system, Contact Lake belt, Northwest Territories, Canada: Mineralium Deposita, v. 49, p. 199–215.

Stormer, J.C., Pierson, L.M., and Tacker, R.C., 1993, Variation of F and Cl X-Ray intensity due to anisotropic diffusion in apatite during electron microprobe analysis: American Mineralogist, v. 78, p. 641–648.

Torab, F., and Lehmann, B., 2007, Magnetite-apatite deposits of the Bafq district, Central Iran: Apatite geochemistry and monazite geochronology: Mineralogical Magazine, v. 71, p. 347–363.

Van Achterbergh, E., Ryan, C.G., Jackson, S.E. and Griffin,W.L., 2001, Data reduction software for LA-ICP-MS: appendix. In: Sylvester, P.J. (Ed.), Laser Ablation-ICP-Mass Spectrometry in the Earth Sciences: Principles and Applications, Mineralog. Assoc. Canada (MAC) Short Course Series, Ottawa, Ontario, Canada, v. 29, p. 239– 243.

Westhues, A., Hanchar, J.M., Whitehouse, M.J. and Martinsson, O., 2016, New constraints on the timing of host-rock emplacement, hydrothermal alteration, and iron oxide-apatite mineralization in the Kiruna district, Norrbotten, Sweden: Econmic Geology, v. 111, p. 1595–1618.

Young, E.J., Myers, A.T., Munson, E.L. and Conklin, N.M., 1969, Mineralogy and geochemistry of fluorapatite from Cerro de Mercado, Durango, Mexico: US. Geological Survey Professional Paper. 650(D), 84– 93.

Zirner, A.L., Marks, M.A., Wenzel, T., Jacob, D.E., and Markl, G., 2015, Rare earth elements in apatite as a monitor of magmatic and metasomatic processes: The Ilímaussaq complex, South Greenland: Lithos, v. 228–229, p. 12–22.

RATIONALE OF CHAPTER 5

Apatite with irregular zoning, jagged crystal edges, dissolution pits and secondary REE-rich mineral inclusions of monazite and allanite were described from bedrock samples and interpreted in Chapter 4. These characteristics represent distinct features of apatite growth within IOAA systems and subsequent remobilization of elements. Of these characteristics, the dissolution pits are the most frequent and are ubiquitous within the studied GBMZ samples. Inclusions of monazite and allanite are found in the apatite from most of the samples with allanite being the dominant REE-bearing phase where late, low temperature calcic alteration is present. The CL response of fluorapatite from the GBMZ is an indication of metasomatic alteration with the green to yellow-green color originating where the manganese activator dominates and a blue color originating from REE activation. Chapter 5 focuses on the usefulness of apatite as an indicator mineral in till. It investigates chemical and physical characteristics of apatite picked from the heavy mineral concentrated fraction of the till samples as well as methodological aspects to be considered when using apatite as an indicator mineral. This chapter was written as a manuscript to be published as a joint NTGS-GSC Open File.

CHAPTER 5: The use of apatite as an indicator mineral of IOA and IOCG deposits in till from the Great Bear magmatic zone

5.1. INTRODUCTION

Apatite is commonly recognized as an indicator of growth environment (Harlov, 2015; Hughes and Rakovan, 2015). Apatite major and trace element chemistry can be used to fingerprint metasomatic processes (Harlov et al., 2002; Bonyadi et al., 2011; Budzyń et al., 2011; Harlov, 2015) as well as discriminate various types of mineral deposits (Belousova et al., 2002; Bouzari et al., 2011; Mao et al., 2015; Mao et al., 2016). Cathodoluminescence (CL) characterization of apatite can also be used as an exploration tool based on variations in the color response, intensity and zonation to discriminate between apatite from systems of interest (e.g. porphyry and carbonatite) and apatite from non-mineralized host rocks (e.g. Kempe and Götze, 2002; Mitchell, 2014). Normandeau et al. (in press, see Chapter 4) identified associations between textural, chemical and CL characteristics of apatite and various metasomatic alterations occurring within rocks of the Great Bear magmatic zone (GBMZ). These observations also highlight the importance of individual apatite grain characterization if their trace element composition is to be used to infer a crystallization environment through a statistical approach (e.g.: Belousova et al., 2002; Mao et al., 2016). The work presented here will test if textural, chemical and CL characteristics can be applied to the use of apatite as an indicator mineral of IOA and IOCG deposits in till from the GBMZ.

5.2. METHODOLOGY

5.2.1. Field procedures

The sampling strategy was designed to collect till containing signatures of iron oxide alkali altered systems and associated IOA to IOCG mineralization from the GBMZ as well as till derived from non-mineralized host rocks and from the regional background. 101 till samples and 95 bedrock samples were collected for the recovery of indicator minerals (Tables 5.1 and 5.2). In the Sue Dianne (n=30) and the Fab system (n=23) areas, till samples were collected proximal to, up-ice and down-ice from mineralization. Till samples (n=25) were also collected near other known showings within large IOAA systems, in the GBMZ background (n=9) as well as in the regional background east of the GBMZ (n=5). Bedrock samples were collected from mineralized (n=57) and non-mineralized (n=23) rocks of various IOA to IOCG deposits or prospects and IOAA systems, and from least altered GBMZ (n=13) rocks and regional rocks from the Wopmay metamorphic zone and Slave Craton (n=2). Rocks from the Sue Dianne deposit also include samples from the nearby satellite Brooke Zone showing. Detailed till and bedrock sample locations and descriptions are provided in Chapters 2, 3 and 4 and in Appendix 1.

5.2.2. Indicator mineral recovery

Heavy mineral processing, concentration and grain picking of till and bedrock samples were performed by Overburden Drilling Management Ltd. Ottawa, (ODM) according to standard procedures (Fig 5.1) followed at the GSC for GEM projects (Plouffe et al., 2013) as described in Normandeau and McMartin (2013; see Chapter 2). Table concentrates were washed with an

oxalic acid solution prior to the heavy liquid separation at a density threshold of 3.2 S.G. After a ferromagnetic separation, the non-ferromagnetic heavy mineral concentrates (NF-HMC) were sieved in three distinct size fractions (0.25 to 0.5 mm, 0.5 to 1 mm, and 1 to 2 mm) and each fraction was examined for potential indicator mineral grains. Mineral species were first identified and picked by trained personnel, and checks were performed on selected grains using SEM-energy dispersive x-ray spectrometer (EDS) to confirm mineral identity at ODM. Apatite counts were reported as % of the >1 amp non-paramagnetic fraction of the 0.25-0.5 mm NF-HMC size fraction (Tables 5.1 and 5.2). The number of apatite grains picked for further analysis in the 0.25-0.5 mm and 0.5-1 mm fractions were also reported. One apatite grain was found in each of the 1-2 mm fraction of two till samples (10CQA2029A1 and 10CQA2036A1). When a specific mineral species was present in a large amount, only a representative population was picked for further study (usually about 20 grains). All apatite original counts and picking results (S.G. >3.2) are provided in Normandeau and McMartin (2013) and in Appendix 1 of the thesis.

Subsequent to these standard procedures, the NF-HMC from a selection of samples having high apatite abundance was re-picked in order to provide additional unmounted apatite grains for CL characterization prior to mounting. Fifty additional grains per sample were picked from 5 bedrock and 5 till samples (S.G. > 3.2), and from 3 bedrock and 5 till samples (3.2 > S.G. > 3.0). The additional re-picking results (S.G. > 3.2 and 3.2 > S.G. > 3.0) are presented in Table 5.3.

5.2.3. Binocular microscope and SEM images of selected grains

The texture of randomly selected grains from till and disaggregated bedrock samples was studied using binocular and scanning electron microscopy (SEM). Backscattered electron images (BSE) and energy dispersive X-ray spectroscopy analysis (EDX) were performed on the 2009 samples using the Hitachi S-3200N variable pressure SEM at the GSC Microbeam Laboratory and for the 2010 samples using the Hitachi S-3000N variable pressure SEM at the Facility for Electron Microscopy Research (FER) at McGill University. The beam was set at 25 kV in variable pressure mode (set at 20 Pa). Single-point, non-quantitative compositional data were obtained using EDX with the INCA analysis software. Readings were integrated over a period of 50 seconds and taken at multiple locations in order to provide complete identification of polymineralic grains. Representative binocular and BSE data, as well as an observation summary document are provided in Normandeau and McMartin (2013) (see Appendix 1).

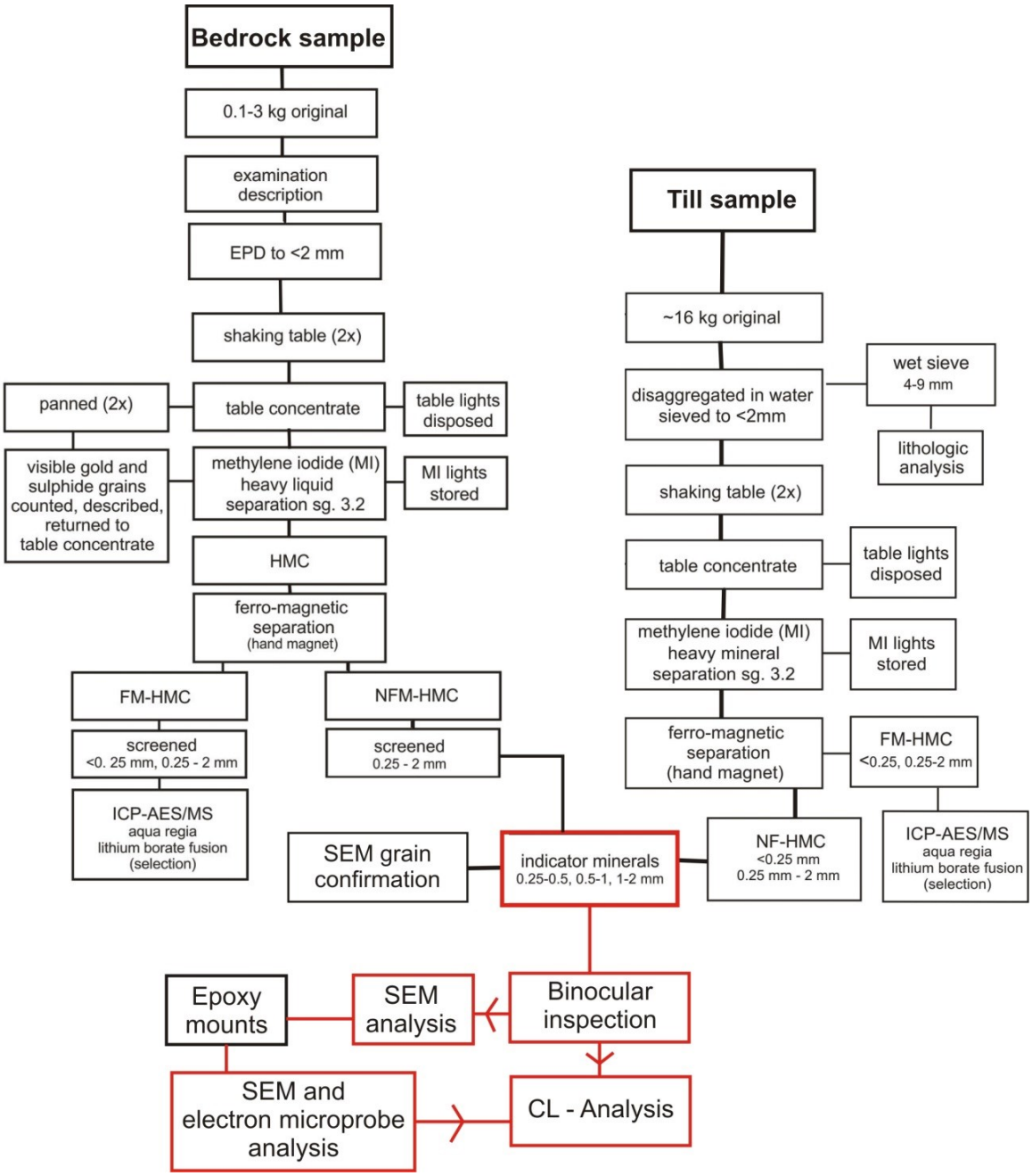

Figure 5.1: Generalized flow sheet showing steps in till sample processing for indicator mineral recovery. Black boxes represent steps taken by commercial laboratories; red boxes represent the additional observations and analysis performed by the thesis author on apatite grains.

5.2.4. Electron microprobe analysis

Picked apatite grains were mounted on 25-mm epoxy-impregnated stubs at SGS Lakefield Research Laboratory. The grains were analyzed to confirm their identity and quantify their chemical composition. Analyses were conducted at the GSC Microbeam Laboratory using a CAMECA SX50 electron microprobe (EMP) equipped with four wavelength-dispersive spectrometers. Operating conditions were 20 kV accelerating voltage and 10 nA beam current using a focused spot. Count times on peak were 10 seconds, with 5 seconds off-peak. Standards comprise a range of natural and synthetic pure metals, simple oxides and simple compounds. The analysed grains were classified (or re-classified when necessary) by K. Venance (GSC) and I. Kjarsgaard (2009 results only) on the basis of their chemical composition. 31 grains out of 773 picked as apatite were identified as species other than apatite and were excluded from further analyses. Theoretical chemical compositions of mineral end-members (LeMaitre, 1982) were used to calculate cut-off values (at approximately 50:50 mol %) for members of binary solid solution series. Some of the grain mounts were not suitable for work on a per-grain basis. EMP work on grain mounts at the GSC is done in automated mode: the coordinates of clean spots away from cracks and impurities are loaded off-line. Some of the grains were heterogeneous (comprising multiple phases) or the phase of interest comprised only a minor component of the grain. The chemical results for the 0.25-1 mm apatite are provided in Appendix 1-XV.

5.2.5. Cathodoluminescence (CL) microscopy

Cathodoluminescence optical microscopy and photomicrography were conducted at the department of Earth and Planetary Sciences of McGill University using a qualitative low vacuum Relion system set to a 4.0 kV beam with an exposure time of 3 to 4 seconds, and a gain of 5. A preliminary CL activation was performed to scan samples using a 250–400 milliseconds exposure. Low exposure time was used to reduce the loss of signal through time (luminescence aging; Murray and Oreskes, 1997). CL analysis were performed on picked grains mounted on epoxy stubs after carbon coating removal using a 1 micron polishing powder as well as on the unmounted grains re-picked at a later stage. During CL microscopy of unmounted grains, measurements were performed with beam voltages varying from 2 kV to 3.5 kV and the exposure time was set from 10 seconds to 20 seconds.

Setting		Number of samples	Proportion (%) of apatite grains in NF-HMC (>1 amp) (0.25 - 0.5 mm)	Number of apatite grain picked NF-HMC (>1 amp) (0.25 - 0.5 mm)	Number of apatite grain picked NF-HMC (>1 amp) (0.5 - 1.0 mm)
GBMZ background and other samples					
	GBMZ background	(n=9)	0 to 1	0 to 20	0 to 1
	Slave Craton and east of the Wopmay fault zone	(n=5)	traces to 10	1 to 20	0 to 4
Down-ice of IOAA showings within the GBMZ					
	Hottah Lake	(n=8)	0 to 2	0 to 20	0 to 1
	Stew Zone (NICO area)	09MOB037	0	0	0
	LCL	09MOB043	traces	16	17
	UR	09MOB041	0	0	0
	Dry	10CQA2061A1	traces	6	0
	DV-3	10CQA2034A1	traces	1	0
	DV-8	10CQA2031A1	traces	2	0
	Grouard Lake South	10CQA2041A1	traces	2	0
	Jackpot-McPhoo	10CQA2052A1	traces	8	0
	Jackpot-McPhoo	10CQA2055A1	1	0	2
	MRB	09MOB032	0.5	20	0
	HS-1 (NICO area)	09MOB030	3	20	0
	OUR (NICO area)	09MOB036	traces	1	1
	Lou Lake (NICO area)	09MOB038	0	0	0
	Rainy Lake 1 (Terra mine area)	10CQA2046A1	traces	12	0
	UR	09MOB040	0	0	0
	Torrie Lake - Unnamed	10CQA2059A1	traces	10	0
	Tatie	09MOB045	0	0	0

Table 5.1: Apatite grain counts and number of grains picked in non-ferromagnetic heavy mineral concentrates (0.25-1 mm; SG>3.2) of till samples.

Setting	Number of samples	Proportion (%) of apatite grains in NF-HMC (>1 amp) (0.25 - 0.5 mm)	Number of apatite grain picked NF-HMC (>1 amp) (0.25 - 0.5 mm)	Number of apatite grain picked NF-HMC (>1 amp) (0.5 - 1.0 mm)
Sue Dianne deposits and local background				
Down-ice (< 200m)	09MOB002	3	20	0
Down-ice (< 500m)	09MOB021	10	20	0
Down-ice (< 500m)	09MOB022	traces	20	0
Down-ice (< 500m)	09MOB023	traces	20	0
Down-ice (< 500m)	09MOB024	15	20	0
Down-ice (< 1000m)	09MOB025	20	20	0
Down-ice (< 1000m)	09MOB026	0	0	0
Down-ice (< 1000m)	09MOB027	0	0	0
Down-ice (< 1000m)	09MOB028	2	20	0
Down-ice (< 1000m)	09MOB029	4	20	0
Up - ice (< 200m)	09MOB001	2	20	0
Sue Dianne deposit local background				
Marian River Batholith	(n=7)	traces to 20	20	0
Undifferentiated porphyry	(n=9)	0 to 20	0 to 20	0
Undifferentiated volcanic	(n=3)	0 to 12	0 to 22	0
Fab system and local background				
Down-ice (< 200m)	09MOB042	0	0	0
Down-ice (< 250m)	10CQA2016A1	1	20	0
Down-ice (< 250m)	10CQA2019A1	traces	20	0
Down-ice (< 250m)	10CQA2021A1	traces	1	0
Down-ice (< 300m)	10CQA2007A1	15	20	19
Down-ice (< 500m)	10CQA2003A1	0.5	20	0
Down-ice (< 500m)	10CQA2004A1	0.5	20	0
Down-ice (< 500m)	10CQA2008A1	4	20	9
Down-ice (< 500m)	10CQA2015A1	traces	2	0
Down-ice (< 2000m)	10CQA2009C1	4	20	0
Down-ice (< 2000m)	10CQA2011A1	0.5	20	0
Down-ice (< 2000m)	10CQA2012A1	2	20	0
Down-ice (< 2000m)	10CQA2022A1	5	20	1
Up - ice (< 500m)	(n=2)	traces to 1	5 to 20	6 to 30
Fab system local background				
Undifferentiated porphyry	(n=3)	0.5 to 10	20	0 to 1
Undifferentiated granit	(n=5)	traces to 15	20	0 to 20

Table 5.1 (cont.): Apatite grain counts and number of grains picked in non-ferromagnetic heavy mineral concentrates (0.25-1 mm; SG>3.2) of till samples.

Setting	Number of samples	Proportion (%) of apatite grains in NF-HMC (>1 amp) (0.25 - 0.5 mm)	Number of apatite grain picked NF-HMC (>1 amp) (0.25 - 0.5 mm)	Number of apatite grain picked NF-HMC (>1 amp) (0.5 - 1.0 mm)
GBMZ background and other samples				
GBMZ background - least altered host rock	(n=13)	0 to 5	0 to 3	0
Slave Craton and east of the Wopmay fault zone	(n=2)	0 to traces	0 to 1	0
Sue Dianne deposit				
mineralized rock	(n=9)	0	0	0
non mineralized rock	(n=16)	0 to traces	0 to 1	0
Fab system				
mineralized rock	(n=5)	0	0	0
non mineralized rock	(n=7)	0	0	0
Other IOAA systems within the GBMZ				
NICO - mineralized rock	(n=2)	0	0	0
Dennis showing - mineralized rock	(n=2)	10	45	0
Terra mine - mineralized rock	(n=12)	0 to 99	0 to 7	0 to 1
JLD - mineralized rock	(n=2)	0 to 5	0 to 20	0 to 1
LCL - mineralized rock	(n=1)	0	0	0
UR - mineralized rock	(n=1)	0	0	0
Dry - mineralized rock	(n=1)	0	0	0
Grouard Lake South - mineralized rock	(n=2)	0	0	0
Jackpot-McPhoo - mineralized rock	(n=1)	0	0	0
Other showings - mineralized rock	(n=19)	0	0	0

Table 5.2: Apatite grain counts and number of grains picked in non-ferromagnetic heavy mineral concentrates (0.25-1 mm; SG>3.2) of disaggregated bedrock samples.

Sample		Location	S.G.	number of apatite grain picked	Cathodoluminescence (CL)
Till	09MOB031	~ 700 m Down-ice of the Sue Dianne deposit	>3.2	50	>50% of grains with blue or blue and green CL response, multiple grains with red spots and lines
			3.0-3.2	50	
	09MOB023	~ 300 m Down-ice of the Sue Dianne deposit	>3.2	50	~ 30 % of grains with faint blue-green CL. Occasional grain with red spots
			3.0-3.2	50	
	09MOB025	~ 300 m Down-ice of the Sue Dianne deposit	>3.2	50	~ 30 % of grains with faint blue-green CL. Occasional grain with red spots
			3.0-3.2	50	
	10CQA2007A1	~ 250 m Down-ice of a showing from the Fab system	>3.2	50	Green CL, 50% of grains zoned based on CL intensity, >50% uniformely green
	10CQA2036A1	Regional sample ~15 km east of the Fab system	>3.2	50	Green CL, 50% of grains zoned based on CL intensity, >50% uniformely green
			3.0-3.2	50	
Bedrock	09CQA1170D3	JLD showing - mineralized rock	>3.2	50	Green CL, grains are zoned based on CL intensity
	09CQA145E4	Dennis showing - mineralized rock	>3.2	50	Green and Green and blue zoned CL, presence of CL red dots
			3.0-3.2	50	
	09CQA1045C8	Dennis showing - mineralized rock	>3.2	50	Blue and blue-green zoned grains. Many faces partially hidden by hematite
			3.0-3.2	50	
	10cqa2054b1	Grouard Lake - altered volcanic rocks	>3.2	50	Green CL, grains are zoned based on CL intensity. Many faces partially hidden by hematite
	09CQA128B2	Terra mine altered - volcanic rock	>3.2	50	No CL response (grains covered in hematite)

Table 5.3: Additional apatite re-picking results and cathodoluminescence characterization from till and bedrock non-ferromagnetic heavy mineral concentrates (0.25-0.5 mm).

5.3. RESULTS

5.3.1. Apatite abundance

Although marginally heavy (S.G. = 3.16–3.22), apatite is a common mineral recovered in till samples from the GBMZ; it was present in 85 out of the 101 till samples (S.G. >3.2). Observed grains vary in size from the lowest limit of the recovered size fraction (0.25 mm) to the highest limit (2 mm) and may occur from trace amounts (1-3 grains/sample) to a significant proportion (20%) of the non-paramagnetic fraction of the NF-HMC of till samples (Table 5.1). In disaggregated bedrock, apatite was much less abundant than in till and recovered in only 11 out of the 95 samples, although it occurs in abundance in a few samples from the JLD and the Dennis showing, and in a sample from the Terra mine deposit where it constitutes 99% of the non-paramagnetic fraction (Table 5.2). Apatite is also relatively abundant in one sample collected far from any IOAA in the GBMZ least altered background. Although observed in thin sections from Sue Dianne deposit and Fab system bedrock samples (Chapter 4; Appendix 3), apatite was not recovered in the NF-HMC of disaggregated mineralized bedrock samples from these systems. The apatite grains observed in thin sections from these mineralized systems varied in size from 20 μm to 3 mm; therefore, apatite grains should have been recovered in the picked size fractions. Crystal disintegration during rock sample disaggregation under the EPD, or oversight during mineral picking, could be at cause.

5.3.2. Apatite color and shape

Under the binocular microscope, picked apatite grains are colorless to lightly colored, either pale blue, green or light pink (Fig. 5.2). No correlation was established between apatite color and apatite source or location, in either till or bedrock. Apatite grain shapes are anhedral to subhedral, with a number of faces following the apatite crystal habits (Fig. 5.3), similar to apatite observed in thin sections from bedrock samples (Lypaczewski et al. 2013; Chapter 4). Atypical euhedral apatite grains are present only in apatite picked from disaggregated bedrock from less altered samples (e.g. 09CQA1010A4, Fig. 5.2d).

5.3.3. Apatite surface reaction features

Surfaces of apatite grains picked from till and disaggregated bedrock samples are systematically overgrown by plates and rosettes composed of a calcium-rich phase, confirmed through EDS (Fig. 5.3). The plates and rosettes are likely the result of a chemical reaction between the apatite surface and the oxalic acid used to wash the table concentrates as part of the heavy mineral recovery process at Overburden Drilling Management. Apatite grains recovered without the use of any acid wash at McGill University facilities from a selected GBMZ bedrock sample are distinctly lacking the Ca-rich mineral overgrowth (Fig. 5.3d). This confirms that the plates and rosettes are not the result of metasomatic processes or post-glacial weathering of the till. Apatite grain edges are typically jagged due to dissolution by oxalic acid.

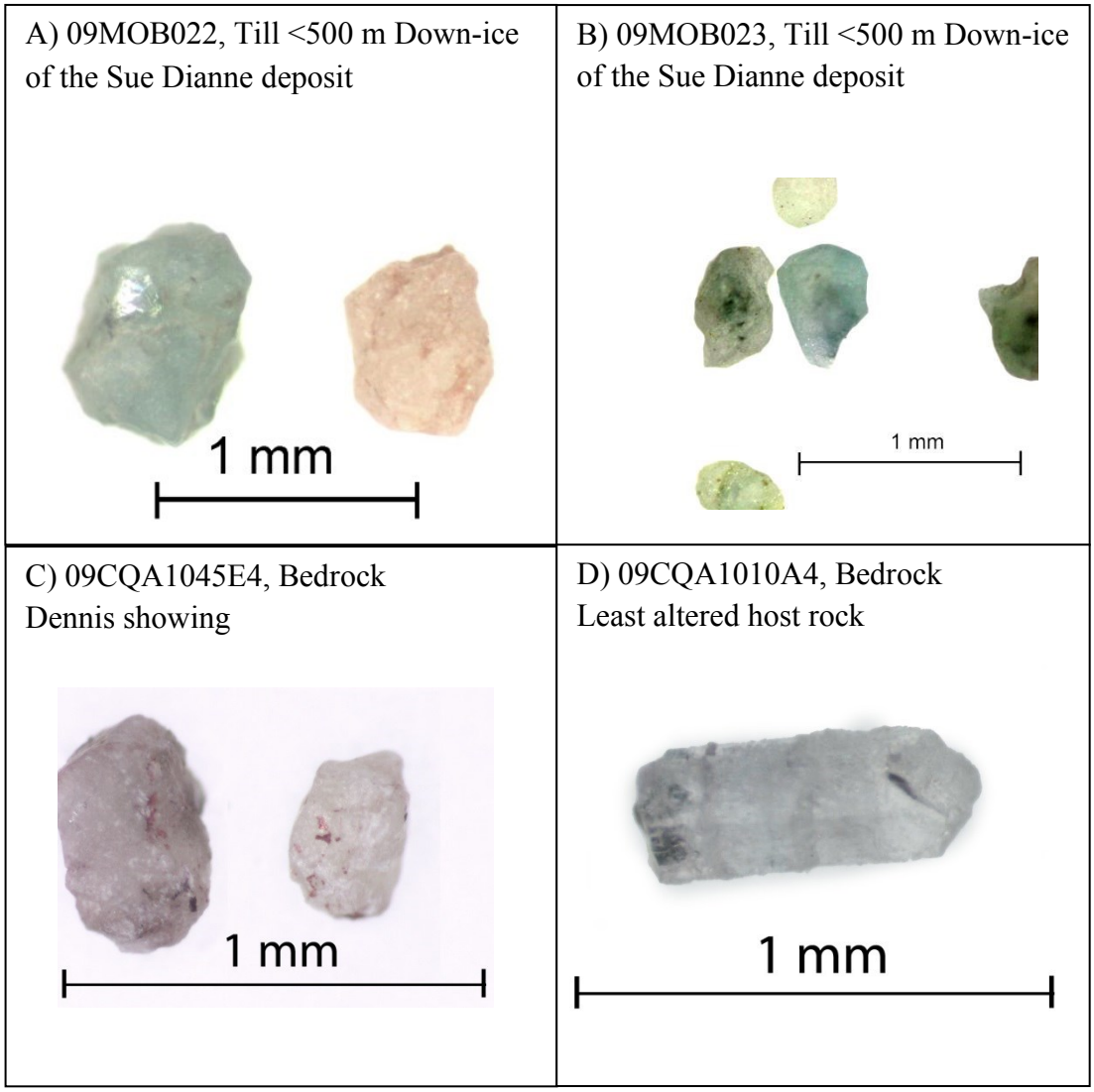

Figure 5.2: Representative colors of picked apatite grains from the NF-HMC of till (a,b) and bedrock (c,d) under the binocular.

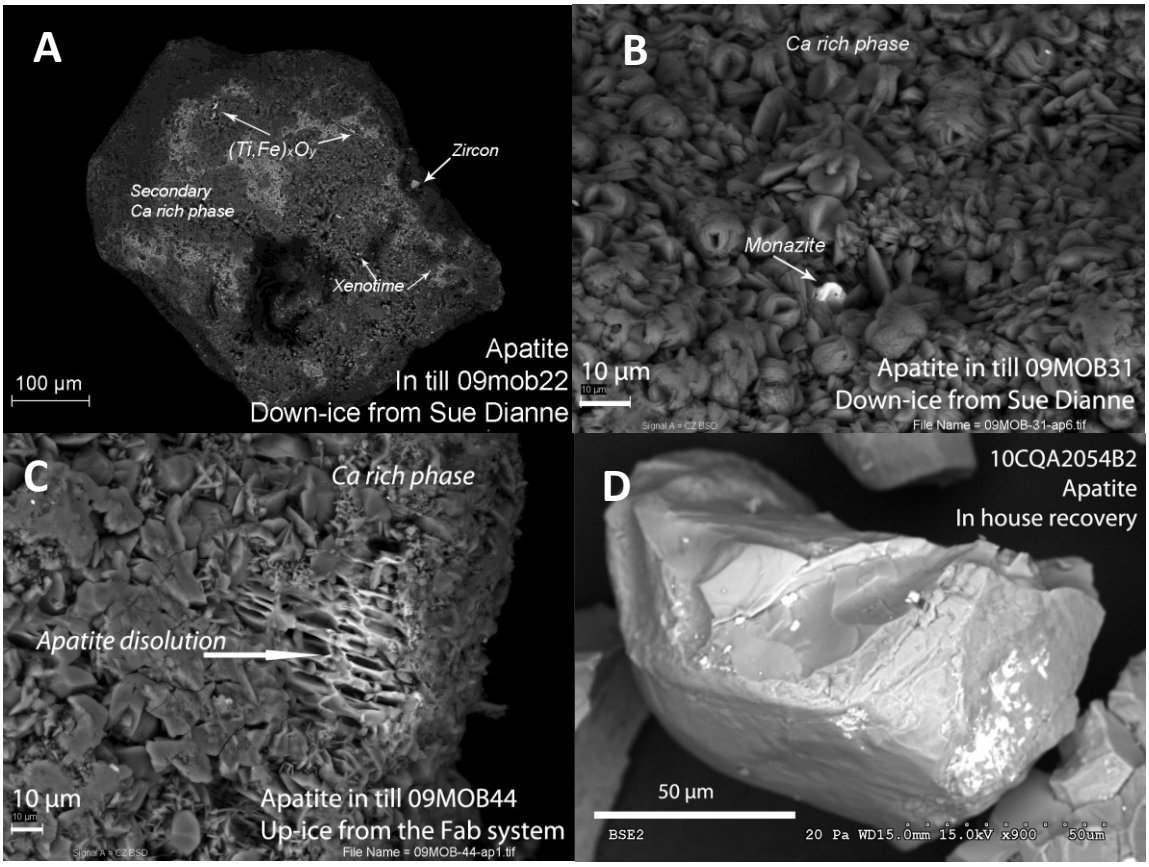

Figure 5.3: BSE images of apatite grains picked from till and disaggregated bedrock samples; a) apatite with iron oxide and REE-rich inclusions; b) plates and rosettes composed of a Ca-rich phase coating the surface of an apatite grain; c) dissolution of apatite and Ca-rich plates; d) apatite grain recovered at McGill U. facilities lacking the plates and rosettes.

5.3.4. Mineral inclusions and dissolution pits in apatite

Apatite grain surfaces commonly have inclusions of iron (± titanium) oxide and/or REE-rich phases, possibly monazite, xenotime and/or allanite. They may be observed on a picked grain surface (Fig. 5.3a,b, 5.4c,d) or within grains (Fig 5.5b,c). These inclusions are found in greater abundance in grains picked from till samples down-ice of IOA to IOCG mineralization and IOAA systems (e.g. Fig 5.5c) but may also be found in grains from the less altered GBMZ background. They have not been observed on apatite grains picked from till samples located outside the GBMZ, over the Slave Craton and Wopmay metamorphic zone. Dissolution pits were observed within polished apatite grains (Fig 5.5b, c) as well as on the surface of apatite grains (Fig 5.3c). The pits observed on picked grain surfaces are large (~ 10 μm) and form mosaics (Fig. 5.3c). They are only visible on rare surfaces lacking Ca-rich overgrowth. In contrast, the dissolution pits visible within mounted and polished apatite grains are small (< 5μm) and isolated (Fig. 5.5b, c).

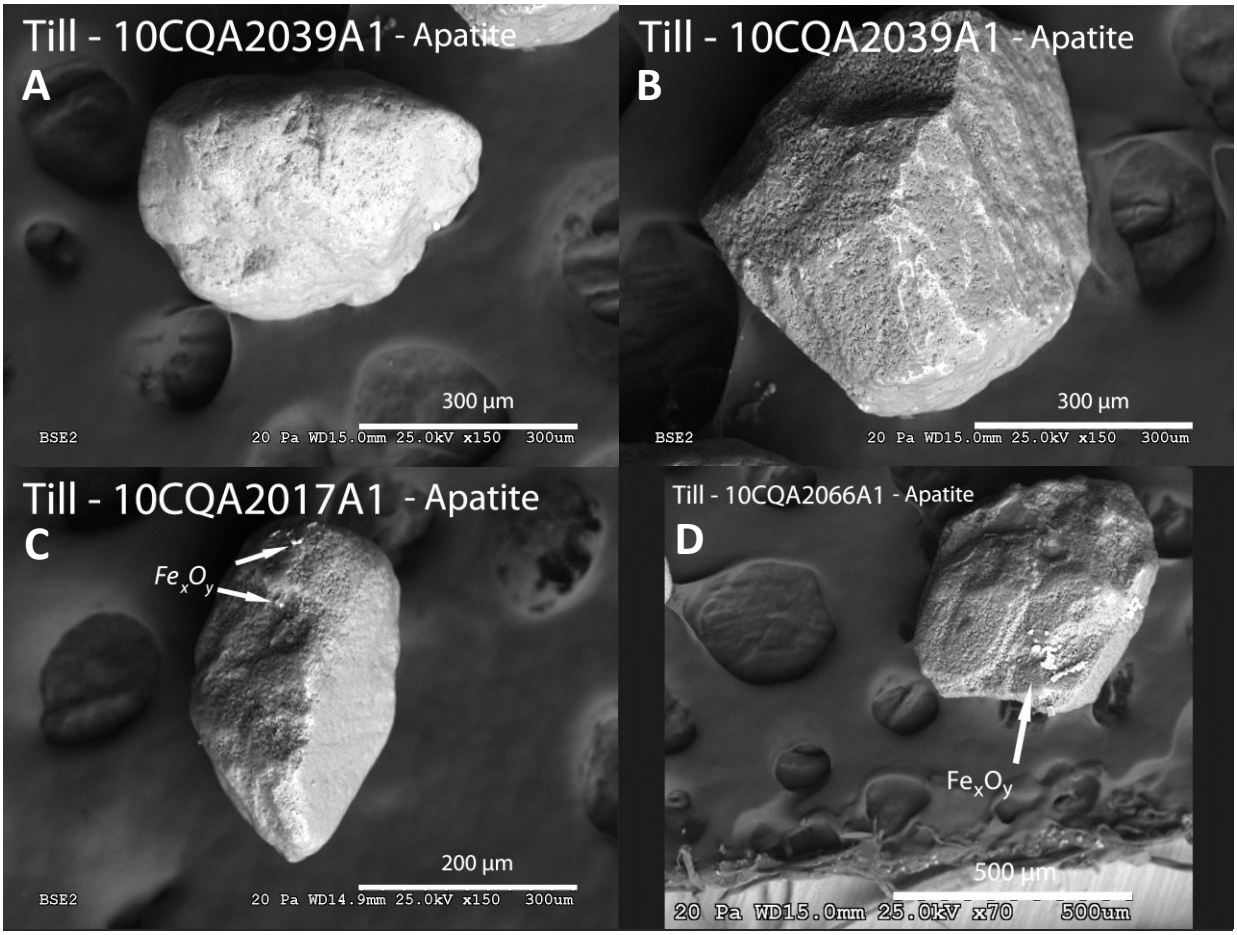

Figure 5.4: BSE images of apatite grains picked from GBMZ till samples; a) grain with rounded edges; b) grain with sub-angular edges; c) apatite recovered up-ice of the Fab system with sub-angular edges and iron oxide inclusions; d) apatite recovered down-ice of the Hottah system with sub-angular edges and iron oxide inclusions.

5.3.5. Cathodoluminescence (CL) response

Most apatite grains picked from till samples and polished on a mount display a green to yellow-green CL response. These grains are uniform or zoned in patchy green CL color of different intensity. Blue CL from a mounted till apatite grain was observed on a single occasion from sample 09MOB028 collected ~ 700 m down-ice of the Sue Dianne deposit. Unmounted apatite grains with a blue CL response was found in 3 of the 5 re-picked till samples (Table 5.2), all located less than ~ 700 m down-ice of the Sue Dianne deposit. This blue CL response may be seen throughout the grain or in small areas within generally green CL colors (Fig. 5.6a and b). When present in till samples, the proportion of blue CL apatite grains varies from ~ 30% to > 50% of the observed 50 grains. Results are identical in the S.G. >3.2 and in the 3.2 >S.G. >3.0 fractions (Table 5.2). Other CL response in till includes orange and red colored inclusions on apatite grains (Fig 5.6b). These were observed in till samples 09MOB028 (down-ice of Sue Dianne) and 09MOB008 (Sue Dianne local background) from mounted and polished apatite and in all till samples with blue CL from unmounted grains.

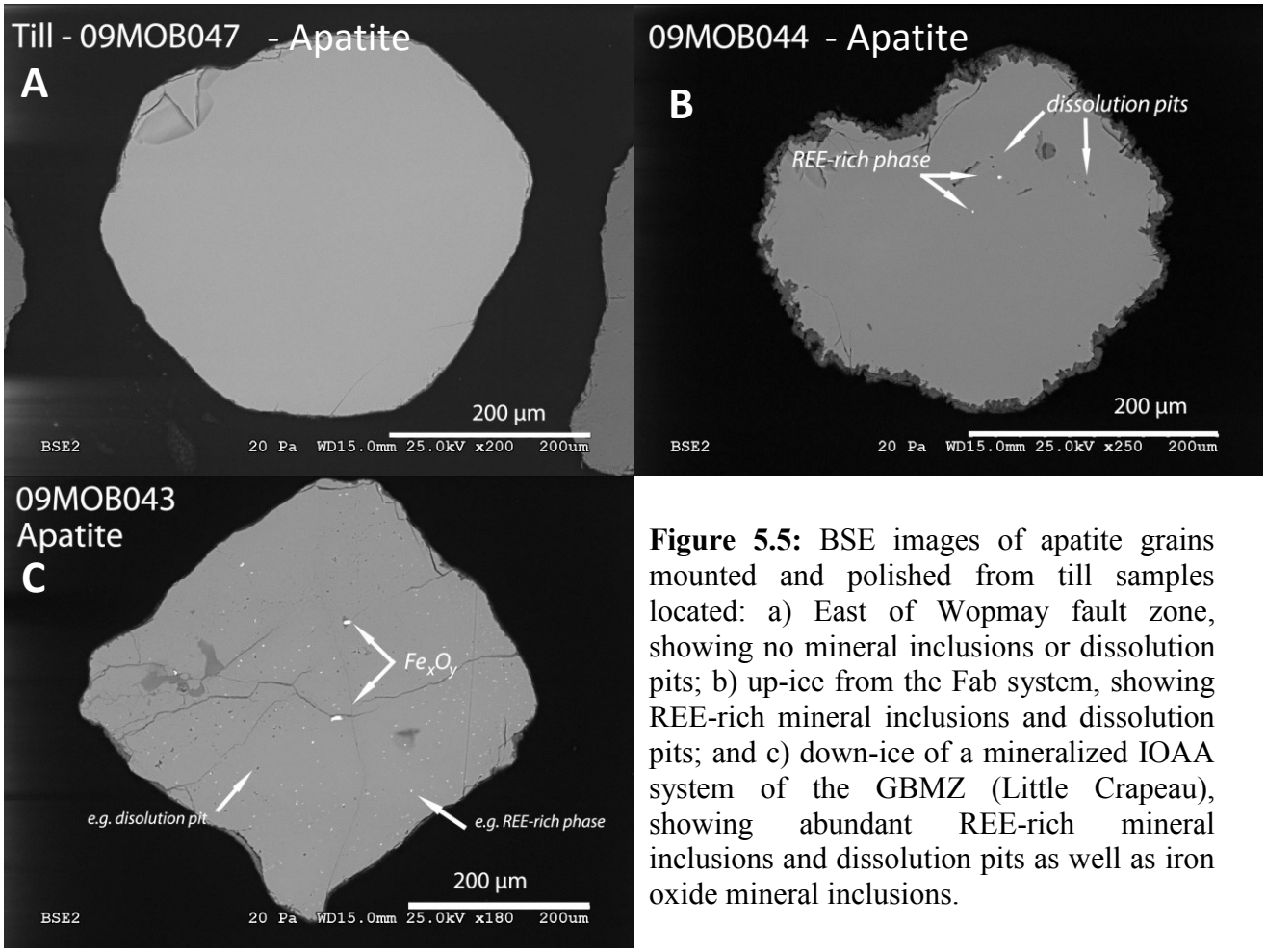

Figure 5.5: BSE images of apatite grains mounted and polished from till samples located: a) East of Wopmay fault zone, showing no mineral inclusions or dissolution pits; b) up-ice from the Fab system, showing REE-rich mineral inclusions and dissolution pits; and c) down-ice of a mineralized IOAA system of the GBMZ (Little Crapeau), showing abundant REE-rich mineral inclusions and dissolution pits as well as iron oxide mineral inclusions.

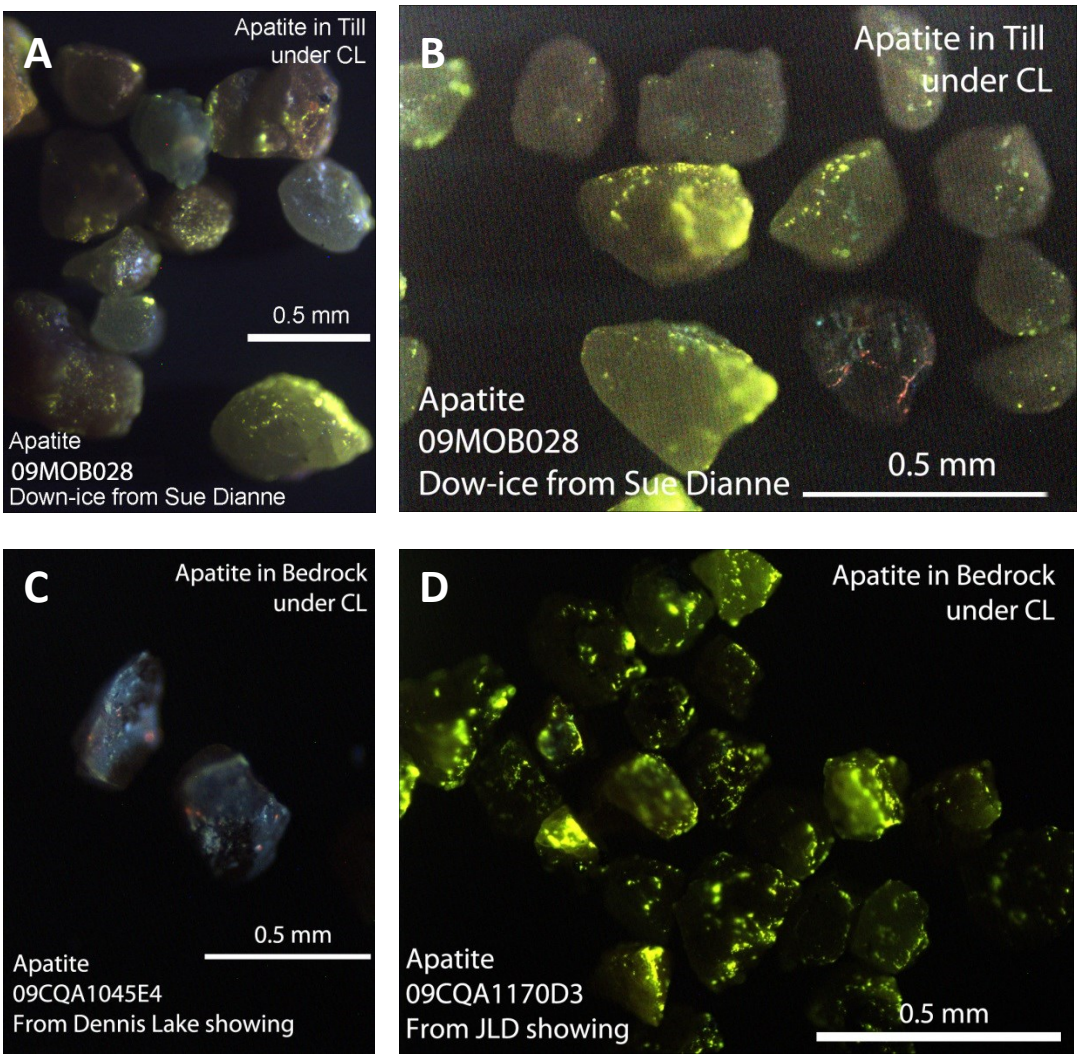

Figure 5.6: Cathodoluminescence of apatite grains picked from till (a,b) and bedrock (c,d) samples prior to mounting and polishing (S.G.>3.2).

5.3.6. Apatite chemical composition

The discrimination diagrams of Belousova et al. (2002) were used to plot the composition of apatite (Fig. 5.7). In general, compositions of picked apatite from till and bedrock samples overlap and fall over a large range of compositional fields including granitoids, granite pegmatites, mafic rocks and iron ores. Discrimination between apatite from various locations

with respect to IOAA systems and mineralization (down-ice, up-ice, mineralized bedrock, background) using these plots is elusive. One anomalous grain picked from till collected down-ice of the Sue Dianne system (~ 600 m) falls within the carbonatite field. This grain also contains 2.78 wt% Cl and was the only chloroapatite recovered within this study. No chloroapatite was identified in local bedrock samples, meaning an association with mineralization cannot be confirmed.

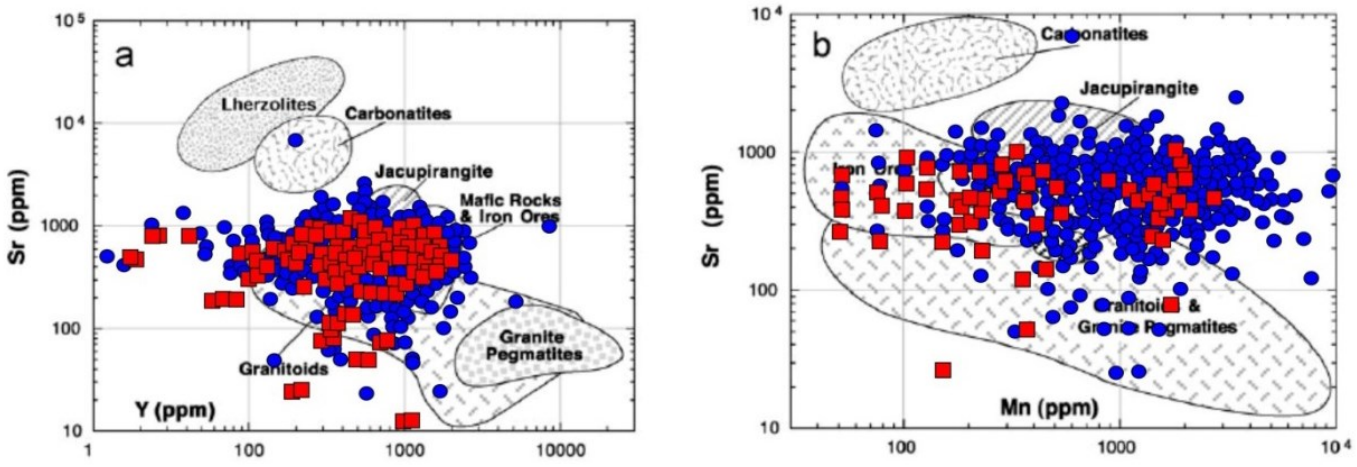

Figure 5.7: EMP– Sr, Y and Mn results for all picked apatite grains plotted against discriminant diagrams of Belousova et al. (2002). Red squares represent grains recovered from disaggregated bedrock samples (n=120); blue circles represent grains recovered from till samples (n=583).

5.4. DISCUSSION

Apatite occurs in till from all across the GBMZ and is occasionally more abundant in till collected down-ice of IOA or IOCG mineralization or in the local background of mineralized systems over intensely altered rocks. Apatite grains recovered from till therefore represent a mixture of grains from background sources and potential mineralized targets. Mapping apatite abundance alone therefore may be misleading. In addition, the absence of picked apatite grains from disaggregated bedrock samples from known apatite-rich localities (e.g. Fab system and Sue Dianne deposit) suggests that variability introduced during the picking procedure may have occurred in the till samples as well. As apatite is an unconventional indicator mineral (i.e., not part of any standard laboratory mineral picking packages), it is expected that identification results may be operator dependent in experimental stages. Alternatively, the lower apatite counts recovered in bedrock may be related to the disintegration of the apatite crystals during the disaggregation procedure to <2 mm sizes, which is different from the sieving procedures for the till samples.

Apatite grains described in bedrock thin sections from the GBMZ IOAA systems and IOCG deposits vary in size from 20 μm to 3 mm (see Chapter 4), leaving a portion of the grains below the commonly picked size fractions in indicator mineral studies (0.25-2 mm). As with other indicator minerals, automated energy dispersive X-ray spectroscopy identification procedures such as QEMSCAN or MLA could be used to target grains smaller than 0.25 mm (e.g.: Agnew, 2014; Layton-Matthews et al., 2014). It is unclear however if this size fraction

would be adequate for cathodoluminescence (CL) characterization, and identification of textural features.

A surface reaction between the apatite and an oxalic acid solution used during heavy mineral recovery produces a Ca-rich mineral overgrowth on apatite grains. This Ca-rich mineral overgrowth consists of plates and rosettes that provide an unusual satin luster to apatite grains making the grains distinct from other colorless to lightly colored translucent minerals within the NF-HMC and therefore facilitating their identification under the binocular. This surface overgrowth does not prevent the observation of the CL response or the presence of mineral inclusions; however it does cause dissolution of apatite at the grain surface. This dissolution creates large (~ 10 μm) pits that may be visible on grain surfaces and jagged edges visible on polished apatite grains. Compositional analysis of mounted apatite should therefore not be made near grain edges.

Small (< 5 μm) dissolution pits due to metasomatism, similar to those found in bedrock, are observed in most apatite grains picked from till samples collected over the GBMZ. These pits are located within the grains, away from crystal edges and may be randomly distributed or may follow internal fractures. Furthermore, iron oxide and REE-rich inclusions are found on the surfaces of many apatite grains. The abundance of REE-rich mineral inclusions in apatite is, to some extent, linked to the intensity of metasomatic remobilization (see Chapter 4). The mineral identification of the REE-rich inclusions could help vector towards more evolved IOCG deposits by using allanite as an indication of low temperature calcic alteration as opposed to monazite resulting from high or low temperature potassic and/or sodic alterations. As both the dissolution pits and the mineral inclusions were absent from apatite collected in till over the Wopmay

metamorphic zone and the Slave Craton, these features could serve as a regional exploration tool to identify large IOAA rich areas. The elaboration of a quantification method of these features could potentially help vector toward intense alteration zones at a local exploration scale.

Within the GBMZ bedrock samples, apatite grains displaying a blue cathodoluminescence response instead of a green to yellow-green response are REE rich and Mn poor (see Chapter 4). A comprehensive relationship between Mn - REE mobility and the complex metasomatic histories of the GBMZ IOAA systems is still lacking; however, the blue CL response in apatite was only observed in intense IOAA alteration associated with mineralization (i.e.: Sue Dianne deposit, Terra mine, Fab system and Dennis showing). A blue CL response in a high proportion of re-picked apatite was found in all till samples collected less than ~ 700 m down-ice of the Sue Dianne Deposit, presumably derived from the mineralization. The re-picking showed no differences in CL characterization between grains picked within the S.G. >3.2 and grains picked within the 3.2.>S.G.>3.0. Red or orange CL responses in calcite were identified in association with fluorapatite from calcic alteration phases within IOAA system rocks (i.e. Chapter 4). Therefore, red and orange CL spots and lines in picked apatite grains from till are interpreted to result from calcite within polymineralic grains. Blue and red CL responses in apatite offer a promising vectoring potential as it may successfully discriminate apatite down-ice of IOCG deposits. However, additional testing is required to verify this potential due to the small number of samples used in the CL analysis of unmounted grains. The near absence of blue CL response in the mounted apatite grains picked from till may be due to the lower number of grains picked compared to the re-picking number (1 to 20 vs 50) or to different CL settings used on grain mounts (4 kV, 3 to 4 sec) versus unmounted grains (2 to 3.5 kV, 10 to 20 sec).

5.5. CONCLUSION AND RECOMMENDATIONS

Apatite proved to have potential as an indicator mineral in till towards IOAA systems and IOA to IOCG deposits in the GBMZ. A blue cathodoluminescence (CL) response in apatite grains is due to low Mn and high REE content in metasomatised apatite. Orange and red CL spots and lines on apatite grains are due to calcite and are linked to calcic alteration within IOAA metasomatism. Both of these CL responses were observed in a high proportion of apatite from till samples collected down-ice of the Sue Dianne deposit and contrast with the commonly green to yellow-green CL colors of apatite throughout the GBMZ. Likewise, zoning of the green CL response, metasomatic dissolution pits and REE-rich mineral inclusions can discriminate the GBMZ apatite from the Wopmay zone and Slave Craton apatite at the regional scale. The abundance of dissolution pits and REE-rich mineral inclusions may potentially be used as a vector towards IOAA systems where metasomatism is more intense, providing further testing and the elaboration of a quantification method. Mapping apatite abundance alone is not recommended as a practical method since high apatite concentrations in the NF-HMC of till samples may be influenced by IOA and IOCG mineralization, but also by variable occurrences in GBMZ altered and least-altered background rocks. Similarly, chemical composition of selected apatite grains picked from bedrock and till samples was not conclusive to differentiate apatite from altered, mineralized and background settings in the GBMZ.

Heavy mineral separation protocols specific to apatite can be adjusted to take into account its lower density. The specific gravity threshold during heavy liquid separation may be adjusted from 3.2 S.G. to 3.0 S.G. to facilitate recovery without introducing sampling bias.

Oxalic acid wash can be used despite a resulting artifact of Ca-rich mineral overgrowth on apatite. This overgrowth may facilitate apatite identification due to an induced change in surface texture to a satin luster that sets it apart from other semi-translucent lightly colored heavy minerals. Cathodoluminescence (CL) characterization of apatite is better performed on handpicked grains without being mounted and polished. The conventional size fraction of 0.25 to 2 mm was adequate both for CL and SEM characterization. The presence of apatite in host rocks creates a dilution of grains in till therefore picking of no less than 50 grains per sample is recommended for CL characterization. Future work includes the elaboration of a practical guide to the use of apatite as an indicator mineral of IOA and IOCG deposits.

5.6. ACKNOWLEDGMENTS

This work stems from the Geomapping for Energy and Minerals (GEM) IOCG/Multiple Metals Great Bear Region project at the Geological Survey of Canada (Natural Resources Canada) conducted in partnership with the Wopmay Bedrock Mapping project of the Northwest Territories Geological Survey. The first author was funded by the Research Affiliate Program of Natural Resources Canada. Katherine Venance and Pat Hunt of the Geological Survey of Canada Microbeam Laboratory are recognized for their contributions with EMP analysis. Thanks are due to Stu Averill and Overburden Drilling Managment for insights and guidance as well as astounding work in experimental laboratory procedures. The authors are also grateful to Cameron Butler and Philip Lypaczewski for their participation to this project during their undergraduate studies at McGill University. Research was performed under Aurora Research Institute Scientific Research licenses 14548 and 14649.

5.6. REFERENCES

Agnew, P., 2014, Micro-analytical innovation for indicator mineral exploration; in McClenaghan, B. and Layton-Matthews D. (eds) Application of Indicator Mineral Methods to Exploration, Workshop 2, 27th International Applied Geochemistry Symposium (IAGS 2014), Tucson, Arizona, April 2014, p. 11–12.

Belousova, E., Griffin, W., O'Reilly, S.Y., and Fisher, N., 2002, Apatite as an indicator mineral for mineral exploration: Trace-element compositions and their relationship to host rock type: Journal of Geochemical Exploration, v. 76, p. 45–69.

Bonyadi, Z., Davidson, G.J., Mehrabi, B., Meffre, S., and Ghazban, F., 2011, Significance of apatite REE depletion and monazite inclusions in the brecciated Se–Chahun iron oxide–apatite deposit, Bafq district, Iran: Insights from paragenesis and geochemistry: Chemical Geology, v. 281, p. 253–269.

Bouzari, F., Hart, C., Barker, S., and Bissig, T., 2011, Porphyry Indicator Minerals (PIMS): A new exploration tool for concealed deposits in south-central British Columbia: Geoscience BC Report, 2011-17, 31 p.

Budzyń, B., Harlov, D.E., Williams, M.L., and Jercinovic, M.J., 2011, Experimental determination of stability relations between monazite, fluorapatite, allanite, and REE-epidote as a function of pressure, temperature, and fluid composition: American Mineralogist, v. 96, p. 1547–1567.

Harlov, D.E., 2015, Apatite: A fingerprint for metasomatic processes: Elements, v. 11, p. 171–176.

Harlov, D.E., Andersson, U.B., Förster, H.-J., Nyström, J.O., Dulski, P., and Broman, C., 2002, Apatite–monazite relations in the Kiirunavaara magnetite–apatite ore, northern Sweden: Chemical Geology, v. 191, p. 47–72.

Hughes, J.M., and Rakovan, J.F., 2015, Structurally robust, chemically diverse: Apatite and apatite supergroup minerals: Elements, v. 11, p. 165–170.

Kempe, U., and Götze, J., 2002, Cathodoluminescence (CL) behaviour and crystal chemistry of apatite from rare-metal deposits: Mineralogical Magazine, v. 66, p. 151–172.

Layton-Matthews, D., Hamilton, C. and McClenaghan M.B., 2014, Mineral chemistry: modern techniques and applications to exploration: in McClenaghan, B. and Layton-Matthews D. (eds) Application of Indicator Mineral Methods to Exploration, Workshop 2, 27th International Applied Geochemistry Symposium (IAGS 2014), Tucson, Arizona, April 2014, p. 1–10.

Mao, M., Rukhlov, A.S., Rowins, S.M., Spence, J., and Coogan, L.A., 2015, Detrital apatite trace-element compositions: A robust new tool for mineral exploration: British Columbia Ministry of Energy and Mines, British Columbia Geological Survey, GeoFile 2015-09, 1 p.

Mao, M., Rukhlov, A.S., Rowins, S.M., Spence, J. and Coogan, L.A., 2016, Apatite trace element composition: A robust new tool for mineral exploration: Economic Geology, v. 111, p. 1187–1222.

Mitchell, R.H., 2014, Cathodoluminescence of apatite, in Coulson, I.M., ed., Cathodoluminescence and its application to geoscience: Mineral Association of Canada, Short Course Series, v. 45, p. 143–167.

Normandeau, P.X., McMartin, I., 2013, Composition of till and bedrock across the Great Bear magmatic zone: field database and analytical results from the GEM IOCG-Great Bear Project, GSC Open File 7307, 26 p.

Normandeau, P.X., Harlov, D.E., Corriveau, L., Paquette, J., McMartin, I., in press, Characterization of fluorapatite within iron oxide alkali-calcic alteration systems of the Great Bear magmatic zone: a potential metasomatic process record: The Canadian Mineralogist.

Plouffe, A., McClenaghan, M.B., Paulen, R.C., McMartin, I., Campbell, J., and Spirito, W., 2013, Processing of unconsolidated glacial sediments for the recovery of indicator minerals: protocols used at the Geological Survey of Canada: Geochemistry, Exploration, Environment, Analysis, v. 13, p. 303–316.

CHAPTER 6: Conclusions

This thesis presents results from a research study aimed at developing surface glacial drift exploration methods applied to iron oxide alkali-altered (IOAA) systems and associated iron oxide-apatite (IOA) to iron oxide copper-gold (IOCG) deposits in the Great Bear magmatic zone (GBMZ), Northwest Territories, Canada. It is based on the documentation of the surficial geology context and the characterization and analysis of the matrix and heavy mineral fractions of till samples collected by the author, coupled to comparisons with bedrock mineralogy and geochemistry. The main conclusions drawn from each chapter are summarized below and the challenges to glacial sediment prospecting in the GBMZ are outlined before concluding with recommendations for possible future work.

6.1. SUMMARY OF FINDINGS

Surficial geology field interpretations as well as till and bedrock samples were collected in 2009 and 2010 as part of the Geo-mapping for Energy and Minerals (GEM) IOCG/Multiple Metals Great Bear Region project of the Geological Survey of Canada (Natural Resources Canada). Surficial geology field observations indicate a discontinuous thin till cover, sparingly affected by glaciolacustrine reworking below 300 m a.s.l. Till is generally fresh and sampling of unaltered material, below the B-horizon, was performed in hand-dug pits at an average depth of 50 cm to avoid the effects of post-glacial weathering in the soils. The dominant ice-flow direction is towards the west-southwest in the southern part of the GBMZ and gradually shifts to

west-northwestward in the north. Although older indicators of glacial flow directions were measured, glacial dispersal trains follow the dominant, more recent trends. Short glacial transport distances were inferred mainly through the dispersal of heavily metasomatised clasts found less than 800 m down-ice of their source, or from scattered single-element geochemical anomalies (<2 km).

Possible vectoring elements to IOAA systems and IOA to IOCG deposits throughout the GBMZ in the till matrix geochemistry include Fe, Co, Ni, Cu, As, Mo, Bi, La, Th, U and W. All investigated IOAA systems showed one or a combination of these elements in anomalous concentrations up to 2 km down-ice of outcropping mineralization, regardless of the variable sampling density. Na, Ca and K concentrations in till analyzed after a near total digestion of the silt + clay-size fraction are influenced by IOAA alteration. Na, Ca and K concentrations in till collected over or down-ice of IOAA system tend to have a greater variability, yet systematic relations between these element concentrations and specific bedrock alterations were elusive. La and Th digestion method ratios (i.e., the concentration of an element given after a near total digestion over the concentration of that same element given after a partial digestion method) from the silt + clay-sized fraction of till represent a simple and economic vectoring tool to IOAA alteration as demonstrated for the Sue Dianne deposit. Digestion method ratios show a variation in the resistivity to acid digestion of the minerals hosting La or Th or a change of the mineral host itself to a phase with a different resistance to acid digestion. Due to the extent of the alteration halo, the mapping of La and Th digestion method ratios better defines the geochemical anomaly in till and extends the dispersal train to ~ 3 km down-ice of the Sue Dianne deposit.

In order to develop an indicator mineral exploration method specific to the GBMZ deposits and their alteration halos, apatite was studied *in situ* in bedrock samples as well as in

non-ferromagnetic heavy mineral concentrates of till and disaggregated bedrock samples. In bedrock, apatite from the GBMZ consistently displays textural features resulting from IOAA metasomatism. Dissolution pits caused by LREE remobilization are ubiquitous within altered systems and the less altered granitic rocks. However, they are more abundant in strongly altered bedrock samples. Inclusions of monazite and allanite are present in apatite from most of the altered or mineralized bedrock samples. Allanite is the dominant REE-bearing phase where late, low temperature calcic alteration is present. The cathodoluminescence (CL) response of apatite from the GBMZ is an indication of metasomatic alteration with a green to yellow-green color observed where the Mn activator dominates and a blue CL response observed from rare-earth elements (REE) activation. The latter is detected only if the REE activation dominates over the Mn. Patchy CL zonation in a single grain of apatite, in most cases, indicates an originally light REE rich apatite with localized LREE leaching consistently accompanied by pitting. The blue CL response was only observed in intense IOAA alteration associated with mineralization. The CL response of apatite grains, their Th and U content, and the sporadic presence of monazite and/or allanite inclusions in apatite grains are consistent with their role in the metasomatic history of the GBMZ IOAA systems. The textural and geochemical characteristics point to an important role for apatite as a recorder of the processes and geochemical signature of alterations during mineralization.

The textural and CL characterization of apatite grains in till, rather than their relative abundance, has better potential as an indicator mineral method towards IOAA systems and IOA to IOCG deposits in the GBMZ. Cathodoluminescence (CL) characteristics can be photographed on 0.25-0.5 mm size apatite grains picked from till before or after they have been mounted in an epoxy plug and polished. Blue CL apatite or blue zones in green CL apatite, as well as orange

and red CL spots and lines on apatite grains, were found in abundance (>30% of unmounted grains) in three till samples, all collected less than ~ 700 m down-ice of the Sue Dianne deposit. These grains contrast with the green to yellow-green CL colors commonly seen in apatite throughout the GBMZ. Therefore the study of CL response colors of a number of apatite grains (min ~ 50 grains) prior to mounting on epoxy stub for geochemical analysis provides a promising method for vectoring of IOA to IOCG deposits that contain metasomatised apatite. The observation of patchy zoning, as opposed to concentric zoning, in apatite grains showing the green CL response, metasomatic dissolution pits and REE-rich mineral inclusions in mounted and polished apatite grains discriminates the GBMZ apatite from the Wopmay zone and Slave Craton apatite at the regional scale.

6.2. CHALLENGES TO GLACIAL SEDIMENT PROSPECTING IN THE GBMZ AND POSSIBLE FUTURE WORK

Surface exploration using glacial sediments as a prospecting medium in the GBMZ is challenged by the fact that multiple mineralized outcrops occur in close proximity, rather than there being few widely spaced point sources. This distribution adds complexity to interpretations of glacial dispersal patterns and detection of mineral deposits. Furthermore, the sheer size of alteration halos from IOAA systems and IOA to IOCG deposits, typically exceeding tens of kilometers, presents an additional difficulty as true background values needed to define anomalies are difficult to obtain. The field mapping of bedrock alteration zones attributed to IOCG and IOAA systems also remains a challenge due to overprinting and retrograde alteration. These factors complicate the tracing of geochemical anomalies in till to a single type of alteration or mineralization. Likewise, the large diversity of system types, geochemistry and ore

mineralogy now documented within the GBMZ challenges the goal of finding common vectoring methods. Moreover, the discontinuity of the till cover in the GBMZ constrains the design of any till sampling strategy.

Further work on the elaboration of a drift prospecting method towards IOA to IOCG deposits and IOAA systems should favor a study area with a continuous till cover such as the northern portion of the GBMZ, located above the tree-line. This region is also free from the post glacial effects of Glacial Lake McConnell on till, such as waves, current and lake ice action. Till sampling would also be facilitated by the ubiquitous presence of frostboils, a geomorphic feature of tundra environments easily recognized in the field and known to provide relatively unweathered material for till sampling which would reduce field variability and alleviate constraints on sample location sites. Further studies on IOAA and IOCG signatures within the till matrix should continue to use both partial and total digestion methods to elaborate on digestion method ratios. As well, the clay and the silt+clay-sized fraction should be obtained to preferentially target metal enrichments and alteration signatures respectively.

Cathodoluminescence (CL) studies of detrital apatite could be carried out on the heavy indicator mineral concentrate prior to grain picking as the apatite could potentially be differentiated from other responding minerals. To facilitate the capture of apatite, the density threshold used for the separation of the heavy minerals can be adjusted to >3.0 S.G. as opposed to the standard >3.2 S.G. The possibility of differentiating apatite sources through CL response and textural characteristics could also be evaluated using a finer mineral fraction (< 0.25 mm). A combination of CL and automated energy dispersive X-ray spectroscopy identification procedures such as QEMSCAN or MLA could be used to test this hypothesis.

Appendix 1 – Open File 7307 dataset

Composition of till and bedrock across the Great Bear magmatic zone: Quaternary field database and analytical results from the GEM IOCG-Great Bear Project

Complete Open File 7307 can be downloaded from Natural Resources Canada, (http://geoscan.nrcan.gc.ca/starweb/geoscan/servlet.starweb?path=geoscan/downloade.web&search1=R=292560) and contain the following files:

OF7307 Appendices:

I. Field site descriptions

II. Ice-movement indicators

III. Sample descriptions

IV. Till geochemistry, <0.002 mm, ICP-MS, modified aqua regia digestion

Va. Till geochemistry, <0.063 mm, ultratrace ICP-MS, modified aqua regia digestion

Vb. Till geochemistry, <0.063 mm, ICP-MS, 4-acid digestion

VI. Till geochemistry, <0.063 mm, INAA

VII. Till Au-Pt-Pd <0.063 mm, fire assay/ICP-MS

VIII. Till matrix color and sand-silt-clay distribution

IX. Till carbon content, <0.063 mm, LECO / LOI

Xa. Till matrix mineralogy, <0.063 mm (QEMSCAN)

Xb. Till matrix mineralogy, <0.002 mm (XRD)

XI. Till pebble counts, 4-9 mm, % counted

XII. Till and bedrock gold grain and indicator mineral counts

XIII. Till and bedrock FM-HMC geochemistry (<0.25 mm and 0.25-2 mm)

XIV. Binocular and SEM photographs of selected grains

XV. Electron microprobe analysis of grains from NFM-HMC

Appendix 2 – LA-ICP-MS- Fluorapatite

Trace Element Concentrations MDL filtered.
All values are reported in ppm

	11UPA86B4				09CQA1170D3			09CQA0128B2					3507A				09CQA1045C8				09CQA1045E4			
Element	JL09A31	JL09A32	JL09A33	JL09A34	JL09A39	JL09A40	JL09A41	JL09A22	JL09A23	JL09A24	JL09A25	JL09A26	JL09A27	JL09A28	JL09A29	JL09A30	JL09A46	JL09A47	JL09A48	JL09A49	JL09A42	JL09A43	JL09A44	JL09A45
Na23	511.43	450.44	366.63	230.58	232.25	257.96	261.37	1733.13	1710.53	2301.91	1420.71	1557	1600.38	326.74	836.03	1337.15	109.88	194.4	121.02	148.14	144.43	113.42	145.48	156.14
Mg25	96.23	46.58	49.98	346.95	250.73	53.35	42.74	179.89	170.68	134.35	173.8	169.12	179.75	13472.57	2156.15	182.21	4.46	75	11.3	9.76	3.77	5.21	5.8	6.4
Al27	4.9	1.79	2.49	108.18	237.54	13.61	130.25	3.35	1.44	16.29	<0.73	<1.00	<1.22	771.79	328.62	<1.24	<1.29	53.14	<1.28	5.12	7.26	<1.43	3.39	68.56
Si29	999.69	1343.76	1010.07	1167.52	1703.9	1006.15	204.01	2491.84	2407.9	1442.81	2374.22	2191.2	2461.82	27004.15	8045.55	2488.5	1990.24	2233.37	1125.24	609.94	1734.65	1766.57	2116.78	2276.04
P31	191509.6	184412.4	177051.3	175873.9	188897.1	185884.6	200728.7	187609.7	182611.2	90010.69	180285.1	178981.6	194656.2	254.99	186805.9	177798.4	170685.8	166976	176886	178632.6	164320.5	178538.2	172567.4	169388.3
S34	<444.84	537.62	1017.2	602.74	<325.42	<306.69	<316.78	<421.69	<356.89	<323.82	<209.13	<277.87	<331.67	2183.45	371.48	<317.84	655.79	<286.02	614.96	<336.65	550.62	505.76	<273.53	420.53
K39	5.7	<3.89	<4.15	5.49	143.83	18.91	7.02	7.85	<3.50	36.83	<2.20	<2.98	<3.64	214.58	24.95	<3.68	<3.62	14.5	6.04	<3.56	5.78	<4.05	<3.13	<3.01
Ca42	393078.1	393077.8	393077.5	393077.1	398078.2	394504.3	393074.6	393080.4	393080.2	393079.9	393079.7	393079.5	393079.2	393079	393078.7	393078.4	398075.2	391642.6	393786.1	400217.7	393074.1	395217.8	395932	387355.4
Ca43	383782.6	378746.5	390292.2	382063.6	391970.4	386766.3	392568.1	387587.2	388127	381619.4	388843.1	389581.2	390655.8	391433.9	384609	385170.3	390691.3	379457.1	391126.9	396436.8	370043.3	389129.7	381345.7	384801.5
Sc45	<0.23	<0.177	<0.186	0.171	0.22	0.214	<0.17	<0.174	<0.149	<0.15	<0.093	<0.128	<0.15	0.79	<0.163	<0.16	<0.165	<0.14	<0.16	<0.16	0.23	<0.173	<0.141	<0.139
Mn55	90.69	83.1	86.41	80.83	1986.82	2299.99	2497.1	146.43	144.32	135.86	146.51	148.1	151.89	8760.28	196.38	148.67	109.27	97.37	82.01	70.23	51.03	39.56	44.96	46.85
Fe57	465.88	422.01	426.29	851.93	1366.15	478.21	662.16	845.87	819.28	3858.3	837.18	817.94	858.47	7127.26	11211.63	833.44	263.74	4894.62	321.09	256.45	292.75	322.18	316.83	373.53
Cu65	<0.51	<0.43	<0.45	<0.44	1.17	<0.39	<0.37	0.55	<0.36	8.33	0.34	<0.29	<0.42	68.84	2.11	0.67	0.43	4.25	0.54	<0.40	0.91	0.64	1.65	1.25
Zn66	<3.69	4.29	<2.99	<2.92	5.65	<2.74	6.99	<2.86	<2.49	13.92	4.01	<2.10	<2.63	155.37	12.87	<2.64	<2.63	<2.26	<2.64	<2.64	<2.86	<3.07	<2.33	<2.20
As75	336.39	349.3	386.42	461.43	514.84	550.32	281.34	66.34	63.62	73.06	55.6	59.56	66.29	661.81	170.88	58.51	592.75	484.87	893.31	436.79	333.81	445.77	333.91	275.95
Sr88	117.6	123.11	118.62	104.26	91.17	94.44	92.1	405.28	401.56	338.12	404.23	399.12	401.72	102.05	300.56	397.54	102.64	91.57	107.29	81.66	104.21	161.63	106.29	94.9
Y89	398.21	411.49	347.01	267.4	2385.61	2105.36	1042.46	1104.77	1128.95	1332.3	990.63	979.15	1080.07	211.29	809.87	1030.76	470.43	921.62	628.09	467.87	245.24	275.27	375.14	384.33
Mo95	<0.162	<0.095	<0.088	<0.080	0.107	0.198	0.15	<0.132	<0.108	<0.074	<0.046	<0.093	0.18	0.68	0.32	<0.103	<0.078	0.32	0.076	2.39	<0.093	<0.143	<0.072	0.063
Sn118	<0.35	<0.26	0.43	<0.26	<0.29	<0.26	<0.25	<0.28	<0.25	1.19	<0.164	<0.205	0.34	1.93	1.79	<0.24	<0.22	<0.25	<0.29	<0.22	<0.26	<0.30	<0.20	<0.23
Ba137	0.72	0.214	0.268	0.64	1.95	0.63	1.58	1.78	1.28	9.91	1.52	1.66	1.27	6.43	12.15	1.96	0.233	1.77	0.34	0.207	1.61	1.42	1.85	0.83
La139	1631.32	1786.26	1453.34	844.68	75.86	146.41	290.61	6053.77	6113.9	7955.2	5007.12	4901.37	5604.12	73.65	2960.48	4881.06	2029.64	2128.18	739.97	298.94	2090.08	1781.53	2471.23	2613.74
Ce140	3184.74	3405.55	2648.76	1583.15	332.07	536.43	931.48	11296.46	11352.04	15895.29	10025.88	9686.92	11092.31	44.19	6175.31	9916.53	4360.16	4623	1821.47	846.72	4061.12	3733.39	4821.74	4940.08
Pr141	282.27	297.53	226.34	140.6	74.05	94.23	111.85	1106.93	1109.98	1371.23	993.76	977.63	1074.49	14.92	595.5	963.2	405.02	435.29	194.07	106.65	350.99	342.4	397.42	415.08
Nd146	930.93	952.48	745.21	465.29	525.22	581.55	451.2	3778.94	3785.41	4578.67	3506.64	3408.74	3535.19	72.23	2095.56	3304.65	1321.07	1483.05	732.32	444.66	1071.31	1047.39	1137.12	1181.28
Sm147	118.84	121.91	95.28	62.64	283.78	299.79	150.2	503.71	501.77	600.5	470.72	460.07	489.53	12.68	304.91	458.82	148.35	218.05	128.31	92.05	106.94	103.96	110.81	114.86
Eu151	11.9	12.76	10.84	7.38	59.87	57.34	24.43	34.07	34.35	39.72	31.07	30.59	32.47	1.51	21.2	29.89	19.53	27.34	16.67	14.71	15.44	12.57	13.29	13.89
Gd157	94.91	100	79.93	54.32	429.34	435.41	187.8	358.73	350.95	427.79	324.44	322.34	348.92	26.07	223.83	326.47	105.39	175.45	118.46	94.3	69.03	70.62	85.56	86.36
Tb159	11.74	12.44	9.54	6.7	74.17	74.65	29.82	42.32	42.3	51.67	38.73	37.95	41.92	4.11	28.59	37.99	12.64	23.41	15.53	11.98	6.85	8.01	10.12	10.33
Dy163	65.71	65.09	53.07	38.27	449.01	425.39	174.39	217.41	213.94	264.86	198.87	194.11	218.46	23.07	151.83	206.02	67.4	133.77	88.59	65.23	35.54	42.6	54.71	55.72
Ho165	13.94	13.32	11.48	7.99	81.86	77.65	35.34	41.33	41.92	48.83	37.69	36.93	40.69	5.42	30.19	38.25	13.75	27.88	19.32	14.32	7.41	8.86	11.86	11.87
Er167	33.24	36.04	30.23	22.27	205.56	173.91	95.07	101.53	100.17	126.46	91.03	89.93	101.07	14.55	75.1	87.91	36.54	77.96	52.86	39.07	19.66	22.14	30.51	30.24
Tm169	4.83	4.66	3.88	2.86	27.06	23.24	12.34	12.04	12.1	15.3	10.96	10.81	11.88	2.35	8.9	10.86	4.87	10.57	7.35	5.21	2.54	2.82	3.96	3.9
Yb173	27.68	30.84	25.98	18.17	171.69	138.95	79.93	60.63	59.14	76.99	56.9	53.25	57.46	16.09	43.94	57.07	28.78	52.58	42.06	32.76	13.76	15.26	20.86	21.47
Lu175	4.18	4.76	3.83	2.97	23.18	17.98	11.78	5.98	6.01	7.41	5.52	5.25	6.06	2.11	4.36	5.51	4.18	5.07	4.82	5.2	1.26	1.358	2.12	2.18
Hf177	0.12	<0.029	<0.046	<0.00	0.023	0.03	0.042	<0.047	0.041	0.26	0.038	<0.033	<0.033	0.34	0.042	<0.038	<0.038	0.05	0.056	<0.040	<0.034	<0.046	<0.026	<0.038
Bi209	0.33	0.208	0.185	0.38	4.26	5.99	1.03	0.027	<0.017	0.205	0.0189	<0.0102	0.042	2.88	0.97	0.038	1.93	2.35	1.68	1.05	1.48	2.39	1.34	0.91
Th232	51.72	55.51	43.93	18.83	0.656	4.08	8.04	223.72	252.3	308.76	164.15	159.14	254.35	0.95	142.43	217.31	153.11	122.03	57.4	3.34	225.34	226.36	216.01	215.24
U238	10.08	11.27	8.64	5.13	6.23	7.41	2.28	34.43	33.56	34.99	29.4	28.6	34.54	1.91	40.18	34.65	62.34	70.04	26.14	2.59	138.63	129.14	158.42	167.09

Trace Element Concentrations
All values are reported in ppm

	11UPA86B4				09CQA1170D3			09CQA0128B2					3507A				09CQA1045C8				09CQA1045E4			
Element	JL09A31	JL09A32	JL09A33	JL09A34	JL09A39	JL09A40	JL09A41	JL09A22	JL09A23	JL09A24	JL09A25	JL09A26	JL09A27	JL09A28	JL09A29	JL09A30	JL09A46	JL09A47	JL09A48	JL09A49	JL09A42	JL09A43	JL09A44	JL09A45
Na23	511.43	450.44	366.63	230.58	232.25	257.96	261.37	1733.13	1710.53	2301.91	1420.71	1557	1600.38	326.74	836.03	1337.15	109.88	194.4	121.02	148.14	144.43	113.42	145.48	156.14
Mg25	96.23	46.58	49.98	346.95	250.73	53.35	42.74	179.89	170.68	134.35	173.8	169.12	179.75	13472.57	2156.15	182.21	4.46	75	11.3	9.76	3.77	5.21	5.8	6.4
Al27	4.9	1.79	2.49	108.18	237.54	13.61	130.25	3.35	1.44	16.29	****	****	<****	771.79	328.62	0.45	0.19	53.14	****	5.12	7.26	****	3.39	68.56
Si29	999.69	1343.76	1010.07	1167.52	1703.9	1006.15	204.01	2491.84	2407.9	1442.81	2374.22	2191.2	2461.82	27004.15	8045.55	2488.5	1990.24	2233.37	1125.24	609.94	1734.65	1766.57	2116.78	2276.04
P31	191509.6	184412.4	177051.3	175873.9	188897.1	185884.6	200728.7	187609.7	182611.2	90010.69	180285.1	178981.6	194656.2	254.99	186805.9	177798.4	170685.8	166976	176886	178632.6	164320.5	178538.2	172567.4	169388.3
S34	66.75	537.62	1017.2	602.74	207.59	236.89	311.31	285.18	<****	<****	<****	212.11	108.43	2183.45	371.48	167.17	655.79	109.99	614.96	<****	550.62	505.76	<****	420.53
K39	5.7	<****	0.12	5.49	143.83	18.91	7.02	7.85	1.07	36.83	0.75	0.52	3.5	214.58	24.95	<****	0.37	14.5	6.04	<****	5.78	0.58	2.07	2.75
Ca42	393078.1	393077.8	393077.5	393077.1	398078.2	394504.3	393074.6	393080.4	393080.2	393079.9	393079.7	393079.5	393079.2	393079	393078.7	393078.4	398075.2	391642.6	393786.1	400217.7	393074.1	395217.8	395932	387355.4
Ca43	383782.6	378746.5	390292.2	382063.6	391970.4	386766.3	392568.1	387587.2	388127	381619.4	388843.1	389581.2	390655.8	391433.9	384609	385170.3	390691.3	379457.1	391126.9	396436.8	370043.3	389129.7	381345.7	384801.5
Sc45	****	*****	0.015	0.171	0.22	0.214	****	0.088	0.09	0.01	*****	*****	0.08	0.79	0.063	0	0.049	0.1	****	****	0.23	0.091	*****	*****
Mn55	90.69	83.1	86.41	80.83	1986.82	2299.99	2497.1	146.43	144.32	135.86	146.51	148.1	151.89	8760.28	196.38	148.67	109.27	97.37	82.01	70.23	51.03	39.56	44.96	46.85
Fe57	465.88	422.01	426.29	851.93	1366.15	478.21	662.16	845.87	819.28	3858.3	837.18	817.94	858.47	7127.26	11211.63	833.44	263.74	4894.62	321.09	256.45	292.75	322.18	316.83	373.53
Cu65	0.31	0.38	****	****	1.17	0.32	****	0.55	0.03	8.33	0.34	0.25	0.04	68.84	2.11	0.67	0.43	4.25	0.54	****	0.91	0.64	1.65	1.25
Zn66	<****	4.29	<****	<****	5.65	1.2	6.99	1.8	<****	13.92	4.01	0.33	****	155.37	12.87	<****	0.65	0	1.05	<****	0.72	<****	****	1.26
As75	336.39	349.3	386.42	461.43	514.84	550.32	281.34	66.34	63.62	73.06	55.6	59.56	66.29	661.81	170.88	58.51	592.75	484.87	893.31	436.79	333.81	445.77	333.91	275.95
Sr88	117.6	123.11	118.62	104.26	91.17	94.44	92.1	405.28	401.56	338.12	404.23	399.12	401.72	102.05	300.56	397.54	102.64	91.57	107.29	81.66	104.21	161.63	106.29	94.9
Y89	398.21	411.49	347.01	267.4	2385.61	2105.36	1042.46	1104.77	1128.95	1332.3	990.63	979.15	1080.07	211.29	809.87	1030.76	470.43	921.62	628.09	467.87	245.24	275.27	375.14	384.33
Mo95	*****	0.03	0.063	0.004	0.107	0.198	0.15	*****	*****	*****	0.042	0	0.18	0.68	0.32	*****	0.068	0.32	0.076	2.39	*****	*****	*****	0.063
Sn118	****	****	0.43	0.19	****	****	****	****	0.01	1.19	*****	0.082	0.34	1.93	1.79	0.16	0.15	****	****	****	****	****	0.08	****
Ba137	0.72	0.214	0.268	0.64	1.95	0.63	1.58	1.78	1.28	9.91	1.52	1.66	1.27	6.43	12.15	1.96	0.233	1.77	0.34	0.207	1.61	1.42	1.85	0.83
La139	1631.32	1786.26	1453.34	844.68	75.86	146.41	290.61	6053.77	6113.9	7955.2	5007.12	4901.37	5604.12	73.65	2960.48	4881.06	2029.64	2128.18	739.97	298.94	2090.08	1781.53	2471.23	2613.74
Ce140	3184.74	3405.55	2648.76	1583.15	332.07	536.43	931.48	11296.46	11352.04	15895.29	10025.88	9686.92	11092.31	44.19	6175.31	9916.53	4360.16	4623	1821.47	846.72	4061.12	3733.39	4821.74	4940.08
Pr141	282.27	297.53	226.34	140.6	74.05	94.23	111.85	1106.93	1109.98	1371.23	993.76	977.63	1074.49	14.92	595.5	963.2	405.02	435.29	194.07	106.65	350.99	342.4	397.42	415.08
Nd146	930.93	952.48	745.21	465.29	525.22	581.55	451.2	3778.94	3785.41	4578.67	3506.64	3408.74	3535.19	72.23	2095.56	3304.65	1321.07	1483.05	732.32	444.66	1071.31	1047.39	1137.12	1181.28
Sm147	118.84	121.91	95.28	62.64	283.78	299.79	150.2	503.71	501.77	600.5	470.72	460.07	489.53	12.68	304.91	458.82	148.35	218.05	128.31	92.05	106.94	103.96	110.81	114.86
Eu151	11.9	12.76	10.84	7.38	59.87	57.34	24.43	34.07	34.35	39.72	31.07	30.59	32.47	1.51	21.2	29.89	19.53	27.34	16.67	14.71	15.44	12.57	13.29	13.89
Gd157	94.91	100	79.93	54.32	429.34	435.41	187.8	358.73	350.95	427.79	324.44	322.34	348.92	26.07	223.83	326.47	105.39	175.45	118.46	94.3	69.03	70.62	85.56	86.36
Tb159	11.74	12.44	9.54	6.7	74.17	74.65	29.82	42.32	42.3	51.67	38.73	37.95	41.92	4.11	28.59	37.99	12.64	23.41	15.53	11.98	6.85	8.01	10.12	10.33
Dy163	65.71	65.09	53.07	38.27	449.01	425.39	174.39	217.41	213.94	264.86	198.87	194.11	218.46	23.07	151.83	206.02	67.4	133.77	88.59	65.23	35.54	42.6	54.71	55.72
Ho165	13.94	13.32	11.48	7.99	81.86	77.65	35.34	41.33	41.92	48.83	37.69	36.93	40.69	5.42	30.19	38.25	13.75	27.88	19.32	14.32	7.41	8.86	11.86	11.87
Er167	33.24	36.04	30.23	22.27	205.56	173.91	95.07	101.53	100.17	126.46	91.03	89.93	101.07	14.55	75.1	87.91	36.54	77.96	52.86	39.07	19.66	22.14	30.51	30.24
Tm169	4.83	4.66	3.88	2.86	27.06	23.24	12.34	12.04	12.1	15.3	10.96	10.81	11.88	2.35	8.9	10.86	4.87	10.57	7.35	5.21	2.54	2.82	3.96	3.9
Yb173	27.68	30.84	25.98	18.17	171.69	138.95	79.93	60.63	59.14	76.99	56.9	53.25	57.46	16.09	43.94	57.07	28.78	52.58	42.06	32.76	13.76	15.26	20.86	21.47
Lu175	4.18	4.76	3.83	2.97	23.18	17.98	11.78	5.98	6.01	7.41	5.52	5.25	6.06	2.11	4.36	5.51	4.18	5.07	4.82	5.2	1.26	1.358	2.12	2.18
Hf177	0.12	0.003	*****	0	0.023	0.03	0.042	0.004	0.041	0.26	0.038	0.022	*****	0.34	0.042	*****	0.002	0.05	0.056	*****	*****	*****	0	0.006
Bi209	0.33	0.208	0.185	0.38	4.26	5.99	1.03	0.027	0.012	0.205	0.0189	0.0076	0.042	2.88	0.97	0.038	1.93	2.35	1.68	1.05	1.48	2.39	1.34	0.91
Th232	51.72	55.51	43.93	18.83	0.656	4.08	8.04	223.72	252.3	308.76	164.15	159.14	254.35	0.95	142.43	217.31	153.11	122.03	57.4	3.34	225.34	226.36	216.01	215.24
U238	10.08	11.27	8.64	5.13	6.23	7.41	2.28	34.43	33.56	34.99	29.4	28.6	34.54	1.91	40.18	34.65	62.34	70.04	26.14	2.59	138.63	129.14	158.42	167.09

1 sigma error.
All values are reported in ppm

	11UPA86B4				09CQA1170D3			09CQA0128B2					3507A				09CQA1045C8				09CQA1045E4			
Element	JL09A31	JL09A32	JL09A33	JL09A34	JL09A39	JL09A40	JL09A41	JL09A22	JL09A23	JL09A24	JL09A25	JL09A26	JL09A27	JL09A28	JL09A29	JL09A30	JL09A46	JL09A47	JL09A48	JL09A49	JL09A42	JL09A43	JL09A44	JL09A45
Na23	77.44	69.72	58.28	37.67	43.35	49.28	51.32	205.08	207.89	287.49	182.14	205.04	216.56	45.74	119.33	196.03	24.62	44.58	28.62	35.79	29.31	23.49	30.89	33.95
Mg25	18.69	8.84	9.58	66.62	55.92	12.41	10.61	24.31	23.88	20.45	25.62	25.71	28.69	2163.23	356.69	31.49	1.74	21.26	3.84	3.41	1.94	1.63	1.93	1.98
Al27	1.73	0.76	0.73	5.67	13.1	1.11	7.53	0.61	0.61	1.61	0.34	0.44	0.82	38.31	16.33	0.76	0.71	3.57	0.98	1.02	1.2	0.6	0.76	4.09
Si29	246.29	246.15	192.08	219.1	356.38	218.53	106.77	358.9	354.46	247.7	356.88	337.36	397.54	4275.87	1299.7	420.47	471.77	545.79	294.79	177.6	387.76	391.02	479.4	523.99
P31	118398	115999.4	113340.6	114604.5	134860.9	135207.8	148767.7	100780.7	99463.37	49737.22	101110.1	101928.3	112613	150.95	111647.3	108060.9	139071.6	138670.9	149735.7	154135.2	124098.5	137407.4	135354.1	135410
S34	535.39	2781.83	5352.22	3238.9	1286.23	1499.44	2035.06	1397.92	191.61	1596.65	601.23	1029.3	574.27	10670.29	1840.1	858.57	5140.33	931.34	5271.3	2157.18	3707.58	3524.18	773.07	3164.41
K39	4.95	2.42	2.01	2.11	33.91	4.99	3.24	2.06	1.82	6.6	1.04	1.33	2.61	37.45	4.77	2.32	1.98	4.99	3.26	2.87	3.25	1.72	2.02	1.8
Ca42	12574.71	12463.65	12453.2	12446.43	12638.46	12503.01	12488.53	12443.2	12449.82	12515.65	12439.96	12441.25	12479.13	12495.68	12445.62	12466.31	12618.26	12449.93	12514.79	12707.54	12492.17	12512.89	12553.28	12271.91
Ca43	28102.99	28309.67	29902.27	30009.48	34912.93	35290.46	36740.67	22584.87	23177.12	23441.43	24369.78	25029.69	25780.16	26503.66	26639.6	27381.84	41263.12	41077.2	43358.11	44992.79	35496.87	38206.5	38379.63	39667.92
Sc45	0.21	0.099	0.09	0.078	0.13	0.093	0.12	0.076	0.079	0.14	0.044	0.056	0.11	0.18	0.075	0.1	0.092	0.12	0.12	0.11	0.14	0.075	0.084	0.073
Mn55	4.96	4.36	4.58	4.35	116.79	137.78	152.7	6.45	6.46	6.37	6.73	6.91	7.31	421.31	9.63	7.48	7.44	6.84	5.89	5.15	3.31	2.55	2.98	3.14
Fe57	174.21	161.1	167.55	344.57	640.84	231.08	329.6	236.59	236.57	1149.26	257.12	259.18	281.16	2402.1	3895.31	299.04	151.71	2892.45	195.78	160.93	150.45	169.8	172.04	208.57
Cu65	0.53	0.28	0.21	0.19	0.51	0.25	0.27	0.21	0.19	1.83	0.14	0.15	0.3	14.8	0.52	0.3	0.27	1.61	0.4	0.27	0.5	0.29	0.63	0.49
Zn66	3.44	1.97	1.49	1.35	2.67	1.56	3.04	1.28	1.34	3.69	1.07	0.94	1.82	33.22	3.1	1.62	1.46	1.89	2.09	2.06	2.14	1.33	1.44	1.28
As75	96.34	102.31	116.03	142.06	179.85	197.11	103.41	15.2	14.95	17.76	13.69	15.03	17.24	175.39	46.42	16.37	247.07	207.35	391.74	196.5	125.83	172.21	132.33	112.15
Sr88	4.19	4.14	3.98	3.5	3.22	3.3	3.3	12.97	12.9	11.08	13.03	12.91	13.14	3.47	9.84	13.11	3.71	3.41	4	3.07	3.75	5.67	3.8	3.4
Y89	18.23	18.93	16.22	12.7	123.53	110.94	56.02	43.86	45.42	54.5	40.92	41.02	46	9.21	35.48	45.9	27.75	55.46	38.55	29.28	13.47	15.34	21.32	22.24
Mo95	0.064	0.061	0.056	0.036	0.097	0.098	0.11	0.05	0.056	0.026	0.03	0.042	0.11	0.27	0.11	0.06	0.062	0.18	0.073	0.98	0.039	0.059	0.04	0.05
Sn118	0.32	0.15	0.19	0.13	0.22	0.19	0.18	0.12	0.13	0.4	0.084	0.095	0.21	0.58	0.49	0.16	0.14	0.22	0.44	0.15	0.19	0.24	0.13	0.21
Ba137	0.3	0.09	0.071	0.098	0.31	0.13	0.29	0.16	0.16	0.98	0.13	0.15	0.24	0.69	0.76	0.26	0.084	0.34	0.14	0.099	0.31	0.16	0.25	0.13
La139	67.45	74.47	61.39	36.17	3.55	6.88	13.89	224.5	229.05	301.78	191.52	189.58	219.53	3.01	118.66	198.22	105	112.13	39.72	16.36	101.17	87.55	123.54	132.87
Ce140	138.55	149.91	118.38	71.87	16.43	26.94	47.64	433.81	441.25	626.65	399.46	391.06	454.32	1.91	259.87	423.62	243.9	263.66	105.9	50.19	211.26	197.56	259.92	271.21
Pr141	12.47	13.2	10.2	6.43	3.72	4.78	5.8	42.65	43.31	54.34	39.76	39.64	44.25	0.68	25.2	41.4	22.86	25.07	11.41	6.4	18.44	18.27	21.62	22.99
Nd146	81.88	85.56	68.67	43.99	56.49	64.07	51.07	262.2	269.43	334.71	262.64	261.97	278.97	6.05	174.04	281.71	169.11	194.7	98.6	61.39	124.18	124.37	138.49	147.48
Sm147	6.83	6.48	5.13	3.44	17.03	18.23	9.52	21.91	22.22	27.49	21.48	21.36	23.38	0.93	14.97	23.03	10.25	15.48	9.38	6.89	7	6.73	7.39	7.77
Eu151	0.77	0.63	0.53	0.37	3.09	2.97	1.37	1.35	1.4	1.78	1.27	1.27	1.45	0.15	0.94	1.37	1.15	1.68	1.07	0.96	0.91	0.7	0.78	0.81
Gd157	5.76	5.54	4.48	3.11	26.75	27.57	12.35	16.1	16.07	20.35	15.31	15.49	17.31	1.64	11.41	17.04	7.66	13.09	9.09	7.39	4.8	4.79	6	6.13
Tb159	1.03	1.05	0.83	0.59	7.38	7.6	3.13	2.76	2.84	3.59	2.72	2.73	3.12	0.35	2.22	3.03	1.5	2.85	1.94	1.54	0.76	0.88	1.15	1.2
Dy163	5.15	4.95	4.11	3.04	39.83	38.61	16.3	12.91	13.01	16.67	12.63	12.62	14.65	1.74	10.61	14.78	7.1	14.45	9.83	7.42	3.49	4.17	5.51	5.73
Ho165	0.74	0.62	0.53	0.37	4.04	3.87	1.83	1.6	1.65	2.02	1.51	1.5	1.72	0.29	1.28	1.66	0.78	1.62	1.15	0.87	0.43	0.47	0.66	0.66
Er167	1.98	1.7	1.43	1.06	10.18	8.69	4.99	3.95	3.97	5.37	3.65	3.66	4.34	0.85	3.2	3.88	2.1	4.58	3.21	2.42	1.21	1.2	1.72	1.7
Tm169	0.31	0.22	0.18	0.13	1.23	1.06	0.61	0.45	0.46	0.66	0.42	0.42	0.5	0.15	0.36	0.46	0.26	0.57	0.42	0.3	0.16	0.14	0.21	0.2
Yb173	2.33	2.16	1.83	1.31	13.44	11.08	6.66	3.27	3.29	4.67	3.25	3.11	3.61	1.24	2.77	3.74	2.7	5.08	4.18	3.33	1.33	1.33	1.9	1.97
Lu175	0.31	0.25	0.2	0.16	1.25	0.97	0.68	0.25	0.26	0.39	0.24	0.23	0.31	0.15	0.21	0.28	0.27	0.35	0.34	0.36	0.11	0.085	0.14	0.14
Hf177	0.1	0.018	0.014	<0.00	0.023	0.022	0.039	0.021	0.025	0.11	0.016	0.018	0.01	0.11	0.019	0.021	0.021	0.042	0.04	0.013	0.011	0.018	0.016	0.022
Bi209	0.11	0.06	0.053	0.1	1.26	1.81	0.33	0.013	0.011	0.068	0.0077	0.0058	0.021	0.66	0.23	0.017	0.68	0.86	0.63	0.4	0.48	0.78	0.45	0.31
Th232	3.33	3.53	2.85	1.26	0.078	0.33	0.66	11.48	13.2	16.57	8.94	8.85	14.48	0.1	8.44	13.17	13.29	10.87	5.25	0.34	17.86	18.32	17.9	18.24
U238	0.87	0.9	0.7	0.43	0.6	0.72	0.25	2.13	2.13	2.33	1.95	1.94	2.43	0.18	2.93	2.6	6.84	7.89	3.03	0.33	13.81	13.15	16.54	17.86

Minimum detection limits (99% confidence).
All values are reported in ppm

	11UPA86B4				09CQA1170D3			09CQA0128B2					3507A				09CQA1045C8				09CQA1045E4			
Element	JL09A31	JL09A32	JL09A33	JL09A34	JL09A39	JL09A40	JL09A41	JL09A22	JL09A23	JL09A24	JL09A25	JL09A26	JL09A27	JL09A28	JL09A29	JL09A30	JL09A46	JL09A47	JL09A48	JL09A49	JL09A42	JL09A43	JL09A44	JL09A45
Na23	7.11	5.36	5.7	5.47	5.32	4.89	5.07	5.55	4.86	4.54	3.06	4.14	5.03	7.03	5.19	5.08	4.82	4.19	4.68	4.76	5.25	5.46	4.21	4.01
Mg25	2.08	1.67	1.74	1.89	1.92	1.72	2.05	1.8	1.62	1.63	1.04	1.37	1.68	2.17	1.8	1.48	1.9	1.68	1.62	1.75	1.91	2	1.44	1.42
Al27	1.7	1.29	1.44	1.38	1.36	1.27	1.32	1.31	1.14	1.09	0.732	1	1.22	1.71	1.25	1.24	1.29	1.13	1.28	1.28	1.36	1.43	1.13	1.09
Si29	178.24	136.36	144.62	139.56	135.67	125.82	132.91	141.07	123.3	114.76	75.54	104.47	131.62	181.72	133.31	128.86	125.54	109.21	122.85	123.19	135.09	143.57	109.16	103.34
P31	20.71	15.43	16.22	15.32	15.14	14	14.44	16.43	13.97	13.2	8.71	11.57	14.99	20.57	15.34	15.01	13.2	11.79	13.57	13.29	14.86	15.3	11.89	11.23
S34	444.84	335.98	345.23	330.59	325.42	306.69	316.78	421.69	356.89	323.82	209.13	277.87	331.67	453.35	330.96	317.84	317.83	286.02	324.86	336.65	328.93	347.65	273.53	260.51
K39	5.18	3.89	4.15	4	3.93	3.61	3.76	3.97	3.5	3.27	2.2	2.98	3.64	5.1	3.75	3.68	3.62	3.13	3.5	3.56	3.91	4.05	3.13	3.01
Ca42	125.88	94.41	101.84	97.07	94.64	86.62	90.18	93.82	83.59	77.88	51.75	71.46	91.28	126.51	90.59	90.67	84.81	75.15	84.67	84.23	94.04	98.01	75.49	70.21
Ca43	152.06	117.92	130.62	126.59	124.79	112	118.71	116.06	101.17	98.84	67.59	88.6	102.95	161.7	115.56	113.8	111.35	99.03	117.07	114.96	128.28	131	98.62	93.7
Sc45	0.234	0.177	0.186	0.168	0.179	0.157	0.169	0.174	0.149	0.145	0.0934	0.128	0.154	0.218	0.163	0.164	0.165	0.14	0.161	0.162	0.169	0.173	0.141	0.139
Mn55	0.618	0.461	0.507	0.501	0.48	0.459	0.476	0.466	0.411	0.389	0.264	0.361	0.433	0.607	0.454	0.434	0.447	0.395	0.442	0.446	0.487	0.505	0.389	0.379
Fe57	12.66	9.27	10.39	9.56	9.84	8.87	9.4	9.61	9.03	8.22	5.26	7.28	8.86	12.49	9.12	8.97	9	7.99	8.38	9.11	9.55	10.06	7.68	7.18
Cu65	0.513	0.431	0.45	0.441	0.439	0.394	0.374	0.377	0.356	0.369	0.245	0.292	0.425	0.449	0.375	0.351	0.372	0.363	0.385	0.404	0.465	0.449	0.365	0.355
Zn66	3.69	2.86	2.99	2.92	2.93	2.74	2.83	2.86	2.49	2.3	1.51	2.1	2.63	3.7	2.71	2.64	2.63	2.26	2.64	2.64	2.86	3.07	2.33	2.2
As75	0.521	0.461	0.475	0.447	0.387	0.421	0.413	0.472	0.416	0.328	0.233	0.32	0.406	0.498	0.414	0.346	0.394	0.428	0.464	0.399	0.458	0.498	0.333	0.354
Sr88	0.00841	0.00621	<0.00000	0.0177	<0.00000	0.00757	<0.00000	0.0106	0.0119	0.00649	<0.00000	0.0114	0.0111	0.0108	0.00571	<0.00000	0.0128	0.012	0.0214	0.00547	0.0102	0.0224	0.0144	0.0106
Y89	0.00715	0.0139	0.0058	0.00531	0.015	0.0226	0.0164	0.00525	0.00931	0.0162	0.00599	<0.00000	0.0164	0.013	0.00688	0.00474	0.00964	0.0054	0.0291	<0.00000	0.00859	0.0174	0.0272	0.00516
Mo95	0.162	0.0946	0.0877	0.0799	0.0945	0.0793	0.0922	0.132	0.108	0.0739	0.0464	0.0934	0.0872	0.15	0.0948	0.103	0.0777	0.0503	0.0409	0.0914	0.0926	0.143	0.0717	0.0589
Sn118	0.352	0.26	0.261	0.261	0.287	0.259	0.245	0.277	0.253	0.228	0.164	0.205	0.246	0.336	0.251	0.238	0.217	0.251	0.291	0.22	0.263	0.302	0.203	0.225
Ba137	0.0489	0.0806	<0.00000	0.0514	0.0324	0.0618	0.0337	0.0882	0.0494	0.0466	<0.00000	0.0358	<0.00000	0.0893	<0.00000	0.0458	0.0735	0.0782	0.067	0.0546	0.0479	0.0358	0.0371	0.0352
La139	0.00622	<0.00000	0.00874	0.00923	<0.00000	0.0068	0.00428	<0.00000	0.0386	0.0245	0.0107	0.00644	<0.00000	0.00985	0.00424	<0.00000	0.00936	0.0115	0.0198	<0.00000	0.0122	0.0285	0.0448	0.0334
Ce140	0.0101	0.00432	<0.00000	0.0123	0.0087	0.0178	0.00404	0.0061	0.0251	0.023	0.022	0.00677	0.00672	0.0142	0.00399	0.00549	<0.00000	0.0185	0.0345	0.01	0.0211	0.0458	0.0599	0.0347
Pr141	0.00962	<0.00000	0.0039	0.0186	0.00452	0.00431	0.00664	0.00707	0.00885	0.00264	0.00598	0.00248	0.00318	<0.00000	0.00463	0.0045	0.00562	0.00257	0.0107	0.0044	0.00746	0.0158	0.0221	0.0115
Nd146	<0.00000	0.0493	<0.00000	0.216	0.0343	0.0627	0.0206	<0.00000	0.0461	0.0329	0.0682	0.0218	0.0396	0.0386	0.0407	0.0485	<0.00000	0.0618	0.0449	0.0193	<0.00000	0.082	0.077	0.0747
Sm147	<0.00000	0.0255	0.0281	0.133	0.0397	0.0218	0.0336	0.0361	0.0404	0.0426	0.0225	0.031	0.0324	0.0316	0.0333	<0.00000	0.0232	<0.00000	0.0701	<0.00000	<0.00000	0.0253	0.0262	0.0556
Eu151	0.0108	0.0195	0.00874	0.0339	0.0143	0.0136	0.0128	0.00794	0.00629	<0.00000	0.00572	0.00557	0.0143	0.0139	<0.00000	0.0124	0.0102	<0.00000	0.0066	<0.00000	0.0106	0.0193	0.00818	0.00776
Gd157	0.0846	0.0509	<0.00000	0.172	0.0324	0.0488	<0.00000	0.0442	0.0286	0.0467	0.0225	0.0179	0.0512	0.0706	0.0235	0.0324	<0.00000	0.0552	0.0211	0.0315	0.0414	0.0669	0.0185	0.0176
Tb159	0.00524	0.00864	<0.00000	0.0267	0.00776	0.0105	0.00624	<0.00000	0.00615	<0.00000	0.00197	0.00471	0.00492	0.00678	0.00619	0.00492	<0.00000	0.00558	<0.00000	<0.00000	0.00628	0.0101	<0.00000	<0.00000
Dy163	<0.00000	0.0269	0.0171	0.138	0.0242	0.0421	0.0205	0.0271	0.0214	0.0202	<0.00000	0.0155	0.014	0.0193	<0.00000	0.0242	0.0141	0.0194	0.0288	0.0136	0.0252	<0.00000	<0.00000	0.0284
Ho165	0.00549	0.00572	<0.00000	0.0276	0.00811	0.00915	0.00533	0.00708	0.00646	0.00745	0.00207	0.0057	0.00516	0.00502	0.00748	0.0063	0.00369	0.00414	0.00475	0.00354	0.00536	<0.00000	0.0072	0.00279
Er167	0.0446	0.0233	<0.00000	0.112	0.0148	0.0199	0.0217	0.0166	0.0227	0.0175	0.0146	0.0259	0.0148	0.0354	<0.00000	0.0148	0.0212	0.0206	<0.00000	0.0144	<0.00000	0.0326	0.0207	0.0161
Tm169	0.0072	0.00375	0.00714	0.0169	0.00476	0.00454	0.0035	0.00534	<0.00000	0.00488	0.00271	0.00457	0.00585	0.00806	0.00849	0.00477	<0.00000	<0.00000	0.00881	<0.00000	0.00703	0.00526	<0.00000	0.00366
Yb173	0.0461	<0.00000	0.0264	0.128	0.0216	0.0291	0.0224	<0.00000	0.0191	0.018	0.0173	0.0169	0.0216	0.0298	0.0222	0.0305	0.0438	0.0301	0.0282	<0.00000	0.0319	<0.00000	<0.00000	0.0439
Lu175	0.00776	0.00404	0.00445	0.0211	0.00363	0.00489	0.00842	<0.00000	0.00457	0.00527	<0.00000	0.00403	0.00365	0.00503	0.00917	0.00364	0.00637	0.00714	0.00821	0.00353	0.00535	<0.00000	<0.00000	0.00279
Hf177	0.04	0.0294	0.0458	<0.00000	<0.00000	0.0178	0.0273	0.0472	0.0289	<0.00000	0.0185	0.0329	0.0326	0.0579	0.0193	0.0375	0.0377	0.0211	<0.00000	0.0404	0.0337	0.046	0.0261	0.0378
Bi209	0.0247	0.014	0.0166	0.00992	0.0208	0.0152	0.0156	0.0219	0.0165	0.02	0.00957	0.0102	0.014	0.024	0.0161	0.00901	0.00876	0.012	0.0122	0.0137	0.0196	0.0124	0.00405	0.0127
Th232	0.00681	0.0087	0.00781	0.072	0.0119	0.0043	0.00811	0.00715	0.004	0.013	0.00363	0.00612	0.00452	0.0108	0.0104	0.00782	<0.00000	0.0154	0.027	0.0124	0.00942	0.00996	0.00894	0.0104
U238	0.011	0.0105	0.00892	0.0346	0.0133	0.004	0.00436	<0.00000	0.00835	0.00497	0.00536	0.00467	0.0112	0.0164	0.00613	<0.00000	0.00737	0.0143	0.0209	0.00408	0.0107	0.0131	0.00961	0.00912

Trace element concentrations normalised to chondrite.
All values are reported in ppm

	11UPA86B4				09CQA1170D3			09CQA0128B2					3507A				09CQA1045C8				09CQA1045E4			
Element	JL09A31	JL09A32	JL09A33	JL09A34	JL09A39	JL09A40	JL09A41	JL09A22	JL09A23	JL09A24	JL09A25	JL09A26	JL09A27	JL09A28	JL09A29	JL09A30	JL09A46	JL09A47	JL09A48	JL09A49	JL09A42	JL09A43	JL09A44	JL09A45
Na23	0.071	0.0622	0.0506	0.0318	0.0321	0.0356	0.0361	0.239	0.236	0.318	0.196	0.215	0.221	0.0451	0.115	0.185	0.0152	0.0268	0.0167	0.0204	0.0199	0.0157	0.0201	0.0216
Mg25	0.00067	0.00033	0.00035	0.00243	0.00175	0.00037	0.0003	0.00126	0.00119	0.00094	0.00122	0.00118	0.00126	0.094	0.0151	0.00127	0.00003	0.00052	0.00008	0.00007	0.00003	0.00004	0.00004	0.00004
Al27	0.00038	0.00014	0.00019	0.00839	0.0184	0.00105	0.0101	0.00026	0.00011	0.00126	0	0	0	0.0598	0.0255	0	0	0.00412	0	0.0004	0.00056	0	0.00026	0.00531
Si29	0.0062	0.0084	0.0063	0.0073	0.0106	0.0063	0.00128	0.0156	0.015	0.009	0.0148	0.0137	0.0154	0.169	0.0503	0.0156	0.0124	0.014	0.007	0.0038	0.0108	0.011	0.0132	0.0142
P31	83.27	80.18	76.98	76.47	82.13	80.82	87.27	81.57	79.4	39.14	78.38	77.82	84.63	0.111	81.22	77.3	74.21	72.6	76.91	77.67	71.44	77.63	75.03	73.65
S34	0	Inf	Inf	Inf	0	0	0	0	0	0	0	0	0	Inf	Inf	0	Inf	0	Inf	0	Inf	Inf	0	Inf
K39	0.0067	0	0	0.0064	0.168	0.0221	0.0082	0.0092	0	0.0431	0	0	0	0.251	0.0292	0	0	0.017	0.0071	0	0.0068	0	0	0
Ca42	29.12	29.12	29.12	29.12	29.49	29.22	29.12	29.12	29.12	29.12	29.12	29.12	29.12	29.12	29.12	29.12	29.49	29.01	29.17	29.65	29.12	29.28	29.33	28.69
Ca43	28.43	28.06	28.91	28.3	29.03	28.65	29.08	28.71	28.75	28.27	28.8	28.86	28.94	29	28.49	28.53	28.94	28.11	28.97	29.37	27.41	28.82	28.25	28.5
Sc45	0	0	0	0.0198	0.025	0.025	0	0	0	0	0	0	0	0.091	0	0	0	0	0	0	0.027	0	0	0
Mn55	0.0308	0.0283	0.0294	0.0275	0.676	0.782	0.849	0.0498	0.0491	0.0462	0.0498	0.0504	0.0517	2.98	0.0668	0.0506	0.0372	0.0331	0.0279	0.0239	0.0174	0.01345	0.0153	0.0159
Fe57	0.00168	0.00152	0.00153	0.0031	0.0049	0.00172	0.0024	0.00304	0.00295	0.0139	0.00301	0.00294	0.0031	0.0256	0.04	0.003	0.00095	0.018	0.00116	0.00092	0.00105	0.00116	0.00114	0.00134
Cu65	0	0	0	0	0.007	0	0	0.0033	0	0.05	0.00203	0	0	0.41	0.0125	0.004	0.0026	0.0253	0.0032	0	0.0054	0.0038	0.0098	0.0074
Zn66	0	0.0093	0	0	0.0122	0	0.0151	0	0	0.0301	0.0087	0	0	0.336	0.0279	0	0	0	0	0	0	0	0	0
As75	117.21	121.71	134.64	160.78	179.39	191.75	98.03	23.12	22.17	25.46	19.37	20.75	23.1	230.59	59.54	20.39	206.53	168.95	311.26	152.19	116.31	155.32	116.35	96.15
Sr88	9.88	10.35	9.97	8.76	7.66	7.94	7.74	34.06	33.74	28.41	33.97	33.54	33.76	8.58	25.26	33.41	8.62	7.69	9.02	6.86	8.76	13.58	8.93	7.97
Y89	176.98	182.88	154.23	118.84	1060.27	935.71	463.32	491.01	501.76	592.13	440.28	435.18	480.03	93.91	359.94	458.12	209.08	409.61	279.15	207.94	109	122.34	166.73	170.81
Mo95	0	0	0	0	0.077	0.144	0.105	0	0	0	0	0	0.13	0.49	0.235	0	0	0.23	0.055	1.73	0	0	0	0.046
Sn118	0	0	0.171	0	0	0	0	0	0	0.47	0	0	0.136	0.77	0.71	0	0	0	0	0	0	0	0	0
Ba137	0.211	0.063	0.079	0.188	0.571	0.185	0.462	0.523	0.376	2.91	0.447	0.488	0.373	1.89	3.56	0.574	0.068	0.52	0.1	0.061	0.473	0.416	0.542	0.243
La139	4445.02	4867.19	3960.06	2301.59	206.71	398.94	791.85	16495.28	16659.14	21676.29	13643.37	13355.22	15270.08	200.68	8066.7	13299.9	5530.35	5798.85	2016.27	814.54	5695.03	4854.31	6733.59	7121.91
Ce140	3327.83	3558.57	2767.77	1654.28	347	560.53	973.33	11804.03	11862.11	16609.49	10476.36	10122.17	11590.71	46.18	6452.78	10362.1	4556.07	4830.73	1903.32	884.77	4243.59	3901.14	5038.39	5162.05
Pr141	2060.4	2171.77	1652.11	1026.27	540.55	687.82	816.43	8079.8	8102.04	10008.95	7253.7	7136.01	7842.98	108.9	4346.73	7030.67	2956.34	3177.33	1416.58	778.45	2561.98	2499.25	2900.85	3029.79
Nd146	1309.32	1339.63	1048.12	654.42	738.71	817.93	634.6	5314.97	5324.07	6439.76	4931.98	4794.29	4972.13	101.59	2947.35	4647.89	1858.04	2085.86	1029.99	625.4	1506.77	1473.12	1599.33	1661.44
Sm147	514.46	527.76	412.46	271.16	1228.47	1297.81	650.22	2180.57	2172.15	2599.56	2037.76	1991.63	2119.19	54.88	1319.97	1986.23	642.22	943.94	555.46	398.49	462.95	450.05	479.68	497.24
Eu151	136.79	146.71	124.56	84.83	688.19	659.14	280.76	391.58	394.83	456.54	357.17	351.6	373.19	17.33	243.68	343.61	224.54	314.27	191.67	169.08	177.47	144.53	152.79	159.69
Gd157	310.16	326.81	261.22	177.51	1403.08	1422.9	613.71	1172.31	1146.91	1398	1060.26	1053.38	1140.27	85.2	731.48	1066.89	344.41	573.38	387.11	308.17	225.59	230.79	279.61	282.23
Tb159	202.33	214.5	164.56	115.54	1278.75	1287.03	514.17	729.6	729.39	890.9	667.76	654.28	722.79	70.89	492.92	654.93	217.92	403.65	267.76	206.56	118.04	138.06	174.46	178.13
Dy163	172.48	170.85	139.28	100.44	1178.51	1116.51	457.72	570.62	561.52	695.17	521.97	509.48	573.37	60.56	398.5	540.73	176.9	351.12	232.53	171.2	93.28	111.82	143.61	146.26
Ho165	163.83	156.57	134.94	93.86	961.94	912.49	415.33	485.66	492.63	573.85	442.85	434.01	478.13	63.67	354.72	449.47	161.57	327.62	227.06	168.26	87.1	104.11	139.35	139.46
Er167	133.5	144.73	121.42	89.42	825.55	698.44	381.8	407.76	402.3	507.87	365.58	361.18	405.91	58.43	301.61	353.04	146.73	313.11	212.3	156.89	78.95	88.93	122.55	121.44
Tm169	135.72	130.8	109.12	80.39	760.11	652.79	346.58	338.18	339.79	429.79	308	303.59	333.58	66.06	249.9	305.19	136.79	296.81	206.45	146.46	71.35	79.23	111.13	109.63
Yb173	111.61	124.35	104.75	73.26	692.28	560.29	322.31	244.46	238.47	310.45	229.45	214.72	231.68	64.87	177.16	230.12	116.05	212.03	169.6	132.09	55.5	61.52	84.1	86.57
Lu175	109.78	125	100.4	78.01	608.28	471.86	309.18	157.04	157.62	194.46	144.82	137.92	159.17	55.49	114.5	144.62	109.61	132.96	126.53	136.59	33.2	35.65	55.73	57.26
Hf177	0.69	0	0	0	0.13	0.17	0.23	0	0.23	1.44	0.211	0	0	1.91	0.24	0	0	0.28	0.31	0	0	0	0	0
Bi209	1.96	1.25	1.11	2.3	25.52	35.88	6.18	0.16	0	1.23	0.113	0	0.25	17.24	5.79	0.23	11.57	14.08	10.08	6.26	8.89	14.34	8.01	5.44
Th232	1216.86	1306.11	1033.66	443.08	15.44	96.09	189.17	5263.98	5936.4	7265.02	3862.37	3744.55	5984.7	22.43	3351.37	5113.13	3602.7	2871.41	1350.59	78.64	5302.08	5326.06	5082.57	5064.41
U238	826.48	923.59	708.31	420.52	510.55	607.75	186.83	2821.93	2750.68	2867.9	2410.06	2344.36	2830.77	156.72	3293.78	2840.27	5109.92	5740.9	2142.24	212.39	11363.46	10584.88	12984.95	13696.13

Mean Raw CPS background subtracted.
All values are reported in ppm

	11UPA86B4				09CQA1170D3			09CQA0128B2					3507A				09CQA1045C8				09CQA1045E4			
Element	JL09A31	JL09A32	JL09A33	JL09A34	JL09A39	JL09A40	JL09A41	JL09A22	JL09A23	JL09A24	JL09A25	JL09A26	JL09A27	JL09A28	JL09A29	JL09A30	JL09A46	JL09A47	JL09A48	JL09A49	JL09A42	JL09A43	JL09A44	JL09A45
Na23	126213	144295	115316	71414	67366	83508	85252	563257	573129	829850	761733	622739	550618	79383	272920	436869	38335	71111	40496	50942	44387	33854	53476	59770
Mg25	1919	1202	1263	8611	5756	1364	1098	4863	4740	4000	7671	5550	5058	266871	57212	4824	121	2136	293	260	91	122	167	191
Al27	689	326	444	18979	38696	2470	23801	638	282	3420	0	0	0	107806	61504	84	37	10840	0	980	1248	0	696	14651
Si29	2484	4329	3192	3630	4944	3256	665	8254	8209	5284	12913	8878	8568	66287	26504	8195	6928	8150	3756	2092	5325	5265	7767	8695
P31	2478610	3103042	2930058	2871219	2918963	3213659	3505585	3168782	3181595	1688440	5033575	3731076	3494174	3235	3189196	3042021	3235051	3328796	3236576	3370641	2711140	2868914	3424965	3511481
S34	60	638	1196	703	228	290	382	274	0	0	0	284	127	1856	432	197	814	140	706	0	632	558	0	581
K39	1681	0	44	2028	49622	7275	2721	3065	432	15940	480	250	1442	62441	9748	0	151	6274	2389	0	2107	203	902	1247
Ca42	1089808	1409872	1379945	1354886	1270724	1403257	1406863	1495533	1533277	1640964	2428214	1802672	1543636	1085340	1452387	1448003	1518617	1566362	1440904	1505522	1324048	1291759	1592619	1621775
Ca43	243068	310465	313265	301204	286562	315129	321888	335015	344207	362465	546882	407031	349718	246521	324315	323973	341504	347706	327864	341590	285586	291422	351485	369158
Sc45	0	0	8	97	114	126	0	54	56	5	0	0	48	356	38	0	30	69	0	0	129	49	0	0
Mn55	32694	38816	39560	36375	831519	1073052	1172572	70991	71938	72669	116256	87455	76975	3128110	94020	71091	54650	51025	39292	34566	22554	16964	23727	25724
Fe57	4450	5219	5163	10135	15026	5855	8147	10903	10857	54862	17656	12833	11555	67566	142433	10568	3426	66494	3979	3257	3385	3608	4359	5338
Cu65	26	43	0	0	120	36	0	63	3	1064	64	35	5	5916	243	77	52	549	64	0	98	67	214	169
Zn66	0	321	0	0	382	90	531	139	0	1190	508	30	0	8885	987	0	53	0	82	0	51	0	0	112
As75	23061	31118	33837	39826	41780	49872	25703	5909	5852	7244	8213	6573	6302	44497	15457	5303	58032	49779	83905	42164	28748	37301	34423	29634
Sr88	69886	94754	89457	77282	62835	72568	71250	326033	331791	299517	530743	389649	336347	60162	237435	313510	84767	79292	85006	66513	75909	114283	92519	86002
Y89	278517	373057	308490	233794	1944237	1913689	954186	1035412	1088266	1378705	1521377	1119472	1060213	146192	751641	955893	459859	944489	588830	450811	211399	230356	386502	412259
Mo95	0	3	8	0	13	27	20	0	0	0	9	0	25	68	43	0	10	49	10	348	0	0	0	10
Sn118	0	0	138	61	0	0	0	0	2	425	0	33	118	473	592	52	54	0	0	0	0	0	31	0
Ba137	73	28	34	81	232	83	211	243	180	1496	341	277	182	650	1647	265	33	266	47	29	203	173	279	130
La139	1311418	1862228	1486323	849911	71221	153315	306435	6476536	6734274	9415481	8802770	6420127	6307254	58469	3154515	5199908	2283688	2509601	797931	331166	2075390	1717203	2932127	3228045
Ce140	2717394	3766872	2872990	1688908	330177	594820	1039997	12895398	13332051	20044926	18767654	13501955	13276549	37289	6990377	11217797	5194901	5773343	2080383	993708	4269610	3810027	6057259	6460021
Pr141	293532	401044	299145	182753	89704	127297	152148	1542281	1590708	2109632	2269055	1661830	1568169	15348	821731	1328056	588119	662593	270207	152595	449597	425758	608353	661463
Nd146	155752	206600	158525	97360	102489	126572	98892	845255	871144	1131512	1286455	931225	829393	11947	465052	732945	309206	363894	164364	102564	221134	209888	280542	303414
Sm147	17171	22842	17512	11327	47917	56477	28502	97115	99552	127965	148942	108423	99097	1809	58411	87863	30106	46403	24984	18426	19117	18047	23688	25572
Eu151	5524	7682	6397	4285	32436	34653	14865	21120	21913	27213	31608	23172	21125	691	13050	18394	12698	18633	10395	9424	8849	6997	9107	9910
Gd157	13733	18765	14713	9837	72583	82114	35671	69211	69690	91251	102770	76055	70724	3727	42940	62609	21391	37338	23061	18869	12350	12268	18301	19234
Tb159	11189	15385	11580	8001	82698	92856	37364	53673	55243	72506	80727	58935	55943	3870	36125	47993	16921	32858	19938	15807	8079	9175	14276	15177
Dy163	15569	20004	16001	11355	124479	131573	54333	68466	69372	92294	102947	74876	72414	5395	47664	64673	22445	46708	28297	21412	10430	12141	19200	20361
Ho165	12703	15750	13321	9120	87304	92376	42341	49807	52063	65221	74821	54674	51789	4867	36419	46163	17567	37324	23647	17997	8361	9700	15982	16647
Er167	7445	10471	8620	6247	53876	50845	27991	30127	30622	41564	44467	32749	31640	3214	22278	26083	11479	25670	15914	12080	5450	5960	10110	10428
Tm169	4747	5935	4858	3522	31103	29796	15931	15688	16237	22078	23512	17274	16315	2279	11579	14143	6710	15260	9706	7073	3088	3329	5749	5903
Yb173	4247	6136	5071	3489	30775	27782	16094	12384	12437	17397	19098	13315	12344	2438	8936	11605	6186	11846	8666	6934	2610	2808	4726	5064
Lu175	3809	5628	4436	3392	24726	21400	14124	7217	7462	9899	10957	7779	7718	1899	5261	6648	5349	6801	5920	6566	1428	1489	2866	3066
Hf177	21	0	0	0	4	7	9	0	9	66	14	6	0	59	9	0	0	12	13	0	0	0	0	1
Bi209	209	173	151	311	3270	5140	893	21	10	186	25	7	37	1795	813	31	1798	2297	1504	961	1212	1901	1309	926
Th232	37957	52845	41034	17308	563	3910	7753	218042	253235	333098	263112	190103	261122	690	138502	211314	157653	131702	56652	3389	204659	199590	234483	243228
U238	7934	11504	8658	5059	5741	7625	2361	35904	36051	40409	50466	36592	37982	1483	41879	36121	69017	81287	27744	2826	135290	122367	184837	202992

Appendix 3 – Open File 7319

Petrographic and cathodoluminescence characterization of apatite from the Sue Dianne and Brooke Zone IOCG mineralization systems, Great Bear magmatic zone, Northwest Territories

Lypaczewski, P., Normandeau, P.X., Paquette, J., and McMartin, I., 2013. Petrographic and cathodoluminescence characterization of apatite from the Sue Dianne and Brooke Zone IOCG mineralization systems, Great Bear magmatic zone, Northwest Territories; Geological Survey of Canada, Open File 7319. doi: 10.4095/292369

Complete Open File 7319 can be downloaded from Natural Resources Canada, (http://geoscan.nrcan.gc.ca/starweb/geoscan/servlet.starweb?path=geoscan/downloade.web&search1=R=292369):

In addition to the Open File report bellow, the following appendices are available with the download:

OF7319 Appendices:

A. Photomicrographs of thin sections in PPL and CL modes
B. Backscattered electron and EDX images on apatite crystals
C. Detailed observations of thin sections

OF7319 Report:

ABSTRACT

Apatite is the main REE-bearing phase in 18 thin sections from two mineralized systems and their host rocks, the Cu-Ag-(Au) Sue Dianne IOCG deposit and the nearby Brooke Zone, located within the southern Great Bear magmatic zone, Northwest Territories, Canada. The thin

sections show a range of IOCG-related alterations and igneous protoliths. Apatite occurs in all thin sections, in amounts ranging between traces to 5-10%. It can be divided into four populations on the basis of size, cathodoluminescence (CL) response and petrographic association: 1) small euhedral apatite (20-40 μm), occurring in clusters of 5 to 20 grains, generally free of inclusions, found in the volcaniclastic samples; 2) single apatite crystals (60-80 μm) with pitted edges, numerous fluid inclusions and sometimes monazite and hematite inclusions; 3) large single apatite crystals (100-300 μm) within epidote veins, sometimes associated with scheelite; and 4) large fractured apatite crystals (0.5 to 4 mm) with heavy hematite staining associated with hydrothermal breccias. The first 3 populations have a green to yellow CL response and the third population shows some irregular zoning. The fourth population shows a blue CL tint, with irregular green zones throughout grains or near the crystal rims. In that fourth population, mineral inclusions with an orange CL response are likely calcite. Group 3 and 4 also show a heterogeneous REE distribution within crystals under EDX. Given the overprinting of multiple alteration types in many of the specimens, additional work is needed to relate these apatite populations to specific alteration stages associated with IOCG-type mineralization. However, the presence of apatite coarse enough to be picked from glacial sediment samples and showing distinctive CL signatures in rocks related to IOCG mineralization suggests potential as an indicator mineral method.

INTRODUCTION

While apatite has potential to be a good indicator mineral in iron oxide copper-gold (IOCG) Kiruna-type deposits where it is a major mineral of the ore zone (Bonyadi, 2011), it is also present as an accessory mineral throughout the IOCG spectrum. It has been found to be a good resistate mineral in both weathered and glaciated terrains (De Toledo et al., 2004; Bouzari et al., 2011). For example, apatite is commonly present in till from the Great Bear magmatic zone (GBMZ) in amounts ranging between traces to 20% of the heavy mineral fraction (0.25-0.5 mm, separated at S.G.>3.2) with values above 2% found over or down-ice from IOCG systems (Normandeau et al., 2011). It has the ability to record geochemical conditions during its formation or subsequent alteration (Harlov et al., 2002; Harlov et al., 2005; Bouzari et al., 2011). Rare earth elements (REEs), as well as Sr^{2+}, Fe^{2+} and Mn^{2+}, can be incorporated in apatite's Ca^{2+}

sites, usually related to the Ca^{2+} + P^{5}+ -> REE^{3+} + Si^{4+} coupled substitution (Coulson and Chambers, 1996). The variations in Mn, Fe and REEs concentrations impart different colors to apatite in cathodoluminescence (CL) (Kempe & Gotze, 2002) allowing a preliminary assessment of compositional variation between and within grains. Apatite can also incorporate chalcophile elements, allowing the recognition of grains derived from mineralized zones (Belousova et al., 2002).

An undergraduate research project from McGill University, in partnership with the Geo-mapping for Energy and Minerals (GEM) IOCG Great Bear Project at the Geological Survey of Canada, was undertaken to identify and characterize the texture and habits of the apatite and other REE-bearing phases present in the magnetite to hematite group Cu-Ag-(Au) IOCG Sue Dianne deposit (Mumin et al. 2010) and the nearby Brooke Zone and their host rock lithologies, located in the southern Great Bear magmatic zone, Northwest Territories, Canada (Figure X.1). The results of this work will assist an ongoing doctoral research project by Philippe X. Normandeau at McGill University, which aims to develop a drift prospecting approach to IOCG exploration in glaciated terrain. This study was accomplished using transmitted light and cathodoluminescence optical petrography, together with backscattered electron imaging and energy dispersive x-ray spectroscopy analysis from a scanning electron microscope on a selection of bedrock thin sections.

METHODOLOGY

Sample selection

Samples from outcrops near and within the Sue Dianne and Brooke Zone IOCG mineralization systems (Figure X.2) were selected from a suite of samples collected as part of the GEM IOCG Great Bear project in 2009 and 2010. The samples consisted of 13 polished thin sections accompanied by field descriptions of the sampled units. Table X.1 provides the sample locations. These samples were selected to represent a range of IOCG alterations (Table X.2) within the various lithologies exposed near the two mineralized complexes (Corriveau et al., 2010). Sue Dianne mineralization surface samples (09CQA1009A1, 09CA1009B1) are from the hematite-dominated iron oxides zone (Camier, 2002; Mumin et al., 2010). A drill core sample from the Terra mine (3507A) high temperature IOCG system, was added to the selection to

better represent the non outcropping magnetite-dominated zone of Sue Dianne and Brooke Zone as no drill core where available for these systems.

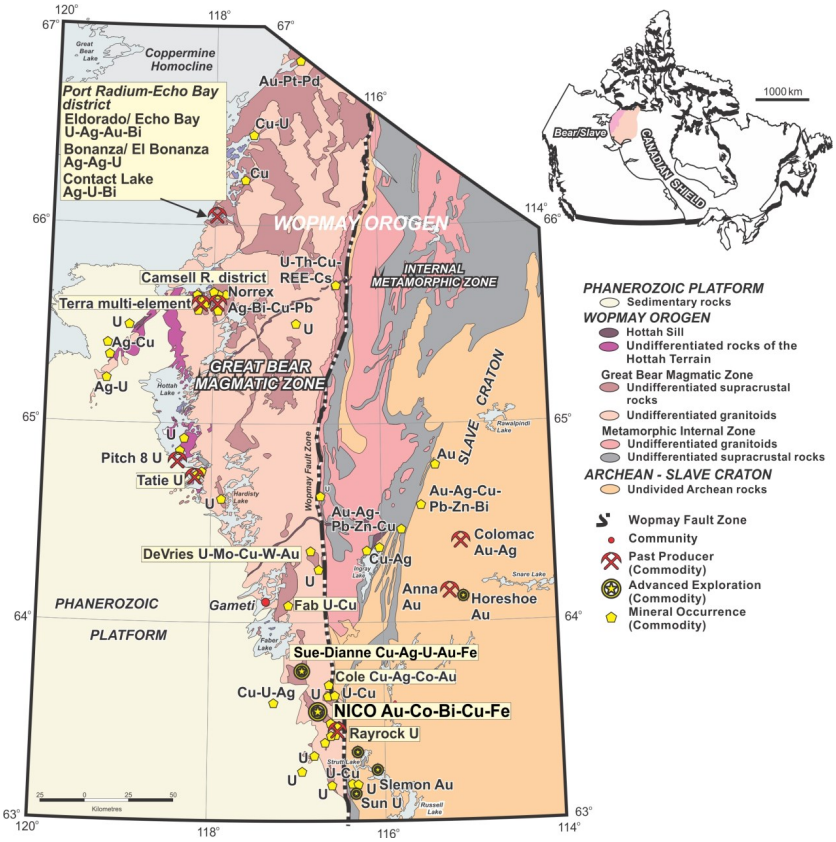

Figure X.1. The Great Bear magmatic zone bedrock geology, mineral occurrences and past-producing mines (modified from Corriveau et al. 2012). The Sue Dianne deposit (and nearby Brooke Zone) is located in the southern part of the GBMZ. Inset map locates the Wopmay orogen (Bear Province) and adjacent Slave craton at the western edge of the Canadian Shield.

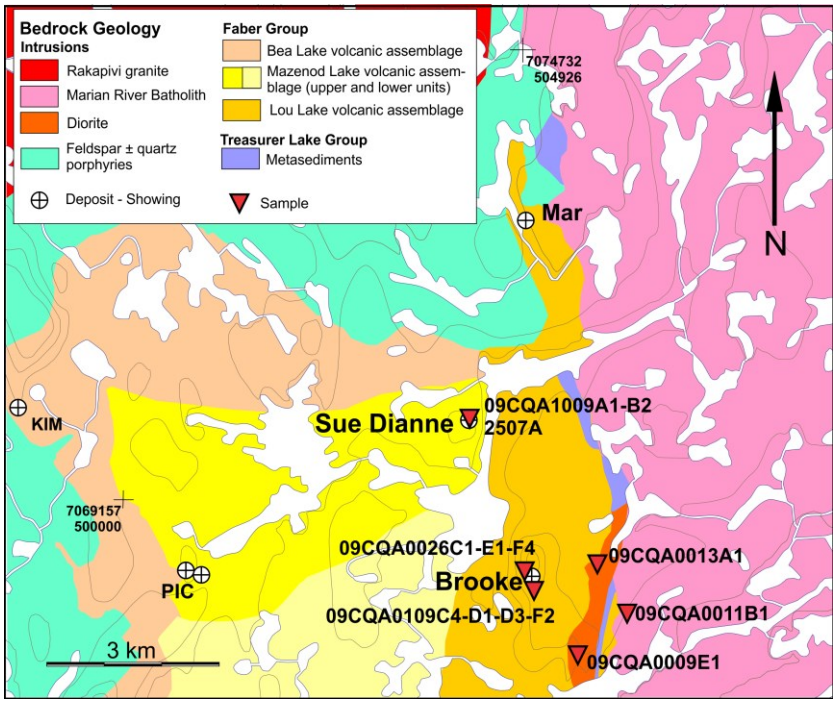

Figure X.2. Regional bedrock geology of the Sue Dianne deposit and Brooke Zone area (from Camier, 2002). Sample site locations are shown.

Table X.1. Summary of sample locations

Sample	Location	Easting	Northing
09CQA0009E01	Regional	505634	7067394
09CQA0011B01	Regional	506131	7067868
09CQA0013A01	Regional	505887	7068580
09CQA0026C01	Brooke Zone	505005	7068450
09CQA0026E01	Brooke Zone	505005	7068450
09CQA0026F04	Brooke Zone	505005	7068450
09CQA0109D01	Brooke Zone	505043	7068270
09CQA0109F02	Brooke Zone	505043	7068270
09CQA0109D03	Brooke Zone	505043	7068270
09CQA0109C04	Brooke Zone	505043	7068270
09CQA0026E04-1	Brooke Zone	505005	7068450
09CQA0026E04-2	Brooke Zone	505005	7068450
09CQA1009A1	Sue Dianne	504266	7070311
09CQA1009B1	Sue Dianne	504266	7070311
3507A	Terra mine, core	4487XX	72763XX
11PUA086B04	Fab	493377	7114864
11PUA538D01	Fab	492742	7115753
11PUA538C01	Fab	492742	7115753
11PUA084C01	Fab	494180	7110513

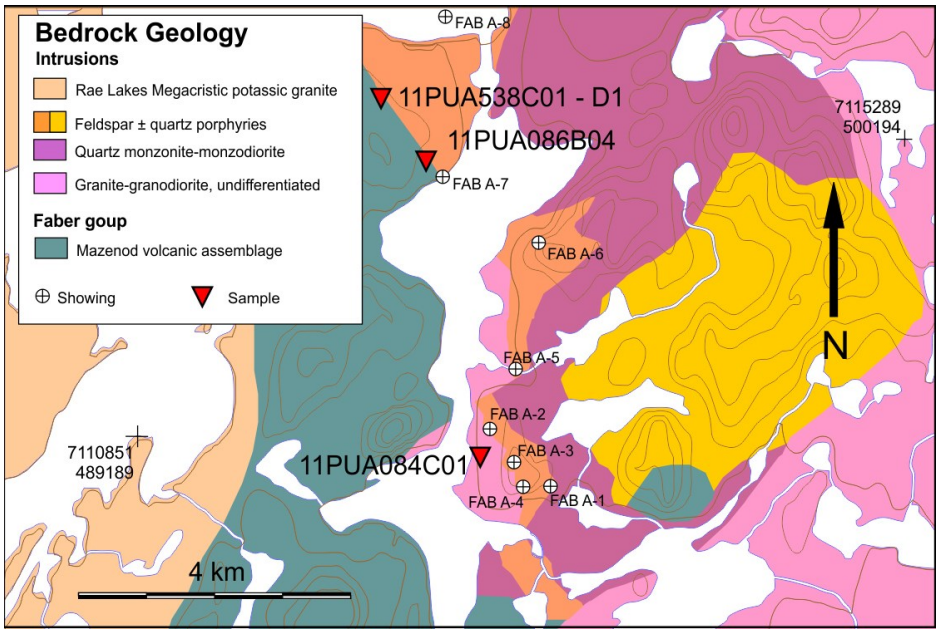

FigureX.3. Regional bedrock geology of the Fab Lake system area (from Gandhi et al., 2001). Sample site locations are shown.

Four additional polished thin sections from a fourth IOCG system (Fab) became available at the end of this study (Fig. X.3; see Fig. X.1 for location of Fab system) (Potter et al., 2012). As they provided a valuable contribution to the apatite characterization in IOCG settings from the GBMZ, their preliminary description was added to this report. It is to be noted however that these last samples are derived from large, thorium-rich, amphibole veins within the Fab IOCG system. Therefore, the samples collected offer a valid representation of the Ca-Fe (HT) alteration of the Fab Lake system, mostly absent at surface in the Sue Dianne system.

Transmitted-light microscopy

Petrographic descriptions using transmitted-light microscopy were completed on each thin section sample using a Leica Model DME polarized microscope. Apatite grains were observed using the 50x objective and 10x ocular, and could only be observed in plane polarized light, as crossed polars made the low birefringence apatite indistinguishable from the surrounding microcrystalline silicates (e.g. feldspar, quartz).

Cathodoluminescence microscopy

Photomicrographs were taken in both transmitted plane polarized light (PPL) and optical CL mode and are provided in Appendix A. Exposure times and settings are included in the file name of each image, according to the format [ThinSectionNumber_PictureNumber – Voltage, Current, Exposure time, Gain]. As such, the filename '*09CQA0109C04_02 - 4.0kV, 0.5 mA, 6.9 s gain 5.0*' refers to the second photograph of thin section 09CQA0109C04, taken in CL mode with a beam set a 4kV and 0.5 mA, a camera exposure time of 6.9 seconds and a gain of 5.

The optimal combination of settings was found to be a 4.0 kV beam with an exposure time of 3-4 seconds, and a low gain of 5. Most importantly, a well-adjusted electron beam focus was required. The optimal focus was found to be about 3 mm wide; a wider beam resulted in an intensity of CL emissions too low to allow a practical exposure time for the photography (under 15 seconds). When scanning through the thin section to locate an area of interest, the gain was adjusted to 25 and exposure times reduced to 250 - 400 milliseconds, allowing for an acceptable refreshing rate of the image. These settings, however, are only good for the initial observation of the samples in CL, due to luminescence aging. Murray and Oreskes (1997) analyzed the variation in CL response with exposure time, and found that the peaks at different wavelengths, produced by specific elements, exponentially decrease in intensity with exposure time, at different rates. In fact, a decrease in intensity by an average of 33% was noted over the first 8 minutes of exposure, often leading to change in the tint of the emission. This effect limits the usefulness of CL in determining the paragenesis of samples, since zoning in apatite grains of metasomatic or magmatic origin shows only faint contrast in CL and is strongly affected by luminescence aging.

Scanning electron microscopy

Petrographic descriptions and CL analysis were used to discriminate populations of apatite according to their texture, CL response and petrographic association. A selection of representative grains from each population was then observed by backscattered electron imaging using a scanning electron microscope. Backscattered electron images (BSE) were taken using the

Hitachi S-3000N variable pressure scanning electron microscope (SEM) at the Facility for Electron Microscopy Research (FEMR) at McGill University. The beam was set at 25 kV in variable pressure mode (set at 20 Pa). Single-point, nonquantitative compositional data were obtained using energy dispersive X-ray spectroscopy analysis (EDX) with the INCA analysis software. Readings were averaged over a live time period of 50 seconds and taken at multiple locations on and around apatite crystals. BSE and EDX data are provided in Appendix B.

RESULTS

Detailed petrographic observations of each thin section, together with a selection of SEM photomicrographs in PPL, CL and backscatter modes, are provided in Appendix C and summarized in Table X.2. Alteration types provided in Table X.2 are based on field observations, portable gamma-ray spectrometer data and bulk geochemistry analysis (Corriveau et al. 2010), while the mineral replacements are those observed in the sample and are most often the result of the late stage lower temperature alterations.

Petrography

09CQA0011B01, 09CQA0009E01: These samples are from the Marian River Batholith bordering the Sue Dianne and Brooke Zone system to the east. 09CQA11B01 is part of the least altered granitic country rock while 09CQA0009E01 is cut within a quartz-feldspars-hematite hydrothermal vein.

09CQA0109F02, **09CQA0013A01:** These two samples are mostly altered to epidote and show evidence of previous alteration phases. The epidotisation is associated with magnetite in 09CQA0109F02 and Mg rich chlorite in 09CQA0013A01. The alteration phases overprinted were not identified.

09CQA0026 series, 09CQA0109D01, 09CQA0109D03, 09CQA0109C04: Many samples consist of hematite-stained tuffs that show mineral replacement of intermediate intensity. Sample 09CQA0026F04 is one of the least replaced of these samples, with potassic feldspar clasts showing only a minor alteration to clay-size material. Other samples show a low amount of clay minerals, numerous monocrystalline clasts and a late microcrystalline silica matrix, all of them

being overprinted by heavy hematite staining. 09CQA0109C04 also shows some minor late epidote alteration. In the samples showing more intense mineral replacements, such as 09CQA0026E04, the feldspar clasts are hardly identifiable, and the matrix is fairly homogeneous.

3507A, 09CQA1009A1, 09CQA1009B1: Mineralized samples from the Sue Dianne deposit and the mineralize sample from the Terra mine drill core are brecciated and show intense replacements. The original mineral assemblages have been completely replaced by iron oxide, clays, chlorite, apatite and a microcrystalline silica matrix.

11PUA086B04, 11PUA538D01, 11PUA538C01, 11PUA084C01: All samples from the Fab Lake system are taken from a large amphibole rich vein. 11PUA086B04 is a coarse grained (>3 mm) assemblage of euhedral amphibole, muscovite and apatite with abundant hematite staining. 11PUA538D01 and 11PUA084C01 are composed of finer grained muscovite and amphibole, with rare apatite and traces of chlorite and clay replacements. 11PUA538C01 is an assemblage of coarse (>5 mm) potassic feldspar, plagioclase and quartz, locally altered to fine grained silica at crystal boundaries. Some potassic feldspar show incipient alteration to clay minerals. Biotite and chlorite are present. All are noteworthy for their more complexly zoned apatite than the samples from the Sue Dianne and Brooke Zone system.

In all cases but for the two samples with major epidote alteration (09CQA0109F02 and 09CQA0013A01), the intensity of replacement generally correlates with the amount of iron oxide present, either in the form of a light hematite staining or a large amount of crystalline magnetite and/or hematite aggregates.

Cathodoluminescence (CL)

In CL, the luminescent phases were found to be apatite, scheelite, calcite with or without the background response of an altered feldspar and/or quartz matrix (Fig. X.4). Calcite emits a characteristic red-orange color and cannot be mistaken for any other mineral specie. Feldspars emit the typical, faint, light blue response. Scheelite has a light blue color similar to that of feldspars but is far brighter. Apatite shows the most variation; it emits a greenish-yellow CL color in the majority of the samples, and a light lilac-blue to green color in the Sue Dianne and Brooke Zone mineralized samples and in the samples from the Fab Lake IOCG system.

CL zoning is present in most apatite grains but is patchy and irregular, with the exception of a few crystals also showing euhedral concentric zoning (09CQA0109C04, 3507A). Similar zoning patterns have been interpreted as the result of metasomatic alteration by Rae et al. (1996). The bright and darker zones in CL highlighting the observed patterns are also visible in the BSE images (Fig. X.5), where brighter zones in CL correspond to darker zones in BSE mode. Kempe and Götze (2002) noted that decreased CL intensity in the core of apatite correlated with an increased quantity of Mn^{2+}, possibly indicating selfquenching at concentrations above 2.0 wt% Mn. These authors observed that the darker zones in CL might be due to increased relative concentrations of weakly responding REEs over strongly responding REEs rather than to a higher concentration of Mn^{2+}. Rae et al. (1996) reported that apatite derived from samples in close proximity to the hydrothermal fluids source had a more contrasting and complex zonation pattern than the ones coming from samples further away from it.

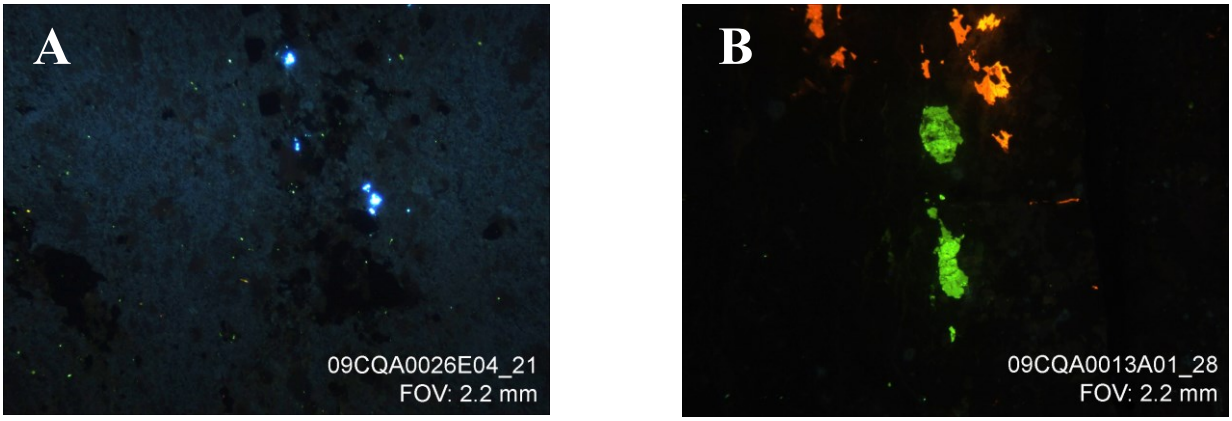

Figure X.4. CL photomicrographs of: A) scheelite crystals (bright blue) in feldspar matrix (faint blue) with micron-sized apatite (green specs); B) calcite (orange) and apatite (green).

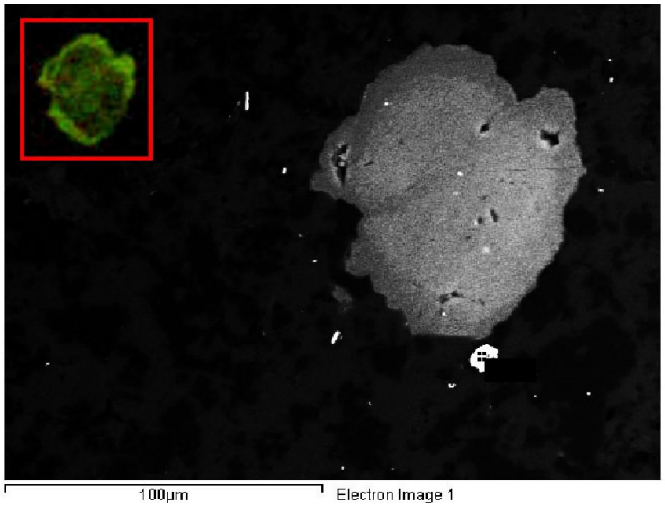

Figure X.5. Apatite grain where darker zones (in BSE) correspond to brighter CL, and inversely. From backscattered electron image 09CQA0026C01_06. BSE; the red square shows the same grain in CL. White dots are mineral inclusions, possibly monazite.

The blue (CL) apatite from the brecciated mineralized zone at Sue Dianne and Terra (09CQA1009A01, 09CQA1009B01, 3507A) shows hematite staining and brecciation during or after its crystallization. The main blue color is replaced by a green color often on the outer edges of the crystals and also along fractures in the apatite or in the form of stringers (09CQA0109C04, 11UPA086B04, 3507A). The green color is likely due to substitution of Ca^{2+} by Mn^{2+}, and the lilac-blue color to substitution of Ca^{2+} by REEs (Kempe & Gotze, 2002). This is supported by the BSE images, where blue zones are of lighter shades (3507A) (Fig. X.6). These zones often show the presence of REEs in quantities above the EDX detection limit. The green zones in CL are darker in BSE images and do not show detectable REEs by EDX analysis.

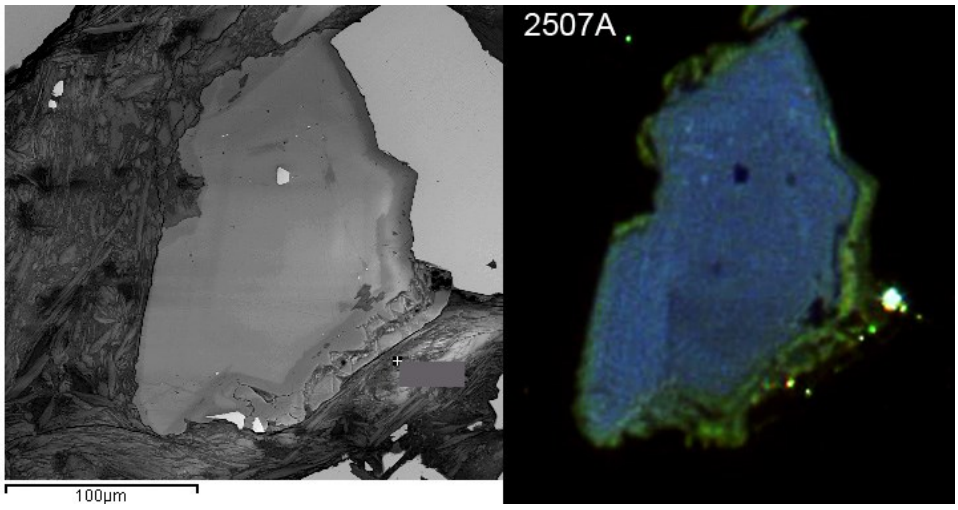

Figure X.6. Same apatite crystal imaged in BSE (SEM, left) and CL (right) showing that the blue CL color matches the brighter (heavier element-enriched) zones where REEs are detected by EDX.

Table X.2. Summary of petrographic and cathodoluminescence observations

ID	Alteration	Mineral replacement	Veins	Apatite location/Association	Apatite size	CL, additional information
09CQA0009E01	Qtz-Hem vein	Chl, Fe. K-spar overgrowth	None	In altered assemblages.	< 30 µm	Rare green-yellow point seen in CL, cannot be seen in PPL
09CQA0011B01	K alteration	Bt, amp -> chl. Plag -> Fe, Clay	Rare; Ep	- Common in chl	60-80 µm	Green-yellow, heterogeneous zonations, euhedral, numerous in chlorite.
				- Rare in feldspars	< 60 µm	
09CQA0013A01	Na-Ca-Fe (HT)	Ep, Si, K, Chl	Common; Ep, Chl	Disseminated in matrix	< 40 µm	Green-yellow, texture visible on larger grains. Numerous red (CL) calcite.
				At vein edges	80-200 µm	
09CQA0109F02	K, K-Fe (HT) ,K-Fe (LT), Ca-Fe (LT) alteration	Clay ± Si (early), Ep, Mag, Minor Pyrite	Numerous; Si (early). Ep ± Mag (Late)	- Early aggregate	40-80 µm	Green-yellow, in veins, homogeneous. Light blue (Intense); scheelite
				- In Ep. Veins	100-300 µm	
09CQA0109C04	K alteration	µm Si, Fe, Clay.	Common, Ep ± Ccp(Py?). Hem, Ep, Si, Clay.	In relict mafic crystals	30-60 µm, 100-180 µm	Grayish-blue-green, green-yellow, commonly show bright rim and zonations.
09CQA0026F04	K±Fe (HT) alteration	µm Si, Fe, Clay.	Few; Mag, Si.	Aggregates	80-120 µm	Green-yellow, heterogeneous zonations.
				Near old veinlets.	60-100 µm	
09CQA0026C01	Fe (HT), K alteration	µm Si, Fe, Clay	Rare; Ep	Dissiminated	50-100µm,	Green-yellow, heterogenous zonations, bright rim; metasomatic alteration.
09CQA0026E01		µm Si, Fe, Clay	Common; Hb, Chl, Mag, Qz.	- Aggregates.	20-40 µm	Green-yellow, heterogeneous zonations. Brownish patch in CL surrounding apatite aggregates.
				- Dissiminated	70-80 µm	
				- Near/in veins.	80-120 µm	
09CQA0109D01	K-Fe (HT to LT) alteration, brecciation	µm Si, Fe, Clay, Minor Ep	Early Si. Breccia; Mag ± Si	- In relict veinlets	70-90 µm	Green-yellow, faint heterogeneous zonations. Striated apatites. Relict mafic (?) zones appear brown in CL.
				- Less often In relict mafic zones	<40 µm	
09CQA0109D03	Fe±K (HT to LT) alteration, brecciation	µm Si, Fe, Clay, Minor Ep	Early Si. Breccia; Mag ± Si	In relict mafic zones	< 40 µm -80 µm	Green-yellow, heterogeneous, bright rim. Striated apatites. Relict mafic (?) zones easily seen in CL.
09CQA0026E04-1	Na (HT), K-Fe (HT) alteration, brecciation	µm Si, Clay, Ep ±Fe	Common; deformed, Py, Ep, Si.	Aggregates	20-30 µm	Green-yellow, minor het. zonations. Numerous blue scheelite.
				Dissiminated	60-80 µm	
09CQA0026E04-2	Na (HT), Fe (HT) alteration, brecciation	µm Si, Fe, Ep ±Clay	Numerous; deformed. Ep, Si, Chl, Mag	Aggregates	20-30 µm	Green-yellow, minor het. zonations. Numerous blue scheelite
				Dissiminated	80 µm	
09CQA1009A01	K-Fe (HT to LT) , brecciation	µm Si, Hm, Chl	Hem, Brecciated	Small, disseminated	30-50 µm, rare 60 µm	Bluish-Green
09CQA1009B01	K-Fe (HT to LT) , brecciation	µm Si, Hm ±Chl	Hem, Brecciated	Rare in relict clasts, often in within large hm.	60 - 80 µm, up to 100 µm	Typical Green. Blue core, Green rim

ID	Alteration	Mineral replacement	Veins	Apatite location/Association	Apatite size	CL, additional information
3507A	K-Fe (HT) alteration, brecciation	Mag, Clay.	Mag, Hem, Brecciated	Dissiminated	0.2 to >3 mm	Blue CL, green where altered. Blue concentric zonations in some crystals.
11PUA086B04	Ca-Fe (HT) alteration	-	-	Dissiminated, mantled by muscovite	0.2 to >3 mm	Blue CL, green where altered. Blue concentric zonations in some crystals.
11PUA538D01	Ca-Fe (HT), K-Fe alteration	-	-	Rare, dissiminated	300 to 400 µm	Typical Green. Blue core, Green rim
11PUA538C01	Ca-Fe (HT), K-Fe alteration	-	-	In relict mafic zones	300 to 400 µm	Grayish-blue, green edges
11PUA084C01	Ca-Fe (HT) alteration	-	-	Dissiminated	300 to 500 µm	Typical Green. Blue core, Green rim

Apatite occurrence

Four texturally distinct types of apatite occurrence were observed:

1) Apatite mostly from volcaniclastic samples commonly occurs in dull brownish polycrystalline aggregates of silt and clay size minerals (e.g. 09CQA0026E01). This is the most fine-grained apatite population, with crystals typically ranging between 20-40 μm in size. Apatite crystals from this population are usually free of inclusions and euhedral. The aggregates are associated with hematite staining and magnetite crystals and are often clearly visible in CL, contrasting with the faint blue background from the feldspars (e.g. 09CQA0026E01; 09CQA0011B01). This type of apatite is texturally similar to metasomatic apatite described by Rae et al. (1996) found in association with mafic Ca-rich phases, including aegirine-augite and amphibole, within a heavily metasomatised quartzite.

2) The second population of apatite occurs as single crystals often found within veinlets or patches of slightly coarser microcrystalline silica. These crystals are typically larger than the first type of apatite, ranging between 60-80 μm in size, and they usually show pitted edges, sometimes with a partial hematite coating. This type of apatite commonly contains numerous fluid-filled inclusions (09CQA0109D03), and/or monazite (09CQA0026C01) and hematite (09CQA0011B01) inclusions.

3) The third type of apatite is less common and consists of large crystals ranging between 100-300 μm in size (09CQA0109F02; 09CQA0013A01). These large crystals are mostly occurring in late epidote veins. Scheelite may be present within these same veins. Apatite from this group shows a heterogeneous zoning in CL with the response varying in intensity but not in color.

4) A fourth type of apatite was found in samples from the Sue Dianne and Terra mine mineralized breccia (3507A, 09CQA1009A1, 09CQA1009B1) and from the Fab Lake IOCG system (11UPA086B04, 11UPA538D01, 11UPA538C01, 11UPA084C01). This type of apatite shows larger crystals (0.2 to 3 mm) which display a CL zoning consisting of two characteristic colors: a main blue zone that was shown by SEM-EDX to contain a higher concentration of REEs, and smaller green zones, which have lower concentrations of REEs or concentrations

below detection limit (e.g. 3507A). Usually, the core of these apatite crystals consists of a blue zone; rims and areas bordering fractures are green (e.g. 3507A). This population of apatite is found in three distinct associations: 1) randomly disseminated in massive magnetite, in which case it is often surrounded by clay minerals (3507A); 2) associated with hematite aggregates and chlorite veins in heavily altered samples from Sue Dianne (09CQA1009A1, 09CQA1009B01); and 3) randomly disseminated among the muscovite in the Fab Lake IOCG system samples.

DISCUSSION

The majority of apatite crystals identified in the studied samples show clear evidence of metasomatic alteration in the form of irregular compositional zonation patterns visible in CL. Apatite crystals occur predominantly in aggregates or in deformed, relict veinlets, indicating their early emplacement by hydrothermal fluids and subsequent alteration. Apatite is also abundant in some of the later epidote-bearing veinlets which crosscut hydrothermal minerals such as earlier apatite, clearly indicating numerous distinct episodes of apatite formation and alteration. Because of this complex history, no distinction was possible between a magmatic apatite population present in protolith later affected by hydrothermal fluids (either through overgrowth crystallization or being partially dissolved), and an original hydrothermal apatite population. A few disseminated apatite crystals were observed without any association with veins, aggregates or specific mineral replacements. These apatite crystals do not show any textural or geochemical variation (based on CL and EDX work) from the apatite occurring in aggregates or in veinlets.

Apatite with a blue-green color response in CL is seen in the mineralized samples from Sue Dianne and Terra mine (3507A, 09CQA1009A01 and 09CQA1009B01) and in samples from the Fab Lake system (11UPA086B04, 11UPA538D01, 11UPA538C01, 11UPA084C01). Since samples from those systems show a similar green zoning of the blue apatite along fractures within the crystals and in the form of stringers, we infer that the green zones are secondary in these particular crystals and are associated with REE-depleted fluids present after crystallization in both cases. Fe-rich fluids were subsequently introduced but had little effect on the apatite other than a hematite staining present in both CL zones.

SUGGESTIONS FOR FUTURE WORK

CL optical microscopy has proven to be essential for the identification of fine grained apatite and for the characterization of crystal zoning. Given its potential and low cost, this analytical method is, in our opinion, under-utilized in the study of apatite. Alternatively, apatite could be located by automated EDX scanning for phosphorus. The diagenesis of each of the four apatite populations found in the Sue Dianne, Brooke Zone, Terra mine and Fab Lake systems remains poorly understood. Specific associations between each alteration phases and the textural characteristics of apatite stated above is currently being examined as a continuation of this study.

Only the apatite populations #3 and #4 contain grains large enough to be hand-picked under a binocular. All grains from the first population and most grains from the second population will be incorporated into the silt and clay fraction of the till during glacial attrition. A normalized count of grains with a blue CL response picked from till samples could offer potential for using apatite as an indicator mineral provided that a characterization of apatite from a larger variety of systems across the IOCG spectrum is completed. Reexamination of apatite grains separated from till and bedrock samples from across the GBMZ and regrouped into the four apatite populations, as well as CL characterization prior to mounting, is being completed to better assess the validity of using apatite as an indicator mineral for exploration in the early stages of processing.

ACKNOWLEDGEMENTS

This research was conducted as part of an undergraduate thesis by P. Lypaczewski at McGill University. Samples were collected as part of the Geomapping for Energy and Minerals (GEM) IOCG Project under the leadership of Louise Corriveau at the Geological Survey of Canada, in collaboration with the Northwest Territories Geoscience Office through funding from the Strategic Investments in Northern Economic Development Program at Indian and Northern Affairs Canada. We are grateful to the following: Fortune Minerals Ltd. for logistical support at NICO in 2009 and 2010 and Helen Campbell and John Stix for respectively making the SEM and CL analysis possible. Jean-François Montreuil is thanked for providing a careful review.

REFERENCES

Averill, S. A. 2001. The application of heavy mineral indicator mineralogy in mineral exploration, with emphasis on base metal indicators in glaciated metamorphic and plutonic terrain. In: McClenaghan, M.B. Bobrowsky, P.T. Hall, G.E.M., Cook, S.J. (eds) Drift exploration in glaciated terrain. Geological Society, London, Special Publications, vol. 185, p. 69-82.

Belousova, E.A. Griffin, W.L. O'Reilly, S.Y. Fisher, N.I. 2002. Apatite as an indicator mineral for mineral exploration: trace-element compositions and their relationship to host rock type. J. Geochem. Expl. 76, p. 45–69.

Bonyadi, Z. Davidson,G. Mehrabi, B. Meffre, S. Ghazban, Fereydoun. 2011, Significance of apatite REE depletion and monazite inclusions in the brecciated Se–Chahun iron oxide–apatite deposit, Bafq district, Iran: Insights from paragenesis and geochemistry. Chemical Geology, v. 281, p. 253-269.

Bouzari, F. Hart, C.J.R. Barker, S. and Bissig, T. 2011. Porphyry indicator minerals (PIMS): A new exploration tool for concealed deposits in south-central British-Columbia. Geoscience BC Report 2011-17.

Camier, W. J. 2002, The Sue-Dianne Fe-oxide Cu-Ag-Au breccia complex, southern Great Bear Magmatic Zone, Northwest Territories, Canada: M.Sc. Thesis, University of Western Ontario, London, Ontario, 220 p.

Coulson, I.M. and Chambers, A.D. 1996. Patterns of zonation in rare-earth-bearing minerals in nepheline syenites of the North QoroQ center, South Greenland. Canadian Mineralogist v. 34, p. 1163-1178

Corriveau, L. Williams, P.J. Mumin, A.H. 2010. Alteration vectors to IOCG mineralization: From uncharted terranes to deposits. In Corriveau, L. and Mumin, A.H. eds. Exploring for iron oxide copper-gold deposits: Canada and global analogues; Geological Association of Canada, Short Course Notes 20, p. 89-110

De Toledo, M.C.M. Lenharo, S.L.R. Ferrari, V.C. Fontan, F. DeParseval, P. 2004. The compositional evolution of apatite in the weathering profile of the Catalão 1 alkaline-carbonatitic complex, Goias, Brazil, The Canadian Mineralogist, v. 42, p. 1139-1158.

Gandhi, S.S. Mortensen J.K. Prasad, N. Van Breemen, O. 2001. Magmatic evolution of the southern Great Bear continental arc, northwestern Canadian Shield: geochronological constraints. Canadian Journal of Earth Sciences, v. 38, p. 767-785.

Harlov, D.E. Wirth, R. Förster, H.-J. 2005. An experimental study of dissolution-reprecipitation in fluorapatite: Fluid infiltration and the formation of monazite. Contributions to Mineralogy and Petrology, v. 150, p. 268–286.

Harlov, D.E. and Förster, H.-J. 2003. Fluid-induced nucleation of REE-phosphate minerals in apatite: Nature and experiment. Part II. Fluorapatite. American Mineralogist, v. 88, p. 1209–1229.

Harlov, D.E. Förster, H.-J. Nijland, T.G. 2002a. Fluid-induced nucleation of REE-phosphate minerals in apatite: Nature and experiment. Part I. Chlorapatite. American Mineralogist, v. 87, p. 245–261.

Harlov, D.E. Andersson, U.B. Förster, H.-J. Nyström, J.O. Dulski, P. Broman, C. 2002b, Apatite-monazite relations in the Kiirunavaara magnetite-apatite ore, northern Sweden. Chemical Geology, v. 191, p. 47–72.

Kempe, U. and Götze, J. 2002, Cathodoluminescence (CL) behaviour and crystal chemistry of apatite from rare-metal deposits: Mineralogical Magazine, v. 66, p. 151–172.

Mumin, A.H. Somarin, A.K. Jones, B. Corriveau, L. Ootes, L. Camier, J. 2010. The IOCG-porphyry-epithermal continuum of deposits types in the Great Bear Magmatic Zone, Northwest Territories, Canada. In Corriveau, L. and Mumin, A.H. eds. Exploring for iron oxide copper-gold deposits: Canada and global analogues; Geological Association of Canada, Short Course Notes 20, p. 59-78.

Murray, J.R. and Oreskes, N. 1997. Uses and limitations of cathodoluminescence in the study of apatite paragenesis. Economic Geology, v. 92, p. 368-376

Normandeau, P.X. McMartin, I. Paquette, J. Corriveau, L. 2011. Drift prospecting applied to iron oxide copper gold exploration in the Great Bear magmatic zone, Northwest Territories, Canada. Poster presentation, Geological & Mineralogical Association of Canada (GAC-MAC) annual meeting 2011, 25-27 April, Ottawa.

Potter, E.G. Montreuil, J.-F. Corriveau, L. 2012. Alteration mapping in IOCG systems: Fab Lake case study. Geological Association of Canada – Mineralogical Association of Canada annual meeting, Program with Abstracts, v. 35, p. 110.

Rae, D.A. Coulson, I.M. and Chambers, A.D. 1996. Metasomatism in the North Qoroq centre, South Greenland: Apatite chemistry and rare-earth element transport. Mineral. Mag. v.60, p. 207 -220.

Slave geological province NATMAP project in Northwest Territories, Canada. GSC Open File 2559. Last DIF reviewed: 2006.